Studies on Poly(*N*,*N*-dimethylaminoethyl methacrylate) Composite Membranes for Gas Separation and Pervaporation

by

Jennifer Run-Hong Du

A thesis

presented to the University of Waterloo

in fulfillment of the

thesis requirement for the degree of

Doctor of Philosophy

in

Chemical Engineering

Waterloo, Ontario, Canada, 2008

AUTHOR'S DECLARATION

I hereby declare that I am the sole author of this thesis. This is a true copy of the thesis, including any required final revisions, as accepted by my examiners.

I understand that my thesis may be made electronically available to the public.

Abstract

Membrane-based acid gas (e.g., CO_2) separation, gas dehydration and humidification, as well as solvent dehydration are important to the energy and process industries. Fixed carrier facilitated transport membranes can enhance the permeation without compromising the selectivity. The development of suitable fixed carrier membranes for CO_2 and water permeation, and understanding of the transport mechanism were the main objectives of this thesis.

Poly(*N*,*N*-dimethylaminoethyl methacrylate) (PDMAEMA) composite membranes were developed using microporous polysulfone (PSF) or polyacrylonitrile (PAN) substrates. The PDMAEMA layer was crosslinked with *p*-xylylene dichloride via quaternization reaction. Fourier transform infrared, scanning electron microscopy, adsorption tests, and contact angle measurements were conducted to analyze the chemical and morphological structure of the membrane. It was shown that the polymer could be formed into thin dense layer on the substrates, while the quaternary and tertiary amino groups in the side chains of PDMAEMA offered a high polarity and hydrophilicity.

The solid-liquid interfacial crosslinking of PDMAEMA led to an asymmetric crosslinked network structure, which helped minimize the resistance of the membrane to the mass transport. The interfacially formed membranes were applied to CO_2/N_2 separation, dehydration of CH_4, gas humidification and ethylene glycol dehydration. The membranes showed good permselectivity to CO_2 and water. For example, a CO_2 permeance of 85 GPU and a CO_2/N_2 ideal separation factor of 50 were obtained with a PDMAEMA/PSF membrane at 23^oC and 0.41 MPa of CO_2 feed pressure. At 25^oC, the permeance of water vapor through a PDMAEMA/PAN membrane was 5350 GPU and the water vapor/methane selectivity was 4735 when methane was completely saturated with water vapor. On the other hand, the relative humidity of outlet gas was up to 100 % when the membrane was used as a hydrator at 45^oC and at a carrier gas flow rate of 1000 sccm. For used for dehydration of ethylene glycol at 30^oC, the PDMAEMA/PSF membrane showed a permeation flux of ~1 mol/(m^2 h) and a permeate concentration of 99.7 mol% water at 1 mol% water in feed.

This work shows that the quaternary and tertiary amino groups can be used as carriers for CO_2 transport through the membrane based on the weak acid-base interaction. In the presence of water, water molecules in the membrane tend to form a water "path" or water "bridge" which also help contribute to the mass transport though the membrane. In addition, CO_2 molecules can be hydrated to HCO_3^-, which reaction can be catalyzed by the amino groups, the hydrated CO_2 molecules can transport through the water path as well as the amino groups in the membrane. On the other hand, for processes involving water (either vapor or liquid) permeation, the amino groups in the membrane are also helpful because of the hydrogen bonding effects.

Acknowledgements

I am privileged to work with my two supervisors, Dr. Xianshe Feng and Dr. Amit Chakma. Their vision, knowledge, and scholarship provide me a role model for my future life and career. I will never forget the enjoyment and happiness from reading the manuscripts revised by Dr. Feng, and I am much moved by and deeply respect his professional conscientiousness of science. I will miss the group meetings with Dr. Chakma who always gives me constructive suggestions on my research and career planning, and I am impressed very much by his vitality and innovativeness. I am deeply indebted to their guidance, encouragement, friendship and support over the past four years during my study at Waterloo.

I wish to thank all my colleagues from our membrane group for all their assistance and support during the course of this research. I am much obliged to Dr. Li Liu, Dr. Shude Xiao, Dr. Leon Hung-Liang Hsu and Dr. Yong Zhou for their interest and valuable discussion and advices on the research and thesis writing. I really appreciate the encouragement and consideration that I have received from Dr. Yufeng Zhang. I also want to thank all my great friends as well as my English tutor Dana Krajcir for making graduate school so much fun.

I would like to express my gratitude to my PhD examination committee members, Dr. Phillip Choi, Dr. Jean Duhamel, Dr. Christine Moresoli and Dr. Joao Soares, for their comments on my research and thesis.

I would like to give my special thanks to my parents, grandmother and uncle Jiajun whose endless love, encouragement and support enabled me to complete this thesis.

Finally, research support from the Natural Sciences and Engineering Research Council (NSERC) of Canada is gratefully acknowledged.

To My Dearest Parents

Table of Contents

List of Figures

xiii

xiv

List of Tables

Chapter 1

Introduction

1.1 Background

Membrane-based separation is generally superior to traditional methods in terms of energy consumption and environmental friendliness. At present, commercially available membranes for the separation of small molecules are mostly asymmetric polymeric membranes consisting of two structurally distinct layers: a porous substrate and a nonporous separation layer. The asymmetric membranes can generally be classified into integrally skinned membranes and composite membranes [Pandy and Chauhan, 2001].

Integrally skinned membranes consist of a microporous substrate covered with a very thin nonporous surface layer or "skin". The pore size of the substrate can decrease toward the skin, and the separation occurs almost entirely in the skin, while the microporous substrate provides the membrane with the necessary mechanical strength. The substrate and skin layer of an integrally skinned membrane are made of the same polymer. However, the membrane performance is often affected by the microscopic defects in the skin and composite membranes have been developed as an alternative.

Composite membranes differ from integrally skinned membranes in that the nonporous surface layer and its microporous substrate are made of different polymers. There are two types of composite membranes: resistance or caulked composite membranes and thin-film composite membranes. Resistance composite membranes are prepared by coating the skin of an integrally skinned membrane with a layer of highly permeable material (e.g., silicone rubber) to plug the defects, if any, and the skin of the integrally skinned membrane is predominately responsible for the separation [Feng et al., 2002]. Thin-film composite membranes are prepared by depositing a nonporous layer on top of an integrally skinned membrane, and the deposition layer is predominately responsible for the separation. Several methods have been developed to prepare thin-film composite membranes, including surface coating, in situ polymerization, and interfacial polymerization. Among these methods,

1

interfacial polymerization can minimize the mass transfer resistance through the composite layer because interfacial polymerization is a self-limiting reaction process which helps form an ultrathin layer in the composite membrane.

Poly(*N*,*N*-dimethylaminoethyl methacrylate) (PDMAEMA) is a water soluble polymer with tertiary amino groups in side chains and can be crosslinked into a three-dimensional network containing quaternary amino groups through compete alkylation. A pre-crosslinked PDMAEMA solution can be coated onto a porous substrate to form a dense composite layer. Alternatively, the composite membrane can also be formed by coating an uncrosslinked PDMAEMA layer on a substrate, followed by surface crosslinking. Both approaches can be used to form an ultrathin PDMAEMA layer. The PDMAEMA layers prepared with surface crosslinking may possess an asymmetric structure in terms of crosslinking networks, and they are anticipated to reduce the mass transport resistance and increase the permeation rate. The mass transport through nonporous composite membranes is supposed to follow the solution-diffusion mechanism. By controlling the crosslinked networks, composite membranes based on PDMAEMA can be employed for gas separation, vapor permeation and pervaporation.

Conventional polymeric membranes based on solution-diffusion for permeation often suffer from a trade-off relationship between the permeability and selectivity. Facilitated transport membranes can enhance the permeation of certain components without compromising the selectivity by taking advantage of the active carriers that specifically interact or reversibly react with the target components. Facilitated transport membranes are often in the form of liquid membranes and fixed carrier membranes. Liquid membranes possess a high permeability and a high selectivity, but they are rarely used industrially due to problems associated with instability and carrier loss. Fixed carrier membranes have the advantages of high permselectivity and good stability because the carriers are fixed onto polymer backbone through chemical bond or electrostatic force.

Considering the tertiary or quaternary amino groups on the side chains of crosslinked PDMAEMA, this polymer may exhibit facilitated transport to CO_2. The permselectivity to

2

CO_2 could be achieved by exploiting the weak acid-base interactions between CO_2 and the tertiary amino groups and the electrostatic interactions between CO_2 and quaternary amino groups. The polymer is highly hydrophilic because of the high polarity and the hydrogen bonding between amino groups and water molecules. The amino groups, responsible for the high hydrophilicity, may also be regarded as fixed carriers for water transport through the membrane. In short, the crosslinked PDMAEMA can favor the permeation of acid gases and water molecules. To our knowledge, there is no work reported in the literature on the potential use of PDMAEMA as a membrane material for CO_2 permeation (for instance, in CO_2 capture from flue gas), and water permeation (for gas humidification and dehydration as well as solvent dehydration by pervaporation). This motivates the development of membranes prepared from homopolymer PDMAEMA for CO_2 separation and water permeation in the thesis.

1.2 Research Objectives

The objectives of this research were to study PDMAEMA membranes for CO_2 separation and water permeation based on the relationship of membrane materials, membrane morphologies and separation properties. The research consisted of the followings:

1) Studies of the membrane material, including the polymerization conditions and selection of suitable crosslinking agent for PDMAEMA.

2) Studies of the membrane fabrication technique, including the traditional coating approach and interfacial polymerization approach. It was demonstrated that the interfacial polymerization approach worked better than the traditional coating approach.

3) Applications of the interfacially formed membranes for CO_2 separation from N_2 and other gas separation and pervaporation applications involving water permeation. The mass transport mechanisms and effects of operating parameters on the membrane performance were investigated.

1.3 Outline of the Thesis

This thesis consists of eight chapters. The scope of each chapter is listed as follows:

Chapter 1 presents an overview of the objectives and the rationale of selecting PDMAEMA as the membrane material (i.e., use of a highly polar material for facilitated permeation of CO_2 through acid-base interactions and for permeation of water through hydrogen bonding interaction).

A literature review on the solution-diffusion mechanism for permeation and its various applications (i.e., CO_2 separation, vapor permeation and pervaporation) are presented in chapter 2.

Chapter 3 deals with PDMAEMA composite membranes prepared by the bulk crosslinking and coating approach. The intrinsic separation properties for various gases were demonstrated experimentally.

Considering the advantages of interfacial polymerization/crosslinking for inducing asymmetric structure of the crosslinking networks, attempts were made to develop interfacially formed PDMAEMA membranes, and this is presented in Chapter 4.

Chapters 5, 6 and 7 are concerned with the various applications of the interfacially formed PDMAEMA membranes based on solution-diffusion mechanism, including the separation of CO_2, dehydration of natural gas, humidification of nitrogen, and dehydration of ethylene glycol.

Chapter 8 summarizes the general conclusions and original contributions of the thesis, and recommendations for future work are also presented.

Chapter 2

Literature Review

2.1 Membrane Separation Processes

Membrane separation is based on selective transport of one or some components over the other components in a mixture through a membrane under a driving force (such as a pressure, concentration, temperature or voltage gradient across the membrane) [Koros, 2004]. Many membrane processes, including microfiltration, ultrafiltration, nanofiltration, dialysis, reverse osmosis, pervaporation, gas separation, vapor permeation and electrodialysis, have been used in chemical, environmental, and pharmaceutical industries [Atkinson, 1999].

As one of the most promising separation technologies, membrane separations offer a number of advantages over traditional methods, including 1) simplicity of process design, compactness, light weight, low maintenance, and easy installation; 2) high process flexibility (modular design permitting easy scale up or operation at reduced capacity as necessary); 3) low energy consumption; and 4) environmental friendliness (no secondary pollution) [Freeman and Pinnau, 2004].

Based on applications and mass transport mechanisms, different types of membranes (for instance porous versus dense membranes) should be used. Porous membranes with pores ranging from 100 nm (for ultrafiltration) or up to 10 μm (for microfiltration) are usually employed in the separation of a mixture with large size components [Hofmann et al., 2000] such as clarification of fruit juice, purification of protein, and sterilization of beer. The separation of different species through porous membrane is mainly based on the size sieving mechanism. The permeants are transported by pressure-driven convective flow through tiny pores, and separation occurs because one of the components is excluded from entering the pores of the membrane through which other components can penetrate.

On the other hand, the processes of reverse osmosis, gas separation, vapor permeation and pervaporation for the separation of small molecular mixtures, such as desalination of sea

water, production of oxygen-enriched air, and natural gas dehydration require the membranes to be nonporous. The mass transport through these membranes is usually described by the solution-diffusion mechanism. That is, the permeants dissolve into the membrane material and then diffuse through the membrane down a concentration gradient. To develop membranes for effective gas separation, vapor permeation and pervaporation, a better understanding of the transport mechanism and of the main factors determining the permselectivity of dense nonporous membranes is essential, and the basic principles will be reviewed briefly in the following sections.

2.2 Solution-diffusion Mechanism

2.2.1 Models

Macroscopic Model

As mentioned previously, the mass transport through a dense membrane is best described by the solution-diffusion model, which was first postulated by Graham in 1866. The chemical potential across the membrane can be expressed as a concentration gradient [Basu et al., 2004]. The transport of molecules from the upstream (i.e., high pressure or high chemical potential) side of a membrane to the downstream (i.e., low pressure or low chemical potential) side of a membrane occurs via a 3-step process: 1) sorption of permeants into the upstream side of the membrane; 2) diffusion through the membrane under a concentration gradient; and 3) desorption from the downstream side of the membrane (see Fig. 2-1) [Matson et al., 1983; Wijmans and Baker, 1995; Koros et al., 1996]. The molecular diffusion is usually the slowest and hence the rate-determining step in the permeation process. In contrast, the sorption and desorption of permeants are very fast, and sorption equilibrium is therefore assumed to be established between both the permeant-membrane interfaces [Feng and Huang, 1997; Stern and Koros, 2000].

The permeability coefficient (P) is generally used to characterize how permeable the membrane is and it is equal to the product of the solubility coefficient (S) and diffusion coefficient (D):
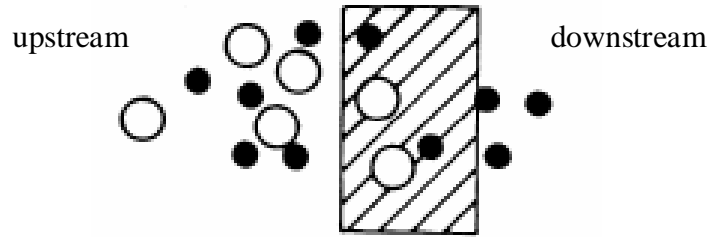
Fig. 2-1. Solution-diffusion mechanism [Zolandz and Fleming, 1992].

$$P = DS \tag{2-1}$$

The solubility coefficient is a thermodynamic parameter [Stern, 1994], and it represents the sorption amount of permeant in the membrane under equilibrium. It is affected by the permeant condensability and the interaction between the permeant and polymer. The solubility of a permanent gas in polymers is rather small because of the weak affinity between permanent gas molecules and a polymer, while the solubility of a condensable gas or an organic solvent in a polymer may be quite large due to their high affinities.

The diffusion coefficient is a kinetic parameter and reflects the mobility of the permeant molecules through a membrane. It depends on the geometrical shape of permeant molecules and the polymer property. The smaller the permeant molecule, the higher the diffusion coefficient. For a given permeant molecule, the polymer properties (i.e., chemical structure and stereochemistry, mobility of polymer segments, steric hindrance, crystallization, and degree of crosslinking) also influence the diffusivity.

The ability of a membrane to separate a mixture is measured by its selectivity. In a binary mixture system consisting of components i and j with component i as the fast permeating species, selectivity can be measured by the ideal separation factor, which is equal to the ratio of their permeability coefficients [Koros, 2002]:

$$\alpha_{i/j} = \frac{P_i}{P_j} = \frac{D_i}{D_j} \times \frac{S_i}{S_j} \tag{2-2}$$

where (D_i/D_j) is the ratio of diffusion coefficients or diffusivity selectivity, and (S_i/S_j) the ratio of solubility coefficients or solubility selectivity. They represent respectively the difference in the diffusivity and solubility of components *i* and *j* in the polymer and thus the contributions of sorption and diffusion to the overall selectivity.

Microscopic Model

Most microscopic models of mass transport in polymers are based on the free volume concept. Owing to conformation constraints of polymers chains (bond angle, steric hindrance), some unoccupied space (< 5 Å in diameter) exists between the polymer chains. Some part of the space is large enough to accommodate foreign molecules [Shah et al., 1989]. The sum of the unoccupied spaces is called the "free volume" or "empty volume". One of the simplest free volume models is that of Fujita [1961]:

$$D_T = R_0 T A_d \exp\left(\frac{B_d}{\upsilon_f} \right) \qquad (2\text{-}3)$$

where D_T is the thermodynamic diffusion coefficient of the permeant, R_0 the gas constant, T the absolute temperature of the system, A_d the proportionality factor, B_d the minimum size of local free volume required for a molecule to permit, and υ_f the fractional free volume in the polymer. Both A_d and B_d are related to the size and shape of the permeant molecules, and the determination of these two parameters was proposed by Fujita [1961]. The free volume or fractional free volume can be estimated by group contribution methods or the *d*-spacing (a measure of the mean intersegmental distance or chain-packing density) determined from the wide-angle X-ray diffraction (WAXD) spectra of polymers [Stern, 1994].

   The dissolution of a gas in rubbery polymers generally follows the Henry's law, Eq. (2-4), and the steady state diffusion of a gas in membranes follows the Fick's First law, Eq. (2-5):

$$C = k_D p \qquad (2\text{-}4)$$

$$N = -D \frac{\partial C}{\partial x} \qquad (2\text{-}5)$$

8

where C is the permeant concentration in the polymer, N the steady state permeation flux, k_D the Henry's Law constant, p the gas partial pressure, and x position coordinate along the flow direction.

Except for the normal free volume elements caused by the incomplete packing of the groups making up the polymer chains, glassy polymers contain excess free volume elements "frozen" in the polymer matrix because the polymer chains cannot rotate freely (see Fig. 2-2). These excess free volume elements in glassy polymers can act as "adsorption sites". Therefore, glassy polymers exhibit excess sorption capacity, and the sorption isotherm can be described by a combination of the Henry's law "dissolved" term C_D, and the Langmuir "hole filling" term C_H. The dual mode sorption was discussed first by Meares in 1954:

$$C = C_D + C_H = k_D p + \frac{C_H' b p}{1 + bp} = (k_D + \frac{C_H' b}{1 + bp})p \qquad (2\text{-}6)$$

where C'_H is the Langmuir capacity constant, and b the affinity constant.
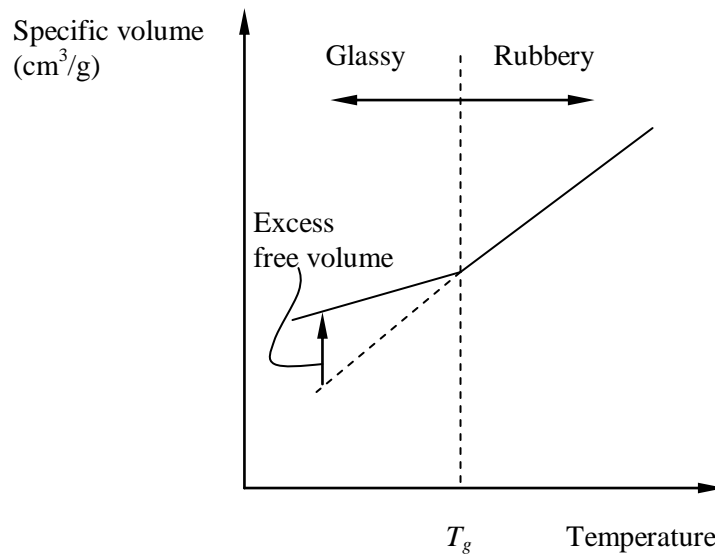
Fig. 2-2. Free volume of a polymer [Baker, 2004]

The sorption of molecules in the Langmuir mode is considerably stronger (more exothermic) than in the dense polymer matrix [Petropoulos, 1994]. However, the molecules sorbed are not completely immobilized in glassy polymers. The mass transfer can be considered to follow the dual mobility or partial immobilization model developed by Petropoulos [1970] and then by Paul and Koros [Paul and Koros, 1976; Koros et al., 1979]:

$$N = -D_D\frac{\partial C_D}{\partial x} - D_H\frac{\partial C_H}{\partial x} = -D_{eff}(C)\frac{\partial C}{\partial x} \tag{2-7}$$

where D_D and D_H are the diffusion coefficients of the two sorbed populations C_D and C_H described in Eq.(2-6), $D_{eff}(C)$ is the effective concentration dependent diffusion coefficient in terms of the gradient in total concentration C. Therefore, P does not change with pressure for rubbery polymers, while P decreases with increasing pressure for glassy polymers [Islam and Buschatz, 2002].

Molecular Model

The transport process in a dense membrane can be visualized as occurring by the "hopping" mechanism [Charati and Stern, 1998; Maier, 1998]. A permeant molecule oscillates most of the time inside a microcavity formed of free volume elements between surrounding polymer chains. Thermally stimulated motions of these chains occasionally open a transient gap of sufficient size as a passage to permit the permeant to "jump" into an unoccupied neighboring microcavity (see Fig. 2-3). These jumps, caused by the concentration gradient, are responsible for the direction of transport. The frequency and magnitude of the jumps depend on the size of the permeant molecules as well as on the free volume of the polymer and mobility of the polymer chains. The smaller the permeant molecules are, the jumps are more frequent and longer, and hence the diffusion rate of the permeant in the polymer is higher. The frequency of the jumps and the chain mobility increase when the temperature is raised; therefore, the diffusivity also increases with increasing temperature.
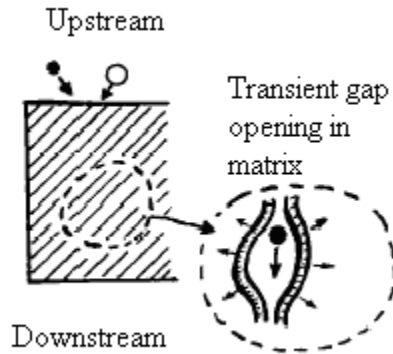
Fig. 2-3. Molecule transport in nonporous membranes [Koros and Fleming, 1993].

2.2.2 Applications Based on the Solution-diffusion Mechanism

The solution-diffusion mechanism applies to reverse osmosis, gas separation, vapor permeation and pervaporation processes. Membrane processes based on a solution-diffusion mechanism are usually classified according to the states of the feed and permeate phases, as shown in Table 2-1. All these processes involve diffusion of molecules in a dense polymer. Once dissolved in the membrane, individual permeants move by the same random process of molecular diffusion. Often, similar membranes can be used in different processes. For example, cellulose acetate membranes developed for desalination by reverse osmosis have

Table 2-1. Classification of membrane processes based on a solution-diffusion mechanism

Membrane process	Feed	Permeate
Gas separation	Gas	Gas
Vapor permeation	Gas	Gas
Pervaporation	Liquid	Gas
Reverse osmosis	Liquid	Liquid

been used in pervaporation dehydration of alcohol and are widely used in separation of carbon dioxide from natural gas, provided that the membranes are all defect-free.

Membrane gas separation has become one of the fast developing industrial separation processes since Monsanto developed the first asymmetric composite hollow fiber membrane for separating hydrogen from ammonia plant purge-gas in the late 1970's. In gas separation, a gas mixture at an elevated pressure is passed across the surface of a membrane that is selectively permeable to one component of the feed mixture, and this component is thus enriched in the membrane permeate side of the membrane. Major current applications of membrane gas separation are 1) the separation of hydrogen from nitrogen, argon and methane in ammonia plants, 2) the production of nitrogen from air, and 3) the separation of carbon dioxide from methane in natural gas operations. Membrane gas separation is an area of considerable research interest, and the applications are expanding rapidly.

Membrane-based vapor permeation is generally grouped to the permeation of condensable gases, such as water vapor and volatile organic compounds (VOCs). Vapor permeation is sometimes regarded as a new application [Sander and Janssen, 1991]. In vapor permeation, the transport of permeating components is carried out from a vapor feed mixture to a permeate vapor phase. Depending on the application, the partial pressure driving force for vapor permeation through the membrane is created by either compressing the feed to an elevated pressure (which is still low enough to prevent condensation) or pulling a vacuum or applying a sweep gas on the permeate side. Vapor permeation is different from permanent gas permeation due to the condensability difference between a vapor and a permanent gas. Different from pervaporation, no phase change occurs during vapor permeation.

Vapor permeation can be used to separate various vapors from gas streams or vapor streams [Nitsche et al., 1998]. VOCs are frequently present in vented gas, inerting nitrogen or air streams discharged into the atmosphere. To prevent the environmental pollution and to recover the VOCs, much attention has been paid to the removal of VOCs from emissions, such as recoveries of vaporous gasoline, vinyl chloride, ethylene, or propylene from industrial waste gas streams [Baker, 2004] as well as higher hydrocarbons recovery from

natural gas or hydrogen-containing off-gas streams in the petrochemical industry [Schultz and Peinemann, 1996]. The industrial application of vapor permeation also involves olefin/paraffin separation in the petrochemical industry [Pinnau and Toy, 2001]. Water vapor permeation is also important; applications can be found in the dehydration of organic mixtures [Salem and Ghoreyshi, 2006], natural gas [Liu et al., 2001a] or compressed air [Ito, 2000], food packaging, humidity control in closed spaces (e.g. air conditioning in building, aviation and space flight) [Cha et al., 1996] and in fuel cells.

Pervaporation is also a relatively new process. Unlike gas separation and vapor permeation, it involves a phase change of permeating species from the liquid to the vapor state. In pervaporation, a liquid mixture contacts one side of a membrane, and the permeate is removed as a low pressure vapor from the other side of the membrane. In pervaporation, the pressure difference across the membrane is usually small, and the driving force for the process is provided by lowering the vapor partial pressure (or activity) on the permeate side of the membrane via vacuum or sweeping [Feng and Huang, 1997]. The partial vapor pressure of a component on the permeate side of the membrane affects its permeation rate significantly. Hence, the down stream vapor pressure must be maintained as low as economically feasible to maximize the driving force for the permeation. Pervaporation, regarded sometimes as a combination of permeation and evaporation, is based on the solubility and diffusivity difference in the membrane, and not on the volatility difference of the components in the feed. Therefore, it is an energy efficient separation technology compared with distillation. This makes pervaporation especially useful in breaking azeotropes [Aptel et al., 1976] which cannot be accomplished by distillation. Because energy is still needed for the vaporization of the permeates, from an energy consumption point of view, pervaporation is especially promising when the concentration of the preferentially permeating species in the feed is low.

The applications of pervaporation can be classified into three categories [Shao and Huang, 2007]. 1) Dehydration of organic solvents. The solvent dehydration was most extensively studied. In the 1980s, Gesellschaft für Trenntechnik (GFT) Co. commercialized the first composite membrane based on a crosslinked poly(vinyl alcohol) supported with a porous

poly(acrylonitrile) substrate for ethanol dehydration [Brueschke, 1983]. Many studies have been carried out for dehydration of various organic solvents (such as benzene [Li et al., 2002], tetrahydrofuran [Rao et al., 2007], cyclohexane [Gómez, et al., 2006], acids [Zhu et al., 1996], ethers, ketones) with different membranes. To date, solvent dehydration is still the dominating application of pervaporation. Most membrane materials used in the dehydration process are hydrophilic. 2) Removal of organic compounds from water, including the removal or recovery of small amounts of organic solvents from contaminated waters, such as benzene, phenol [Boddeker et al., 1990], and chloroform [Brun et al., 1985]. It is effective for waste recovery and pollution control. Hydrophobic materials are usually adopted for these applications. 3) Separation of anhydrous organic solvent mixtures. Motivated by the needs from petrochemical industries, the separation of organic/organic mixtures is being investigated extensively. The solvent mixtures can be subdivided into three categories: polar/non-polar, polar/polar, and non-polar/non-polar [Smitha et al., 2004]. Typical separation systems include alcohol/ether mixtures (e.g., methanol/methyl-*tert*-butyl ether [Dogihere et al., 1994; Jae et al., 1998]), aromatic/alicyclic mixtures (e.g., benzene/cyclohexane [Ray et al., 1997; Inui et al., 1998]), aromatic/aliphatic hydrocarbon mixtures (e.g., benzend/hexane [Yamasaki and Mizoguchi, 1997; Wang et al., 1999]), and isomers (e.g., *p*-xylene/*m*-xylene).

2.3 CO_2 Separation

CO_2 capture and its subsequent use or storage is critical to reduce global warming. Therefore, the separation of CO_2 from industrial sources such as off-gas streams from petrochemical plants or flue gas from coal-fired power plants has attracted attention. Unfortunately, the current generation of commercial gas separation membranes is unsatisfactory for separating CO_2 from flue gas economically. Thus, the development of highly permselective polymeric membranes for CO_2 separation is needed for the membrane process to be viable for greenhouse gas emission control.

2.3.1 Conventional Membrane Materials

The permselectivity of a membrane is related to the state of the polymer: The polymer chains in rubbery polymers are considerably more flexible and rotate more easily than those in glassy polymers. Therefore, rubbery polymers are characterized by a larger free volume and much shorter relaxation time, and exhibit a higher permeability and a lower selectivity than glassy polymers.

The overall selectivity of rubbery polymeric membranes is controlled mainly by the solubility selectivity. Thus, rubbery polymers are well suited for the separation of easily condensable gases. On the other hand, the overall selectivity of glassy polymeric membranes depends mainly on the diffusivity selectivity, and glassy polymers exhibit good selectivity to light gases [Stern and Koros, 2000].

Various rubbery or glassy polymeric membrane materials have been synthesized and investigated for CO_2 separation [Matsumoto et al., 1993; Ismail et al., 1999; Shieh and Chung, 1999; Merkel et al., 2000; Liu et al., 2001b; Ren et al., 2002; 2003; Liu et al., 2004]. Table 2-2 shows the permselectivity of some rubbery and glassy polymers for CO_2/N_2 separation.

It can be seen from Table 2-2 that it is difficult for conventional polymeric membranes to have both a high permeability and a high selectivity. A high permeability is often associated to a low selectivity, and vice versa. This is the well-known permeability/selectivity trade-off relationship. Robeson [1991] did a comprehensive analysis on the literature data for binary gas mixtures from a list of He, H_2, O_2, N_2, CH_4, and CO_2 in an attempt to find an "upper bound" in the permeability and selectivity. An upper bound is observed on a $\log\alpha_{i/j}$ versus $\log P_i$ plot, above which virtually no data exists (see Fig. 2-4). The upper bound permeability-selectivity relationship was described by

$$P_i = k\alpha_{i/j}^n \tag{2-8}$$

where P_i is the permeability of the more permeable gas, n is a constant depending on gas molecular kinetic diameter which can be obtained from the Lennard-Jones potential, k is a constant depending on n, gas condensability and an adjustable parameter [Freeman, 1999].

Table 2-2. Gas permeability and selectivity of rubbery and glassy polymers

Polymer	T (^{o}C)	P_{CO2} (Barrer)	$\alpha_{CO2/N2}$	Reference
Poly (methyl methacrylate)	35	0.62	31	[Stern, 1994]
Polysulfone	35	4.6	25.6	[Koros et al., 1988]
Cellulose acetate	35	5.5	23.9	[Koros et al., 1988]
Polycarbonate	35	6.5	25	[Koros et al., 1988]
Polystyrene	35	12.4	23.8	[Stern, 1994]
6FDA-TAPA Polyimide	35	65	30	[Fang et al., 2001]
Poly (1-trimethylsilyl-1-propyne)	35	28000	5.6	[Stern, 1994]
Natural rubber	25	134	15.4	[Koros et al., 1988]
Poly (cis-isoprene)	35	191	13.2	[Stern, 1994]
Silicone-nitrile copolymer	25	670	20.3	[Koros et al., 1988]
Polydimethylsiloxane	35	4553	3.37	[Koros et al., 1988]

Unit: 1 Barrer = 10^{-10}cm^3(STP) em/(cm^2 s emHg)

Facilitated transport membranes do not follow the simple solution-diffusion mechanism because of the specific interactions or reversible chemical reactions. Therefore, it is possible for a facilitated transport membrane to exceed the "Robeson upper bound".

2.3.2 Carrier Facilitated Transport Membranes

In addition to normal Fickian diffusion, by incorporating active carriers into membranes, facilitated transport membranes can enhance gas permeation [Noble, 1985]. This kind of membrane is similar to biological cell membranes to some extent. The carrier in a facilitated transport membrane interacts or reacts specifically and reversibly with a target permeant to form a permeant-carrier complex, which diffuses to the downstream side of the membrane, where the complex decomposes and releases the permeant and carrier.
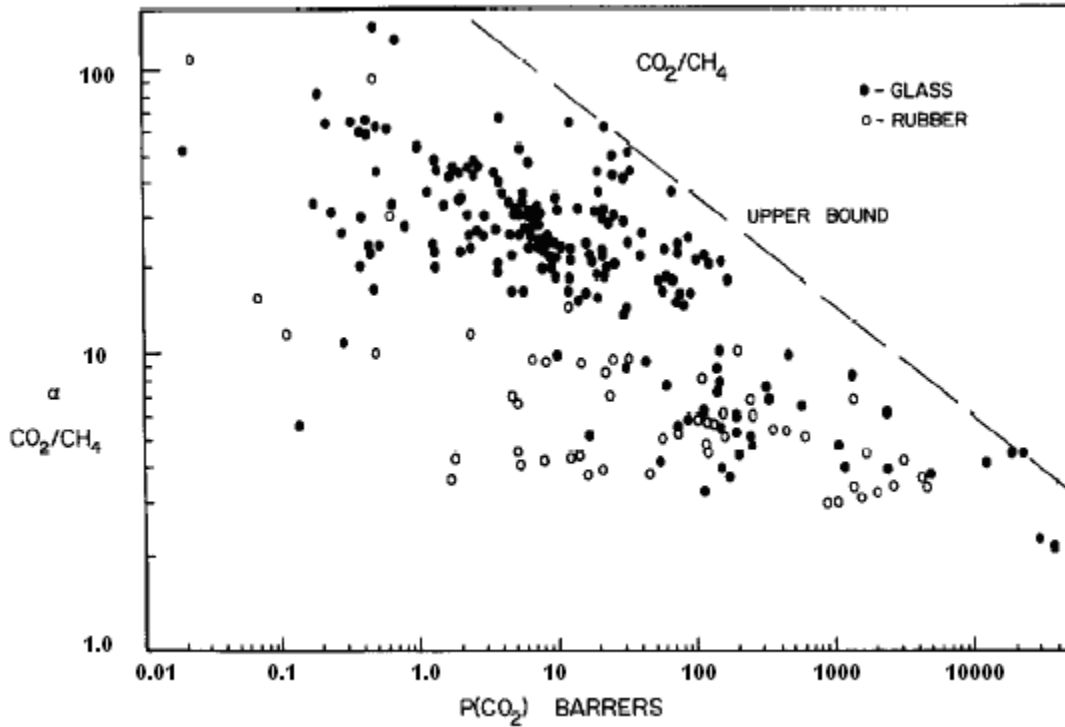
Fig. 2-4. Literature data for CO_2/CH_4 separation factor versus CO_2 permeability [Robeson, 1991].

The concept of using facilitated transport for CO_2 separation is not new. In 1967, Ward and Robb first demonstrated that cellulose acetate membranes with saturated cesium bicarbonate solutions facilitated the separation of CO_2/O_2 mixtures and the separation factor could reach 1500. Since then, facilitated transport has attracted significant interest for CO_2 separation from different gases [Guha et al., 1990; Chakma, 1995; Yamaguchi et al., 1995; Ahmed et al., 1995; Teramoto et al., 2001].

There are two types of facilitated transport membranes according to the mobility of the carriers in membranes. One is a mobile carrier membrane (e.g., liquid membranes) where the carriers can diffuse in the membrane, and the other is a fixed carrier membrane where carriers are immobilized in the membrane matrix.

17

Mobile Carrier Membranes

Studies on facilitated transport were started with liquid membranes. Liquid membranes for CO_2 separation are mainly in the form of supported liquid membranes (SLM) or immobilized liquid membranes. SLM is usually prepared by dissolving carriers in an appropriate solvent and using the solution to fill the pores of a microporous membrane serving as a support. The liquid membrane phase is immobilized by capillary force in the microporous support [Bartsch and Way, 1996].

The first facilitated CO_2 transport SLM was developed by Ward and Robb [1967] using HCO_3^-/CO_3^{2-} as carriers. The facilitated transport process can be illustrated by Fig. 2-5. The reactions between CO_2 and carriers in the membrane are as follows:

$$CO_2 + H_2O \rightleftharpoons H^+ + HCO_3^- \tag{2-9}$$

$$CO_2 + OH^- \rightleftharpoons HCO_3^- \tag{2-10}$$

$$HCO_3^- \rightleftharpoons H^+ + CO_3^{2-} \tag{2-11}$$

where Eqs. (2-9) and (2-10) are slow reactions, while Eq. (2-11) is an instantaneous reaction. When sodium arsenite was added into the membrane liquid to catalyze the reaction given by
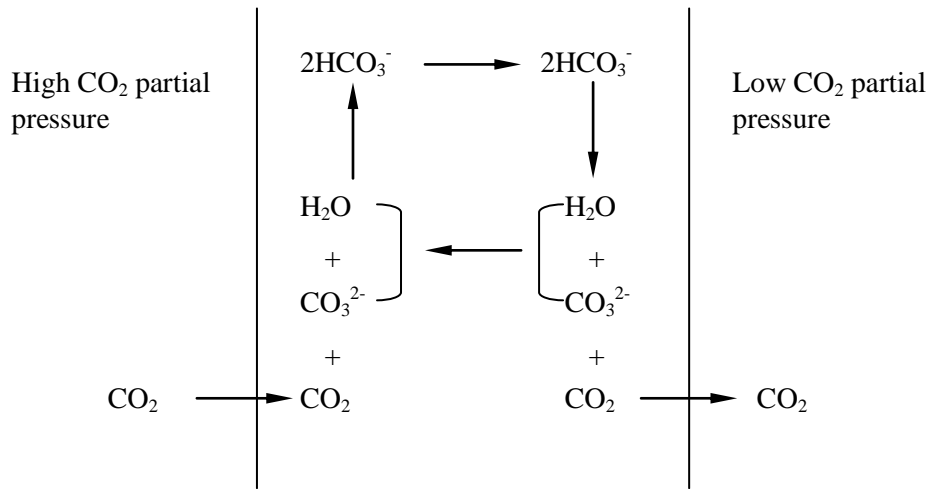
Fig. 2-5. Facilitated transport of CO_2 with HCO_3^-/CO_3^{2-} as carriers [Baker, 2004].

18

Eq. (2-9), the permselectivity of CO_2 was increased. The permeability of CO_2 was 2.14×10^{-7} cm^3(STP) $cm/(cm^2$ s $cmHg)$, and the CO_2/O_2 separation factor was up to 4100. Conventional polymeric membranes do not exhibit such a high separation factor and permeability coefficient.

Teramoto et al. [Teramoto, 1995; Teramoto et al., 1996] used monoethanolamine (MEA) and diethanolamine (DEA) as carriers. Compared to the MEA membranes, the DEA membranes showed a little higher permeation rate of CO_2 since the equilibrium constant of the reaction between CO_2 and MEA is too large for CO_2 to be released rapidly to the receiving phase. When the CO_2 feed partial pressure and the MEA concentration were 5.1 kPa and 4 mol/L, respectively, the separation factor of CO_2/CH_4 was about 2000 and the CO_2 permeance was about 10^{-4} $cm^3/(cm^2$ s $cmHg)$ at $25^{o}C$. CO_2 was suggested to react with the amine as follows:

MEA: $CO_2 + RNH_2 \rightleftharpoons RNHCOO^- + H^+$ (2-12)

   $H^+ + RNH_2 \rightleftharpoons RNH_3^+$ (2-13)

DEA: $CO_2 + R_2NH \rightleftharpoons R_2NH^+COO^-$ (2-14)

   $R_2NH^+COO^- + R_2NH \rightleftharpoons R_2NCOO^- + R_2NH_2^+$ (2-15)
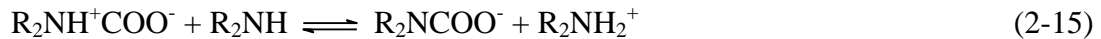
where R is $-CH_2CH_2OH$.

In spite of the high permselectivity, liquid membranes are not yet used industrially due to technical problems. The first problem is the membrane instability caused by the evaporation of the membrane solvent and washout of the carriers, which results in membrane degradation. The second problem is a rather low permeation rate due to the difficulty in preparing very thin liquid membranes. All these problems have hindered the application of liquid membranes [Teramoto et al., 2002].

In order to overcome these drawbacks, Neplenbroek et al. [1992] proposed a "gelled liquid membrane". By applying a homogeneous gel network in the pores of a support, both the mechanical stability (against liquid displacement) and the long-term permeability increased substantially. The flux decreased only slightly because of the open structure of the gel

network. Another technique, by which a thin dense gel layer was applied to the feed side of the membrane, resulted in a specific suppression of the formation of emulsion droplets to avoid the liquid phase loss, and the stability of the membrane was enhanced. The gelled liquid membranes can effectively prevent liquid membrane washout and increase the stability [Nakabayashi et al., 1995]. It is an attractive approach for preparing SLM for CO_2 separation.

Hollow-fiber-contained liquid membranes (HFCLM) were also studied to overcome deficiencies of liquid membranes [Guha, 1991; Sirkar, 1996]. A cylindrical permeator was densely packed with two different sets of hydrophobic microporous hollow fibers. The feed gas at a high pressure flows through the lumen of one set of hollow fibers; a sweep gas or permeated gas flows through the lumen of the other set of hollow fibers. The sweep fibers are intimately commingled with the feed fibers in the middle section of the module but are separated at the ends. In the permeator shell, an aqueous liquid fills the interstitial space between the two sets of hollow fibers and functions as the selective liquid membrane. Any loss of the membrane liquid to the flowing gas can be counteracted by an automatic and continuous supply from an external reservoir. As a result, HFCLM is much more stable than SLM.

Liquid membranes can have a high permselectivity because the diffusion coefficients of gases in liquids are orders of magnitude higher than those in polymeric membranes [Guha et al., 1992] and also because of the reaction between permeant and carrier. However, the stability of liquid membranes is not enough and the operation is complicated. How to improve the stability of liquid membranes and to decrease the membrane thickness for a higher permeance remain targets of future studies.

Fixed Carrier Membranes

One way to improve membrane stability is to immobilize the carriers within the membrane. The carrier fixation is to bind the carrier in the bulk or on the surface of the support membrane through coordination bonds, covalent bonds, or electrostatic forces. The carriers can be fixed in membranes by the following methods:

1) Ion exchange

Ion exchange membranes can be used as the support for fixed carrier membranes. Charged carriers are exchanged into a membrane by ion exchange and kept in the membrane by electrostatic forces so that carriers cannot easily be forced out or washed out from the membrane. This is useful for practical gas separation because of the prolonged service life. Early fixed carrier membranes were mostly prepared by this method. LeBlanc et al. [1980] first reported facilitated CO_2 transport in ion exchange membranes. The results showed that anion exchange membranes containing carbonate and ionized glycinate were effective for CO_2 separation, and the cation exchange membranes with singly protonated ethylenediamine (EDA) had a quite high selectivity for CO_2/N_2. Unprotonated amino groups of EDA reacted reversibly with CO_2 to form a carbamate, and the overall reaction was:

$$CO_2 + 2H_2N(CH_2)_2NH_3^+ \rightleftharpoons {}^+H_3N(CH_2)_2NHCOO^- + {}^+H_3N(CH_2)_2NH_3^+ \qquad (2\text{-}16)$$

The permeability of CO_2 was about 6×10^{-7} cm^3(STP) cm/(cm^2 s cmHg), and the selectivity for CO_2/N_2 was approximately 600 at a CO_2 feed partial pressure of 2.9 kPa at 22°C. This work stimulated researches in this field and a number of studies have been published on the facilitated CO_2 transport through ion exchange membranes [Way, 1987; Noble et al., 1988; Heaney and Pellegrino, 1989; Langevin et al., 1993; Matsuyama et al., 1999a].

Matsuyama et al. [1994a] prepared a cation exchange membrane by plasma-grafting acrylic acid onto a microporous polyethylene membrane and using EDA as the carrier. When the CO_2 feed partial pressure was 4.8 kPa at 25°C, the CO_2 permeance and the CO_2/N_2 selectivity were 1.0×10^{-4} cm^3(STP)/(cm^2 s cmHg) and 4700, respectively.

Quinn and Laciak [1997] prepared a poly(vinylbenzyltrimethylammonium fluoride) membrane by ion exchange to separate CO_2 from CH_4 and H_2. Hydrated fluoride ion $F^- nH_2O$ reacted with CO_2 as a carrier as follows:

$$2[F^- nH_2O] + CO_2 \rightleftharpoons HCO_3^- + HF_2^- (2n\text{-}1)H_2O \qquad (2\text{-}17)$$

At 113 kPa of CO_2 feed partial pressure and 23°C, the CO_2 permeance and CO_2/N_2 selectivity were 7.2×10^{-6} cm^3(STP)/(cm^2 s cmHg) and 629, respectively.

Although electrostatic forces between carriers and ion exchange membranes can help prevent carrier loss to some extent, carriers would be washed out eventually when counter-ions exist. Consequently, ion exchange membranes are still not satisfactory.

2) Grafting modification

Carriers can be grafted on the support membrane and fixed by the coordination bond or covalent bond. Using plasma-grafting, Matsuyama et al. [1994b] deposited an ultra-thin layer of diisopropylamine onto a substrate (a silicone coated porous polyimide membrane). Due to acid-base reaction between CO_2 and the amino groups, the CO_2/CH_4 separation factor and the CO_2 permeance were 17 and 2×10^{-4} cm^3(STP)/(cm^2 s cmHg) respectively at 2 kPa of CO_2 feed partial pressure and 25°C.

Matsuyama et al. [1996] prepared a membrane by low temperature plasma-grafting of *N,N*-dimethylaminoethyl methacrylate onto a polyethylene substrate, and the membrane showed a CO_2 permeance of 5×10^{-6} cm^3(STP)/(cm^2 s cmHg) and a CO_2/N_2 selectivity of 130 at 25°C when the CO_2 partial pressure was 4.8 kPa. They found that both the permeability of CO_2 and selectivity of CO_2/N_2 in wet membranes were higher than those in dry membranes. In dry membranes, facilitated transport of CO_2 was attributed to the weak acid-base interaction between CO_2 and amine moiety, while in wet membranes, the tertiary amino groups were considered to act as a catalyst for the hydration of CO_2 as follows:

$$\text{(2-18)}$$

The problem of grafting modification lies in that the condition of grafting is generally rigorous and it is difficult to scale up for membrane fabrication on an industrial scale.

3) Polymerization or copolymerization

Functional monomers can be used directly to prepare fixed carrier membranes by polymerization or copolymerization. Zhang et al. [2002a; b; c] developed a composite membrane with two kinds of CO_2 carriers, secondary amine and carboxyl groups, by casting hydrolyzed poly(vinylpyrrolidone) on polysulfone substrate. The reaction of the facilitated transport was:

$$RNH(CH_2)_3COO^- + 2H_2O + 2CO_2 \rightleftharpoons 2HCO_3^- + RNH_2^+(CH_2)_3COOH \qquad (2\text{-}19)$$

At 1.3 kPa of CO_2 feed pressure and 26°C, the CO_2 permeance was 7.9×10^{-4} cm^3(STP)/(cm^2 s cmHg) and the CO_2/CH_4 ideal selectivity was 212.

Matsuyama et al. [1999b] prepared a polyethylenimine (PEI)/poly(vinyl alcohol) blend membrane for CO_2/N_2 separation. The primary and secondary amino groups on PEI reacted with CO_2 to form carbamate. The membrane selectivity reached 230 when the CO_2 feed partial pressure was 6.6 kPa at 25°C.

Yoshikawa et al. [1988] synthesized a polymer with a pyridine moiety by radical copolymerization. At 30°C and 24.3 kPa of CO_2 feed pressure, the permeability of CO_2 was 3.4×10^{-11} cm^3(STP) cm/(cm^2 s cmHg) and the ideal separation factor of CO_2/N_2 was 8.7. The results were attributed to the acid-base interaction between CO_2 and the pyridine moiety. By copolymerization of *N,N*-dimethylaminoethyl methacrylate with acrylonitrile, they also developed a membrane that showed a CO_2/N_2 selectivity of 90 and a CO_2 permeance of 2×10^{-7} cm^3/(cm^2 s cmHg) at 6.7 kPa of CO_2 feed pressure and 25°C [1994].

Polymerization or copolymerization is a simple method that can be easily scaled up for practical applications. Various compounds with different functional groups, different backbone and different molecular weight can be obtained by this method. It is one of the most promising methods for making fixed carrier membranes.

In a fixed carrier membrane, the carrier interacts with polymer segments physically or chemically. Carrier molecules can only vibrate within some distance near the equilibrium position and cannot move freely. Therefore, in fixed carrier membranes, the permeation of

the species which interact with the carriers is depressed when compared with mobile carrier membranes where the carriers can move freely. This leads to permselectivity of fixed carrier membranes being lower than that of mobile carrier membranes (see Fig. 2-6). Although mobile carrier membranes tend to have a good permselectivity, from a stability point of view, fixed carrier membranes are more favorable. Therefore, fixed carrier membranes are an important option for CO_2 separation.
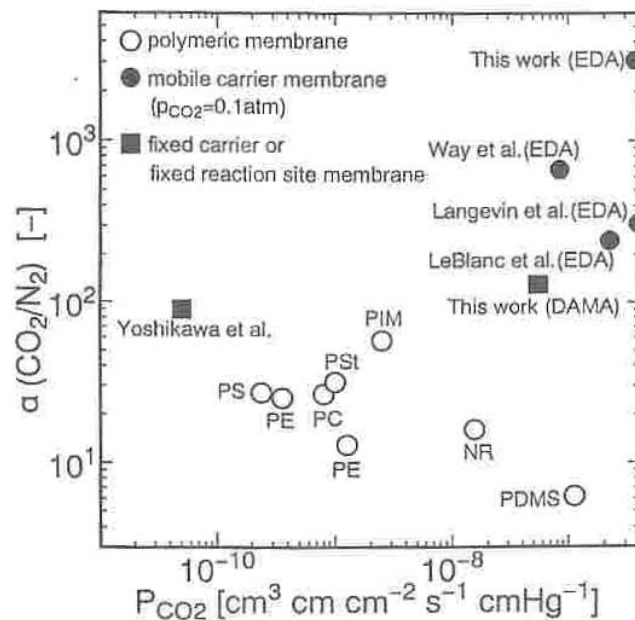
Fig. 2-6. A comparison of permselectivity of conventional polymeric membranes, mobile carrier membranes and fixed carrier membranes for CO_2/N_2 separation [Matsuyama and Teramoto, 1996a].

Transport Models of Carrier Membranes

At present, the facilitated transport mechanism of fixed carrier membranes is not well understood. Only a few mathematical models have been developed to analyze the facilitation in a fixed carrier membrane.

1) Dual sorption model

The dual sorption model, which was originally developed to interpret sorption gases in glassy polymers, has been commonly employed in facilitated transport because it is conceptually analogous to the mass transport in a fixed carrier facilitated transport membrane [Petropoulos, 1994]. It is assumed that there are 2 modes of permeation through the membrane: one is the physical Henry mode and the other is the chemical Langmuir mode. The permeation process includes 4 different diffusion steps, which are consistent with that proposed by Barrer [1984]: diffusion of permeant A through the polymer matrix, diffusion of A from the polymer matrix to a carrier B, diffusion of A through the carriers, and diffusion of A from a carrier to the polymer matrix (see Fig. 2-7).
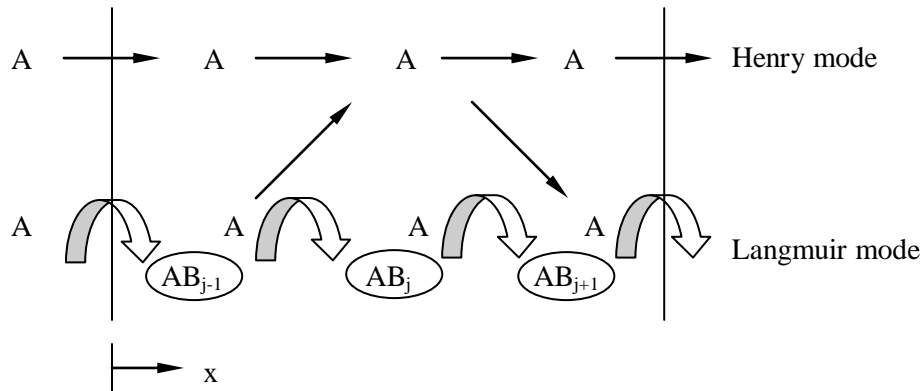
Fig. 2-7. Dual sorption model [Barrer, 1984; Noble, 1990].

A rigorous analysis of the facilitated transport in a fixed carrier membrane was conducted by Noble [1990; 1992] who introduced the concept of "the effective diffusion coefficient" between fixed carriers. In his analysis, the concentration of unreacted fixed carrier was assumed to be constant, implying that there is a large excess of the carriers. A mathematical model was developed. However, the concentration of uncomplexed carriers diminishes as the permeant pressure increases, which is not consistent with the assumption of excess carriers in the model. This causes the model predictions to deviate gradually from the experimental data as the permeant pressure increases. Further, it did not consider the kinetic effect introduced by the chemical reaction either.

25

2) Cussler's model

Cussler et al. [1989] analyzed fixed carrier facilitated transport with the concept of "limited mobility of chained carriers". They assumed that no uncomplexed permeant A can exist in the membrane, and the reaction between a carrier and a permeant occurs only at the surface of the membrane, and is fast. The mobility of the carrier, which is commonly pending on side chains, can allow the complex to encounter a second uncomplexed carrier, resulting in a facilitated transport. Diffusion is only allowed over a limited distance due to the limited mobility of the chained carriers, which in turn, leads to a percolation threshold, i.e., a critical carrier concentration. There is no mass transport when the carrier concentration is below the critical concentration (see Fig. 2-8). However, the existence of such a percolation threshold is unlikely for many systems because facilitated transport has been experimentally observed even at a carrier concentration as low as 0.6 wt% [Tsuchida et al., 1987].
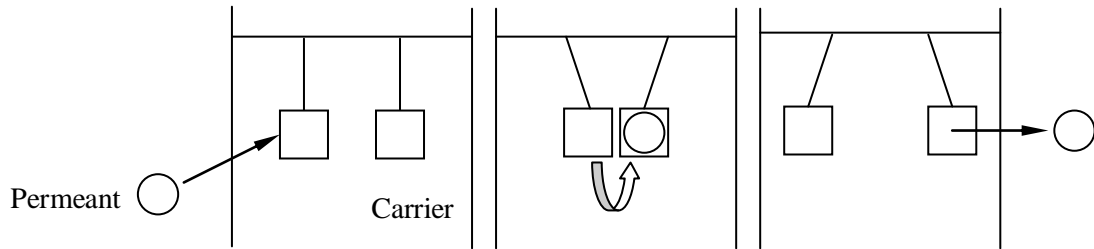
Fig. 2-8. Cussler's model [Cussler, 1989].

3) Resistor-Capacitor circuit model

Kang et al. [1996] demonstrated that the local concentration of a permeant in a fixed carrier membrane instantaneously fluctuated because of a continuous reversible reaction between the permeant and the carrier. The fluctuation in concentration leads to a higher free energy, resulting in facilitation. For mathematical derivation, an analogy was employed between the electric flow in a single parallel resistor-capacitor (RC) circuit and the mass transport in fixed carrier facilitated transport membrane. It was further assumed that a large number of carriers

26

were regarded as one capacitor and the membrane matrix as a resistor, making a single parallel RC circuit. This assumption means that there are only two diffusion pathways, and a permeant dissolved in matrix cannot be transferred through carriers and vice versa. Therefore, Hong et al. [1996; 1999] modified the single RC circuit model into a series of RC circuit model. In this approach a permeant in two elements (matrix and carrier) can change its pathways, exhibiting four diffusional pathways. A sensitivity analysis of the modified RC circuit model showed that the pressure fluctuation at the membrane surface, the initial carrier concentration loaded in the membrane, and the reverse reaction rate constant between the permeant and the carrier were the most significant parameters affecting facilitated transport. The theoretical and experimental results agree fairly well (within less than 5 %) even at a high pressure. However, electron transfer in a circuit and gas transfer in a polymer are not identical although these two transport processes are similar. Such an approach has not been widely used by other researchers.

2.4 Water Vapor Permeation

2.4.1 Materials for Water Vapor Permeation Membranes

The solubility of vapors in a polymer typically increases with increasing size and condensability. A permeant with a high solubility often exhibits strong interactions with each other and with the polymer matrix, resulting in plasticization and swelling of the polymer. Therefore, the solubility coefficient also shows a pressure dependence. Because the overall selectivity of rubbery polymeric membranes is controlled mainly by the solubility selectivity, in the separation of vapor/gas mixtures (e.g., natural gas dehydration), rubbery polymers can be used to permeate the more condensable vapor. Currently, rubbery polydimethylsiloxane (PDMS) is the most commonly used membrane material for separation of vapors from permanent gases. This hydrophobic material can be even used for water vapor/gas separation due to the high condensability of water compared with permanent gases. At 30°C, the water permeability through a PDMS membrane can be up to 4×10^{-6} cm^3(STP) cm/(cm^2 s cmHg) with a H_2O/N_2 permeability ratio of 143 [Metz et al., 2005a].

For different polymers, the water vapor permeability and water vapor/gas selectivity can vary by 5 and 7 orders of magnitude, respectively [Metz et al., 2005a]. Hydrophilic polymers contain sorption sites capable of interactions with water molecules (including dipole-dipole, hydrogen bonding and ion-dipole) [Semenova et al., 1997]. The higher the energy of interaction of water and the active center is, the better the sorption selectivity can be obtained. From this point of view, hydrogen bonding and ion-dipole interactions would yield a high solubility selectivity. The high solubility of water in hydrophilic membrane results in plasticization-induced increases in the diffusion coefficient. On the other hand, water molecules in membranes tend to form clusters due to the hydrogen bonding. The size of the hydrogen bonding clusters also depends on the interaction of the water molecules with the polymer matrix. If the interaction of water-water is larger than that of water-polymer, water uptake is frequently accompanied by larger clustering. Thus, the size of clusters in hydrophobic polymers is usually larger than that in hydrophilic membranes. The molecules in clusters are virtually immobilized relative to the unassociated water leading to a decrease in diffusivity [Barrie et al., 1975; Mensitieri et al., 1995]. Thus, generally, a strong interaction between permeating water molecules and the ionic groups on polymer chains can enhance the solubility and diffusivity of water vapor in a membrane.

The permselectivity for water vapor through many hydrophilic polymeric membranes has been reported. Landro et al. [1991] reported a high H_2O/CH_4 selectivity of $10^3 \sim 10^4$ through amorphous polyurethane membranes. Fu et al. [1994] investigated the permeation of water vapor, oxygen and nitrogen through sulfonated poly(phenylene oxide) (PPO) membranes and found that the selectivity for water vapor over other gases increased remarkably with an increase in the sulfonation degree of PPO. Huang et al. [2003] studied water vapor separation from volatile organic compounds with polyimide dense membranes. Wu et al. [2002] used sulfonated polyethersulfone as a blend material to improve the hydrophilicity of polyimide membranes for dehydration of compressed air. Metz et al. [2005b] studied water vapor/nitrogen transport in poly(ethylene oxide) (PEO)-poly(butylene terephthalte) (PBT) block copolymers, where the hydrophobic PBT segments provide mechanical strength to the

polymer. The water vapor permeability was shown to depend strongly on the polymeric structure and the composition of the polymer.

2.4.2 Channels for Water Penetration

Water is generally regarded to take a different path from a less polar component while diffusing through a membrane. Shimidzu and co-workers [Yoshikawa et al., 1984; 1986; Shimidzu and Yoshikawa, 1991] proposed that the polar groups (i.e. hydrophilicity active sites) in the membrane matrix acted as the fixed carriers for mass transport in the membrane. Unlike the random walk of less polar components, the water molecule jumps from one polar site to another. Water could be also interconnected to form a globule string extending across the membrane thickness and acted as the water transport channel as described in the aggregate model [Gierke et al., 1981]. The water transport channel described with the carrier model and aggregate model is similar with that described with the hydrogen-bonding model proposed by Reid and Breton [1959] to explain the water transport in reverse osmoses with cellulose acetate membranes. It was believed that the "particles" participating in hydrogen bonding (H_2O, H_3O^+, OH^-) diffuse much faster, by jumping from one carbonyl oxygen to another, than inorganic ions incapable of forming hydrogen bonding (e.g., Na^+, Cl^-, etc). After these molecules combine with one side of the membrane, they migrate across the membrane by transferring from one hydrogen bonding site to another and are finally discharged from the downstream side of the membrane.

2.5 Pervaporation Dehydration

2.5.1 Criterion for Selection of Pervaporation Membrane Materials

For pervaporation processes, polymeric membrane materials also suffer the permeability-selectivity trade-off relationship, and the selection of a suitable membrane material is crucial. Since mass transport in the membrane is based on sorption and diffusion, pervaporation membranes should exhibit good sorption characteristics for the preferentially permeating component. A high degree of membrane swelling (like in the membrane vapor permeation) is

often involved. At present, there are several approaches to select membrane material based on solution behavior of permeants in a polymer.

Solubility Parameter Approach

The intermolecular interactions between a permeant and a polymer can be described qualitatively by the Hansen's solubility parameter theory. The overall solubility parameter δ contributing to the cohesion energy density *C.E.D* can be considered to combine three components of dispersion or non-polar forces δ_d, polar forces δ_p, and hydrogen bonding forces δ_h [Hansen, 2007]

$$\delta = (C.E.D.)^{1/2} = \left(\delta_d^2 + \delta_p^2 + \delta_h^2\right)^{1/2} \tag{2-20}$$

The difference in the solubility parameter of a permeant and a polymer Δ is given by

$$\Delta = \left[\left(\delta_{d,S} - \delta_{d,P}\right)^2 + \left(\delta_{p,S} - \delta_{p,P}\right)^2 + \left(\delta_{h,S} - \delta_{h,P}\right)^2\right]^{1/2} \tag{2-21}$$

where the subscripts *S* and *P* refer to the solvent and the polymer, respectively. The smaller the value of Δ, the more favorable the interaction between the permeant and the polymer [Mulder, 1982]. The ratio of Δ_i / Δ_j can thus represent the sorption selectivity between solvents *i* and *j* in the polymer [as cited by Huang, 1991]. The solubility parameter approach is based on the solution of a single permeant in a polymer, which will unsurprisingly lead to a deviation for predicting a sorption selectivity of a binary mixture in the polymer. Incorrect predictions have been observed for situations when the selective permeablity of the membrane is controlled by the preferential diffusion. Therefore, this approach can only be used as a first estimate in the selection of polymeric membrane materials [Feng and Huang, 1997].

Flory-Huggins Thermodynamics Approach

The feed liquid phase and the membrane phase comprising two liquids can be considered to be at a swelling equilibrium. The Flory-Huggins theory is used to describe the state of the

equilibrium. For the permeation of a binary liquid mixture, the Gibbs free energy of mixing of the system ΔG_m can be given by

$$\Delta G_m = RT\left(n_1 \ln \phi_1 + n_2 \ln \phi_2 + n_3 \ln \phi_3 + \chi_{12} u_1 n_1 \phi_2 + \chi_{13} n_1 \phi_3 + \chi_{23} n_2 \phi_3\right) \tag{2-22}$$

where n_i is the mole of the component i, ϕ_i its volume fraction of component i in the tertiary system, u_i the volume fraction of component i in the binary liquid system, and χ_{ij} the binary interaction parameter between components i and j. The subscripts 1, 2, and 3 denote the two liquids and the polymer, respectively. The interaction parameter between the two liquids χ_{12} can be determined from the excess free energy of mixing data ΔG^E as

$$\chi_{12} = \frac{1}{x_1 u_2}\left(x_1 \ln \frac{x_1}{u_1} + x_2 \ln \frac{x_2}{u_2} + \frac{\Delta G^E}{RT}\right) \tag{2-23}$$

The binary interaction parameters χ_{13} and χ_{23} can be evaluated from equilibrium swelling measurements of pure liquid in the polymer and can be given by

$$\chi_{iP} = -\left(\frac{\ln(1-\upsilon_P)+\upsilon_P}{\upsilon_P^2}\right) \tag{2-24}$$

where υ_P is the volume fraction of the polymer. Not only can the Flory-Huggins theory be used to select membrane materials, it can also be used to predict the permeation rate through the membrane by using proper models derived from the free-volume theory [Huang, 1991].

Hydrophilic-hydrophobic Balance Approach

Huang et al. [1988] proposed that the hydrophilic/hydrophobic balance should be considered in the selection of membrane materials. A membrane material with a high affinity to the preferential permeating component can give a high solubility. However, the membrane swelling induced by the sorbed component makes the polymer chains more flexible, and results in increased diffusivities for both permeating components. Thus, an excess swelling of the membrane can lead to a reduced selectivity and mechanical strength. Therefore, the ratio of hydrophilic and hydrophobic groups in a membrane should be adjusted to maintain a

31

proper balance for a good separation performance. Generally, a single polymer does not meet the required hydrophilic/hydrophobic balance. Several techniques have been proposed for improving the membrane structure, including crosslinking, blending a hydrophilic polymer with a relatively hydrophobic polymer, grafting a selective functional group onto an inert membrane, and developing new copolymers composed of both active and inert groups. Although this approach can give a general guideline to improve membrane materials for given separation systems, a quantification of the hydrophilic/hydrophobic balance is lacking.

Contact Angle Approach

It is well known that the surface free energies of a solid (γ_S) and a liquid (γ_L) and the solid-liquid interface free energy (γ_{SL}) are related to the contact angle (β) (see Fig. 2-9) by [Greiveldinger and Rhanahan, 1999]

$$\gamma_S - \gamma_{SL} = \gamma_L \cos\beta \qquad (2\text{-}25)$$
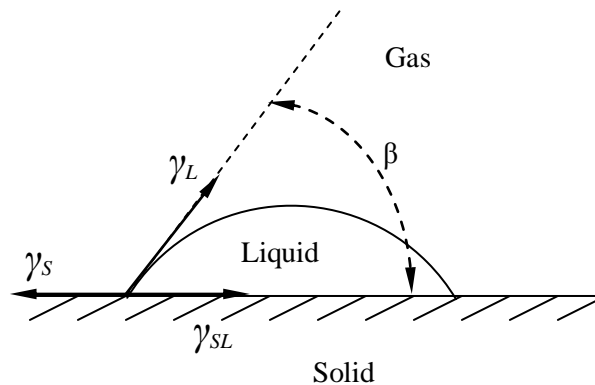
Fig. 2-9. Contact angle and surface free energies of a sessile drop.

The work of adhesion W_a, as an approximation, is given by [Jacob and Berg, 1994]

$$W_a = \gamma_S + \gamma_L - \gamma_{SL} \qquad (2\text{-}26)$$

Thus combining Eqs (2-25) and (2-26) yields

$$W_a = (1 + \cos\beta)\gamma_L \qquad\qquad (2\text{-}27)$$

A low value of contact angle and a high value of work of adhesion favor the spread and dissolving of a liquid onto the surface of a membrane. Though the contact angle approach is straightforward, it can only be used in a preliminary screening of membrane materials since the characteristics of interaction between the components in the liquid mixtures are ignored.

2.5.2 Membrane Materials for Pervaporation Dehydration

Dehydration of organic solvents is presently the dominating application of the pervaporation. According to the criterion of material selection, the solubility of water in membranes increases with the polarity or hydrophilicity of the polymers because of the interactions between water molecules and the polar groups in the polymer [Schult and Paul, 1997a; b]. It is necessary to use hydrophilic polymers to favor the selective permeation of water.

The hydrophilic polymeric materials used for dehydration of organic solvents generally can be divided into two categories based on whether the hydrophilic groups are ionic or non-ionic. Non-ionic groups include -OH, -NHCO-, -OCH$_3$, and -OCOCH$_3$. Polymers with non-ionic hydrophilic groups are represented by poly(vinyl alcohol) (PVA). The hydroxyl groups in PVA can form strong hydrogen bonding, leading to a high selectivity for water permeation from aqueous organic mixtures. PVA is easily swollen and can even be dissolved in water depending on the degrees of polymerization and hydrolysis of poly(vinyl acetate). It is thus often crosslinked to improve the mechanical strength and long-term stability. Dialdehydes, such as glutaraldehyde, are commonly used crosslinking agents for PVA to form a crosslinked polyacetal structure in the presence of a strong acid as a catalyst [Ahn et al., 2005; Zhang et al., 2007d; e]. An aqueous inorganic salt solution or a nonsolvent (e.g., acetone) can be used as a reaction medium to crosslink a preformed PVA film in order to prevent it from dissolving into water during the crosslinking process [Yeom and Lee, 1996]. Other examples of hydrophilic materials in this category are poly(hydroxyl methylene) [Terada et al., 1988] and poly(methyl acrylate) [Itoh et al., 1985].

The materials with ionic hydrophilic groups (i.e., polyelectrolytes) have attracted significant attention. Introduction of ionized groups into membranes can enhance the water selectivity because the ionized groups can hydrate strongly and exclude organic solvents by the salting-out effect [Reineke et al., 1987]. This kind of materials includes polycations or polyanions generated by either naturally occurring or synthetic polymers (see Table 2-3).

Table 2-3. Typical polyeletrolytes for pervaporation dehydration

	Polycation	Polyanion
Natural polymers	Chitosan	Alginic acid
		Cellulose and cellulose derivatives
Synthetic polymers	Poly(vinylpyrrolidone)	Poly(acrylic acid) and salts
	Quaternized ammonium salts	Sulfonated materials

Chitosan, alginic acid and cellulose derivatives are all natural polysaccharides. Chitosan is a typical polycation commercially produced by deacetylation of chitin, which exists naturally in the shell of marine crustaceans [Clasen et al., 2006]. Chitosan membranes can be easily crosslinked using sulfuric acid and aldehydes to improve the separation performance [Sridhar et al., 2001]. Especially, ionically-crosslinked chitosan membranes with sulfuric acid exhibited a high permselectivity due to the presence of divalent ion SO_4^{2-} [Lee et al., 1997; Mochizuki et al., 1989]. A technical obstacle to commercialization of chitosan membranes is the difficulty to control the molecular weight and the degree of deacetylation, which are important to the formation and property of the membranes. Alginic acid is a polyanion obtained from seaweeds. Sodium alginate, the neutralization product of alginic acid and sodium hydroxide, showed excellent selective permeability to water, and the crosslinking is also required to suppress excessive membrane swelling [Huang et al., 1999a].

Poly(acrylic acid) (PAA) is a typical synthetic polyanion used for pervaporation dehydration. It has a high charge density and thus a high hydrophilicity. High molecular

weight PAA, which can be synthesized by radical polymerization, are effective for forming thin membranes and providing high mechanical strength. The carboxyl groups on the side chains can be used as a crosslinking sites. The salt form of PAA membranes has a higher selectivity than the acid form due to the hydration and salt-out effect [Karakane et al., 1991]. Polymers with *N*-substitute groups are another type of synthetic polycations; polymers containing partially quarternized ammonium salts are an example of such polymers.

The elution of mobile counterions often causes a decrease in the separation performance of the polyelectrolyte membranes, and the membranes often need to be regenerated after a certain period. This problem can be solved by introducing fixed counterions by forming polyelectrolyte complexes. Polyelectrolyte complexes can be formed by interaction of two counter-charged polyions or by polymerization of monomers in a polymer matrix. The polyelectrolyte complexes can be regarded as an ionically crosslinked product because the counter-charged groups are mutually blocked to wash out as a result of the Coulombic electrostatic interactions [Semenova et al., 1997].

2.6 Membranes Based on PDMAEMA

The selection of carriers for fixed carrier CO_2 separation membranes should consider the carrier activity and ease of fixation. If the carrier activity is too weak, the facilitated transport effect will not be obvious; if the activity is too strong, stable complexes may be formed making the release of CO_2 at the downstream side of the membrane difficult. A carrier with fast association and dissociation rate constants (preferably with similar magnitudes) is desirable. By far, most carriers used in fixed carrier membranes are amino groups. The facilitated transport is expected to be mainly attributed to the weak acid-base interaction between CO_2 and the amine moiety. However, there are not many studies on this type of membranes in the open literature. On the other hand, according to Shimidzu's carrier model and Gierke's aggregate model, for water permeation, the permselectivity mainly arises from the polarity and free volume of the polymers. One way to fix the carriers is to synthesize the functional polymer, where the carriers become a part of the polymer side chains by chemical bonds. Poly (*N,N*-dimethylaminoethyl methacrylate) (PDMAEMA) has an amine moiety on

35

the side chains and was selected as the functional polymer in this work for preferential permeation of CO_2 and water.

For facilitation to occur, the carrier concentration should be greater than the "critical carrier concentration" (based on Cussler's model), and the carriers should be in large excess (based on Noble's model). More carriers in the membrane tend to yield a better facilitated transport capacity, and a high carrier concentration is expected to lead to a high permselectivity. PDMAEMA has one tertiary amino group on every side chain and can be regarded as a polyamine, which means a high carrier concentration in the membrane.

Matsuyama and Teramoto [1996b] prepared an ion exchange membrane by plasma-grafting acrylic acid and methacrylic acid on a porous substrate and using diamine as carriers. The results showed that the shorter the chain length of the diamine, the higher the CO_2 permselectivity. This indicates that the size of the carrier segment affects gas permeability, and short-chain carriers are needed. The side chains with amino groups in PDMAEMA is not long, which is favorable.

Furthermore, there is an ester group on the side chain. Because the internal rotation activity of C-O is better than C-C, the side chain is flexible which favors the molecular transport according to Cussler's model or the "hopping" mechanism. In addition, PDMAEMA is an inexpensive polymer that can be synthesized easily. It has been used as flocculants [Hurlock, 2000], ion exchange resin [Cunningham, 1977; 1978], mordant for ink printing [Romano and Gallo, 2001], a potential carrier for drug delivery systems [Amiji, 1999]. It has also been disclosed that PDMAEMA can be used to prepare composite membranes for blood purification [Nakano et al., 1988], cationic/anionic mosaic membranes for desalination [Fukutomi et al., 1996] and pervaporation membranes for purification of ethyl *tert*-butyl ether [Streicher, 1997].

PDMAEMA is a linear molecule and is soluble in aqueous solutions. During the course of bulk polymerization, DMAEMA could be auto-crosslinked due to chain transfer to polymer [Odian, 2004]. However, the auto-crosslinking is too weak to prevent PDMAEMA from dissolution in water. Because water or water vapor is present in most cases of gas separation

and pervaporation studied here (e.g., CO_2 separation from flue gas, dehydration and humidification of gases, solvent dehydration by pervaporation), PDMAEMA should be crosslinked to retain membrane stability and durability.

PDMAEMA can be crosslinked by heat treatment. Nakano et al. [1988] prepared a composite membrane by using PDMAEMA as active layer and cuprammonium regenerated cellulose hollow fiber as substrate. The membrane was dried at 40°C under vacuum for 1 h, then heat treated at 120°C for 10 min in a heating dryer before it was used for blood purification. Streicher [1997] prepared a composite membrane by depositing a PDMAEMA-water-ethanol solution on a porous polyacrylonitrile layer which was further supported on a non-woven polyester fabric. The polymer solution was evaporated for 2 min at 90°C. The membrane obtained was then heat treated for 30 min at 125°C. The resulting PDMAEMA layer was 3 μm thick. The membrane was tested for pervaporation of ethanol and ethyl *tert*-butyl ether.

It should be pointed out that the thermal crosslinking may shrink the pores in the substrate, resulting in a low flux. Room-temperature chemical crosslinking may be able to overcome this problem. Du and Zhao [2004a; b] obtained a dense surface composite membrane from PDMAEMA crosslinked by *p*-xylylene dichloride for nanofiltration applications. However, there are few reports on the chemical crosslinking of PDMAEMA in the literature.

Considering the structure of PDMAEMA, the polymer contains a tertiary amino group on the side chain of the monomer unit, which has a relatively high reactivity and can be alkylated or quaternized by halohydrocarbons to form a quaternary ammonium salt:

$$(2\text{-}28)$$
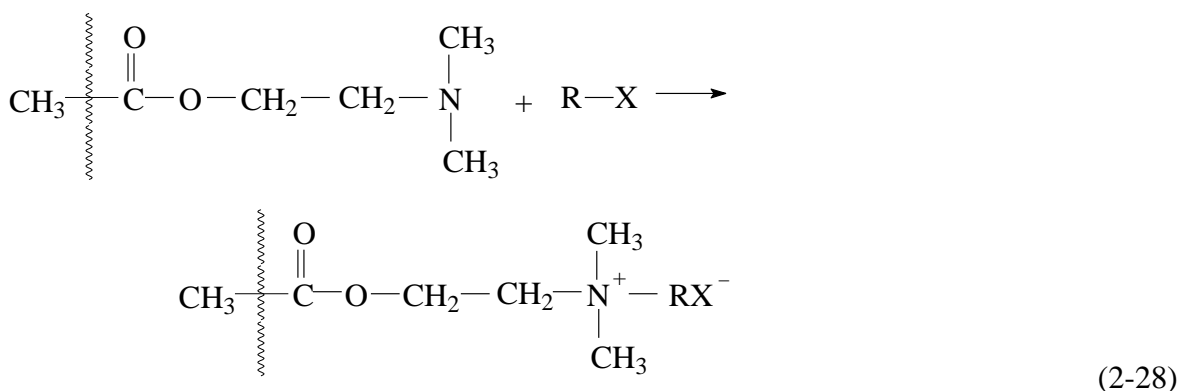
where R-X maybe an alkyl or phenyl monohalide and X^- is the negative mobile counterion. The amino group functions as a nucleophilic reagent, and the halogen atom is replaced by the amino group, thus forming a quaternary ammonium salt.

Mono-halohydrocarbons (such as CH_3I and C_2H_5Br) are commonly used quaternization agents. Treatment of tertiary polyamines with such monohalides, according to the above scheme, leads to water-soluble products. However, the quaternization reaction can also be used to crosslink PDMAEMA with a bifunctional reagent such as an alkyl dihalide. For example,

$$\cdots -CH -\!\!\left(CH_2\right)_{\!\!n}\!\!\overset{\displaystyle R}{\underset{\displaystyle R}{N}} \;+\; X-R'-X \;+\; \overset{\displaystyle R}{\underset{\displaystyle R}{N}}-\!\!\left(CH_2\right)_{\!\!n}\!\!CH-\cdots$$

$$\longrightarrow \;\; \cdots -CH -\!\!\left(CH_2\right)_{\!\!n}\!\!\overset{\displaystyle R}{\underset{\displaystyle R}{\overset{+}{N}}}\!\!{}^-_{}\!X - R' - X^-\,\overset{+}{N}\!\!\overset{\displaystyle R}{\underset{\displaystyle R}{}}-\!\!\left(CH_2\right)_{\!\!n}\!\!CH-\cdots \tag{2-29}$$
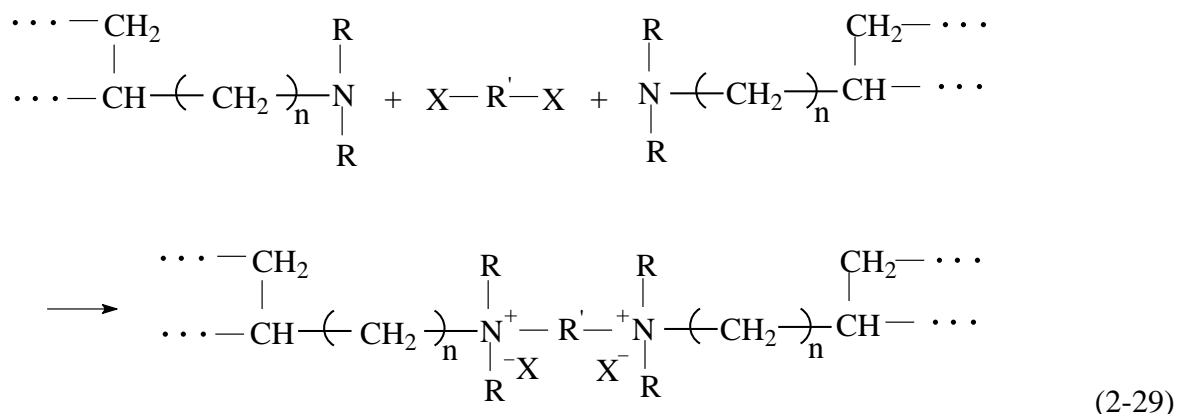
where $X-R'-X$ is an alkyl dihalide, and R and R' may be same or different [Credali et al., 1972].

When a di-halohydrocarbon (e.g., 1,4-dibromobutane) is used, it can undergo a quaternization reaction with two tertiary amino groups from different PDMAEMA molecular chains. That is, quaternization reaction takes place on two different macromolecules to crosslink the polymer. The reaction between the amino group on PDMAEMA and binary halohydrocarbon is as follows:

$$CH_3-\overset{\underset{\displaystyle \|}{O}}{C}-O-CH_2-CH_2-\underset{\underset{\displaystyle CH_3}{|}}{\overset{\overset{\displaystyle CH_3}{|}}{N}} \quad + \quad X-R-X \quad \longrightarrow$$

$$CH_3-\overset{\underset{\displaystyle \|}{O}}{C}-O-CH_2-CH_2-\overset{\overset{\displaystyle CH_3}{|}}{\underset{\underset{\displaystyle CH_3}{|}}{\overset{+}{N}}}-R-\overset{\overset{\displaystyle CH_3}{|}}{\underset{\underset{\displaystyle CH_3}{|}}{\overset{+}{N}}}-CH_2-CH_2-O-\overset{\underset{\displaystyle \|}{O}}{C}-CH_3 \qquad X^- \quad X^-$$

(2-30)
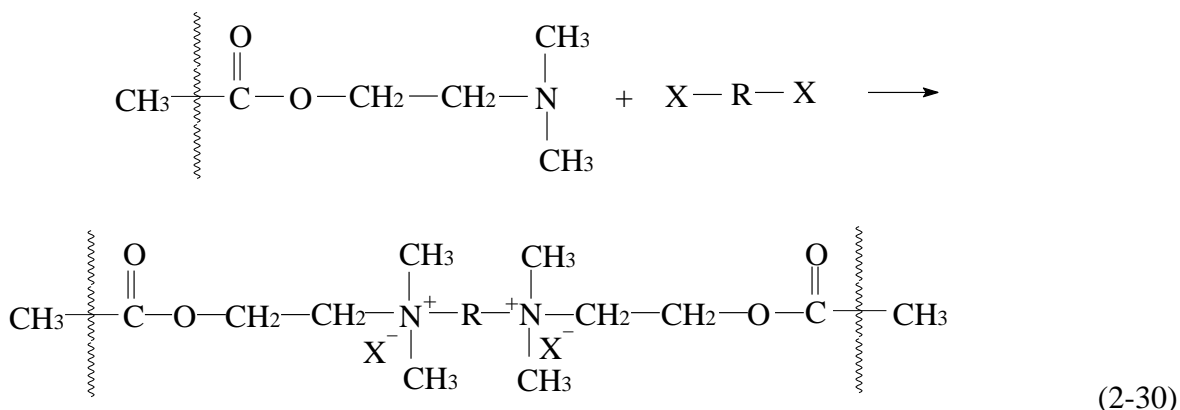
The crosslinking reaction between the polymer and the dihalide takes place in two stages (see Eq. (2-31)), and the second stage is slow. Credali et al. [1972] demonstrated that product II predominates at a ratio of stoichiometric quantities of dihalide to the polymer in equivalents 1:1 and the product is insoluble with a high ion exchange capacity. Excess dihalide gives, for the most part, product I where only half the halogen present is exchangeable. The product obtained with excess dihalide possesses a much lower percentage of crosslinking and therefore swells more in solvents.

$$-N\overset{\displaystyle R}{\underset{\displaystyle R}{<}} \quad + \quad X-R'-X \quad \xrightarrow{\ \text{fast}\ } \quad -\overset{+}{N}\overset{\displaystyle R}{\underset{\underset{\displaystyle R}{X^-}}{<}}-R'-X$$

I

$$-\overset{+}{N}\overset{\displaystyle R}{\underset{\underset{\displaystyle R}{X^-}}{<}}-R'-X \quad + \quad -N\overset{\displaystyle R}{\underset{\displaystyle R}{<}} \quad \xrightarrow{\ \text{slow}\ } \quad -\overset{\overset{\displaystyle R}{|}}{\underset{\underset{\displaystyle R}{|}}{\overset{+}{N}}}-R'-\overset{\overset{\displaystyle R}{|}}{\underset{\underset{\displaystyle R}{|}}{\overset{+}{N}}}- \qquad X^- \quad X^-$$

II

(2-31)
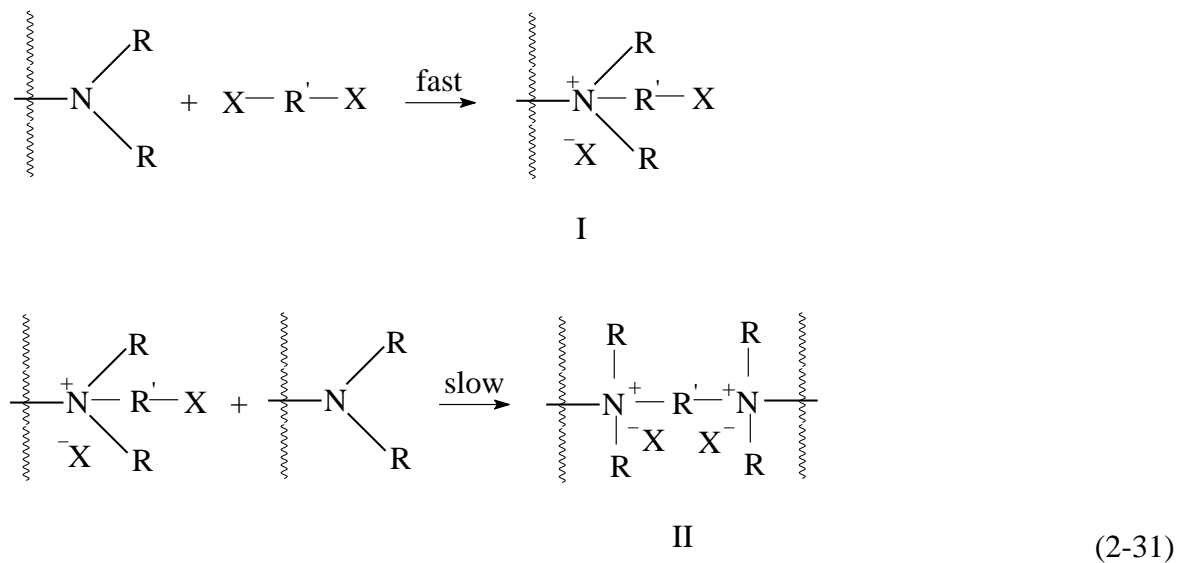
There are several di-halohydrocarbon that can crosslink tertiary amino groups. Their activity and molecular size have a large effect on the crosslinking reaction. For alkylation of an amine, the reactivity of the halogens follows the trend I > Br > Cl. Credali et al. [1972] showed that the reaction was complete in about one hour at 80°C with $C_2H_4I_2$, while the reaction was very slow at about 110°C with Br derivatives. In addition, the structure of halohydrocarbon also affects the crosslinking reaction. Benzyl dihalides of the type

$$X-CH_2-\langle\!\!\bigcirc\!\!\rangle-CH_2-X$$
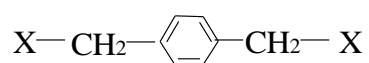
are more reactive than alkyl halides, and their use leads to higher yields of quaternary ammonium salts. This is because the phenylene is an electron attracting substituent and the bond of CH_2-X will break more easily.

On the other hand, the structure of the polymer to be crosslinked (e.g., number and size of the side chains), will also affect the crosslinking reaction. For example, polyethylenimine has a large number of branches, which cause many intramolecular crosslinking reactions. When 1,4-dibromobutane and 1,6-dibromohexane were used as crosslinking agents, it was difficult to achieve adequate intermolecular crosslinking, because the chains of these agents were too short to form the intermolecular crosslinking. 1,9-Dibromononane or 1,10-dibromodecane should be used in this case [Nagaya et al., 1993]. Moreover, the steric effect of the substituents on the amino groups is also important. When the substituents on tertiary amino groups are too big, the steric effect will be too large for the crosslinking reaction to take place. There are only two small methyl substituents on the amino group of PDMAEMA. PDMAEMA can be crosslinked even at room temperature. *p*-Xylylene dichloride was used as the crosslinker in this work in consideration of the PDMAEMA structure and the membrane forming process.

Chapter 3

Bulk Crosslinked PDMAEMA/PSF Composite Membranes[*]

3.1 Introduction

In principle, a high CO_2 permselectivity can be achieved by selectively increasing the solubility and/or diffusivity of CO_2 in the membrane. As such, introducing amino groups onto the polymer chains is expected to enhance the CO_2 permselectivity because of the selective weak acid–base interactions between amino groups and CO_2 molecules that could facilitate the permeation of CO_2. From a membrane manufacturing point of view, it would be simple and straightforward to apply a homopolymer directly to form membranes for practical applications. Therefore, PDMAEMA was selected to be the membrane material for CO_2 separation.

PDMAEMA can be synthesized from *N*,*N*-dimethylaminoethyl methacrylate (DMAEMA) by either anionic or free radical polymerization. Creutz et al. [1997] investigated the synthesis of PDMAEMA by living anionic polymerization of DMAEMA in tetrahydrofuran at $-78^{o}C$ using diphenylmethyl lithium as an initiator. Because the living anionic polymerization requires stringent reaction conditions, the synthesis of PDMAEMA is commonly carried out by radical polymerization in a solution. Kim et al. [2001] prepared PDMAEMA by dissolving 7.8 g of DMAEMA and 0.02 g of 2,2'-azobisisobutyronitrile initiator in 100 ml of a water-ethanol mixture solvent at $75^{o}C$. Toluene and tetrahydrofuran can also be used as the solvent for free radical polymerization of PDMEMA [van de Watering et al., 1998; Huang et al. 1999b]. It should be noted that due to the presence of the solvent in the polymerization process, the purity of the final polymer product will be compromised if the solvent is not removed completely. As one may expect, the residual solvent in the polymer would affect the subsequent membrane formation and membrane properties, and it will be essential to remove the residual solvent before the polymer is used

---

[*] Portions of this work have been published in *J. Membr. Sci.*, 279 (2006) 76-85.

for making membranes. Therefore, as an alternative, free radical bulk polymerization was used to synthesize PDMAEMA in the present work to eliminate the use of solvent during polymerization.

This chapter deals with PDMAEMA membranes for gas separation, with a primary objective of demonstrating the feasibility of using PDMAEMA membranes to separate CO_2 from flue gas for greenhouse gas emission control. Homopolymer of DMAEMA was synthesized by free radical bulk polymerization under mild conditions. Note that the cationic PDMAEMA is highly hydrophilic and that water vapor is present in the flue gas. Although the presence of water vapor was expected to enhance the permeation of CO_2 due to enhanced interactions between amino groups and CO_2 molecules, the PDMAEMA was crosslinked to enhance the stability and durability of the membrane for CO_2 separation from flue gas. *p*-Xylylene dichloride (XDC) was used as the crosslinking agent. The crosslinked membranes were tested for the permeation of N_2 and CO_2, which are the main components in the flue gas. For the purpose of comparison, the permeability of the membrane to other gases (e.g., H_2, O_2, and CH_4) was also evaluated.

3.2 Experimental

3.2.1 Materials

The DMAEMA monomer, containing 2000 ppm monomethyl ether hydroquinone as inhibitor, was purchased from Aldrich Chemicals. Polysulfone (P-1700) was obtained from Amoco Performance Products and was dried at $50^{\circ}C$ in a vacuum oven for 24 h. HPLC grade reagent alcohol containing 90.7 % ethanol, 4.2 % methanol, and 5.1 % isopropanol was purchased from Fisher Scientific and used as the membrane-casting solvent without further purification. Activated carbon (Darco G-60, particle size ∼100 mesh), 2,2'-azobisisobutyronitrile (AIBN), XDC, and heptane were supplied by Sigma–Aldrich. *N,N*-Dimethylacetamide (DMAc) and polyvinylpyrrolidone (PVP, K30, MW ∼40,000) were supplied by Acros Organics and Fluka Chemika, respectively. Acid orange, neutral gray, and basic fuchsine, all acquired from Tianjin Polytechnic University, were used to qualitatively

characterize the charge properties of the membrane. The gases used for the gas permeation experiments were of research grade (99.0-99.998 % pure), and they were supplied by Praxair Specialty Gases and Equipment.

3.2.2 Synthesis of PDMAEMA

PDMAEMA was synthesized via free radical bulk polymerization. The procedure for the polymer synthesis is similar to that described elsewhere [Du and Zhao, 2004a; b]. Briefly, the inhibitor monomethyl ether hydroquinone originally present in the monomer was removed by adsorption on activated carbon before use. 46.6 g of the purified DMAEMA monomer and 0.035 g AIBN initiator were placed into a 500 mL reactor made of polyethylene terephthalate (PET). The reactor was purged with nitrogen for about 5 min to remove oxygen dissolved in the monomer from the system (see Fig. 3-1). Then the reactor was sealed and kept in a thermal bath at 50°C for 1 week. After polymerization, the polymer product was a solid sticking to the reactor wall. The polymer was removed by fracturing the PET reactor and peeling away the fragmented PET. The polymer was then cut into pieces for later use. The glass transition temperature (T_g) of PDMAEMA was measured by a differential scanning calorimeter (Perkin-Elmer DSC-7) to be 19.5°C.
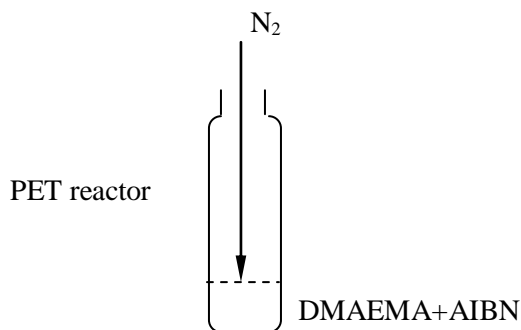
Fig. 3-1. Polymerization process for PDMAEMA.

3.2.3 Membrane Preparation

The polysulfone substrate membrane was prepared through non-solvent induced phase separation method. A mixture of 14 g PSF and 6 g polyvinylpyrrolidone (PVP) were dissolved in 80 mL DMAc at 70°C to form a homogeneous solution, which was then left at 50°C for 24 h in order for air bubbles to be released. The clear polymer solution was cast onto a glass plate to form a thin layer of the polymer solution of 0.28 mm thickness, followed by immersion into non-solvent water at 21°C to undergo coagulation, during which process phase separation of the polymer-solvent system took place, thereby forming an asymmetric microporous membrane. The dissolving of PVP in water can accelerate the initial separation of polymer and solvent to form large pores. The substrate membrane so formed was rinsed with running water for 24 h to wash away the PVP additive completely, and then it was immersed in a glycerol–water solution (volume ratio of 1:1) for 24 h before being dried at ambient conditions. The thickness of the dry PSF microporous membrane was measured to be 0.18±0.01 mm. PDMAEMA/PSF composite membranes were prepared by coating a layer of PDMAEMA onto the PSF substrate (see Fig. 3-2). The PSF membrane was washed with deionized water for 24 h to remove glycerol and then washed with ethanol. PDMAEMA and XDC were dissolved in ethanol separately at pre-determined concentrations, and the PDMAEMA-ethanol and XDC-ethanol solutions were mixed in certain proportions to achieve a predetermined Cl to N molar ratio. Twenty milliliters of the solution was deposited
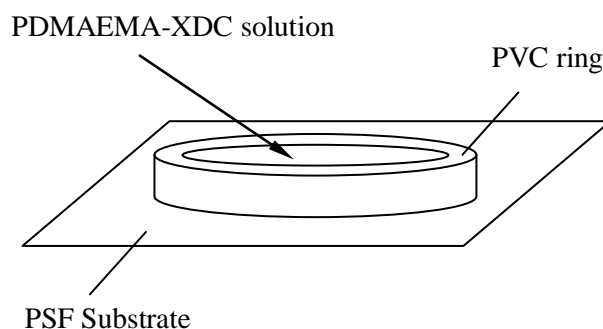
Fig. 3-2. Coating technique for flat-sheet composite membrane.

onto the PSF substrate with the aid of a retainer ring made of poly(vinyl chloride) (10 mm high and 75 mm in diameter) that was adhered on the surface of the PSF substrate. The substrate membrane was positioned horizontally, and the coating solution was allowed to contact the surface of the substrate membrane for a given period of time. Then the excess coating solution was removed, and the membrane was dried in a fume hood at $21^{\circ}C$. The coating process may be repeated for multilayer depositions. The resulting membrane was kept moist by contacting with saturated water vapor in a closed chamber.

3.2.4 Membrane Characterization

Thin films of PDMAEMA prepared with and without crosslinking were examined using Excalibur series Fourier transform infrared (FTIR) spectrometer (Bio-Rad, USA). The uncrosslinked PDMAEMA samples were prepared at $21^{\circ}C$ by casting 50 g/L PDMAEMA in ethanol solution onto a flat polyethylene board followed by drying at $21^{\circ}C$ for 24 h before being peeled off. To prepare the crosslinked PDMAEMA samples, an equal volume of 20 g/L PDMAEMA-ethanol and 11 g/L XDC-ethanol solutions were mixed (molar ratio of atom Cl to N was 1:1), and the solution was cast onto a polyethylene board, followed by solvent evaporation at $21^{\circ}C$ for about 24 h. After peeling off, the PDMAEMA sample was washed with heptane to remove residual XDC crosslinker, and finally it was dried. The thickness of the PDMAEMA samples for FTIR analysis was about 0.26 mm. The morphology of the PDMAEMA/PSF composite membrane was examined under a scanning electron microscope (SEM) (JSM-6460, Jeol, USA). The membrane samples were fractured by quenching in liquid nitrogen, and the specimens were mounted on an aluminum stub and sputter-coated with gold prior to SEM examination. The charge property of the PDMAEMA was investigated using various stain reagents of different charges. Acid orange, neutral gray, and basic fuchsine, which are negatively charged, neutral, and positively charged dyes, respectively, were used to characterize the charge property of the PDMAEMA membrane qualitatively. The PDMAEMA/PSF composite membrane samples were immersed separately in aqueous solutions of the dyes for 3 h, followed by rinsing with pure water three times. The

color of the surface on the PDMAEMA side of the composite membranes was examined visually.

3.2.5 Permeance Measurement

Fig. 3-3 shows a schematic diagram of the experimental setup used for measuring the gas permeance through the PDMAEMA/PSF membranes. The membrane was mounted in a permeation cell (effective membrane area = 16.6 cm^2). A pure gas (i.e., H_2, N_2, O_2, CO_2, and CH_4) was fed through a humidifier, and the gas saturated with water vapor was admitted to the permeation cell. The feed gas pressure was varied in the range of 0.2-0.4 MPa, while the permeate was kept at atmospheric pressure. A thermostatted water bath was used to control the temperature; unless specified otherwise, the test temperature was 23°C. The permeation rate was measured by a bubble flow meter, and the permeance (J) of the gas was calculated by:

$$J = \frac{V}{At\Delta p} \frac{273.15}{T_0} \frac{p_0}{76}$$
(3-1)
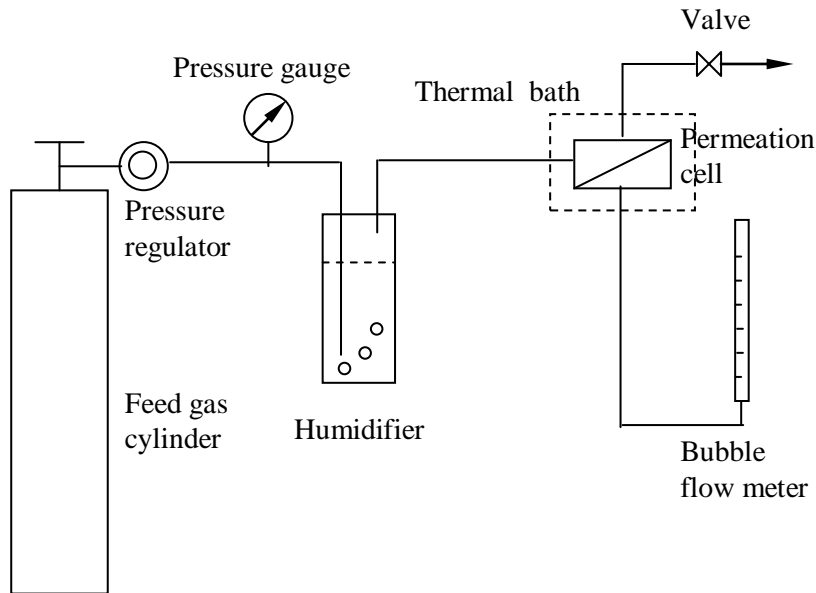
Fig. 3-3. Schematic of experimental setup for permeation measurements.

where V is the volume (cm^3) of the permeate collected at ambient conditions (temperature T_0 (K), pressure p_0 (cmHg)) over a period of time t (s), A the effective area of the membrane (cm^2), Δp the transmembrane pressure difference (cmHg), and J the membrane permeance [cm^3(STP)/(cm^2 s cmHg)]. The membrane permeance is customarily expressed in the unit of GPU [1 GPU = 10^{-6} cm^3(STP)/(cm^2 s cmHg) = 3.35×10^{-10} mol/(m^2 s Pa)]. To evaluate the experimental error, replicate experiments on permeance measurements were performed. Using a given membrane sample the experimental error associated with the test apparatus and procedure was shown to be less than 1 %. Tests with membrane samples cut from the same batch of membrane showed a relative difference within 5 %, which can be considered to be the experimental error in the permeance measurements. Using replicate membranes prepared separately, the relative difference in the permeance was found to be 5-8 %, which represents the reproducibility of the membranes prepared.

The membrane selectivity for a pair of gases was characterized by the ideal separation factor ($\alpha_{i/j}$) defined as their permeance ratio:

$$\alpha_{i/j} = \frac{J_i}{J_j} \qquad\qquad\qquad (3\text{-}2)$$

where subscripts i and j represent the more permeable and the less permeable gases, respectively. Note that humidified feed gas was used in the permeability test because (i) combustion exhaust gasses contain a significant amount of water vapor and (ii) the presence of water vapor is expected to enhance CO_2 permeation. The PDMAEMA is highly hydrophilic and swollen by water vapor, which enhances diffusion of the penetrant through the membrane. In addition, CO_2 is much more soluble in water than N_2 and other non-polar gases. Therefore, the humidified feed will benefit CO_2 permeation from both solubility and diffusivity points of view.

3.3 Results and Discussion

3.3.1 Crosslinking of PDMAEMA

Ethanol, which can dissolve both PDMAEMA and XDC without affecting the PSF substrate, was selected as the solvent during the membrane preparation process. The crosslinking reaction started to occur as soon as the PDMAEMA-ethanol solution was mixed with the XDC-ethanol solution, and the reaction continued after the reacting solution was coated onto the PSF substrate. Unless specified otherwise, the crosslinking was carried out at room temperature for different periods of time. The crosslinking results in the formation of a molecular network by forming quaternary ammonium salt through the reaction between the tertiary amino groups in the side chains of PDMAEMA and the chloromethyl groups in the bifunctional XDC. There are four possible reaction schemes during the crosslinking process, and the possible structures of the crosslinked PDMAEMA are shown in Fig. 3-4.

The changes in the chemical structure of PDMAEMA due to crosslinking was verified by FTIR, as shown in Fig. 3-5, which shows the FTIR spectra of the uncrosslinked and crosslinked PDMAEMA. There is no absorption band from 1675 to 1500 cm^{-1} that corresponds to double bonds for the uncrosslinked PDMAEMA, as shown in Fig. 3-5(a), indicating that there is no C=C bond in the uncrosslinked PDMAEMA membrane. This means that the polymerization of DMAEMA was essentially complete and there were no unreacted residual monomers in the membrane. Fig. 3-5(b) is the FTIR spectrum of PDMAEMA crosslinked by XDC. Note that this sample had been exposed to ambient air (22 ℃, relative humidity ~55 %) and because of the moisture present in the sample, there was a large absorption peak of H_2O at 3367 cm^{-1} covering some absorption peaks of the C-H bond. Nevertheless, it is clear that there is a peak at 1635 cm^{-1}, which is attributed to C=C stretching. Since only XDC molecules in the system have unsaturated carbon bonds in the benzene rings, the presence of benzene rings in the crosslinked PDMAEMA sample thus confirms the chemical crosslinking of PDMAEMA by XDC. The FTIR peaks are summarized in Table 3-1. The crosslinking is further confirmed by the weight change of the dried membrane samples after contacting water; the uncrosslinked PDMAEMA sample

48

underwent a 66 % weight loss, whereas there was essentially no weight change with the crosslinked samples.
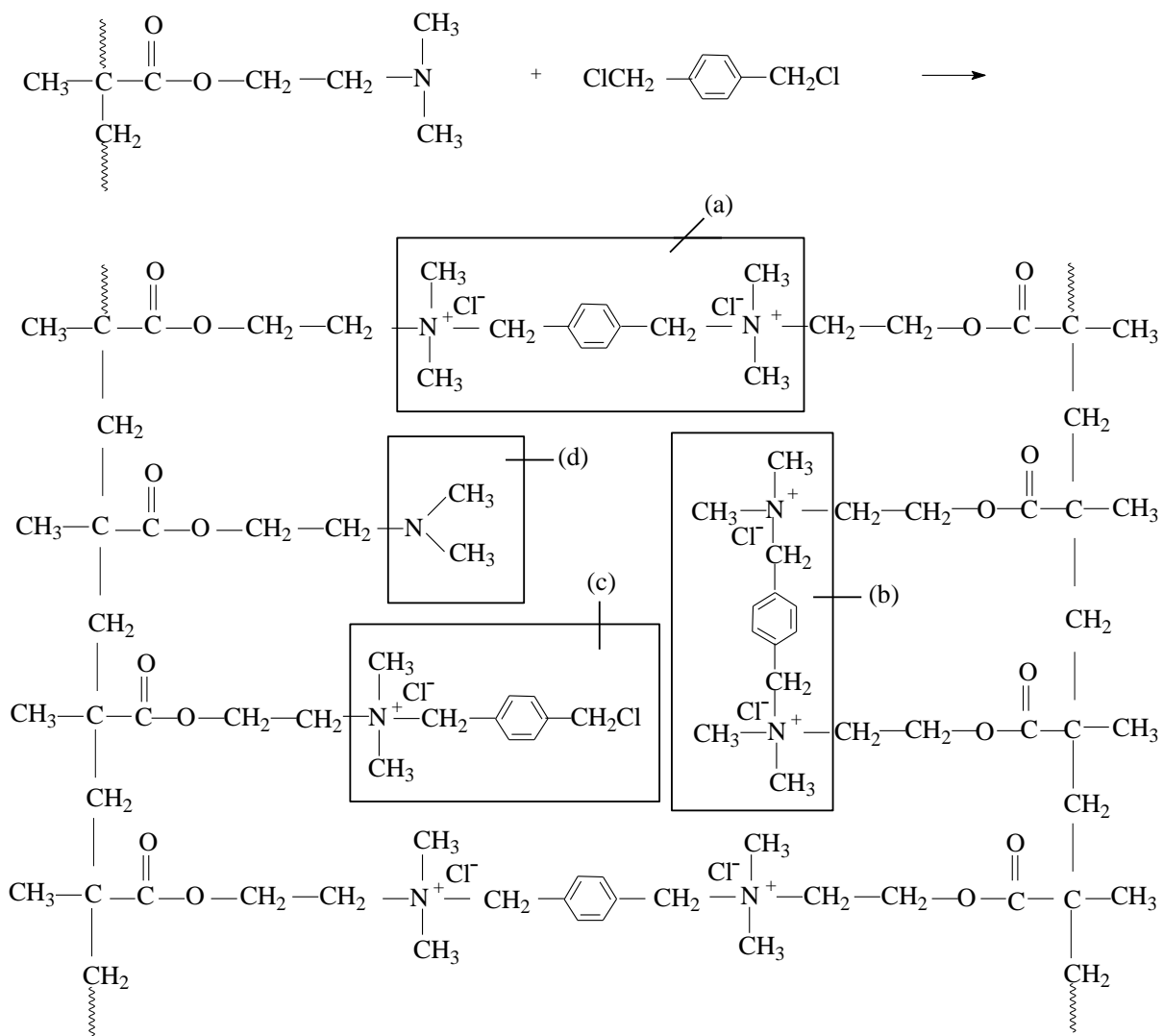
Fig. 3-4. Structure of crosslinked PDMAEMA: (a) intermolecular crosslinking; (b) intramolecular crosslinking; (c) monofunctional reaction of XDC; (d) unreacted tertiary amino group.
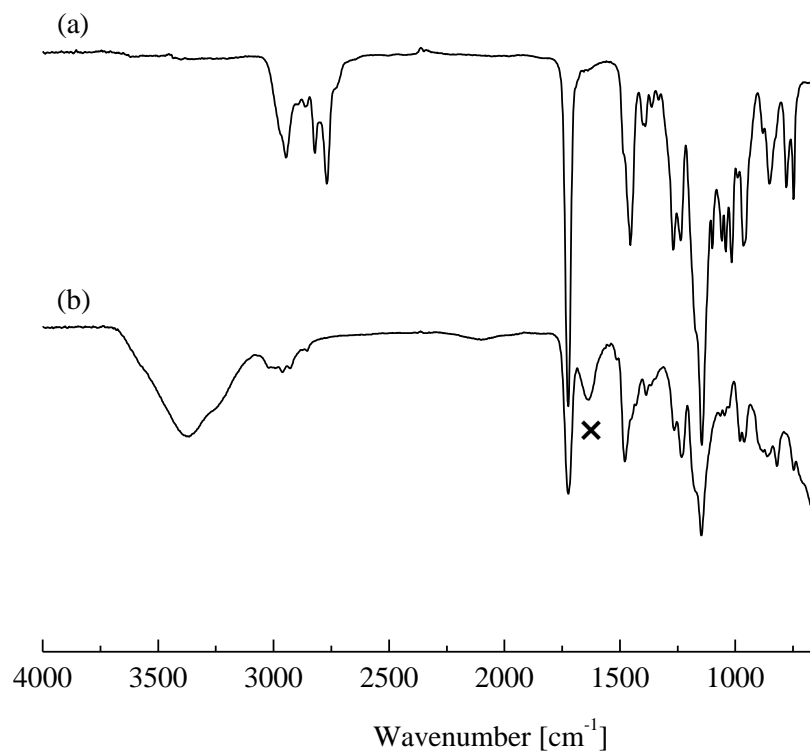
Fig. 3-5. FTIR spectra of uncrosslinked (a) and crosslinked (b) PDMAEMA films.

Table 3-1. Assignment of the FTIR peaks

Wavenumber	group
2946 cm^{-1}, 2821 cm^{-1}, 2769 cm^{-1}, 1479 cm^{-1}, 1455 cm^{-1}	C-H
1723 cm^{-1}	C=O
1635 cm^{-1}	Ph C=C
1269 cm^{-1}, 1233 cm^{-1}	C-O
1145 cm^{-1}, 962 cm^{-1}	C-N

3.3.2 Effect of Membrane Fabrication Parameters on Membrane Performance

The effects of various parameters involved in the membrane formation process on the permselectivity of the resulting membranes were investigated. To study the effect of the polymer concentration in the coating solution, the PDMAEMA-ethanol and XDC-ethanol solutions at different concentrations were mixed with a fixed Cl to N ratio of 1:1, and they were coated on the PSF substrate for 2 h. The permselectivity of the composite membranes formed is shown in Fig. 3-6. With an increase in the PDMAEMA concentration in the coating solution, both CO_2 and N_2 permeance decreased whereas the ideal separation factor increased. This is in agreement with physical reasoning that a higher polymer concentration in the coating solution results in a thicker layer of PDMAEMA in the composite membrane, thus offering a greater resistance to gas permeation through the membrane. The permeance of CO_2 decreased by about 30 % when the PDMAEMA concentration was increased from 10 to 20 g/L, whereas the permeance of N_2 decreased more significantly, resulting in a lesser extent of increase in the ideal separation factor for CO_2/N_2 permeation. This is understandable because a higher polymer concentration will result in a thicker coating layer, which tends to decrease the gas permeance, but the decrease in CO_2 permeance is partially compensated by the increased amino groups in the coating layer that facilitate CO_2 permeation.

Fig. 3-7 shows the effect of coating time on the performance of the PDMAEMA/PSF composite membranes. With an increase in the coating time, the selectivity was improved and the permeation flux decreased. The degree of adsorption of PDMAEMA on the substrate increased with time until adsorption equilibrium was reached. The longer the coating time is, the more PDMAEMA is adsorbed on the substrate, resulting in an increase in the thickness of the coating layer. As such, the resistance of the membrane to gas permeation is increased. However, as expected, when the coating time is sufficiently long, the coating time will not affect the membrane permselectivity any more, because the adsorption of PDMAEMA on the substrate would have been saturated and the thickness of the PDMAEMA deposition layer will no longer increase. It is shown that when the coating time is over 2 h, a further increase
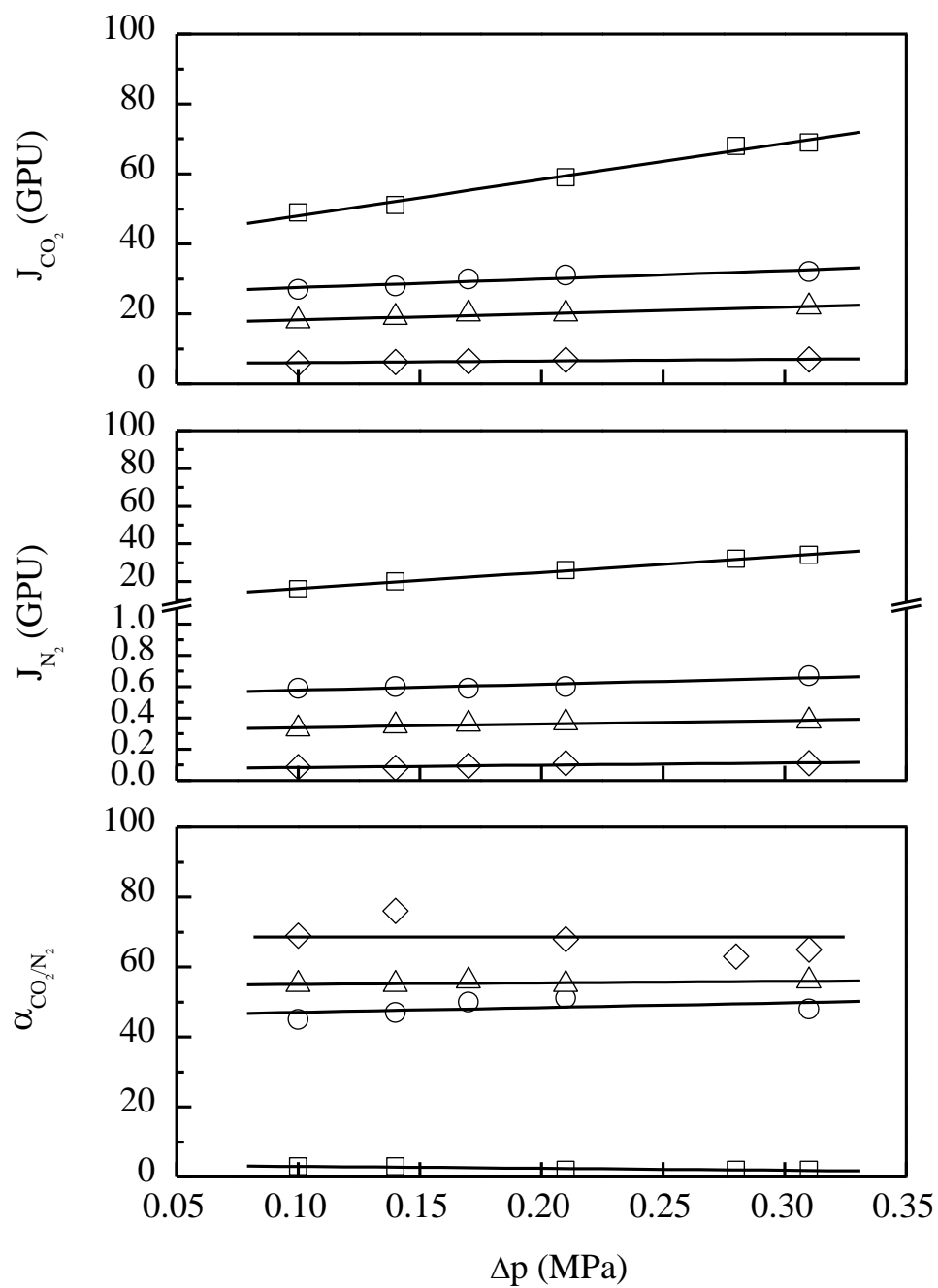
Fig. 3-6. Effect of PDMAEMA concentration in coating solution on the performance of composite membranes (Cl to N ratio 1:1; coating time 2 h): (□) 5 g/L; (○) 10 g/L; (Δ) 20 g/L; (◊) 30 g/L.
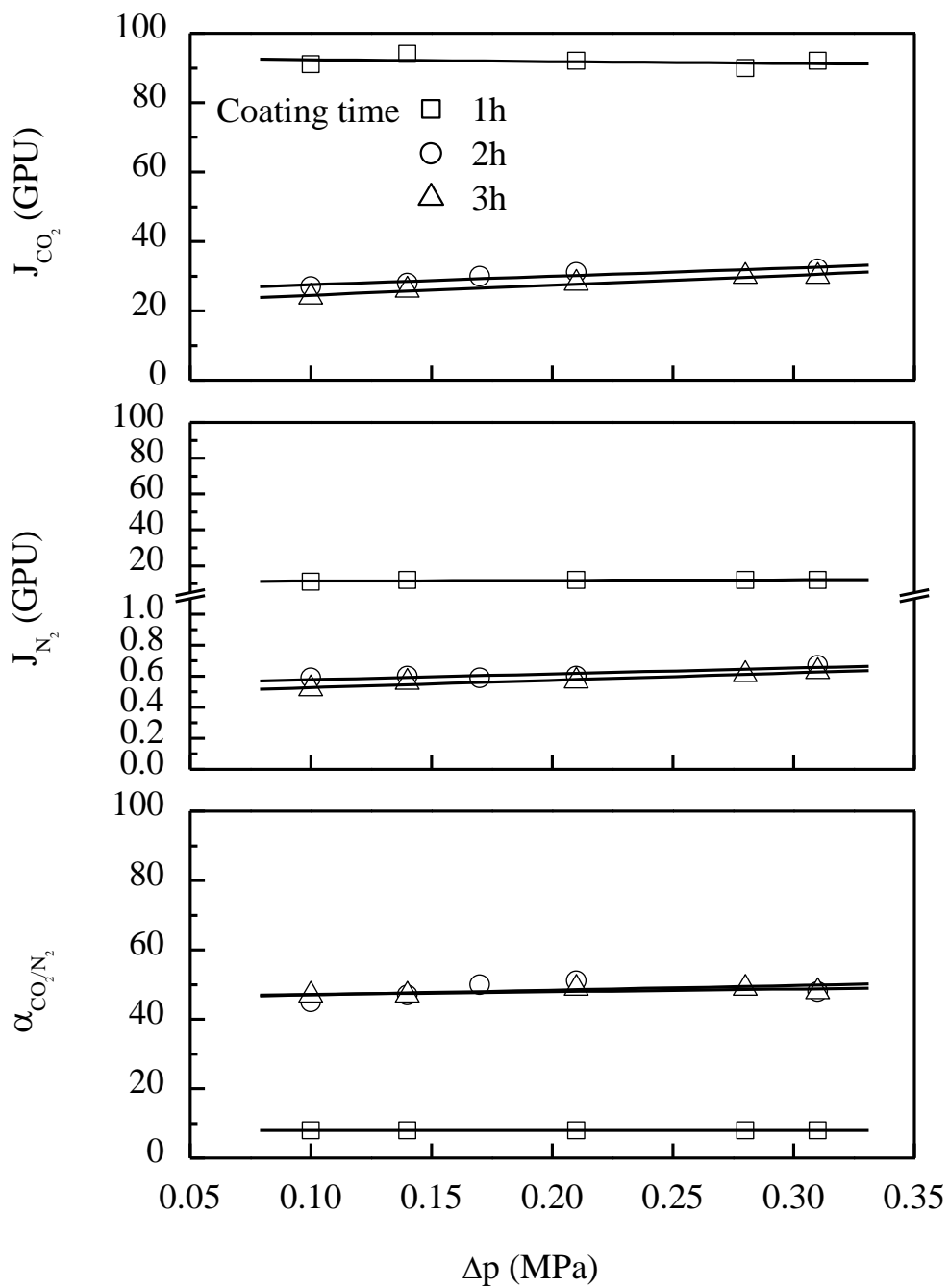
Fig. 3-7. Effect of coating time on the performance of composite membranes (concentration of PDMAEMA in coating solution 10 g/L; Cl to N ratio 1:1).

in the coating time will not influence the membrane permselectivity, and thus a coating time of 2 h was used in subsequent studies.

It is well known that there is no warranty that defect-free composite membranes can be obtained by single coating, and multiple coatings are sometimes needed. To evaluate the effect of the number of PDMAEMA coatings on the performance of the composite membranes, PDMAEMA/PSF composite membranes with single, double, and triple coatings were prepared, and their permselectivities are shown in Fig. 3-8. During the membrane formation process, the overall coating time was controlled to be 2 h. It is shown that as the number of coatings increased, the permeance of the membrane decreased slightly, and the selectivities for double-coated and triple-coated membranes were essentially the same. With an increase in the number of coatings, the top coating layer helps plug the defects that may be present in the pervious coating layer. Membranes with triple coatings were used for further studies, although single coating is preferred from a manufacturing point of view if a defect-free coating layer can be formed.

3.3.3 Membrane Characterization

The surface morphology of the PSF substrate and the PDMAEMA/PSF composite membrane was examined using SEM, as shown in Fig. 3-9 (a and b). It is apparent that there is a significant change in the membrane surface morphology after the PDMAEMA layer was coated onto the PSF substrate. The composite membrane has a uniform and smooth surface.

The asymmetric structure of the membrane was observed by examining the cross-sections of the substrate and the composite membranes under SEM, as shown in Fig. 3-9 (c and d), respectively. An asymmetric structure was found in the PSF substrate, which was composed of a support layer with "finger-like" pores and a denser skin layer with sponge pores (see Fig. 3-9 (c)). In the composite membranes, the top dense layer of PDMAEMA is clearly distinguished from the skin layer of the PSF substrate. The adhesion of the top PDMAEMA layer to the PSF substrate is excellent. The thickness of the PDMAEMA layer can be estimated from the SEM picture to be about 1.0 μm.
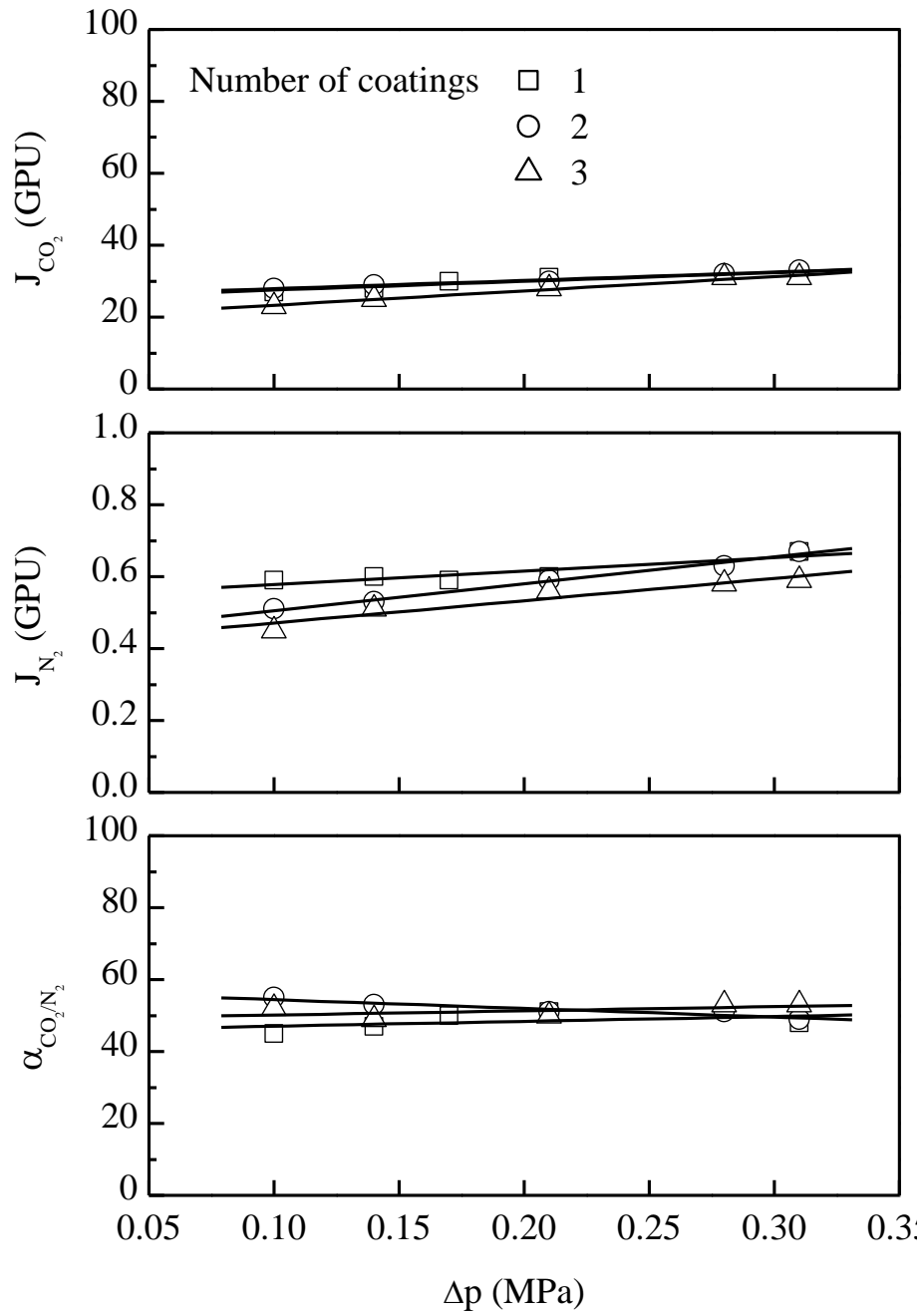
Fig. 3-8. Effect of number of coatings on the performance of composite membranes (concentration of PDMAEMA in coating solution 10 g/L; Cl to N ratio 1:1; coating time: single coating, 2 h; double coatings, 1 h each; triple coatings, 40 min each).
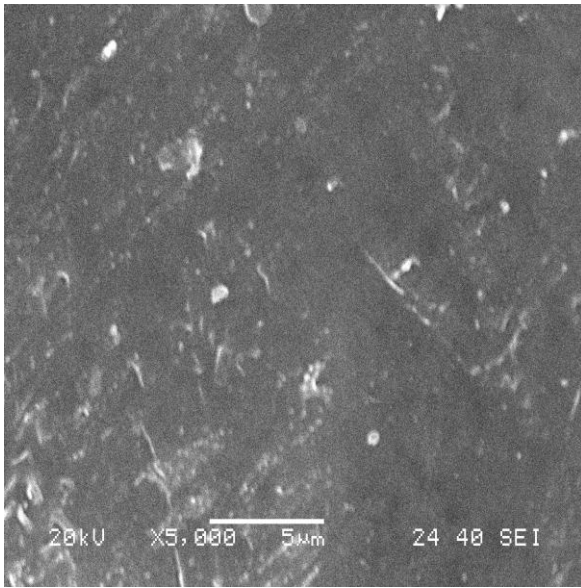
(a)
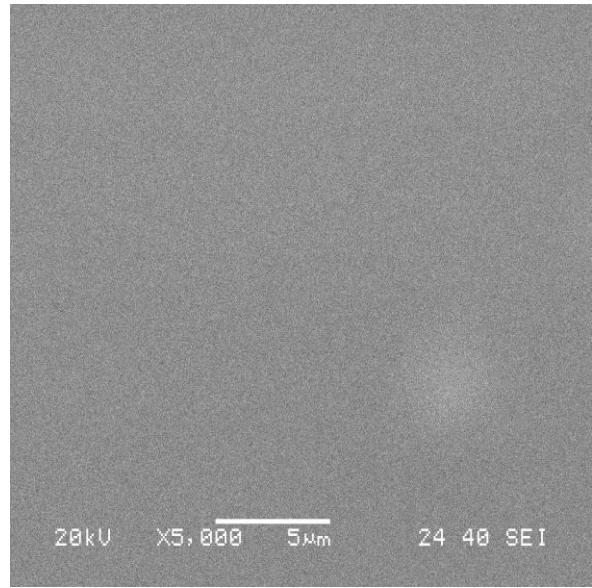
(b)
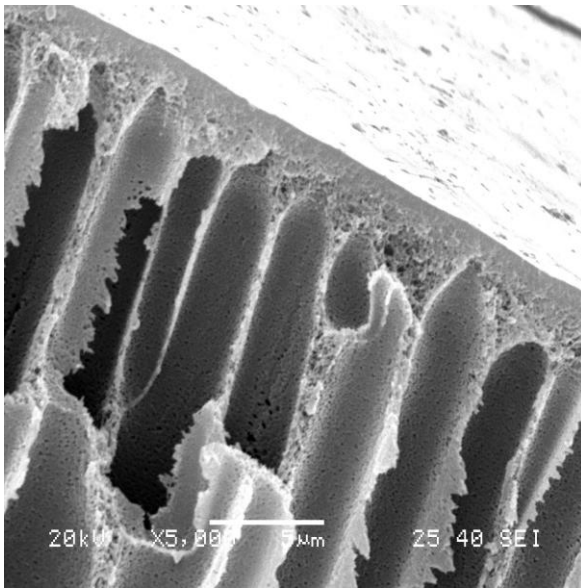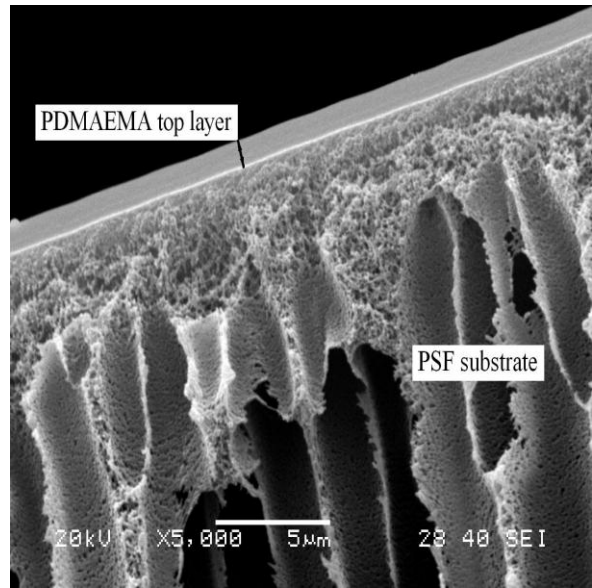
(c)   (d)

Fig. 3-9. SEM images of membrane morphology. (a) Surface of PSF substrate; (b) surface of PDMAEMA/PSF composite membrane; (c) cross-section of PSF membrane; (d) cross-section of PDMAEMA/PSF composite membrane (concentration of PDMAEMA solution 10 g/L; Cl to N ratio 1:1; triple coatings).

The charge property of the composite membrane was qualitatively analyzed with dyes. From a molecular structure point of view, PDMAEMA is converted into a quaternary ammonium salt during crosslinking by quaternization. In aqueous solutions, Cl^-s can be dissociated from the polymer and enter water, resulting in quaternary ammonium groups (-R_4N^+) in the membrane. In addition, PDMAEMA contains unreacted tertiary amino groups, which are subjected to hydration in an aqueous solution:

$$-R_3N + H_2O \rightleftharpoons -R_3NH^+ + OH^- \tag{3-3}$$

Because of the -R_4N^+ and -R_3NH^+ cations in the membrane, the membrane is thus positively charged. Due to electrostatic interactions, negatively charged dye molecules can be adsorbed by the membrane, while positively charged dye molecules will be repulsed. For neutral dye, there is little electrostatic interaction between the membrane and the dye molecules, and the neutral dye will not be well adsorbed on the membrane. The membrane was treated with dyes of different charges (i.e., positive, negative, and neutral), and the color of the membrane was examined. Fig. 3-10 (a) is a photo of the membrane treated with acid orange, a negatively charged dye. The membrane surface was uniformly dyed. Even after rinsing with water for three times, the orange color remained on the membrane surface, showing good affinity of the negatively charged dye molecules and the positively charged membrane surface. Fig. 3-10 (b) shows the membrane treated with neutral gray, a non-charged dye. As expected, the gray color on the membrane surface was very light, indicating its weak adsorption on the membrane surface. After treatment with basic fuchsine, a positively charged dye, no red color could be observed on the surface, as illustrated in Fig. 3-10 (c), showing that the membrane surface did not adsorb the positively charged dye. All these results confirm the cationic nature of the PDMAEMA layer in the composite membranes.
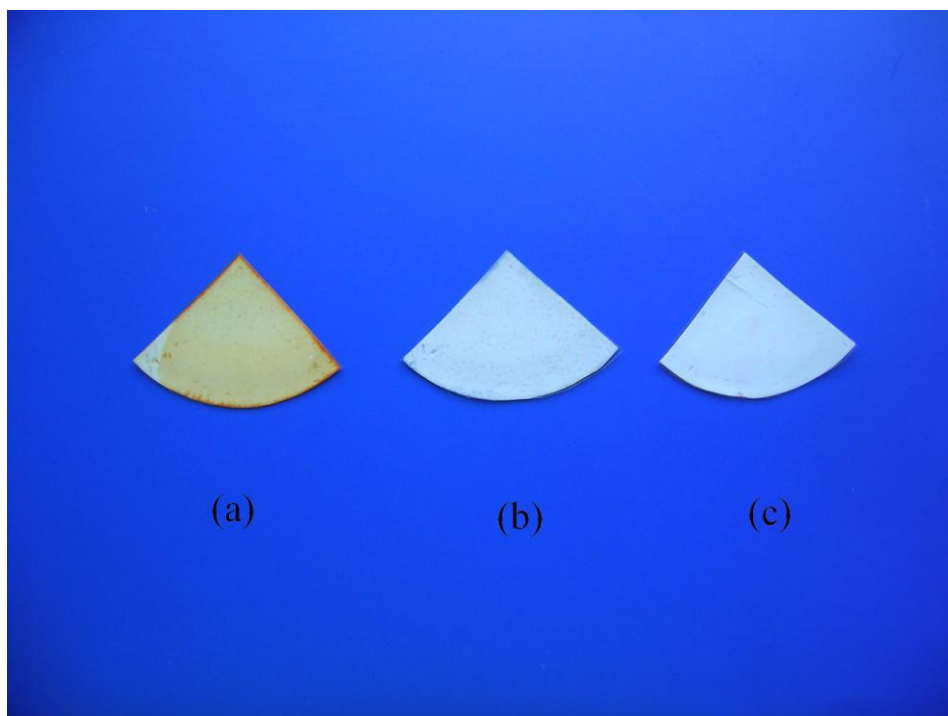
Fig. 3-10. Dye adsorption by PDMAEMA/PSF membrane. (a) Acid orange; (b) neutral gray; (c) basic fuchsine. Membrane formation conditions same as specified in Fig. 3-9.

3.3.4 Permeability of the Membrane

In addition to CO_2 and N_2, the permselectivity of the membrane was also tested with other gases of industrial importance. Fig. 3-11 shows the gas permselectivity through the membrane at different pressures. Clearly, the PDMAEMA/PSF composite membrane has a high permeability to CO_2 and H_2, and a relatively lower permeability to O_2, N_2, and CH_4. The permeability of different gases through the PDMAEMA/PSF membrane followed the order of $N_2 < CH_4 < O_2 < H_2 < CO_2$. The membrane exhibited the best selectivity for the gas pair CO_2/N_2, which is relevant to CO_2 capture from flue gas for greenhouse gas emission control.
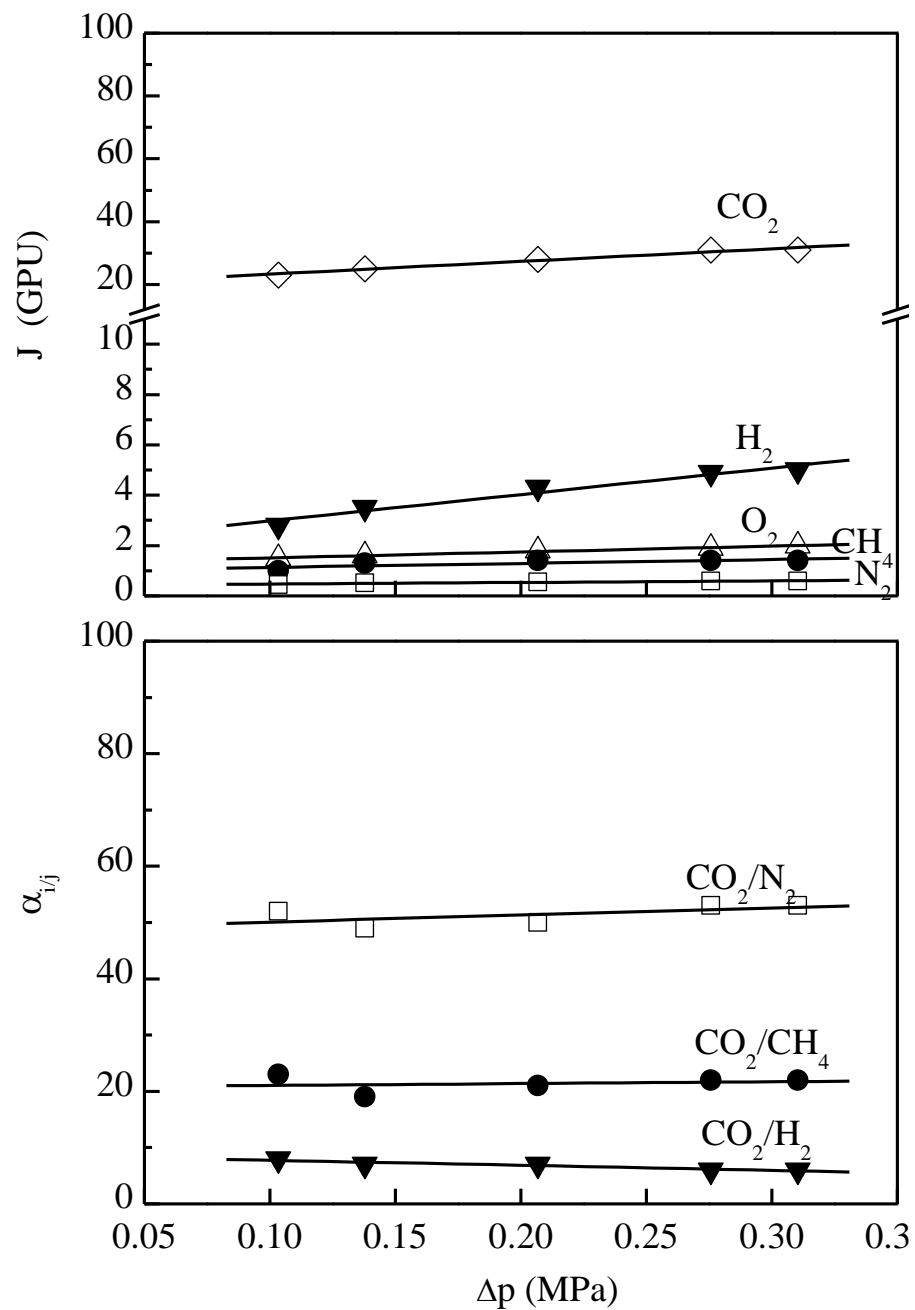
Fig. 3-11. Pressure dependence of permeability and selectivity of various gases through the PDMAEMA/PSF composite membrane. Membrane formation conditions same as those specified in Fig. 3-7.

As mentioned before, the PDMAEMA layer of the composite membrane is believed to dominate the gas permselectivity, and the PSF substrate functions only as a mechanical support. This is confirmed by the data in Fig. 3-12, which shows the permeance of humidified CO_2 and N_2 through the PSF substrate under similar conditions. It can be seen from the permeability data that the PSF substrate is non-selective for gas permeation, and its permeance is about two orders of magnitude higher than the composite membrane. The substantially high permeance of the substrate with essentially no selectivity is due to the pores in the membrane. Using Yasuda and Tsai [1974] technique for pore size determination based on gas permeation, the mean pore size of the dry PSF substrate membrane has been found to be 0.0502 μm.
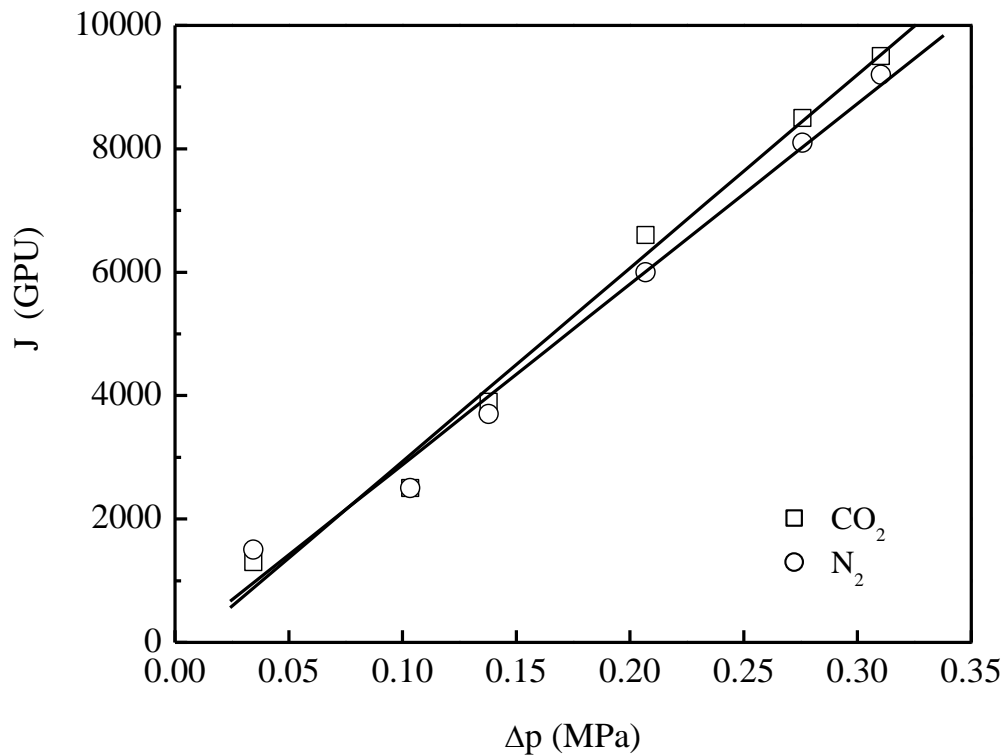
Fig. 3-12. Permeance of CO_2 and N_2 through the polysulfone substrate membrane.

The mass transport in the PDMAEMA layer can be explained from the solution-diffusion model. The permeation is considered to involve sorption of the penetrant into the membrane and molecular movement through the random inter-segmental "holes" produced by the thermal motion of the polymer chains. As a first approximation, the permeability through the membrane is given by the product of solubility and diffusivity coefficients of the penetrant in the membrane. The diffusivity depends on the size and shape of the penetrant. The smaller the gas molecule is, the faster the gas will diffuse in the membrane. The kinetic diameters of H_2 and CO_2 are smaller than other gases studied here [Koros and Paul, 1984], and the diffusivities of these two gases are thus high. On the other hand, the solubility depends to a large extent on the condensability of the penetrant as well as the penetrant–membrane interactions. CO_2 can be considered as a Lewis acid, while the amino groups in the membrane have basic properties. Thus, the solubility of CO_2 in the membrane is enhanced by the weak acid–base interaction between CO_2 molecules and the amine moieties. Furthermore, as mentioned previously, the membrane is positively charged, which limits the solubility of non-polar gases (such as N_2, H_2, O_2, and CH_4) in the membrane. The C=O bond is polar with an electronic cloud leaning to the oxygen atom side because the electronegativity of O is higher than that of C. The positively charged membrane will thus sorb CO_2 more strongly than other gases, and the relatively high solubility of CO_2 in the membrane also favors the permeation of CO_2. Obviously, both the diffusivity and solubility of CO_2 are favorable to CO_2 permeation, leading to a high permeability to CO_2. Fig. 3-11 also shows that the ideal separation factors of CO_2/N_2, CO_2/H_2, and CO_2/CH_4; these gas pairs are of interest for flue gas separation, hydrogen production from fossil fuels and natural gas upgrading. The membrane selectivity is not significantly influenced by the gas pressure in the pressure range tested. The high CO_2/N_2 permselectivity data imply that the homopolymer PDMAEMA can be used to separate CO_2 from flue gas.

A good membrane should possess both a high permeability and selectivity. Unfortunately, membranes with a high permeability often have a low selectivity, and vice versa. In order to evaluate the overall permselective properties, a composite parameter F_J is defined here which

is analogous to the pervaporation separation index used in pervaporation [Feng and Huang, 1997]:

$$F_J = J(\alpha_{i/j} - 1) \tag{3-4}$$

where J is the permeance of the fast permeating component. A zero value of F_J means either a zero flux or zero separation, and the F parameter can be used as a quick and rough estimate of the overall membrane permselectivity, especially when J or α of membranes is in the same order of magnitude. Alternatively, the F parameter may also be defined on the basis of permeability coefficient for homogeneous membranes.

Table 3-2 shows the permselectivity of the membranes obtained in this work and other membranes containing amino groups and nitrogen heterocyclic rings reported in the literature. Although a direct comparison of the membrane performance is difficult because the membranes were tested under different conditions, the data do provide some understanding of the effectiveness of the amino groups and nitrogen heterocyclic rings in the polymers in facilitating the permeation of CO_2. In general, the PDMAEMA/PSF composite membranes showed favorable permselectivity as compared to the copolymerized and the plasma-grafted PDMAEMA membranes [Matsuyama et al., 1996; Yoshikawa et al, 1994]. For example, at 23 ℃ and 412 kPa of CO_2 feed pressure, the permeance of CO_2 was 30 GPU and the CO_2/N_2 ideal separation factor was 53, corresponding to a F parameter value of 1600. The plasma-grafted diisopropylamine membrane [Matsuyama et al., 1994b] and the hydrolyzed polyvinylpyrrolidone membrane [Zhang et al., 2002b] had a high permeance at low partial pressures of CO_2. Although other membranes had higher selectivities, their permeances were generally low. The polyelectrolyte membrane based on polyvinylbenzyltrimethylammonium fluoride [Quinn and Laciak, 1997] also had a high performance for CO_2 separation from N_2 based on the F parameter. It should be pointed out that all the permselectivity data obtained with gas mixtures listed in Table 3-2 are carried out using a sweep gas on the permeate side. As a result, CO_2 is transferred from the feed stream to the sweep gas stream. This process will unlikely be suitable for CO_2 capture from flue gas for greenhouse gas emission control

Table 3-2. Permselectivity of membranes containing amino groups or nitrogen heterocycle rings

Membrane	System	Temp (K)	Pressure (kPa)	α	J_{CO2} (GPU)	F_J (GPU)	Reference
Poly(4-vinylpyridine-co-acrylonitrile)	Pure CO_2 and N_2	303	24.3	9	0.001	0.008	[Yoshikawa et al., 1988]
Poly(N,N-dimethylaminoethyl methacrylate-co-acrylonitrile)	Pure CO_2 and N_2	298	6.7	90	0.2	18	[Yoshikawa et al., 1994]
Plasma-grafted diisopropylamine on Polyimide	CO_2/CH_4 2.0 vol%CO_2	298	101	17	200	3200	[Matsuyama et al., 1988]
Plasma-grafted N,N-dimethylaminoethyl methacrylate on Polyethylene	CO_2/N_2 4.7 vol%CO_2	298	101	130	5	645	[Matsuyama et al., 1996]
Polyvinylbenzyltrimethylammonium fluoride	CO_2/N_2 20 vol%CO_2	296	460	629	7	4400	[Quinn et al., 1997]
	CO_2/CH_4 30.6 vol%CO_2		520	490	3	1500	
	CO_2/H_2 30.6 vol%CO_2		520	43	3	130	
Polyethylenimine/Polyvinyl alcohol	CO_2/N_2 6.5 vol%CO_2	298	101	230	4	920	[Matsuyama et al., 1999b]
Hydrolyzed Polyvinylpyrrolidone on Polysulfone	Pure CO_2 and CH_4	299	1.3	212	800	168800	[Zhang et al., 2002b]
Poly(N,N-dimethylaminoethyl methacrylate)/Polysulfone	Pure CO_2 and N_2	296	412	53	30	1560	This work
	Pure CO_2 and CH_4			22		630	
	Pure CO_2 and H_2			6		150	

as additional separation will be needed to recover CO_2 from the sweep gas. Note that the PDMAEMA/PSF membrane used in this study was not prepared under optimized conditions, and it is possible to further improve the membrane performance by fine tuning the various parameters involved in the membrane formation process. The membrane permeability can be highly improved by using interfacial polymerization approach for membrane formation which is discussed in the following chapter.

The effect of temperature on the permselectivity of the membrane was investigated at a transmembrane pressure difference of 100 kPa. As shown in Fig. 3-13, the gas permeance increases with an increase in temperature, and the temperature dependency of permeance follows an Arrhenius type of relation. The calculated activation energy of permeation is shown in Table 3-3; for comparison, some literature data on the activation energy of permeation are also listed. It appears that CO_2 tends to have a low activation energy of permeation, and E_P increases with an increase in the kinetic molecular diameter of gases except for H_2. Although H_2 has the smallest kinetic diameter, its solubility in the membrane is expected to be low because of its low condensability, and the energy barrier for H_2 to overcome in order to permeate through the membrane is high.

Fig. 3-13 also shows that the membrane selectivity for a given gas pair decreases with an increase in temperature. In general, an increase in temperature will lead to an increase in the diffusivity and a decrease in the solubility. Compared to N_2 permeation, CO_2 is a more condensable gas and the heat effect of dissolution is more significant. Thus, an increase in temperature will increase N_2 permeability more significantly than CO_2, resulting in a decrease in the CO_2/N_2 selectivity. The activation energy is a representation of the significance of temperature dependency of the membrane permeability. If the activation energy of permeation for the fast component is greater than for the slow component, then the selectivity of the gas pair will decrease with an increase in the temperature.
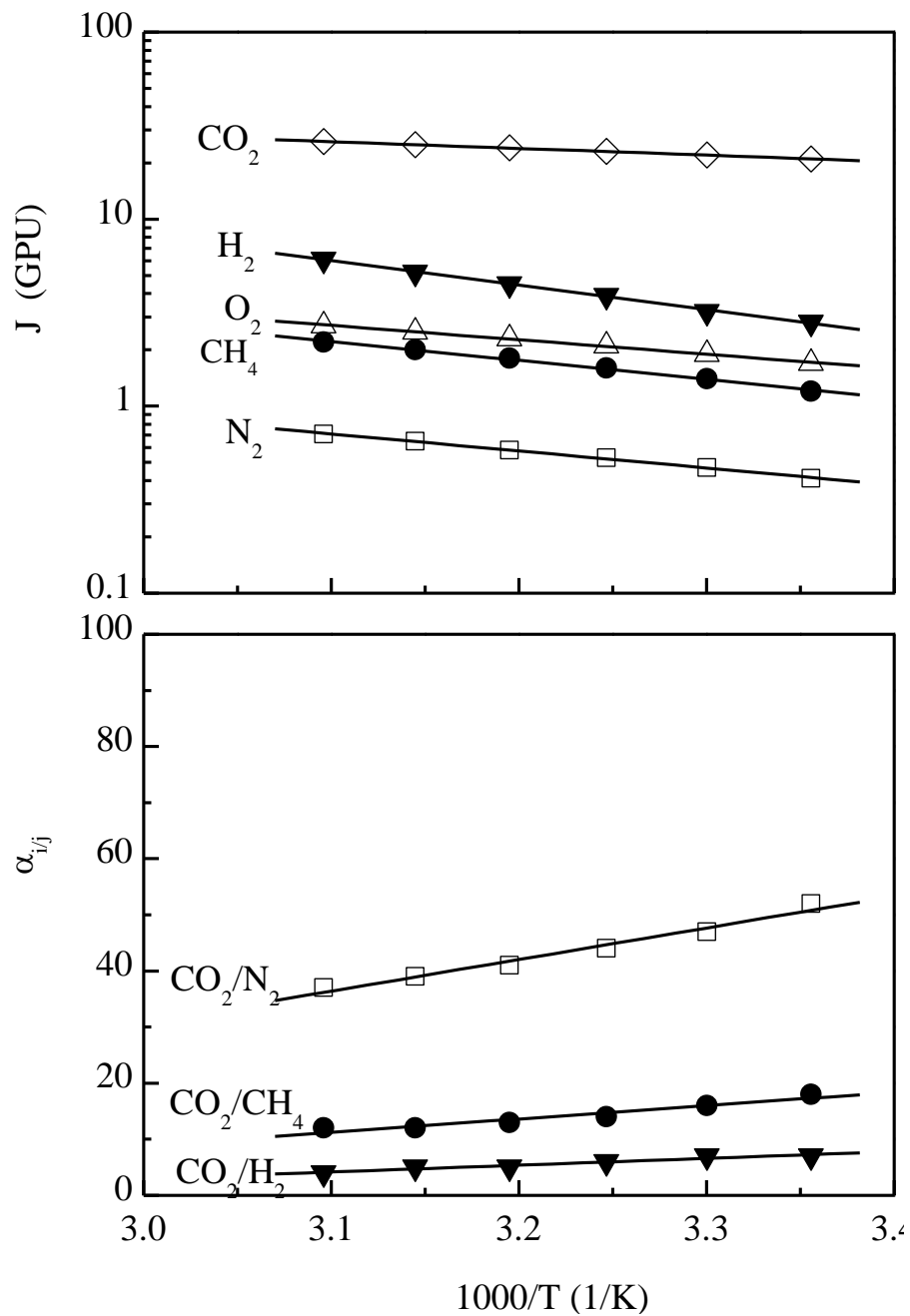
Fig. 3-13. Temperature dependence of permeance and selectivity of various gases through the PDMAEMA/PSF composite membrane. Membrane formation conditions same as those specified in Fig. 3-9.

Table 3-3. Apparent activation energy for permeation (kJ/mol)

Membrane	CO_2	O_2	N_2	CH_4	H_2	Reference
PDMAEMA/PSF	6.8	14.0	17.5	20.0	24.6	This work
Cellulose	7.34	12.58	16.04	15.01	17.48	[Wu and Yuan, 2002]
6FDA-durene polyimide	0.2	2.4	4.45	7.25	-	[Lin and Chung, 2001]
Poly (lactic acid)	6.1	11.1	11.2	13.0	-	[Lehermeier et al., 2001]

3.4 Conclusions

Composite membranes comprised of a PDMAEMA active layer and a PSF substrate were prepared. The PDMAEMA, which was a homopolymer synthesized by free radical bulk polymerization using AIBN as the initiator, was chemically crosslinked by XDC. After crosslinking, the membrane became positively charged, and the thickness of the PDMAEMA layer in the composite membrane was about 1 μm. The concentration of the coating solution and coating time were found to affect the performance of the composite membrane. The permeability of the composite membrane to various gases follows the order of $N_2 < CH_4 < O_2 < H_2 < CO_2$, and the membrane was found to compare favorably with other membranes based on copolymerization and the plasma grafting of DMAEMA in terms of CO_2/N_2 permselectivity. For example, at 23 °C and 412 kPa of CO_2 feed pressure, the permeance of CO_2 was 30 GPU and the CO_2/N_2 ideal separation factor was 53. The gas permeance through the PDMAEMA/PSF membrane increases with an increase in temperature, and the temperature dependency of membrane permeance follows an Arrhenius type of relation. The apparent activation energy for the permeation of N_2, CH_4, O_2, H_2, and CO_2 through the membrane was found to be 17.5, 20.0, 14.0, 24.6, and 6.8 kJ/mol, respectively.

Chapter 4

Interfacially formed PDMAEMA/PSF Composite Membranes[*]

4.1 Introduction

The cationic bulk-crosslinked PDMAEMA membranes showed a fairly high permselectivity to CO_2/N_2, as shown in Chapter 3. The bulk crosslinking reaction leads to a uniform crosslinking. While crosslinking generally improves membrane selectivity, the permeability tends to decrease due to the restricted chain flexibility of the polymer matrix. In order to minimize the mass transfer resistance through the membrane while retaining a high selectivity of the membrane, interfacial crosslinking was attempted in the present study.

Interfacial polymerization based on reactions between monomers or crosslinking of a reactive pre-polymer layer has been used commercially for making thin film composite membranes for reverse osmosis [Peterson, 1993]. One of the best-known examples of interfacially formed composite membranes is Cadotte's NS-100 membrane based on polyethylenimine crosslinked with toluene-2,4-diisocyanate [Cadotte, 1985]. Typically, to prepare a composite membrane by interfacial polymerization, a microporous substrate is soaked in a solution containing the reactive monomer or polymer (e.g., polyamines), and it is then brought into contact with an immiscible solution containing another monomer or crosslinking agent (e.g., diacid chloride). A crosslinked polymer layer forms on the surface of the substrate at the interface of the two immiscible solution phases, and the thin film so formed will act as a barrier to further contacts between the reacting species, resulting in a less crosslinked polymer layer under the surface layer and in the pores of the substrate. This is thus a self-limiting process that helps form a very thin crosslinked layer in the composite membrane. The kinetics of film growth by interfacial reactions has been studied recently for different systems [Song et al., 2005; Ji et al., 2000].

Interfacial polymerization has now become a well-established method to prepare thin film composite membranes from amine polymers especially for reverse osmosis and nanofiltration. Unfortunately, such membranes usually do not yield sufficient permselectivity when used for gas separation where the membrane is dry. One of the problems is the presence of minute defects in the active layer because an extremely thin layer of densely crosslinked polymer only forms at the surface, and microvoids may be developed when the membrane is dried. In addition, the densely crosslinked or interfacially polymerized layer is confined to a very thin layer at or near the surface of the porous substrate, where the immiscible reacting solutions are in contact. In the substrate, the pores of the substrate will be filled with less crosslinked hydrogel. When the membrane is used for reverse osmosis or nanofiltration, the substrate remains highly water-swollen and offers little resistance to water passage. However, the membrane should be dry for gas separation, and the hydrogel initially present in the substrate will become rigid and stiff upon drying, leading to a substantial resistance to gas permeation. As a result, defect-free interfacial composite membranes often exhibit a low gas permeability [Castro et al., 1991].

In spite of the aforementioned issues, it is encouraging that interfacial composite membranes have shown great promise for gas separations. Liang and Martin [1991] prepared a poly(N-methylpyrrole) membrane by vapor–liquid interfacial polymerization onto a microporous alumina substrate, and the membrane showed a CO_2 permeance of 2 GPU and a CO_2/N_2 selectivity of 17.6. Petersen and Peinemann [1997] prepared a polyamide composite membrane by liquid–liquid interfacial polymerization, and the membrane showed a CO_2 permeance of 54 GPU and a CO_2/N_2 selectivity of 24. More recently, Zhao et al. [2006] developed an interfacial composite membrane from trimethylene tetramine and trimesoyl chloride, and heat treatment was found to help stabilize the membrane performance for CO_2/N_2 separation.

To eliminate the surface microvoids that could be caused by the solvents involved in the interfacial reaction during membrane formation, a solid–liquid interfacial reaction was exploited in the present work. Instead of monomeric amine, polymeric amine was chosen in this work to minimize the penetration of amine solution into the pores of the substrate so as

68

to minimize the membrane resistance. PDMAEMA with amine moieties on side chains used as the polyamine was coated on a PSF substrate and air-dried before contacting with the crosslinking solution. The chemical crosslinking occurred at the solid–liquid interface between the PDMAEMA solid layer and a *p*-xylylene dichloride (XDC)-heptane solution. The resulting composite membranes were tested for permeation of N_2 and CO_2, which are the main components of flue gas.

The separation performance of a membrane is determined not only by its chemical structure, but by its morphology as well. The interfacial crosslinking is expected to induce a thin crosslinked layer on the membrane. Therefore, the top layer of the composite membrane would possess an asymmetric structure in terms of crosslinking networks, which is anticipated to be more advantageous than its homogeneous counterpart as far as the permeation flux is concerned. The distinctive morphology of the opposite surfaces of the interfacially crosslinked PDMAEMA membranes was confirmed experimentally. On the other hand, considering that water vapor is present in flue gas and it enhances the permeation of CO_2, the hydrophilicity of the surface layer of the composite membrane was analyzed.

4.2 Experimental

4.2.1 Materials

Diiodomethane (99%), glycerol (≥99%), and formamide (≥99%) were supplied by Sigma–Aldrich. Ethylene glycol (99.4%) was purchased from Fisher Scientific. All other materials were the same as those described in Chapter 3.

4.2.2 Membrane Preparation

The polysulfone substrate membrane was prepared by the phase inversion technique; the detailed procedure has been described in Chapter 3. The composite membranes were prepared by interfacial crosslinking of a layer of PDMAEMA on the PSF substrate (see Fig. 4-1). The PSF substrate was washed with deionized water for 24 h to remove glycerol. Then 20 mL of PDMAEMA-ethanol solution at a given concentration was deposited onto the PSF

substrate with the aid of a retainer ring adhered on the surface of the PSF substrate. The coating solution was allowed to contact the surface of the substrate membrane for a certain period of time, and then the excess coating solution was removed and the membrane was air dried in a fume hood at 21 °C, thereby forming a thin solid layer of PDMAEMA on the substrate. Then, 20 mL of an XDC–heptane solution at a given concentration was deposited onto the coated PDMAEMA surface where the crosslinking reaction took place on the solid–liquid interface. To prevent heptane loss due to evaporation during the crosslinking reaction, the reaction was carried out in a closed chamber filled with heptane vapor. After a certain period of reaction time, excess crosslinking solution was removed and the membrane surface was washed with heptane three times to remove the remaining XDC on the membrane surface. After drying, the membrane was kept moist by contacting with saturated water vapor in a closed chamber.
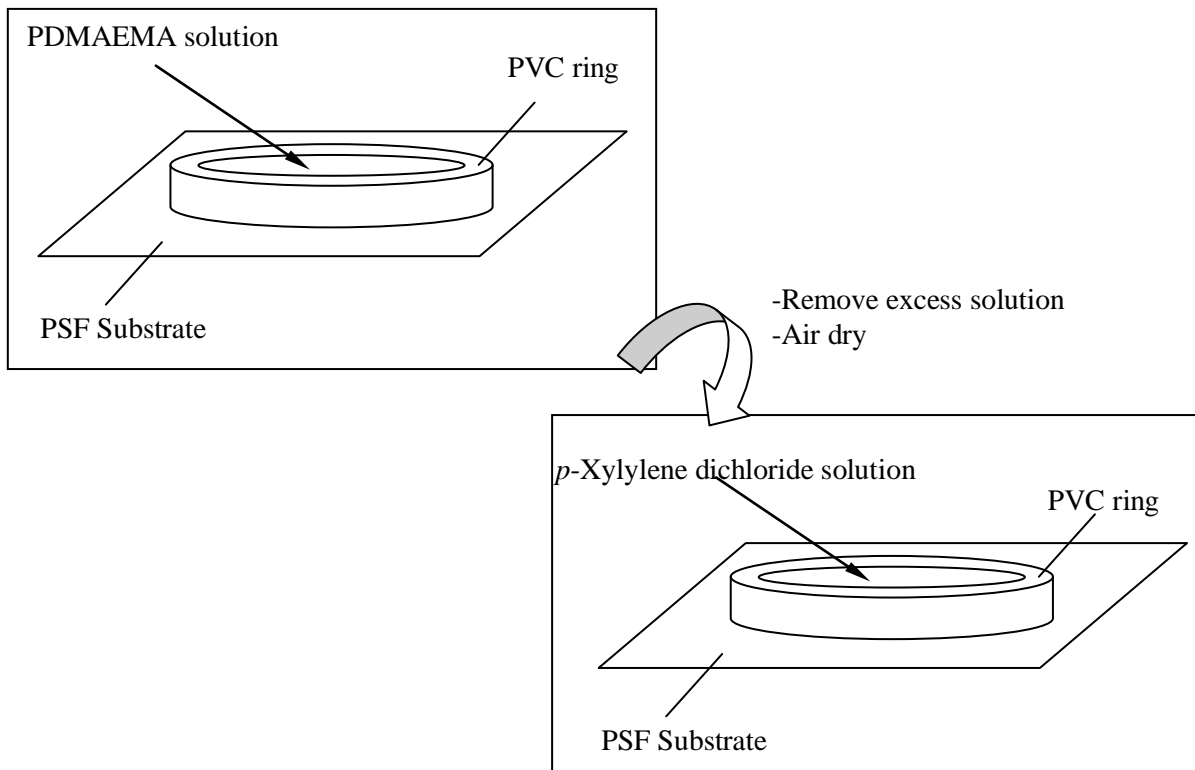
Fig. 4-1. Interfacially crosslinking technique for flat-sheet composite membrane.

4.2.3 Morphology Characterization

To verify the heterogeneity of the structural composition along the thickness of the PDMAEMA layer, the membrane samples were subjected to "erosion" with water and the weight change of the membrane was determined. Initially, the membrane samples were fully dried and weighed before being rinsed with deionized water for 48 h at 23 ℃. The uncrosslinked PDMAEMA dissolved in water. Afterwards, the membranes were dried and weighed again. The weight loss in the membranes was evaluated by

$$\Delta W = \frac{W - W'}{A} \qquad\qquad (4\text{-}1)$$

where ΔW is the weight loss per membrane area after immersion in water, A the area of the dry membrane sample prior to water rinsing, and W and W' are the dry weights of the membrane sample before and after rinsing with water. The membrane samples used for weight change measurements were prepared by coating a PDMAEMA layer of different thicknesses onto the PSF substrate followed by crosslinking with XDC at a concentration of 10 g/L in heptane for a given period of time.

Further, to look at the morphology of the interfacially formed PDMAEMA layers, thick films of different thicknesses without the PSF substrate were also prepared by coating PDMAEMA–ethanol solution onto a Teflon plate. The dried PDMAEMA surface was allowed to contact with 20 mL of 1 g/L XDC–heptane solution for 24 h to accomplish interfacial crosslinking. After drying, the films were immersed in deionized water for 6 days to wash out the uncrosslinked PDMAEMA in the film. The membrane structure before and after water washing was examined under scanning electron microscopy (SEM, JSM-6460, Jeol, USA). The change in the membrane morphology caused by water erosion was also used to confirm the asymmetric crosslinking density across the membranes.

4.2.4 Contact Angle Measurements

Contact angle measurements with different probe liquids were performed using a contact angle meter (Cam-plus Micro, Tantec Inc.). To correlate the contact angle with the degree of crosslinking of the membrane, different concentrations of the crosslinking solution (1−10 g/L

XDC in heptane) were used in the interfacial crosslinking reaction while maintaining a constant reaction time of 5 h and a temperature of 21 ℃. The membrane samples were air dried at ambient temperature prior to contact angle measurements. The contact angle values reported represent the mean values (±standard deviations) of at least five measurements. The surface free energy of the composite membrane was determined from the contact angle data.

4.3 Results and Discussion

4.3.1 Characterization of Membrane Structure

The interfacial crosslinking reaction occurs at the solid–liquid interface between the PDMAEMA layer and the XDC solution. The reaction results in the formation of a crosslinked molecular network by forming quaternary ammonium salt through alkylation reaction between the tertiary amino groups in the side chains of PDMAEMA and the chloromethyl groups in the bifunctional XDC. The change in the amino groups on PDMAEMA due to the alkylation reaction has been verified by X-ray photoelectron spectroscopy reported elsewhere [Du and Zhao, 2004a]. Interfacially XDC-crosslinked PDMAEMA nanofiltration membranes have been reported to have good water flux and MgSO$_4$ rejection [Du and Zhao, 2004a;b].

Fig. 4-2 is a schematic diagram illustrating the "concentration" profile of crosslinked sites in the membrane as time proceeds during the interfacial crosslinking. There are two extreme cases. In Case (a), the crosslinking is controlled by the mass transfer only. The crosslinking occurs initially on the exterior surface, and the crosslinker needs to diffuse through a progressively increasing thickness of the crosslinked layer to crosslink the interior. There is a sharp boundary in the membrane between the crosslinked and the uncrosslinked portions. On the other hand, in the extreme case of reaction control (Case b) where there is no diffusional resistance, the crosslinking occurs uniformly (but not instantaneously) throughout the membrane, and the concentration of the crosslinked sites in the membrane is "homogeneous" along the membrane thickness but increases with respect to time. A general case (Case c) is shown in which the concentration profile of crosslinked sites changes continuously with

respect to position and time. For the interfacial crosslinking studied here, the mass transfer resistance is not likely to be unimportant considering the relatively low magnitude of diffusivity of liquid molecules in a dense solid polymer. It is therefore anticipated that similar to other interfacially polymerized membranes [Freger, 2003; Freger and Srebnik, 2003], the PDMAEMA/PSF composite membrane will have an asymmetric structure in the PDMAEMA layer in terms of the crosslinked sites. While the surface layer is non-porous, it consists of a network of macromolecular chains connected through crosslinks (thereby forming macromolecular meshes). After the tertiary amino groups on the outermost PDMAEMA layer have reacted with XDC to form a crosslinked layer, the diffusion and penetration of XDC to reach the interior will be restricted. This "self-limiting" effect will lead to a non-uniform crosslinking along the thickness of the PDMAEMA layer, unless the crosslinking time is sufficiently long. Beneath the highly crosslinked outer surface, the unreacted amino groups in the interior are less crosslinked and thus the polymer chain mobility is less restricted. It is therefore expected that the unreacted amino groups will be favourable for high permeability, while the crosslinked surface layer will dominate the selectivity of the membrane.
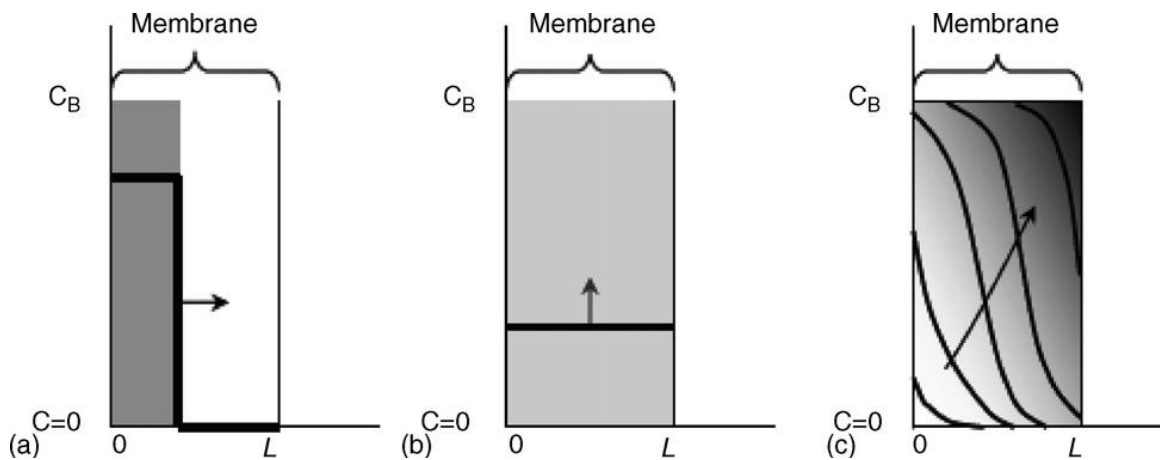
Fig. 4-2. A schematic instantaneous concentration profile of crosslinked "sites" in the membrane during crosslinking, illustrating two extreme cases (a) diffusion control and (b) reaction control and a general case (c). Arrows indicate direction of movement profile with respect to time.

The distinctive morphologies of the opposite surfaces of the interfacially crosslinked PDMAEMA layer have been confirmed experimentally. Because PSF does not dissolve in water, the weight loss of the membrane caused by water "erosion" can be regarded as the elution of uncrosslinked PDMAEMA which is soluble in water. Fig. 4-3 shows the weight loss of the PDMAEMA/PSF composite membranes with different thicknesses of PDMAEMA layers. The thickness was controlled by coating PDMAEMA–ethanol solution onto the PSF substrate for different times. There was little or no change in the weight when the PDMAEMA layer was very thin, showing that the whole polymer layer was adequately crosslinked and could not be washed away by water. However, as the PDMAEMA layer becomes thicker, the crosslinking agent will not be able to penetrate the whole film to crosslink the amino groups, resulting in a portion of the PDMAEMA layer uncrosslinked beneath the surface layer. For a relatively thick PDMAEMA layer, the approximate linear relationship between the weight loss and the PDMAEMA thickness appears to indicate that at a given crosslinking agent concentration for a given period of crosslinking time, the crosslinked layer that is insoluble in water is more or less the same. This implies that for a thick layer of PDMAEMA, the XDC penetration depth is almost the same, independent of the overall PDMAEMA thickness. It is expected that with an increase in the reaction time, more XDC molecules will be able to penetrate the coating layer to crosslink PDMAEMA and consequently the membrane weight loss will be decreased. This is indeed the case, as shown in Fig. 4-4. The data in Fig. 4-4 further show that the reduction in the weight loss is less drastic as the reaction time increases, which agrees with the reasoning that the crosslinked layer functions as a barrier for the crosslinking molecules to diffuse inside to further crosslink PDMAEMA in the interior of the coating layer.

In addition, the structure of the PDMAEMA layer can be observed under SEM. In order to examine the membrane structure clearly, a thick PDMAEMA film formed by interfacial crosslinking was prepared on a Teflon plate so that the crosslinking took place on the top surface. Fig. 4-5 (a1) and (b1) shows the SEM images of the top surface of the PDMAEMA film before and after washing with water, respectively. Because of the evaporation of volatile ethanol during film formation, there were a few "ruffles" on the surface of the dried film
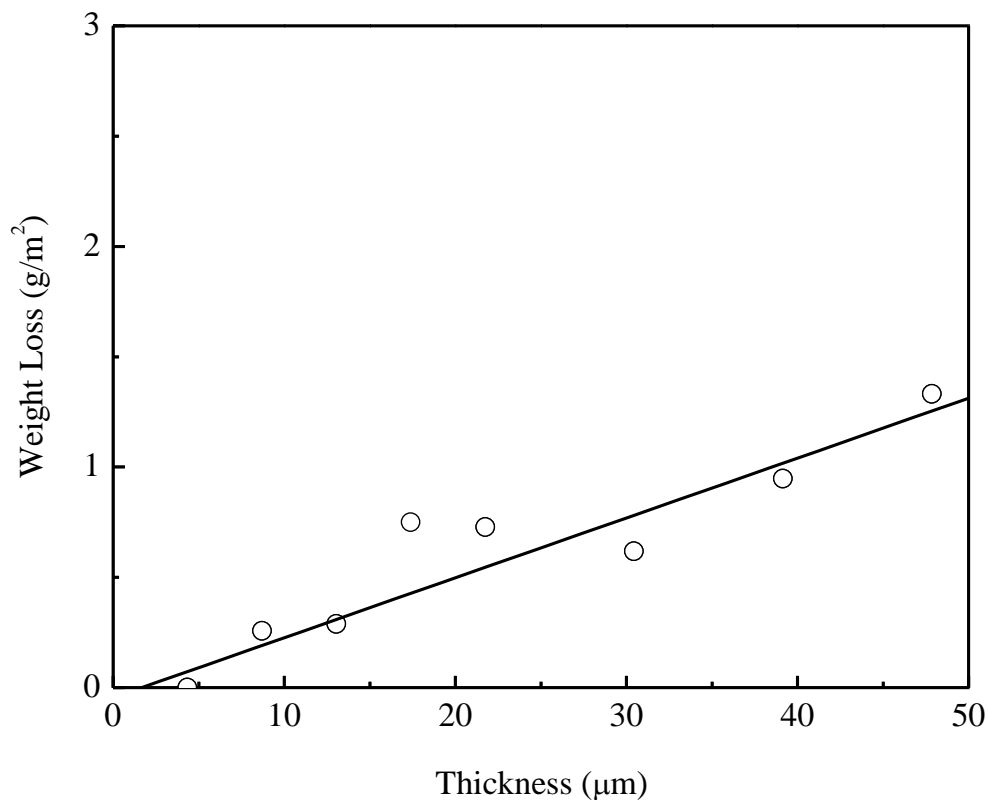
Fig. 4-3. Effect of PDMAEMA layer thickness on the weight change of PDMAEMA/PSF composite membranes (crosslinker concentration 10 g/L, crosslinking time 5 h).

formed, as shown in Fig. 4-5 (a1). After washing in water, the membrane was swollen. Upon drying, the membrane shrunk, and some wrinkles developed on the surface, as shown in Fig. 4-5 (b1). However, no visible pores or defects were observed, showing that the top surface of the crosslinked layer is dense. The bottom surface of the film, which did not contact the crosslinking solution directly, showed different structures, as shown in Fig. 4-5 (a2) and (b2). While there were no pores detectable on the bottom surface of the film before washing in water, a lot of cavities with sizes up to about 5 μm were developed after washing with water.
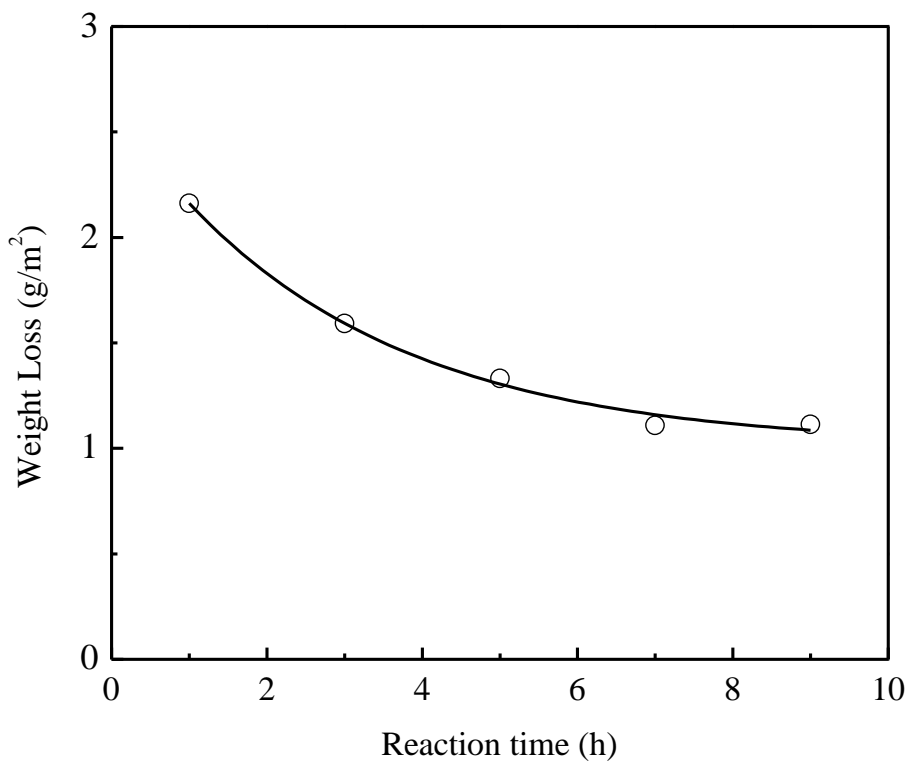
Fig. 4-4. Effect of interfacial crosslinking reaction time on the weight change of PDMAEMA/PSF composite membranes (crosslinker concentration 10 g/L).

A comparison between the top and the bottom surfaces (see Fig. 4-5 (b1) and (b2)) of the washed film clearly indicates that there is a structural change across the film. The cross-section of the water-washed film is shown in Fig. 4-6; it is shown that there is a dense layer near the top surface, a transitional region in the middle, and a loose structure near the bottom. The crosslinked top surface of PDMAEMA cannot be washed out, whereas the uncrosslinked PDMAEMA near the bottom surface can be washed out by water, leaving behind visible cavities near the bottom surface.
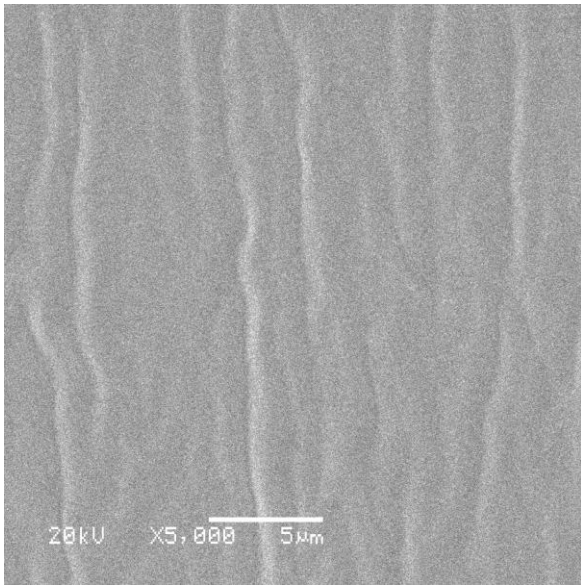
(a1)
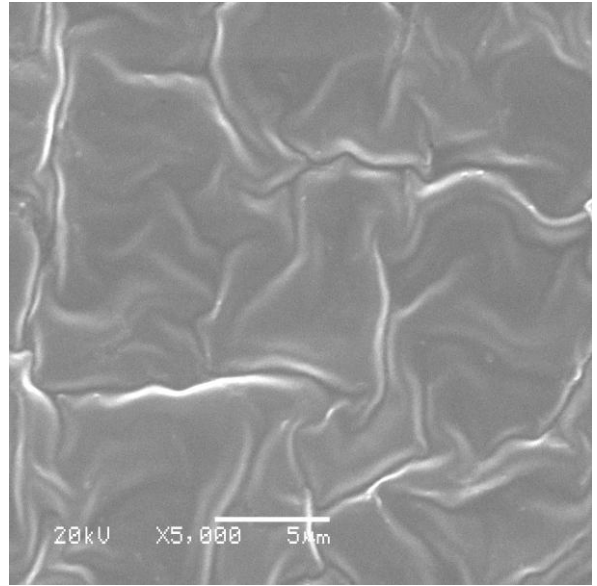
(b1)
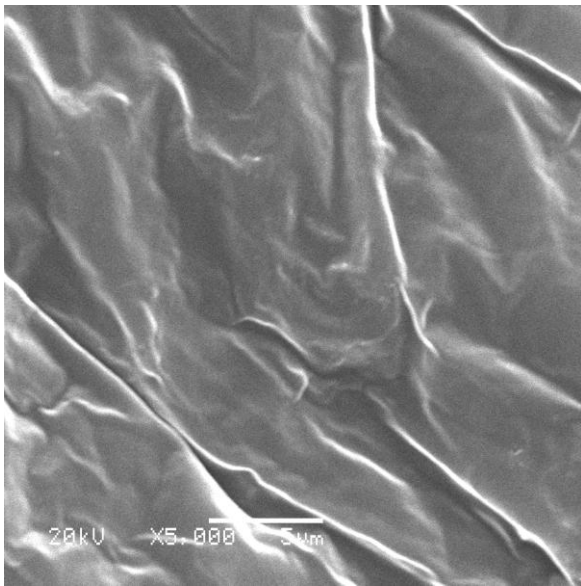
(a2)
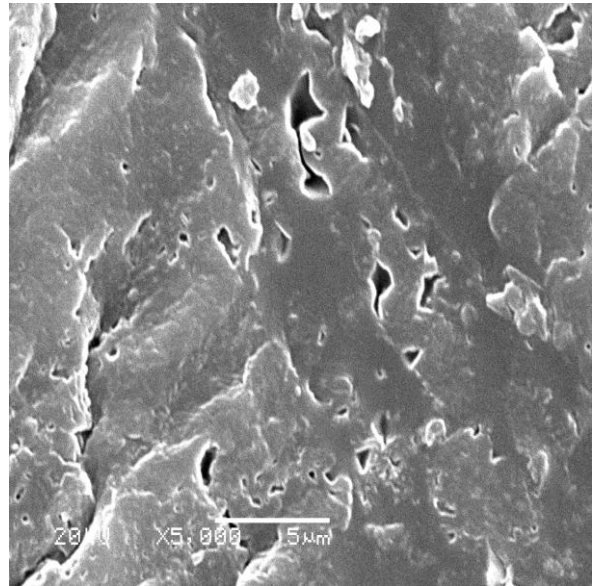
(b2)

Fig. 4-5. SEM images of PDMAEMA films via interfacial crosslinking. (a1) and (a2) show the top and bottom surfaces of the unwashed film, (b1) and (b2) show the top and bottom surfaces after water rinsing (crosslinker concentration 1 g/L, crosslinking time 24 h, water rinsing time 6 days).

(a)   (b)
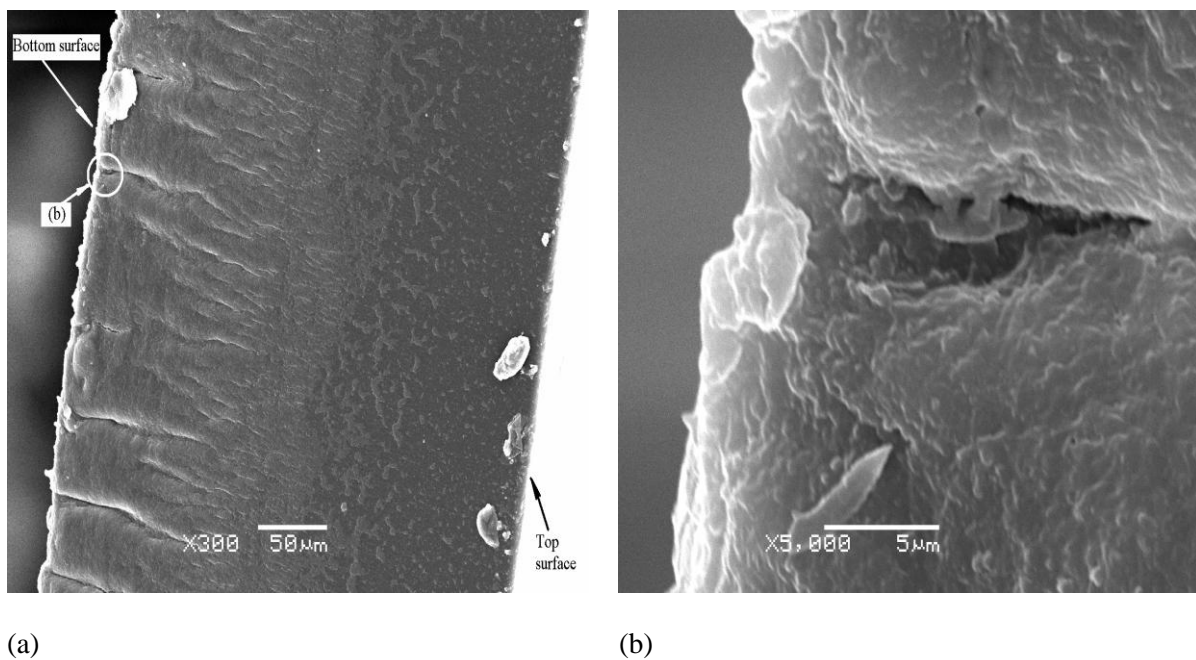
Fig. 4-6. The cross-section of interfacially formed PDMAEMA film (crosslinker concentration 1 g/L, crosslinking time 24 h, rinsing time 6 days). A magnified view is shown in (b).

The above analysis demonstrates the asymmetric structure of the PDMAEMA layer in the interfacial composite membrane after water "erosion". There are more unreacted tertiary amino groups near the substrate than at the top surface, which is considered favourable for facilitating the permeation of CO_2.

4.3.2 Surface Free Energy

It is well known that the permeability of a gas in a dense membrane depends mainly on the solubility and diffusivity. The polymer chain segments movement is limited in dry membranes. For hydrophilic membranes, the membrane can be swollen by water vapor, which is present in the combustion flue gas. The membrane resistance to the gas transport can be reduced due to the higher mobility of polymer chains and the enhanced solubility of CO_2 in the water swollen membranes. Therefore, it is anticipated that membranes with high hydrophilicity will favour the permeation of CO_2 through the membrane in the presence of

water vapor. Contact angle measurements were conducted to assess the surface hydrophilicity and the surface free energy of PDMAEMA crosslinked by XDC.

The contact angle was mainly determined by the surface properties, and the surface properties of the interfacially crosslinked membrane are not significantly influenced by the interior PDMAEMA beneath the surface with a lower degree of crosslinking. In addition to measuring the contact angle of water on the membrane surface that can be used to characterize the hydrophilicity of the membrane surface, contact angle measurements with different probe liquids were performed to obtain additional surface thermodynamic information that is unavailable from water contact angle data alone.

The total surface free energy, γ^{Tot}, can be considered to consist of two components [van Oss, et al. 1987]; one is the apolar or Lifshitz–van der Waals component γ^{LW} (which includes London dispersion, Debye induction, and Keesom orientation forces), and the other is the polar or Lewis acid–base component γ^{AB} that depends on the electron-donor (Lewis base) (γ^-) and electron-acceptor (Lewis acid) (γ^+) properties:

$$\gamma^{Tot} = \gamma^{LW} + \gamma^{AB} \qquad (4\text{-}2)$$

where $\gamma^{AB} = 2\sqrt{\gamma^- \gamma^+}$. The total work of adhesion is given by [Köstler et al, 2005]:

$$W_a = (1 + \cos\beta)\gamma_L^{Tot} = 2\sqrt{\gamma_S^{LW}\gamma_L^{LW}} + 2\sqrt{\gamma_S^+\gamma_L^-} + 2\sqrt{\gamma_S^-\gamma_L^+} \qquad (4\text{-}3)$$

where subscripts S and L indicate the solid phase and liquid phase, respectively. Eq. (4-3) implies that the contact angles of at least three different probe liquids (with known surface free energy values) on the solid surface are needed to determine three surface free energy components of a solid (γ_S^{LW}, γ_S^+ and γ_S^-) mathematically [Wu et al., 1995]. A group of liquids consisting of two polar and one apolar liquid are frequently used in the literature, but minor uncertainties in the known or measured quantities may lead to unrealistic results when solving a set of three linear equations [Köstler et al, 2005; Volpe and Siboni, 1997; 2000]. To increase the accuracy of the estimation, five probe liquids (four polar and one apolar) were used in the present work. The surface free energy components of the probe liquids are shown

in Table 4-1. The unknowns $\sqrt{\gamma_S^{LW}}$, $\sqrt{\gamma_S^+}$, and $\sqrt{\gamma_S^-}$ were solved from Eq. (4-3) by the least square regression.

Table 4-1. Literature values (in mJ/m²) of electron-acceptor γ_L^+, electron-donor γ_L^- and Lifshitz–van der Waals γ_L^{LW} components of liquid surface free energy γ_L^{Tot} at 20 °C [Wu et al, 1995]

Liquid	γ_L^+	γ_L^-	γ_L^{AB}	γ_L^{LW}	γ_L^{Tot}
Water	25.5	25.5	51.0	21.8	72.8
Glycerol	3.92	57.4	30.0	34.0	64.0
Formamide	2.28	39.6	19.0	39.0	58.0
Ethylene glycol	1.92	47.0	19.0	29.0	48.0
Diiodomethane	0	0	0	50.8	50.8

Fig. 4-7 shows the contact angle of water on the membrane surface and the corresponding work of adhesion at different concentrations of XDC in the crosslinking solution during interfacial crosslinking. Clearly, the contact angle of water on the membrane surface was reduced by the interfacial crosslinking, leading to an increase in the work of adhesion. PDMAEMA is known to have a high hydrophilicity, and the surface crosslinking can prevent PDMAEMA from dissolving in water. The increase in the surface hydrophilicity of the membrane caused by the crosslinking is attributed to the higher hydrophilicity of quaternary ammonium salt formed by the crosslinking than that of the tertiary amines in the uncrosslinked PDMAEMA. When the majority of tertiary amino groups on the membrane surface are converted to $-R_4N^+$ groups, further quaternization of the amino groups beneath the surface layer will not affect the $-R_4N^+$ groups on the membrane surface any more, and consequently the surface hydrophilicity of the membrane will essentially remain the same when the XDC concentration is high enough. It should be pointed out that after crosslinking,

the membrane became more stable because of the crosslinked structure whereas the membrane surface hydrophilicity was increased. Baines et al. [1996] also observed that quaternization of the amino groups in the PDMAEMA component in a PDMAEMA-*b*-MMA block copolymer greatly enhanced its water uptake in aqueous solutions.
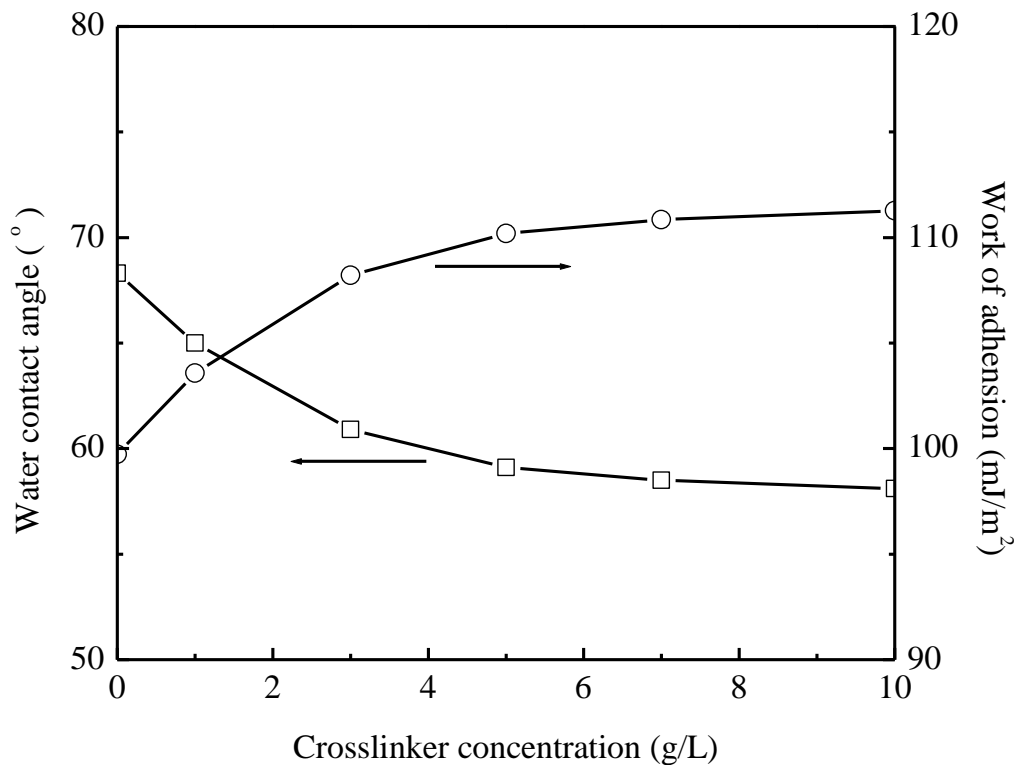
Fig. 4-7. Contact angle and work of adhesion of water on membrane surface as a function of crosslinker concentration (concentration of PDMAEMA in coating solution 15 g/L, coating time 15 min, crosslinking time 5 h).

To determine the surface energy properties, the contact angles of diiodomethane, glycerol, formamide and ethylene glycol were also measured on the membrane surface; the experimental data are presented in Table 4-2. Although diiodomethane is an apolar solvent,

the contact angle was found to be even lower than other polar solvents. This could be due to the strong interaction between diiodomethane and the tertiary amino groups on PDMAEMA membranes. For glycerol, formamide and ethylene glycol, which are all water-miscible, the contact angles decreased with an increase in the degree of crosslinking. However, when the concentration of crosslinking agent is high enough, there is no further change in the contact angles. This further indicates the increased hydrophilicity of the crosslinked PDMAEMA.

Table 4-2. Contact angles (in °) of different liquids on the PDMAEMA membrane surfaces interfacially crosslinked at different XDC concentrations

XDC concentration (g/L)	Water	glycerol	formamide	ethylene glycol	diiodomethane
0	68.3±1.0	64.0±2.8	57.5±3.0	41.5±1.0	32.0±1.2
1	65.0±0.7	60.8±1.8	55.0±4.5	39.0±1.4	29.2±2.5
3	60.9±0.2	55.2±5.0	46.0±1.7	37.9±1.4	27.9±1.3
5	59.1±0.9	53.3±3.0	41.7±1.2	37.1±1.2	29.5±1.2
7	58.5±1.3	53.0±1.3	39.7±1.3	37.0±3.5	28.3±1.5
10	58.1±1.7	53.0±2.9	38.5±1.3	37.5±3.5	29.9±1.5

The surface free energy data calculated from the contact angle values were listed in Table 4-3. The total surface free energy of the membranes prepared under various crosslinking conditions explored is in the range of 42.8–47.8 mJ/m². It is shown that the interfacial crosslinking leads to an increase in the surface free energy, and the polar component of the surface free energy is influenced by the interfacial reaction dramatically. This is expected considering the polar $-R_4N^+$ groups induced on the membrane surface by the crosslinking. On the other hand, the Lifshitz–van der Waals component did not change substantially, and it was around 45 mJ/m² for all samples. This is in agreement with the reported γ^{LW} values

which were found to be around 40–45 mJ/m^2 for almost all known polar polymer surfaces [van Oss, 1994]. The γ^+ component values were considerably small for all membrane samples. A small γ^+ value is an indication of residual hydration [van Oss et al., 1997; Farhat et al., 1999]. The increase in γ^+ with an increase in XDC concentration during interfacial crosslinking shows that more residual water can be retained in the surface layer as the surface becomes more hydrophilic. On the other hand, there is usually a strong correlation between the membrane hydrophilicity and γ^- value, and thus the value of γ^{AB}, which represents the overall polar component of surface free energy, is also a measure of the degree of residual hydration [van Oss et al., 1997]. It is mainly the increase in γ^{AB} caused by the crosslinking that results in a variation in the overall surface free energy of the membrane.

Table 4-3. The component and total surface free energy (in mJ/m^2) of PDMAEMA membranes

XDC concentration (g/L)	γ_S^{LW}	γ_S^+	γ_S^-	γ_S^{AB}	γ_S^{Tot}
0	42.7	0.000	14.5	0.07	42.8
1	43.9	0.001	16.7	0.24	44.1
3	44.9	0.046	18.7	1.84	46.7
5	44.5	0.109	19.7	2.93	47.4
7	45.1	0.103	20.0	2.86	48.0
10	44.6	0.124	20.4	3.18	47.8

4.3.3 Effect of Membrane Fabrication Parameters on Membrane Performance

The effects of various parameters involved in the membrane formation process on the permselectivity of the resulting membranes were investigated. The effect of PDMAEMA coating time on the permselectivity of the composite membranes was tested, and the results

are shown in Fig. 4-8. As the PDMAEMA coating time increases, more PDMAEMA will be deposited on the microporous membrane substrate. Consequently, the permeance of both CO_2 and N_2 decreases. The decrease in N_2 permeance appears to be more significant than CO_2, and the selectivity tends to increase slightly. When a sufficiently large amount of PDMAEMA was deposited onto the substrate so that the crosslinkable amino sites reach maximum on the membrane surface, a further increase in the coating time will not improve the membrane selectivity anymore, whereas the permeance will continue to decrease due to the increased PDMAEMA layer thickness. It is expected that after the PDMAEMA adsorption on the substrate reaches equilibrium, the coating time will no longer affect the membrane performance. The data in Fig. 4-8 show that under the experimental conditions tested, when the PDMAEMA deposition time is over 15 min, the deposition time has little impact on the membrane selectivity, and thus a coating time of 15 min was used in subsequent studies.

To study the effect of the polymer concentration in the PDMAEMA solution on the membrane performance, different concentrations of PDMAEMA–ethanol solutions were deposited on the PSF substrate for a given period of time (i.e., 15 min). The permselectivity of the resulting composite membranes is shown in Fig. 4-9. As one may expect, with an increase in the PDMAEMA concentration in the coating solution, both CO_2 and N_2 permeance decreased, whereas the CO_2/N_2 permeance ratio increased. At relatively low PDMAEMA concentrations (i.e., 5–15 g/L), the membrane selectivity increases significantly with an increase in the PDMAEMA concentration. However, at a PDMAEMA concentration greater than 15 g/L, the polymer concentration has little influence on the membrane selectivity. Compared with the composite membranes formed by bulk crosslinking, which have been reported in Chapter 3, the interfacially formed composite membranes have a higher permeance while the membrane selectivity is essentially the same. For example, at a PDMAEMA concentration of 20 g/L, the permeance of the interfacially crosslinked membrane was 67 GPU, while it is about three times the permeance of the bulk crosslinked membrane, whereas both membranes exhibited a CO_2/N_2 permeance ratio of around 50. The

Fig. 4-8. Effect of PDMAEMA deposition time on the permeation performance of the composite membranes. Concentration of PDMAEMA in coating solution 15 g/L, crosslinker concentration 10 g/L, and crosslinking time 5 h.
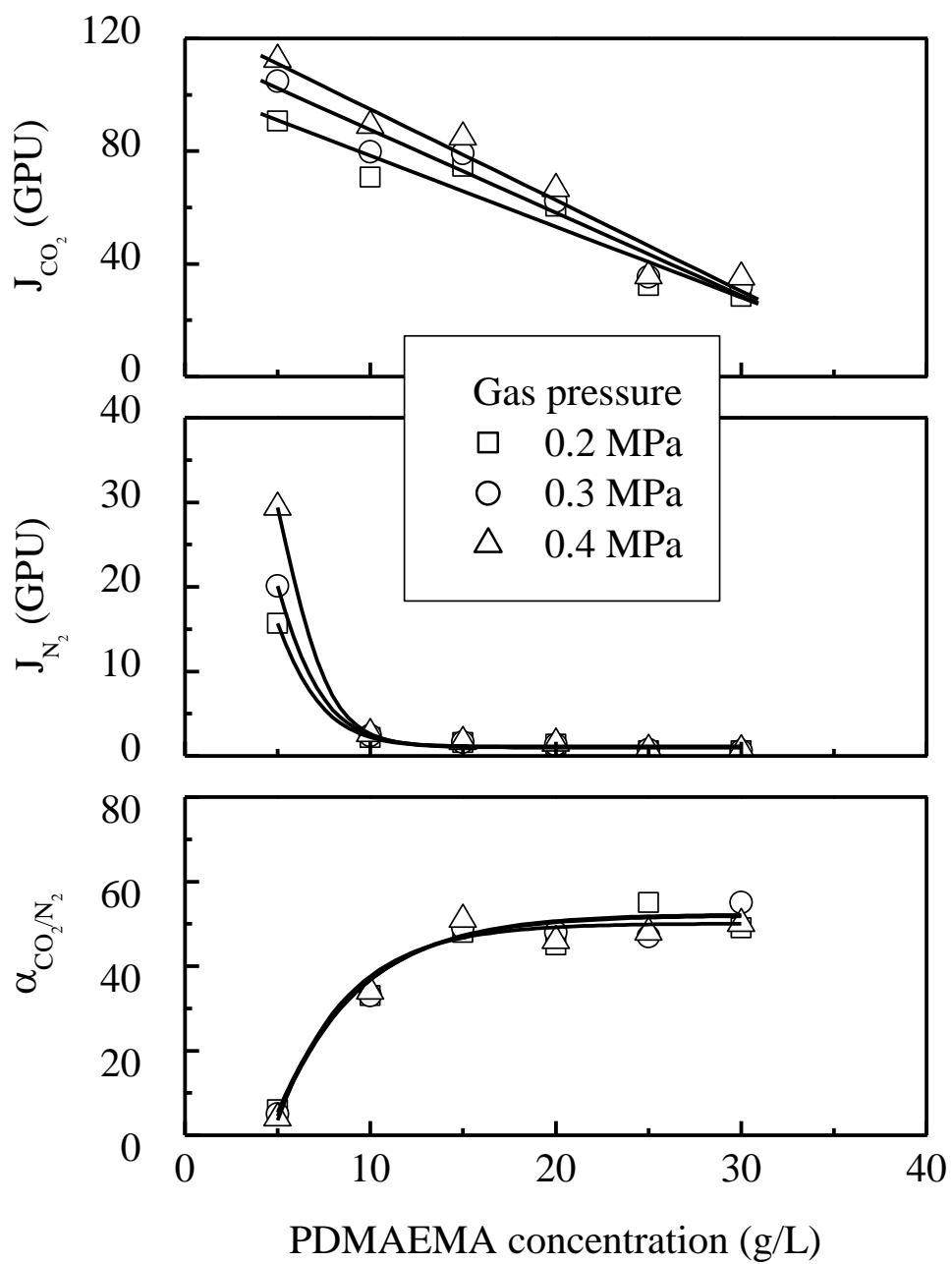
Fig. 4-9. Effect of PDMAEMA concentration on the permeation performance of the composite membranes. PDMAEMA coating time 15 min, crosslinker concentration 10 g/L, and crosslinking time 5 h.

cross sectional structure of the PDMAEMA/PSF composite membrane prepared by the interfacial crosslinking is shown in Fig. 4-10. Although the thickness of the PDMAEMA layer in the interfacially formed composite membrane (ca. 1.5 μm) is comparable with the bulk-crosslinked membrane, the higher permeance of the interfacial composite membrane is derived from its thin crosslinked layer. In the interfacially formed membrane, only the surface layer is highly crosslinked, which is responsible for the selectivity, whereas the less crosslinked loose structure beneath the surface layer has a high chain mobility that favors gas permeation. The permeance data demonstrate that the composite membranes with an interfacially crosslinked layer are more advantageous over the bulk-crosslinked composite membranes. By incorporating a gradient of crosslinking density, the membrane permeability can be improved without compromising the selectivity.
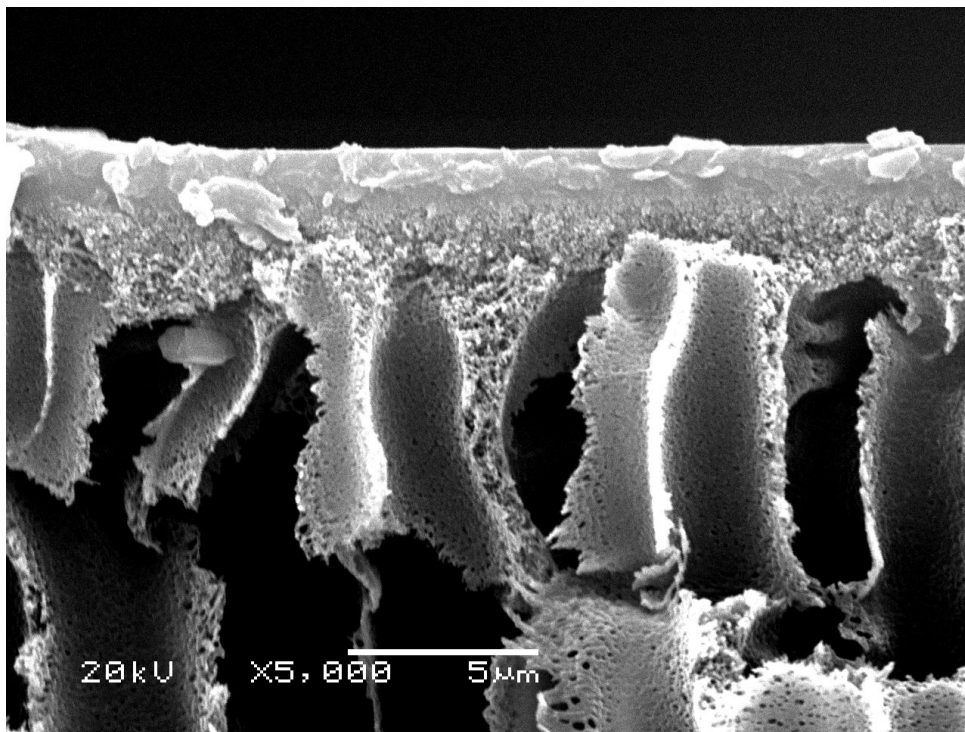
Fig. 4-10. Cross-section of a PDMAEMA/PSF composite membrane. Concentration of PDMAEMA in coating solution 15 g/L, coating time 15 min, crosslinker concentration 10 g/L, crosslinking time 5 h.

The effect of interfacial reaction time on the permselectivity of the composite membranes is shown in Fig. 4-11. As shown by the weight change analysis (see Fig. 4-4), the degree of crosslinking increases with the reaction time. The network structure of PDMAEMA becomes more rigid as the reaction time increases, and the mobility of the polymer chain segments decreases. Consequently, the gas permeance through the membrane decreases and the selectivity increases.

Fig. 4-12 shows the performance of the membranes prepared with different concentrations of crosslinking agent for a crosslinking time of 5 h. When the XDC concentration was low, the permeance of the membrane to CO_2 and N_2 was high, but the selectivity was quite low. As the crosslinker concentration increases, the degree of crosslinking on the membrane surface will increase, which tends to increase the membrane selectivity. However, at a higher concentration of XDC in the crosslinking solution, the crosslinking agent XDC will penetrate the PDMAEMA layer more deeply because of the large driving force for XDC to diffuse in PDMAEMA, resulting in a greater extent of crosslinking across the PDMAEMA layer. This tends to decrease the gas permeation flux. On the other hand, as mentioned before, the hydrophilicity of the PDMAEMA layer increases when crosslinked with XDC, and the membrane can accommodate more water molecules, thereby swelling the membrane and thus enhancing the CO_2 permeation. Therefore, the reduced polymer chain flexibility due to crosslinking is partially compensated by the increased free volume in the membrane. In addition, the presence of water molecules in the membrane also enhances the solubility aspect for CO_2 permeation because of the preferential dissolution of CO_2 in water over N_2. The above reasoning agrees with the permeance data shown in Fig. 4-11 and Fig. 4-12, where the decrease in CO_2 permeance is less significant than the decrease in N_2 permeance with an increase in the crosslinker concentration or crosslinking time.

Comparing the performance of interfacially formed PDMAEMA composite membranes with that of the bulk crosslinked counterpart, the asymmetric structure in the active layer of interfacially formed membranes favors the permeation of gases without compromising the selectivity. Therefore, the interfacially formed PDMAEMA composite membranes were tested further for separation of CO_2 mixtures and other applications in the following chapters.
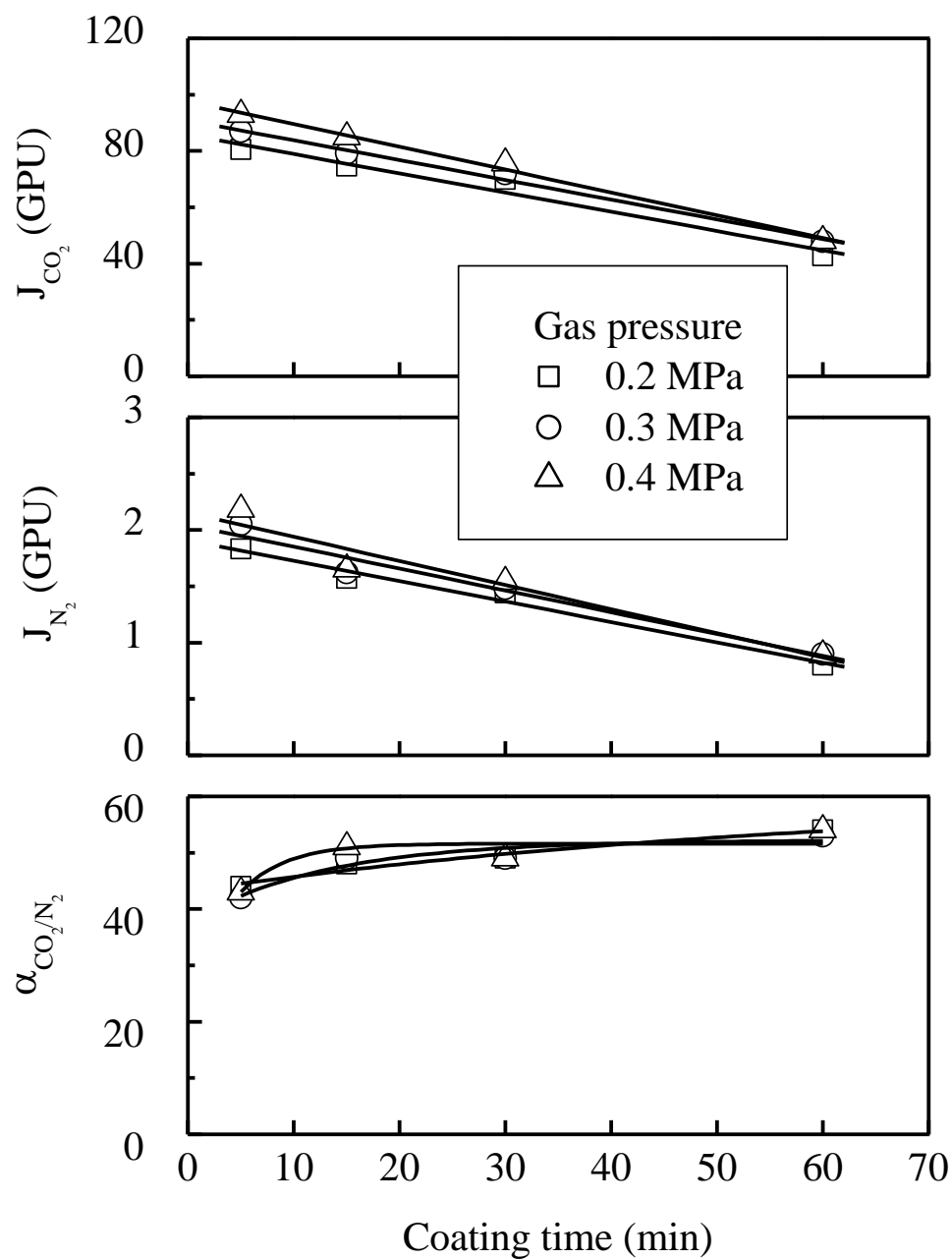
88
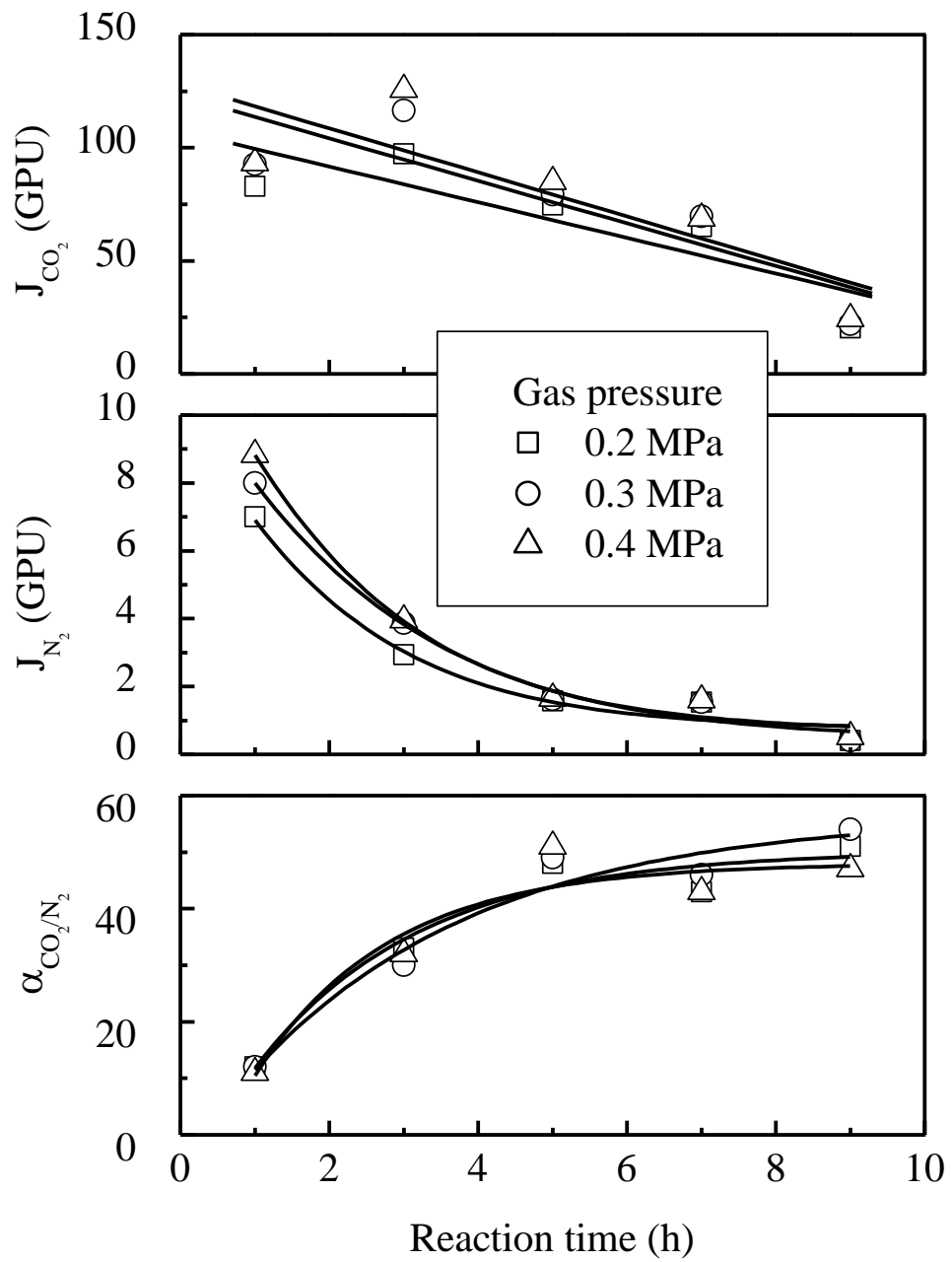
Fig. 4-11. Effect of crosslinking time on the permeation performance of the composite membranes. Concentration of PDMAEMA in coating solution 15 g/L, coating time 15 min, and crosslinker concentration 10 g/L.
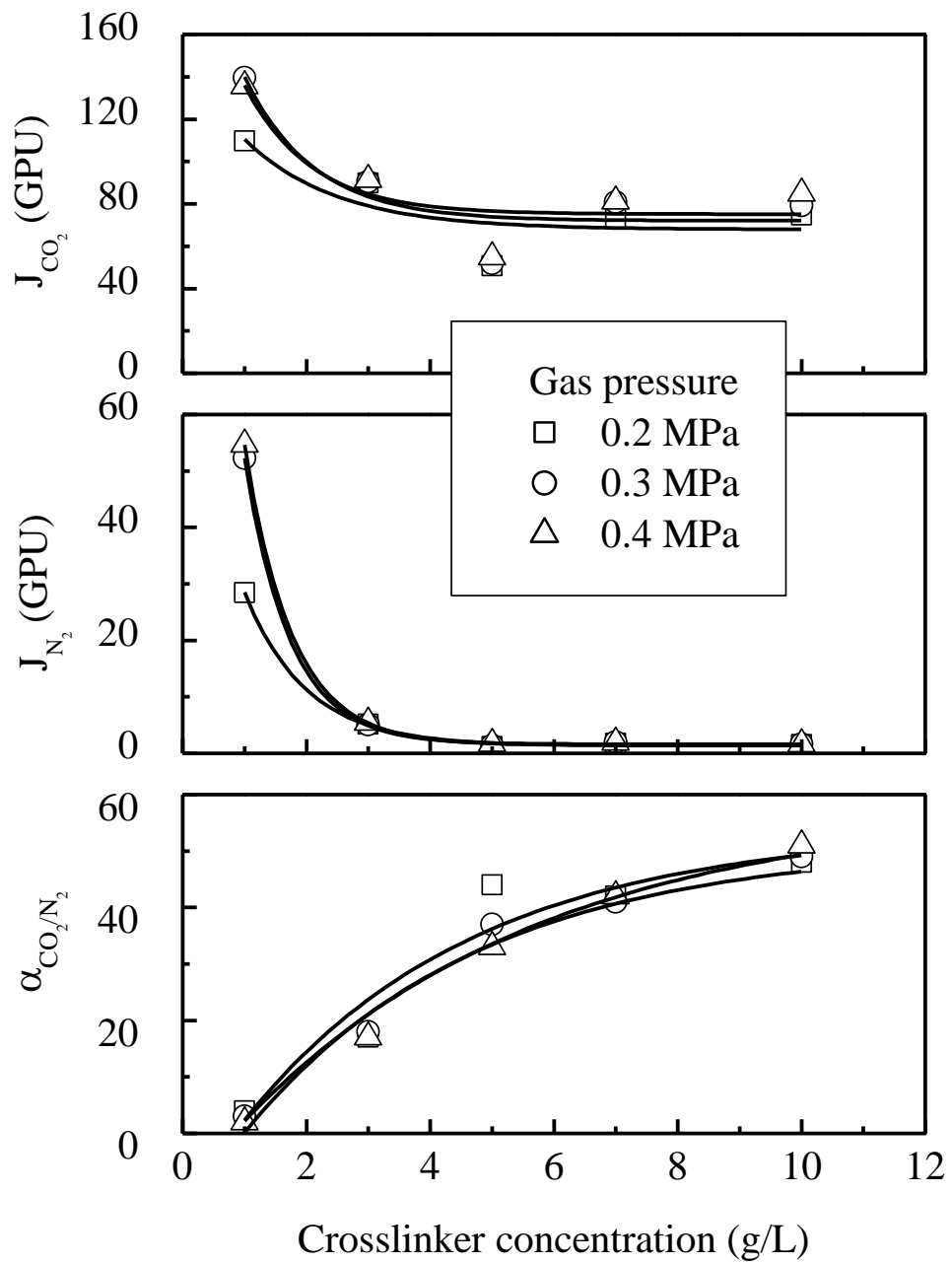
Fig. 4-12. Effect of crosslinker concentration on the performance of the composite membranes Concentration of PDMAEMA in coating solution 15 g/L, coating time 15 min, and crosslinking time 5 h.

4.4 Conclusions

Poly(N,N-dimethylaminoethyl methacrylate)/polysulfone (PDMAEMA/PDF) composite membranes were prepared via solid–liquid interfacial crosslinking. PDMAEMA was used as a reactive polymer to form the active layer, which was crosslinked by p-xylylene dichloride (XDC) through complete alkylation. It was shown that the permselectivity of the composite membranes was affected by the PDMAEMA concentration in the polymer coating solution, the coating time of the PDMAEMA solution, the concentration of the crosslinking agent and crosslinking time. The membrane was found to compare favorably with membranes prepared by bulk crosslinking. A three-fold increase in the membrane permeance for CO_2 permeation was achieved. At 23 °C and 0.41 MPa membranes with a CO_2 permeance of 85 GPU and a CO_2/N_2 permeance ratio of 50 were obtained at a crosslinker concentration of 10 g/L for a crosslinking time of 5 h.

Chapter 5

Gas Transport through PDMAEMA membranes

5.1 Introduction

For gas separations involving CO_2, the gas mixture is usually wet or saturated with water vapor. Normally water plays an important role in gas transport through a dense membrane based on the solution-diffusion mechanism. The diffusion of a gas through a membrane depends on the mobility of polymer segments and the size of the free volume. In a dry membrane, the mobility of polymer segments is limited, and the free volume is small. In a humidified membrane, on the other hand, the solubility of a gas can be improved by the dissolution and hydration in water. The mobility of the polymer segments and the size of the free volume tend to increase with water induced swelling of the membrane, and the resistance to diffusion of a gas thus decreases. As a result, the water sorbed in the membrane increases both the solubility and diffusivity of a gas in the membrane. Especially, the dissolved water molecules have a tendency to form clusters and distribute themsleves in the membrane into water paths as another transport passage when the water content in the membrane is high enough [Schult and Paul, 1996a]. In this case, the gas molecules will permeate through the water paths as well. As such, the gas transport in a water-swollen membrane can be regarded as the sum of the transport in the polymer matrix and the transport in the water phase. Because the solubility and diffusivity of a gas in water is usually much higher than in the polymer matrix, the permeability of a gas will be influenced by the water paths in the water-swollen membrane. Therefore, for hydrophilic membranes, the gas permeability can be improved significantly by the presence of water, though the thickness of the membrane may increase owing to the swelling by water. Higuchi et al. [1984] found that the permeability of O_2 in a wet cellophane membrane was about 10^4 times higher than that in a dry state because of the continuous water paths in the water wet membrane. Park and Lee [2001] also showed that for gas permeation through a water-swollen layer, the gas molecules mainly passed through the free volume, which was filled by water, resulting in improved gas

92

permeability. In this chapter, the effect of water on the gas transport of CO_2 and N_2 through PDMAEMA membranes was investigated.

For gas mixtures, the presence of one component may affect the permeation of the other, which is called a coupling effect. This effect arises as a result of interactions between the components in the mixture or with the polymer. Consequently, the use of pure gas permeation data cannot reveal the coupling effects, which may be positive or negative. Positive coupling effect is caused by swelling or plasticizing of a polymer matrix. A permeant, particularly strongly sorbing permeant (e.g. CO_2, H_2O, VOCs), when the sorbed concentration in a polymer matrix is high enough, can induce significant increases in the local segmental motion of the polymer, leading to an increased diffusion coefficient [Ismail and Lorna, 2002; Kapantaidakis et al., 2003]. Negative coupling effect is due to the competitive sorption and diffusion between components in a membrane. There are fixed amounts of sorption sites and transport pathways in a membrane which will get "saturated" or "occupied" at a certain sorbed concentration. The competition among the competing components for the limited number of sorption sites and transport pathways causes depression of the permeability of one component by the other [Barrer, 1984; Barbari, 1989]. The plasticization and the competitive sorption and diffusion, which have opposite effects on gas permeation, influence the overall transport of mixed gas through membranes. Therefore, comparing with pure gas permeation, either an increase or a decrease or a constant in the permeability of one component due to the presence of another component is possible [Donohue, 1989; van den Broeke et al., 1999; Liu et al., 2005].

As mentioned previously, there is a great need for membrane-based CO_2 separation in many industrial fields such as flue gas separation, natural gas sweetening or hydrogen production. In this chapter, the effect of feed composition on the permeation and separation of several CO_2 mixtures (i.e., CO_2/N_2, CO_2/CH_4, and CO_2/H_2) was analysed by comparing with pure gas permeation data to investigate the influence of coupling effects on the permeation of mixed gases. The effects of other operating parameters (such as stage cut and feed pressure) on the performance of the membrane were also studied.

5.2 Experimental

5.2.1 Membrane Preparation

The PSF substrate membrane was prepared by the phase inversion technique using PVP as an additive; the detailed procedure has been described in Chapter 3. The interfacially formed PDMAEMA/PSF composite membrane was prepared by crosslinking a PDMAEMA layer on the PSF substrate with a heptane solution of XDC; the general procedure for PDMAEMA crosslinking was the same as that described in Chapter 4. In this chapter, 20 mL of 15 g/L PDMAEMA-ethanol solution was brought into contact with the surface of the PSF substrate for 15 min. Then the excess coating solution was removed, followed by air drying in a fume hood. The coated PDMAEMA surface was exposed to 20 mL of 10 g/L XDC-heptane solution and an alkylation reaction took place on the solid-liquid interface. After 5 h of reaction, the excess crosslinking agent was removed and the membrane surface was washed with heptane three times to remove the remaining XDC on the membrane surface before the membrane was air dried.

5.2.2 Gas Permeation Measurements

The gas permeation measurements were carried out by the traditional volumetric technique. The experimental procedure and apparatus for pure gas permeation measurements were the same as used before (see Chapter 3). A schematic diagram of the apparatus for binary mixed gas permeation measurements is shown in Fig. 5-1. The PDMAEMA/PSF composite membrane was mounted in the permeation cell, which had an effective permeation area of 16.6 cm^2. The feed gas was humidified by passing through a water bubbler before admission to the feed side of the membrane, and the permeate gas exited at atmospheric pressure from the downstream side of the membrane. For dry gas permeation experiment, the humidifier was removed. The operating temperature was maintained at 23°C. The gas composition in binary feed mixtures was controlled by two Matheson mass flow controllers (Model 8270). To evaluate the effect of feed flow rate, pre-mixed binary gas mixtures containing 15 %, 10 % or 5 % CO_2 (balance N_2) were used as the feed, instead of using the on-line mixing system. The residue flow rate was controlled by a mass flow controller. For the tests on the

effects of feed pressure and composition, a relative high residue flow rate (about 60 cm^3(STP)/min) was used in order to minimize the concentration polarization. The flow rates of the permeate and residue streams were measured by bubble flow meters. The compositions of the feed, residue and permeate were determined by an Agilent on-line gas chromatograph (Model 6890N) equipped with a packed column (60/80 mesh Carboxen-1000, 15' × 1/8', Supel Co) and a thermal conductivity detector. The GC operating temperatures were 100°C, 103°C and 150°C for the oven, the injector and the detector, respectively. The permeance (J_i) of an individual component in the mixed gas through the membrane was evaluated by

$$J_i = \frac{Y_i Q_p}{A \Delta p_i}$$ (5-1)
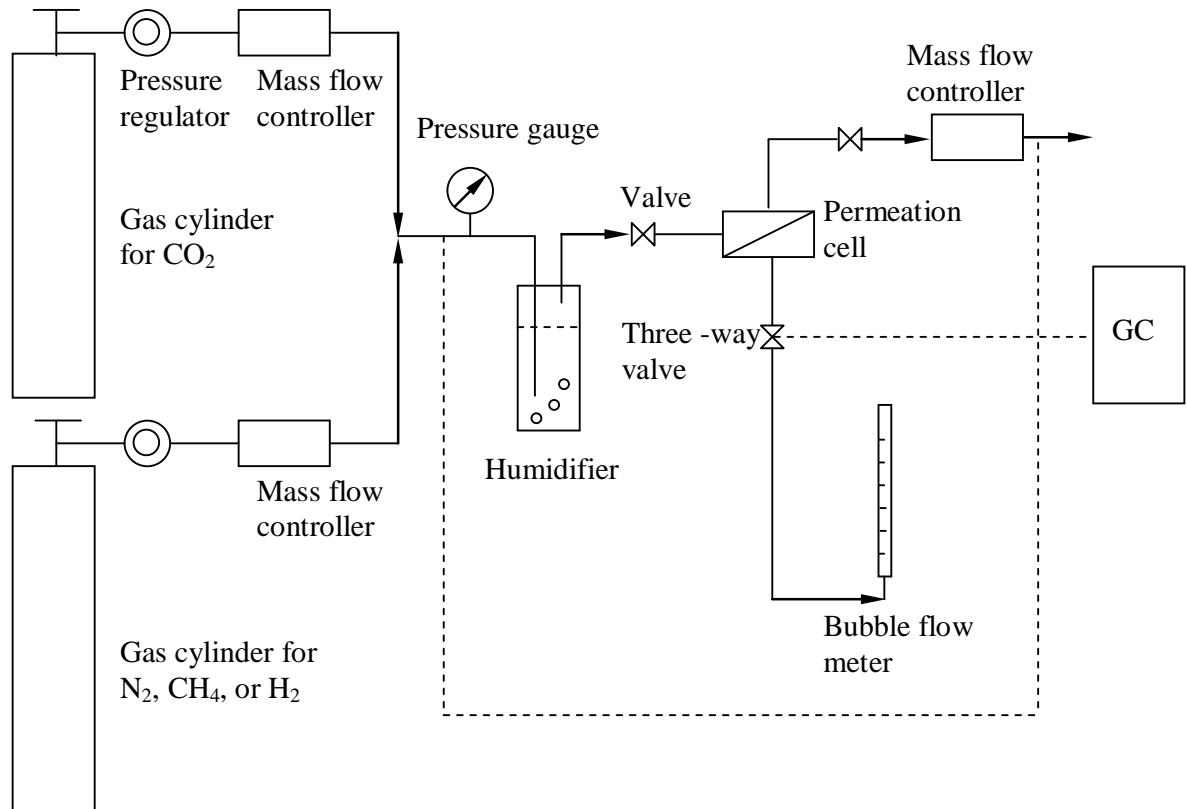
Fig. 5-1. Schematic diagram of experimental setup for mixed gas permeation.

where Q_p is the permeate flow rate, Y_i the mole fraction of gas i in permeate, A the effective area of the membrane, Δp_i the partial pressure difference of gas i across the membrane. Note that all flow rates or fluxes are reported at standard temperature and pressure (STP).

5.2.3 Water Content Measurement

The PDMAEMA membrane was prepared using a stainless steel mesh as the substrate, which does not sorb water, instead of the PSF substrate. The dried film samples of known weights were immersed in deionized water for 1 day at $23^{\circ}C$ to reach sorption equilibrium. Then the films were taken out of water, the water on the film surface was quickly wiped out with Kimwipes, and the film was weighed again. In order to calculate the volume fraction of water content in a swollen membrane, the overall density of the dry PDMAEMA layer was also measured: a PDMAEMA membrane was prepared with a PSF substrate of known weight and it was weighed again. The density of the PDMAEMA layer can be calculated from the area and thickness of the coating layer.

5.3 Results and Discussion

5.3.1 Effect of Water Vapor on Pure Gas Permeation

Figs. 5-2 and 5-3 show the permeation fluxes of CO_2 and N_2 through the composite membrane with and without the presence of water vapor. From Fig. 5-2 (b) and Fig. 5-3 (b), N_2 flux in the dry membrane was found to be proportional to the transmembrane pressure and the permeance was nearly constant, which shows that N_2 transport in the membrane occurs primarily by the simple solution-diffusion mechanism based on the molecular diffusion. While CO_2 transport, due to the interaction of CO_2 with the polymer, does not exhibit a constant permeability. In a dry state, there are two mechanisms for CO_2 transport in the membrane which occur simultaneously: free molecular diffusion and CO_2-carrier complex transport. When the pressure becomes high enough, the carriers available become saturated on the feed side, and the flux of CO_2 due to CO_2-carrier complex transport will approach a constant, while the flux due to free molecular diffusion will continue to increase with pressure. Therefore, the total flux contributed by these two modes of transport will increase
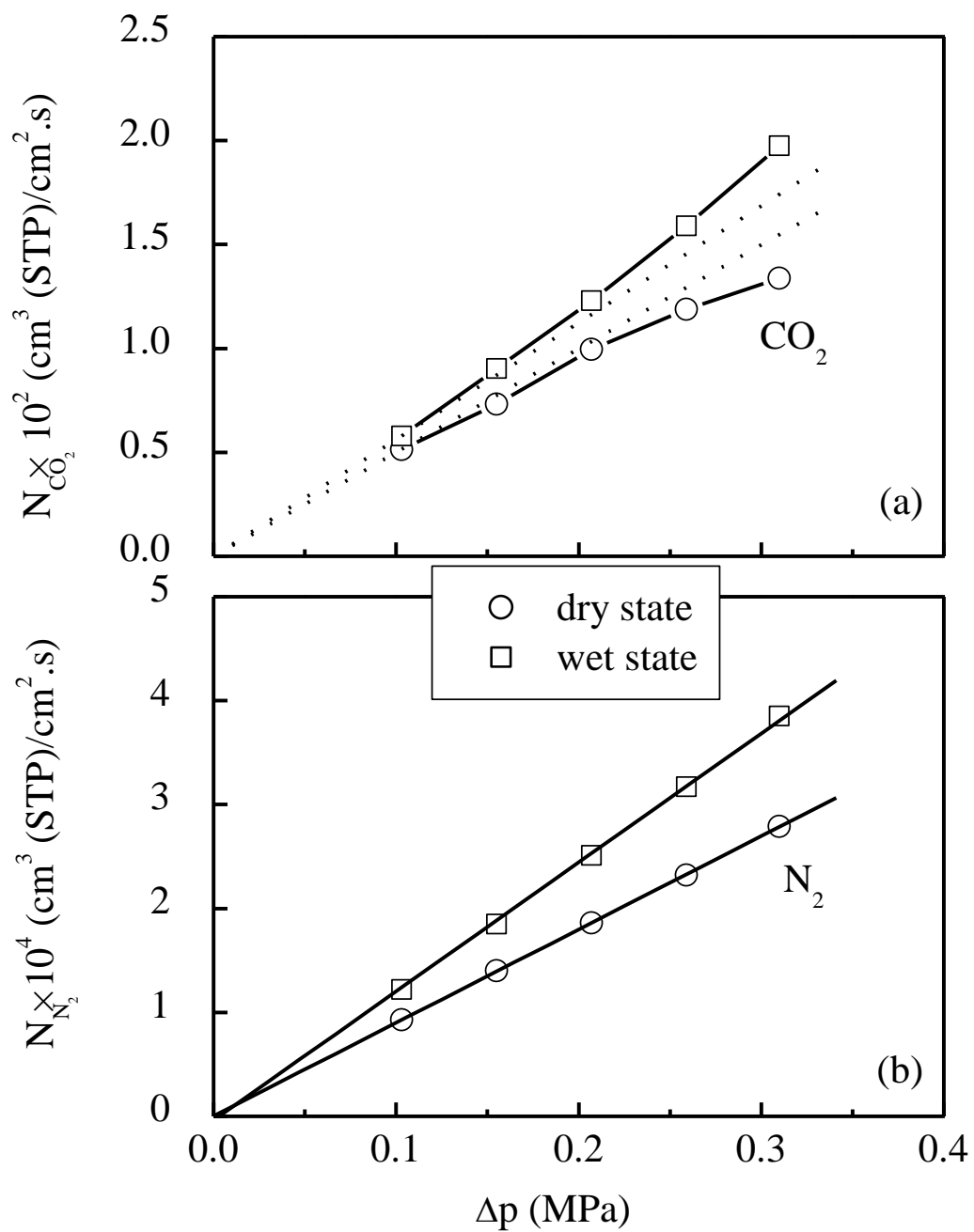
Fig. 5-2. Effects of pressure on the flux of CO_2 and N_2 through humidified and dry membranes.
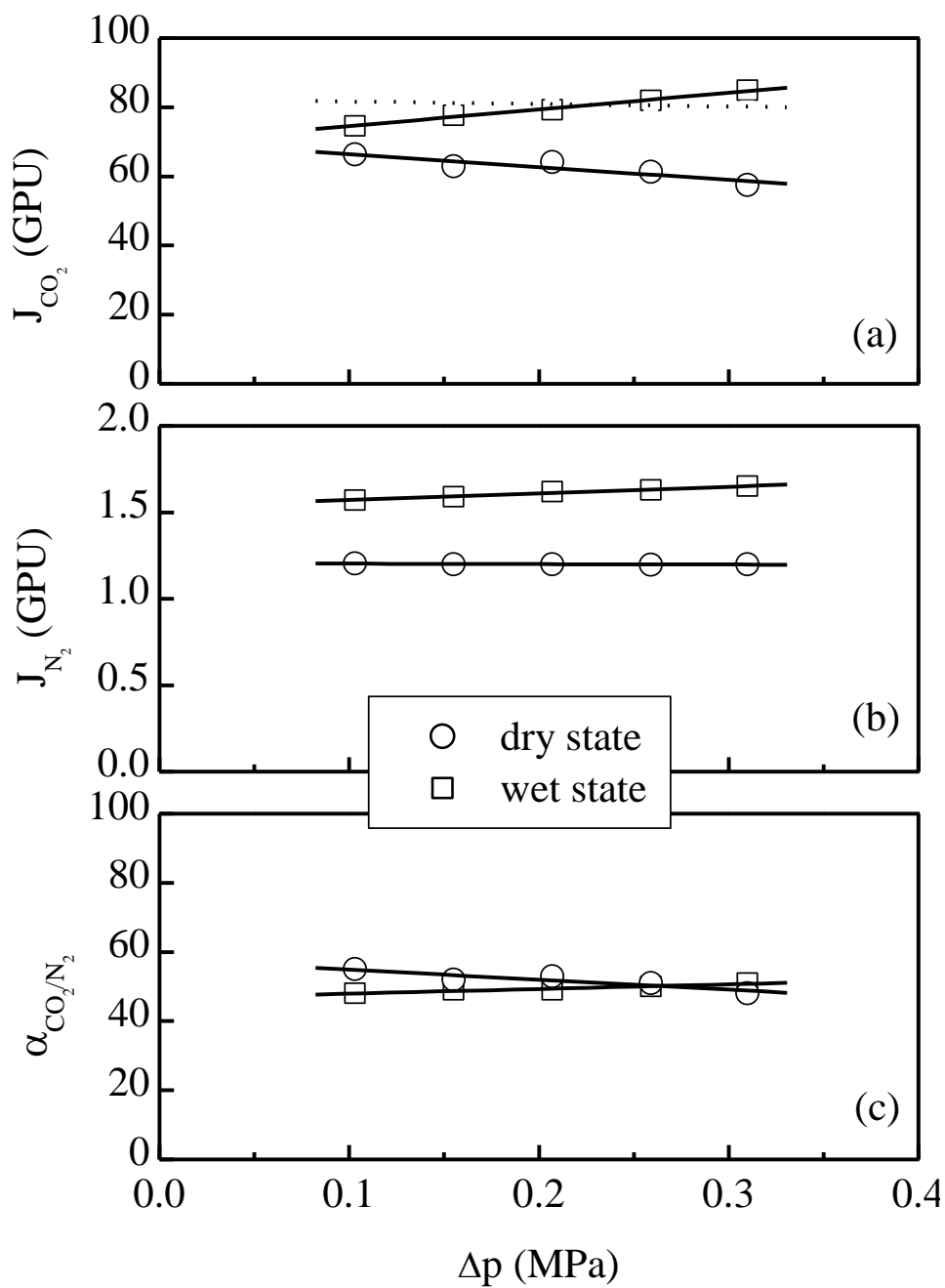
Fig. 5-3. Performance comparison of humidified and dry membranes.

more quickly at lower pressures, while the increasing trend will become slower with an increase in pressure because the carriers are gradually saturated by CO_2 in the feed, as shown in Fig. 5-2 (a). Accordingly, the permeance of CO_2 will decrease with an increase in pressure, as shown in Fig. 5-3 (a). These results are characteristic of the facilitated transport mechanism.

In a wet state, the permeance of a gas through a wet membrane J_w can be regarded as the summation of the permeance through the dry membrane J_d and that through the water path J_{H2O}:

$$J_w = J_d(1-\varepsilon) + J_{H2O}\varepsilon/\tau \tag{5-2}$$

$$J = \frac{P}{l} \tag{5-3}$$

where l is the thickness of the PDMAEMA layer (i.e., 1.5 μm); ε is the water content (volume fraction) in the water-saturated membrane that can be measured by weight and represents the swelling degree of a membrane; τ is the tortuosity of the water path and represents the chain entanglement in a dense membrane. Because N_2 is an inert gas to the polymer and water, the value of τ can be estimated from Eqs. (5-2) and (5-3) using permeation data of N_2 in the dry membrane and that in water. The solubility, diffusivity and the permeability of CO_2 and N_2 in water at 25°C are listed in Table 5-1 [Lide, 2007].

Table 5-1. Permselectivity of gas in water (25°C).

	S (cm^3/cm^3 emHg)	D (cm^2/s)	P (Barrer)	$\alpha_{CO2/N2}$
CO_2	1.01×10^{-2}	1.91×10^{-5}	1923	49.7
N_2	1.94×10^{-4}	2.00×10^{-5}	38.7	

The permeation of CO_2 through the humidified membrane, therefore, can be calculated from the CO_2 permeation data in the dry membrane and the calculated permeability data of

the water path. The results are shown in Fig. 5-3 (a) (dotted line). The calculated permeance of CO_2 through the humidified membrane is lower than the measured value at a high transmembrane pressure difference, demonstrating that the above simple parallel permeation model underestimates the CO_2 permeability at high pressures. It is known that in a wet state, CO_2 molecules can be transformed into small and easy-to-move ions HCO_3^-. Zhang et al. [2002c] characterized a humidified hydrolyzed polyvinylpyrrolidone composite membrane by FTIR with attenuated total reflectance technique and proved that there were complexes of CO_2 with active groups (i.e., secondary amine and carboxyl groups) and complex of CO_2 with H_2O (i.e., HCO_3^-) at the same time. The membrane material may also be subjected to hydration and dissociation in water to form quaternary ammonium cations, as discussed in Chapter 3. Matsuyama et al. [1996] proposed that in this case, the membrane should be called a fixed reaction site membrane or a catalysis membrane. The quaternary ammonium cations or tertiary amino groups can act as a weak base catalyst for the CO_2 hydration reaction. Therefore, in a humidified membrane, carrier facilitated transport of CO_2 through the functional groups in the membrane and water path take place simultaneously. The transport of CO_2 in the water path can be enhanced by the presence of amino groups, while the transport of CO_2 facilitated by the amino group carriers can be improved by the hydration of CO_2. The significance of the mutual effect between water and the amino groups will increase when the CO_2 concentration in the membrane is high.

However, unlike other hydrophilic membranes mentioned before, the gas permeability of both CO_2 and N_2 through the humidified PDMAEMA/PSF membrane was not substantially higher than that of the dry membrane. This is mainly due to the very low resistance of the interfacially crosslinked PDMAEMA layer. The high mobility of uncrosslinked side chains with amino groups beneath the ultrathin crosslinked outer surface results in an effective gas transport even in the absence of water. In terms of selectivity, Fig. 5-3 (c) shows that the ideal separation factor of CO_2/N_2 in the humidified membrane is lower than that in the dry membrane at low pressures; however, it gradually increases to exceed that in the dry membrane when the pressure is sufficiently high. This indicates that at a low CO_2

concentration, the intrinsic selectivity of the membrane measured in the dry state is higher than the intrinsic selectivity in water.

5.3.2 Effect of Stage Cut on Binary Gas Permeation

Stage cut is the ratio of permeate to feed flow rate and the value is in the range of 0 to 1. When a gas mixture passes the surface of a membrane, the driving force decreases gradually because of the permeation through the membrane. Figs. 5-4 and 5-5 show the CO_2 concentration in the permeate and the total permeation flux at various stage cuts. A high CO_2 concentration in permeate was accompanied with a high permeate flux. As the stage cut decreased, the flux and concentration of CO_2 in permeate increased. When the stage cut approaches zero, both the flux and concentration of CO_2 in permeate will reach a maximum, which can be viewed as the maximum obtainable separation of the membrane for a given feed composition. These values can be estimated by extrapolation to 0 stage cut (marked with "*"). Figs. 5-4 (b) and 5-5 (b) show respectively the influences of the stage cut on the permeate CO_2 concentration and total flux relative to their maximum obtainable values at 0 stage cut. Obviously, all these ratios are lower than 1, because the selective permeation always causes depletion of CO_2 in the feed stream. For the binary feed mixture with 15 % of CO_2, when the stage cut changed from 0.15 to 0.01, the relative permeate flux was from 0.81 to 0.98 and the relative CO_2 concentration in permeate was from 0.71 to 0.96. Interestingly, at a given stage cut, the feed concentration did not affect the relative permeate concentration significantly, but the relative permeation flux was affected remarkably by the feed concentration. In the following studies on the effects of feed pressure and composition on the separation of binary CO_2/N_2 mixtures, a stage cut of around 0.01 was maintained.

5.3.3 Effect of Operating Pressure on Binary Gas Permeation

Fig. 5-6 shows the permeation flux of CO_2/N_2 binary mixtures through the PDMAEMA/PSF membrane at different feed pressures (205 - 412 kPa). With an increase in the feed pressure, the total flux and the CO_2 mole fraction in the permeate increased. This trend indicates that a high feed pressure is favourable for the separation of CO_2 from N_2. Similar results on
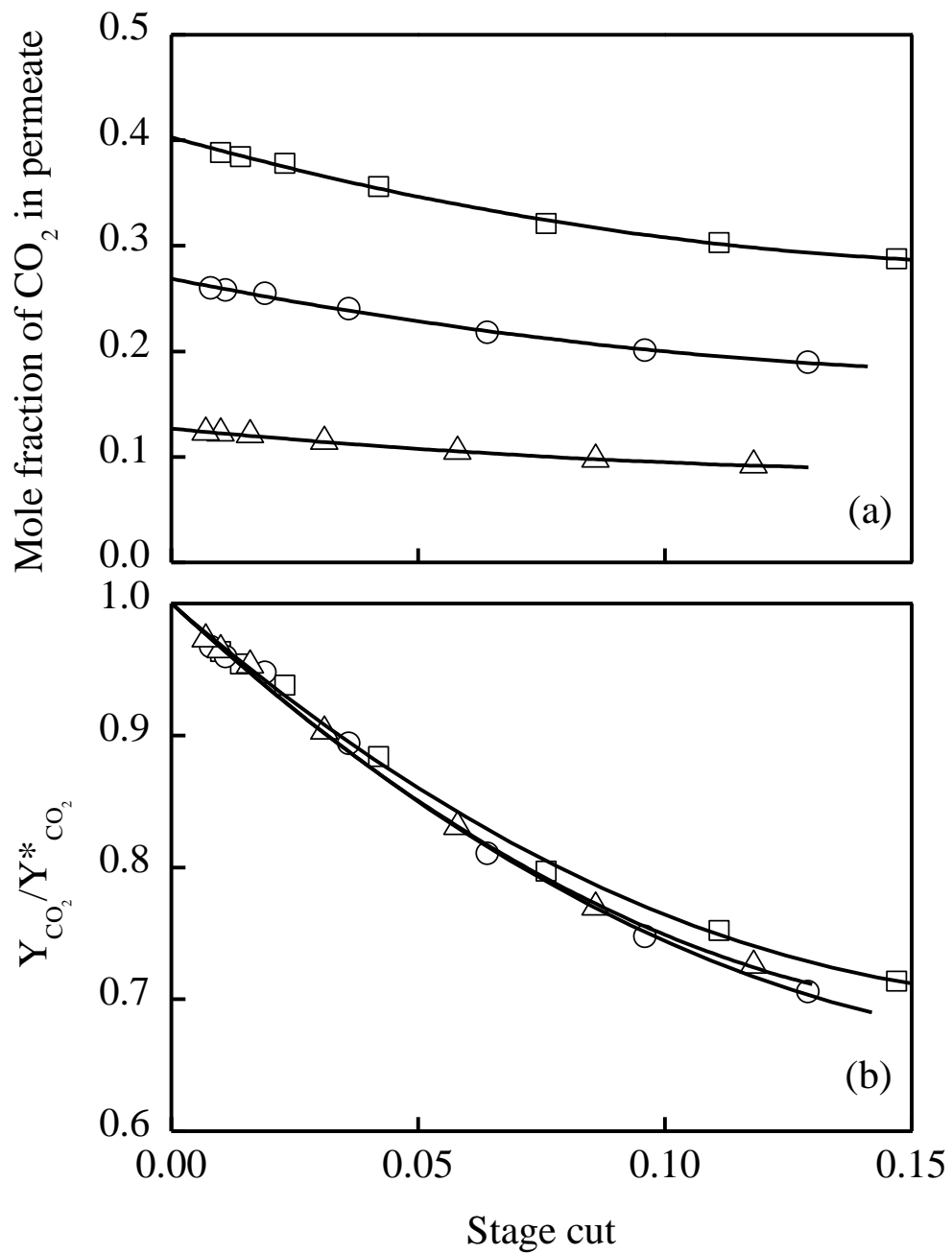
Fig. 5-4. Effect of stage cut on (a) permeate concentration, and (b) permeate concentration relative to the maximum obtainable permeate concentration. Feed pressure, 308 kPa; temperature, $23^{o}C$. ($\square$) 15 % CO_2; ($\circ$) 10 % CO_2; (Δ) 5 % CO_2.
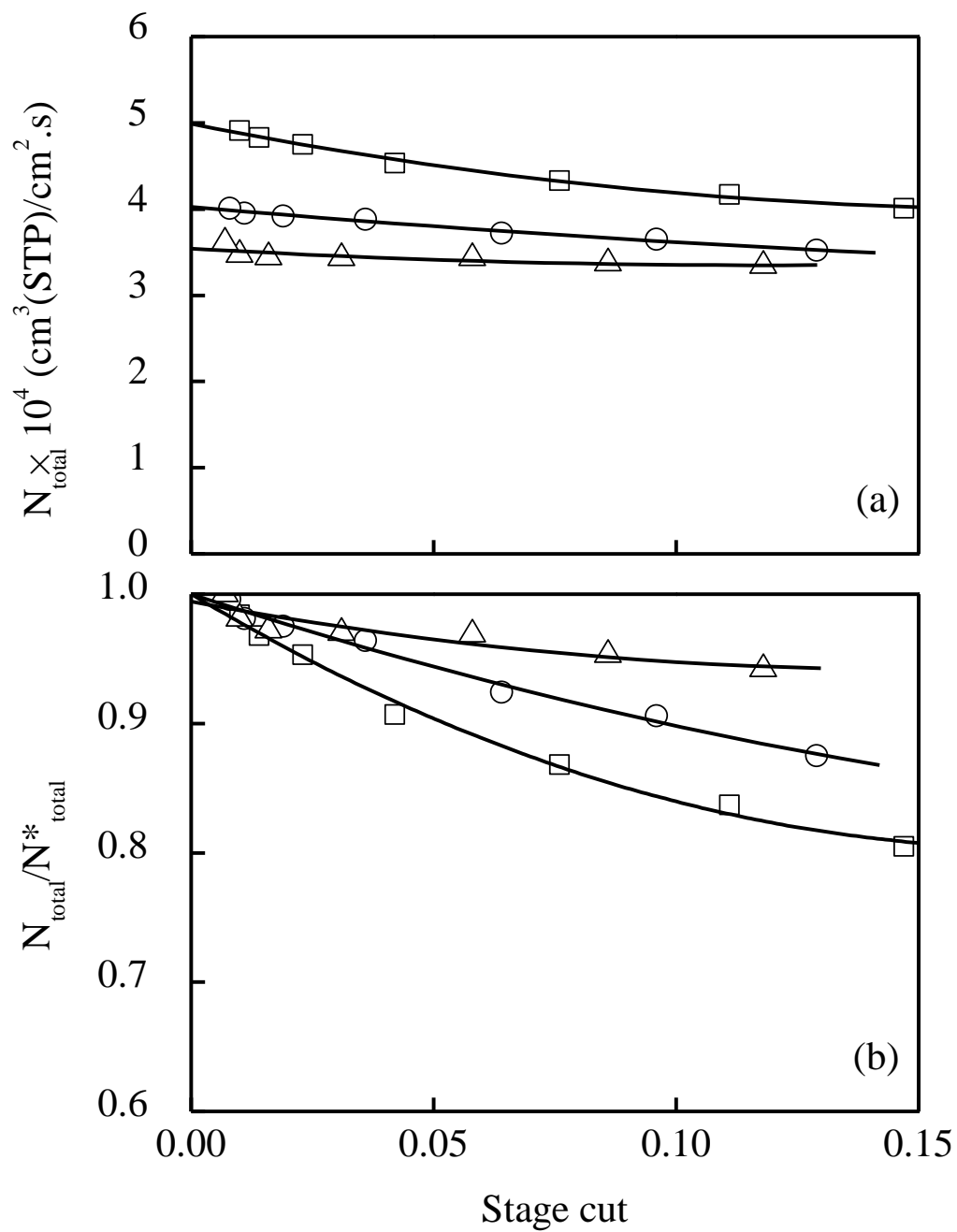
Fig. 5-5. Effect of stage cut on (a) total permeation flux, and (b) normalized permeate flux. Feed pressure, 308 kPa; temperature, 23°C. (□) 15 % CO_2; (○) 10 % CO_2; (Δ) 5 % CO_2.
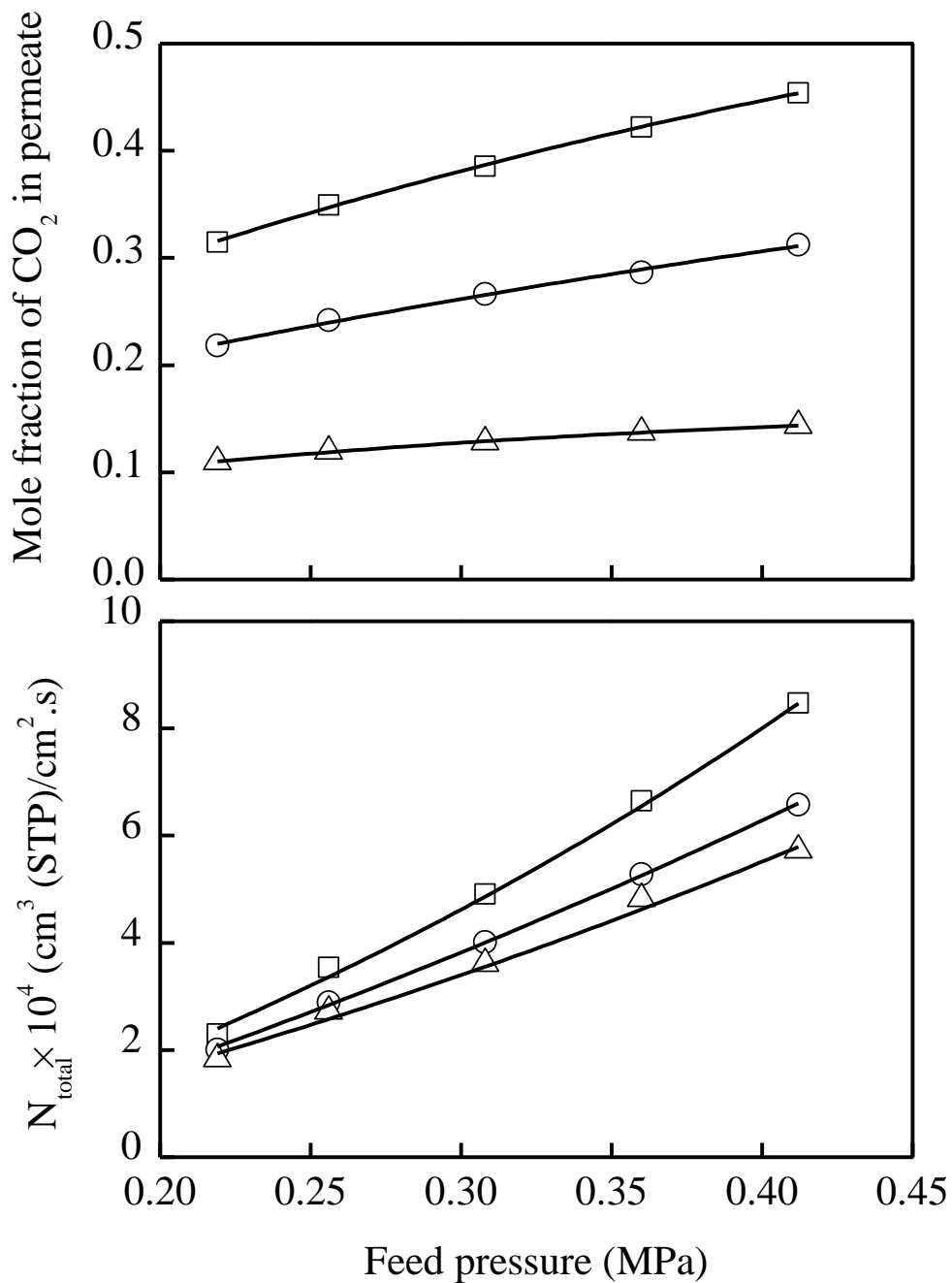
Fig. 5-6. Effect of feed pressure on (a) permeate concentration, and (b) total permeation flux for separation of CO_2/N_2 mixtures. (□) 15 % CO_2; (○) 10 % CO_2; (Δ) 5 % CO_2.

poly(dimethylsiloxane) membrane was reported by Wu et al. [2006]. Figs. 5-7 and 5-8 show the variation of the individual permeance of CO_2 and N_2 with their partial pressure differences. It was shown that at a given partial pressure difference, the permeance of CO_2 in the mixture increases as feed CO_2 concentration increases, while permeance of N_2 in the mixture did not change significantly. This indicates a negative coupling effect on the transport of CO_2, that is, CO_2 permeance was lowered by the presence of N_2.
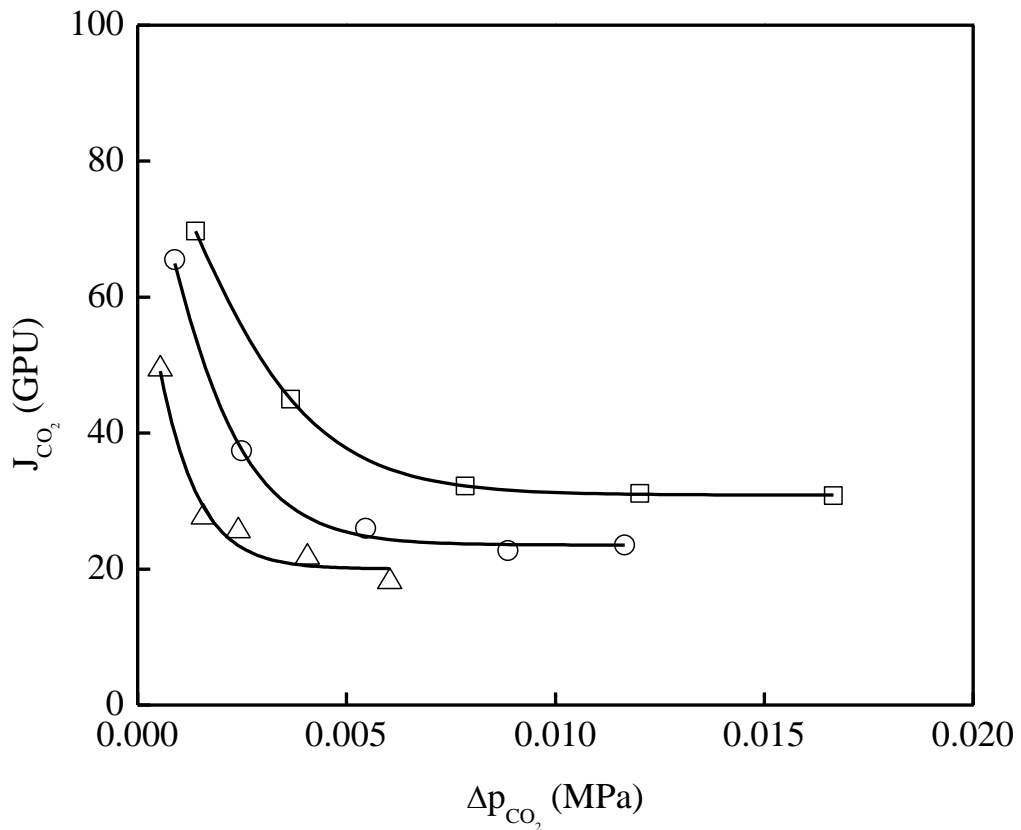
Fig. 5-7. Effect of CO_2 partial pressure difference across the membrane on permeance of CO_2 in CO_2/N_2 mixtures. ($\square$) 15 % CO_2; ($\circ$) 10 % CO_2; ($\triangle$) 5 % CO_2.
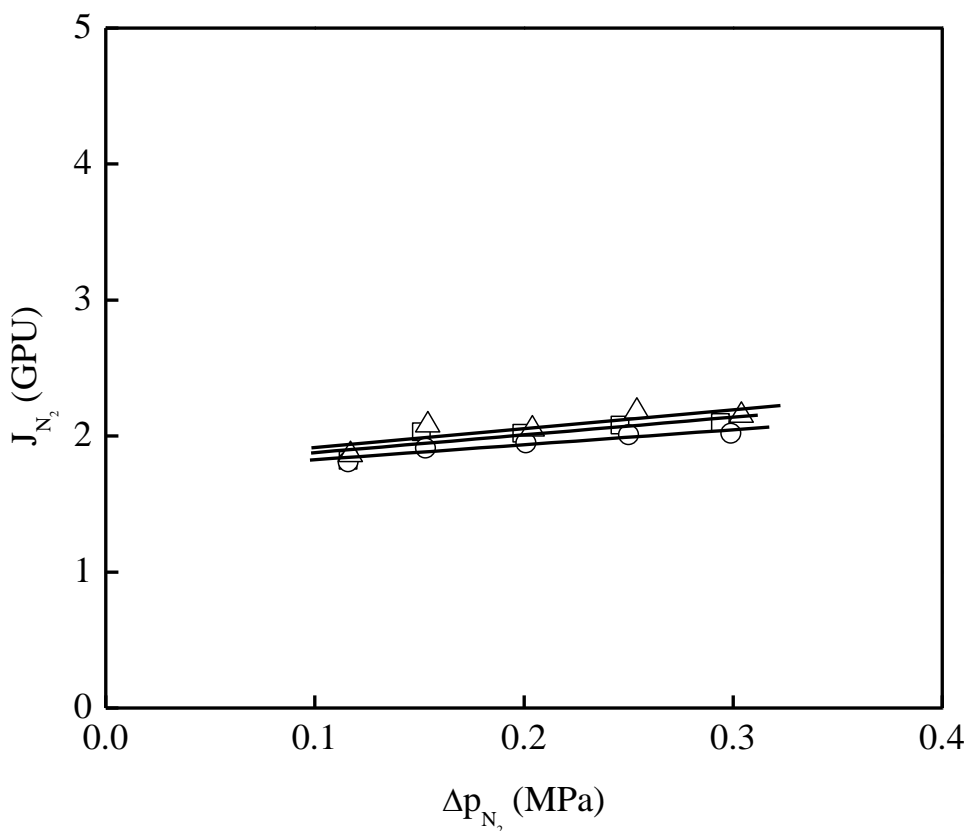
Fig. 5-8. Effect of N_2 partial pressure difference across the membrane on permeance of N_2 in CO_2/N_2 mixtures. (□) 15 % CO_2; (○) 10 % CO_2; (△) 5 % CO_2.

5.3.4 Effect of Feed Composition on Binary Gas Permeation

To investigate the coupling effects in mixed gas permeation, the permeation results of three binary mixtures, CO_2/N_2, CO_2/CH_4, and CO_2/H_2 with different feed compositions are shown in Fig. 5-9. Similar to N_2, both CH_4 and H_2 are inert gas to the PDMAEMA/PSF membrane. The feed pressure was kept constant at 308 kPa in all the measurements. The CO_2 mole fraction in the permeate and total permeation flux of the mixtures are shown as a function of the CO_2 mole fraction in the feed gas. The data presented in Fig. 5-9 (a) show that the permeate concentration of CO_2 is always larger than that in the feed, indicating that CO_2 is

106
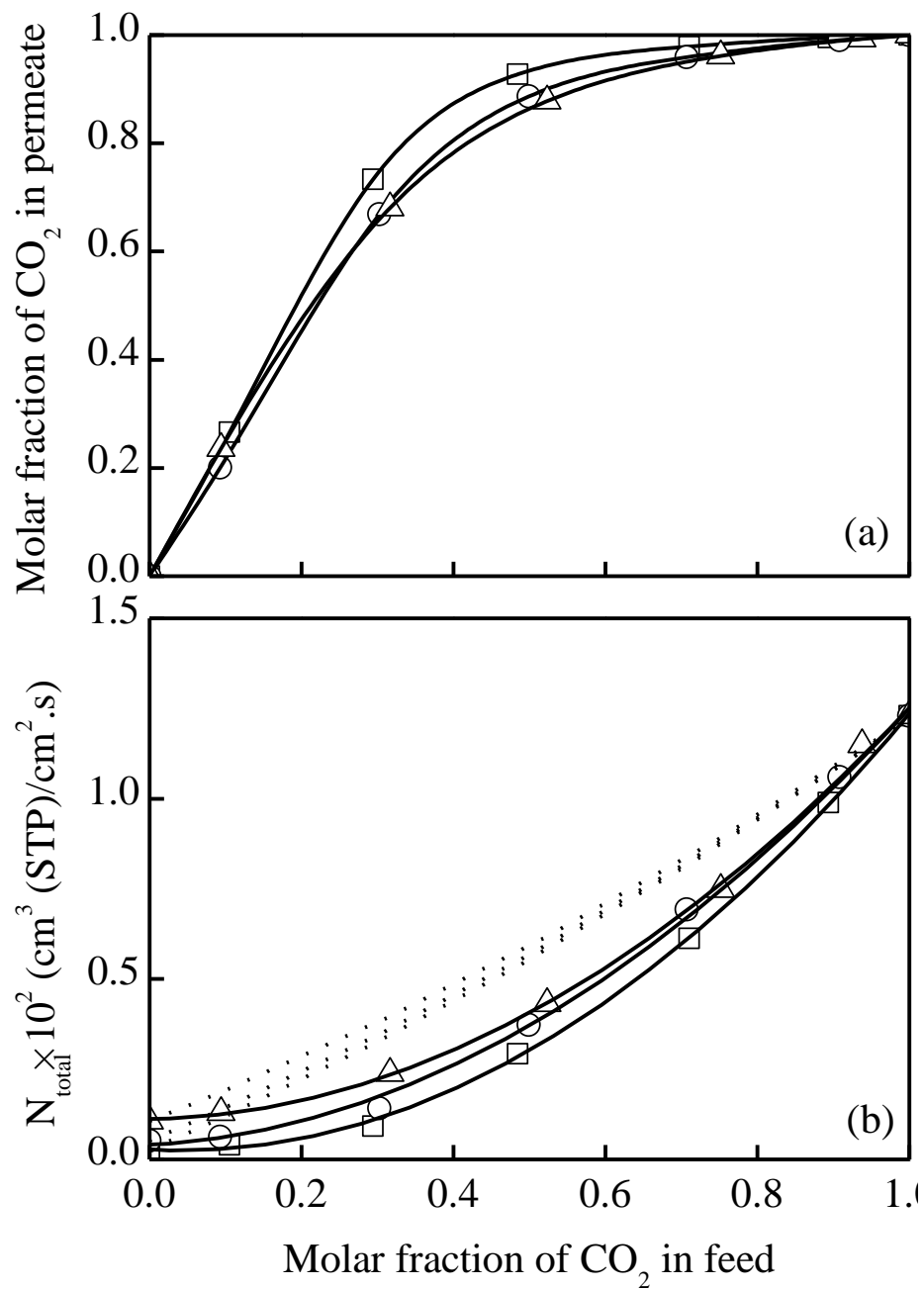
Fig. 5-9. Effect of feed concentration on (a) permeate concentration, and (b) total permeation flux for the permeation of (□) CO_2/N_2, (○) CO_2/CH_4 and (Δ) CO_2/H_2 mixtures. Feed pressure, 308 kPa. Dotted lines in (b) represents the ideal permeation flux.

preferentially transported in all the CO_2/N_2, CO_2/H_2 and CO_2/CH_4 mixtures regardless of feed concentrations. The CO_2 concentration in the permeate increased with an increase in CO_2 concentration in the feed. For all the binary gas mixtures studied, the incremental change in permeate CO_2 concentration appeared to be fast at CO_2 concentrations below 50 % but started to level off at higher CO_2 concentrations. Comparing the permeate concentrations of CO_2 of the three mixtures, the membrane selectivity to CO_2/N_2 is the highest, followed by CO_2/CH_4 and CO_2/H_2.

Fig. 5-9 (b) presents the total permeation fluxes of the mixed gases as compared to the ideal permeation fluxes represented by the dotted lines. The ideal permeation flux is calculated by summing up pure component permeation fluxes at pressures that are equal to the transmembrane partial pressures of the gas mixture [Dhingra and Marand, 1998] as

$$N_{total}^{o} = \sum (X_i N_i^{o})$$ (5-4)

where N_{total}^{o} is the total ideal permeation flux for a mixed gas system at feed pressure p_f, and N_i^{o} is the pure component permeation flux of gas i at a feed pressure $X_i p_f$. No interactions between the permeating gases were assumed for ideal permeation. As expected, with an increase in the mole fraction of CO_2 in the feed, the ideal total permeation flux increased.

To have a better understanding of the coupling effects between the permeating components in the mixtures, the individual permeation fluxes of the components in the mixed gas are plotted as a function of feed composition in Figs. 5-10 and 5-11. The dotted lines in the figures represent the ideal individual permeation flux. It is shown that the permeation fluxes of individual components increased with an increase in their concentrations in the feed. However, the CO_2 permeation flux from the mixtures was lower than pure CO_2 permeation flux at the same transmembrane CO_2 partial pressures. This means that CO_2 permeation was slowed down by the presence of other gases (e.g., N_2, CH_4, and H_2); as a result, the coupling has a negative effect on CO_2 transport. The magnitude of the coupling effect was affected by the feed concentration. When the feed CO_2 mole fraction was about 0.5, the reduction in CO_2 permeation reached its maximum. At a lower concentration of CO_2, due to the large amount of the inert gas, the competition for the limited active sorption sites and diffusion pathways

are significant; whereas at a higher CO_2 concentration, the partial pressure of the inert gas is low, the competitive sorption and diffusion of the inert gas become weaker. Fig. 5-10 also shows that the negative coupling effect on CO_2 flux seemed to be almost independent of the type of the inert gas in the feed mixture (e.g., N_2, CH_4, and H_2). Visser et al. [2005] reported similar results for the permeation of CO_2/N_2 and CO_2/CH_4 mixtures through polyethersulfone/polyimide membranes.
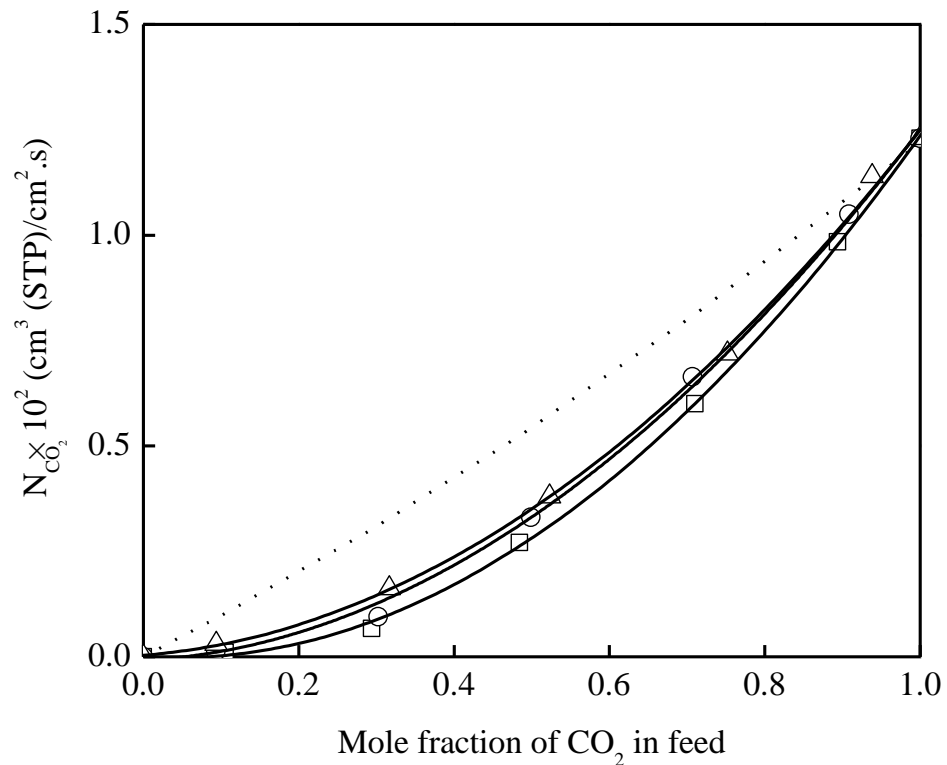
Fig. 5-10. Effect of CO_2 content in feed on partial permeation flux of CO_2 in (□) CO_2/N_2, (○) CO_2/CH_4 and (Δ) CO_2/H_2 mixtures. Feed pressure, 308 kPa. Dotted line represents the ideal permeation flux.

From Fig. 5-11, it appears that the permeation fluxes of N_2, CH_4 or H_2 in the mixtures are higher than the permeation flux of pure gases at pressures equal to the partial pressure in the mixture. With the presence of CO_2, CO_2-induced plasticization loosens the polymer matrix and increases the free volume and segmental mobility, enhancing the diffusivity of the membrane to the permeating species. Therefore, the inert gas permeation flux also increases. This indicates that the presence of CO_2 has a positive effect on the permeation of other permeating components (i.e., N_2, CH_4 and H_2).
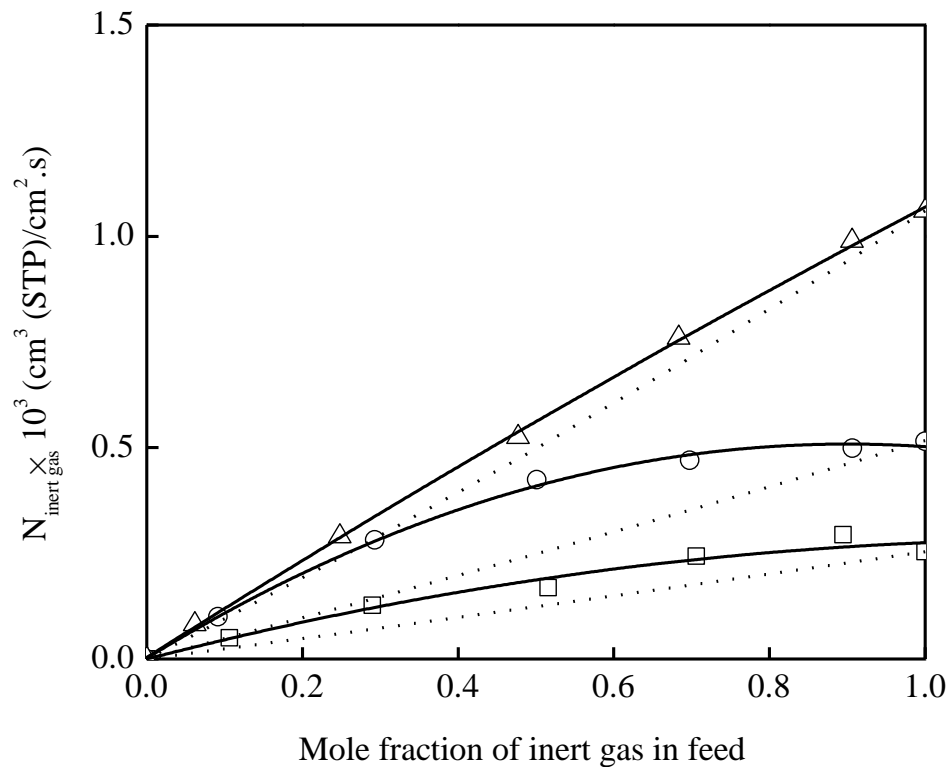
Fig. 5-11. Effect of inert gas (N_2, CH_4, or H_2) content in feed on partial permeation flux of inert gas in (□) CO_2/N_2, (○) CO_2/CH_4 and (Δ) CO_2/H_2 mixtures. Feed pressure, 308 kPa. Dotted line represents the ideal permeation flux.

Huang and Lin [1968] have defined a permeation ratio, θ, to measure the deviation of the actual permeation from the ideal permeation for pervaporation separation. The same concept can be used for gas permeation as well. The permeation ratio for the individual component i can be expressed as

$$\theta_i = \frac{N_i}{N_i^o} \qquad (5\text{-}5)$$

From Fig. 5-12, it is evident that the permeation ratio for inert gases increases with an
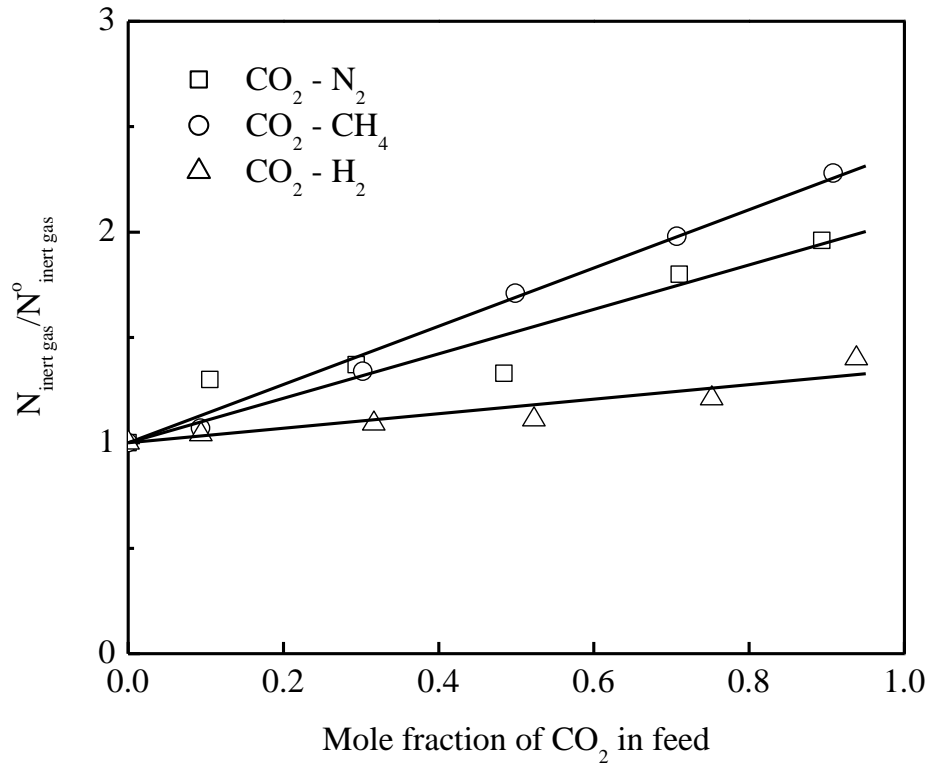
Fig. 5-12. Permeation ratio of N_2, CH_4 and H_2 in binary CO_2/N_2, CO_2/CH_4 and CO_2/H_2 mixtures at different CO_2 feed concentrations. Feed pressure, 308 kPa.

111

increase in the feed CO_2 concentration. It may be noticed that the H_2 permeation ratio is the lowest as compared to permeation of N_2 and CH_4. This result is due to hydrogen's small size, which enables it to diffuse through the membrane more easily. A further increase in the segmental motion of the membrane caused by the plasticization of CO_2 does not affect H_2 diffusivity as much as other gases with larger molecular sizes. As a result, the coupling effect of CO_2 for CO_2/H_2 mixture on H_2 permeation is less significant than on the permeation of N_2 and CH_4 for CO_2/N_2 and CO_2/CH_4 mixtures.

5.4 Conclusions

PDMAEMA/PSF composite membranes were prepared through solid-liquid interfacial crosslinking. The permeation of CO_2 and N_2 was studied with and without the presence of water vapor. The humidified membrane tended to be more permeable than the dry membrane, though the difference was not drastic due to the low resistance of the asymmetric crosslinking structure in PDMAEMA layer.

The PDMAEMA/PSF composite membrane was used to separate binary CO_2/N_2, CO_2/CH_4 and CO_2/H_2 mixtures. The effects of operating conditions (such as stage cut, feed pressure, and feed composition) on the membrane separation performance were studied. Decreasing the stage cut and increasing the feed pressure will increase the CO_2 concentration in the permeate. Increasing the feed CO_2 content led to an increase in the permeation fluxes of both components. The binary mixture permeation and single component permeation was compared in order to evaluate the coupling effect. It was shown that the presence of CO_2 enhanced the permeation of the other permeating components (e.g., N_2, CH_4 and H_2), while the CO_2 permeation was negatively affected by other components.

Chapter 6

Gas Dehydration and Humidification by PDMAEMA membranes

6.1 Introduction

Water vapor transport through polymeric membranes is important for gas dehydration and humidification. In natural gas processing, for example, the raw natural gas from the well is saturated with water. When temperature and pressure vary, the water vapor may condense in the pipeline, causing problems associated with corrosion of the pipeline and formation of solid methane hydrates which can block the pipeline. The water content should be reduced for transmission, storage, or as fuel. Conventionally, the natural gas is treated with absorbent for dehydration. Glycols are commonly used absorbent to dehydrate natural gas at the wellhead. This method is quite efficient for the removal of water from gas, but it involves complex plants with high space requirements which is not very suitable for offshore applications. Membrane dehydration is expected to provide an alternative to absorption operation. When raw natural gas passes through a membrane unit, water will preferentially permeate through the membrane, and dried natural gas is retained in the retentate. A hybrid process involving a membrane separation prior to absorption would also allow a longer cycle of absorption and regeneration, which help reduce energy consumption and prolong service life.

   Another promising application involving water vapor permeation is humidifier which can be used for humidity control as in fuel cells. The proton exchange membrane (PEM) fuel cell is considered as one of the most promising alternative power sources to compete with internal combustion due to its lower overall emission and higher efficiency. Water management is critical to the reliability of PEM fuel cells [Hyun and Kim, 2004]. If the membrane becomes too dry, the proton conductance will be reduced leading to an increased resistive loss and decreased power output, and the local hot spots can dramatically reduce the life of the membrane. On the other hand, excessive water present in the membrane will result in flooding of the cathode and cause the blockage of the gas flow channels, electrodes, and

113

backing layers. Therefore, it is crucial to control the membrane humidity of the fuel cells to avoid dehydration and flooding. At present, bubble humidifiers are widely used. To reduce the size and energy consumption of the humidification unit, membrane humidifiers can be adopted. This can be achieved by flowing the incoming dry gas to one side of a water permeable membrane and flowing the hot water on the other side of the membrane. The membrane will transfer the heat and water vapor from the wet side to the dry side without flooding problems.

At present, not much information on water vapor permeation for gas dehydration or humidification is available. In this chapter, water vapor permeation through PDMAEMA/polyacrylonitrile (PAN) composite membranes prepared with interfacial crosslinking was studied. The effects of the operating parameters (e.g., feed composition, temperature) and the resistance of the PAN substrate membrane on the performance of the membrane for natural gas dehydration was investigated. For the gas humidification, N_2 gas was used in the study and the humidification performance using a membrane humidifier at different gas flow rates and operating temperatures was evaluated. The results will be useful for membrane hydrator in PEM fuel cells or air conditioning systems.

6.2 Experimental

6.2.1 Materials

PAN ultrafiltration membranes with a molecular weight cutoff of 20,000 and a thickness of about 70 μm were supplied by Sepro Membranes. Other materials were used in the same manner as before.

6.2.2 Membrane Preparation

The PAN membranes were used as substrate and rinsed with deionized water before use. The PDMAEMA/PAN composite membranes were prepared by interfacial crosslinking of a PDMAEMA layer on a PAN membrane, similar to the PDMAEMA/PSF membrane described in Chapter 5. 20 mL of 15 g/L PDMAEMA ethanol solution was contacted with

the surface of PAN substrate for 15 min. After the excess solution was removed, the membrane was air dried. Next the so-formed thin PDMAEMA layer was contacted with 20 mL of 10 g/L *p*-xylylene dichloride (XDC) heptane solution for 5 h to achieve the interfacial crosslinking. Then the excess crosslinking solution was removed and the remaining XDC on the membrane was washed out with heptane before the membrane was air dried.

6.2.3 Permeation Test for Gas Dehydration

The permeance of methane through the composite membrane was measured with the traditional constant pressure-variable volume method, and the procedure and apparatus were the same as those described in Chapter 3. In the feed side, a CH_4 gas stream was saturated with water vapor by bubbling the gas through a porous sintered stainless steel ball immersed in water and then through a packed bed of glass balls to minimize carry over of the water mist.

The schematic diagram of the experimental setup for gas dehydration is shown in Fig. 6-1. In the feed side, a feed stream with a certain relative humidity was obtained by mixing a dry methane stream with a methane stream saturated with water. The flow rates of both gas streams were adjusted by mass flow controllers (Matheson Gas, Model 8270) and the humidity was controlled by adjusting the flow rates of the dry and wet streams. The mixed stream was fed continuously to the membrane and the total feed flow rate was kept at 1500 sccm. The bubble humidifier was kept at room temperature. The operating temperature of the permeation cell was controlled at $25{\sim}55^{o}C$ by a water bath. Upon introduction of feed into the permeation cell, water vapor and methane permeated through the membrane and the remainder of the feed left through the retentate line. A paraffin oil seal in the retentate line was used to prevent water vapor in the air from going back to the permeation system. The water contents in both the feed and retentate streams were measured by a dew point meter (Vaisala DRYCAP, Model DM70, Finland). The feed side was held at atmospheric pressure while the permeate side was kept at low pressure (usually 1.7 kPa) by a vacuum pump. The permeate pressure was varied by a needle valve and measured by a vacuum gauge. Water vapor that permeated through the membrane was condensed with a liquid nitrogen trap, and

115

its permeation rate was obtained by weighing the permeate water collected in the condenser for a given time. The water vapor permeance J_{vap} was obtained by the following equations:

$$Q_{vap} = AJ_{vap}(p_f X_{ave} - p_p Y) \tag{6-1}$$

$$Q_{CH4} = AJ_{CH4}[p_f(1 - X_{ave}) - p_p(1 - Y)] \tag{6-2}$$

$$Y = \frac{Q_{vap}}{Q_{vap} + Q_{CH4}} \tag{6-3}$$

where Qs are permeation rates (cm^3(STP)/s); p_f and p_p are the feed and permeate pressures (cmHg), respectively; X_{ave} the average water vapor concentration in the feed side of the membrane, taken as the average molar fractions of water vapor in feed and retentate, and Y the molar fraction of water vapor in permeate. Subscripts f and p represent the feed side and the permeate side, respectively.
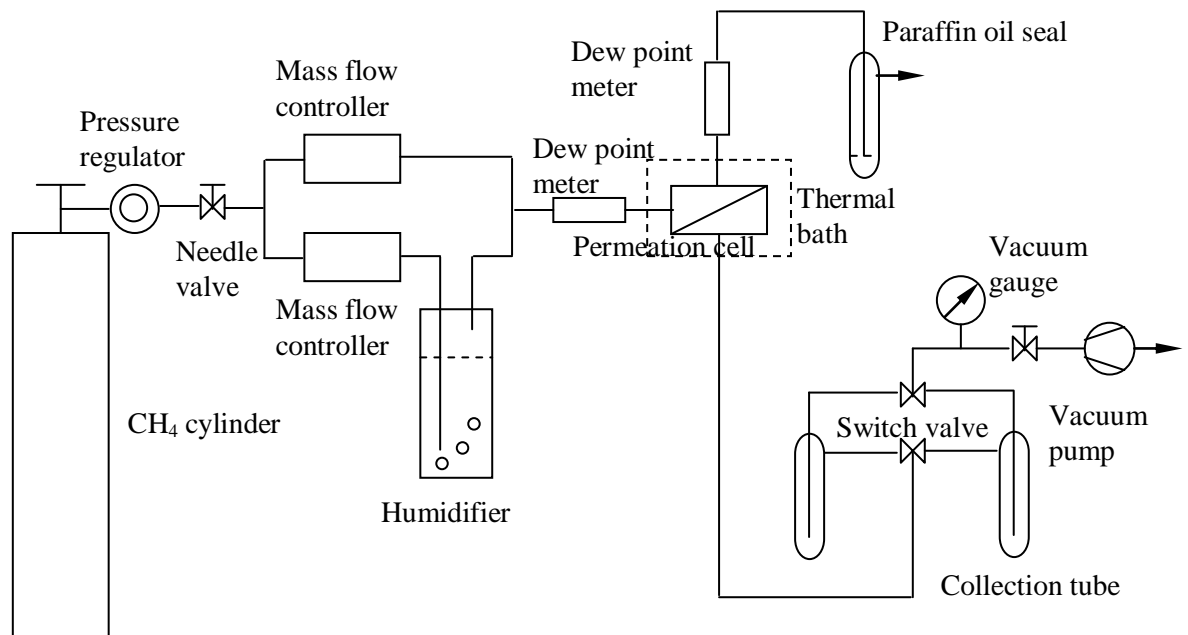
Fig. 6-1. Schematic diagram of experimental setup for methane dehydration.

6.2.4 Permeation Tests for Gas Humidification

The setup for gas humidification is schematically shown in Fig. 6-2. The pressures on both sides were kept at atmospheric pressure. N_2 was used as the carrier gas in the experiments. It was introduced to the permeate side of the permeation cell to purge water vapor which has permeated through the membrane and helped maintain a low water partial pressure. The flow rate of the carrier gas was controlled and measured by a mass flow controller. The water contents in the outlet of the carrier gas streams were measured by a dew point meter. Assuming that only water vapor permeated through the membrane and the permeation of nitrogen through the membrane to the liquid water side was negligible, the water permeation rate was calculated from the carrier gas flow rate and the concentration of water vapor in the outlet gas streams by

$$Y = \frac{Q_{vap}}{Q_{vap} + Q_{gas}} \tag{6-4}$$
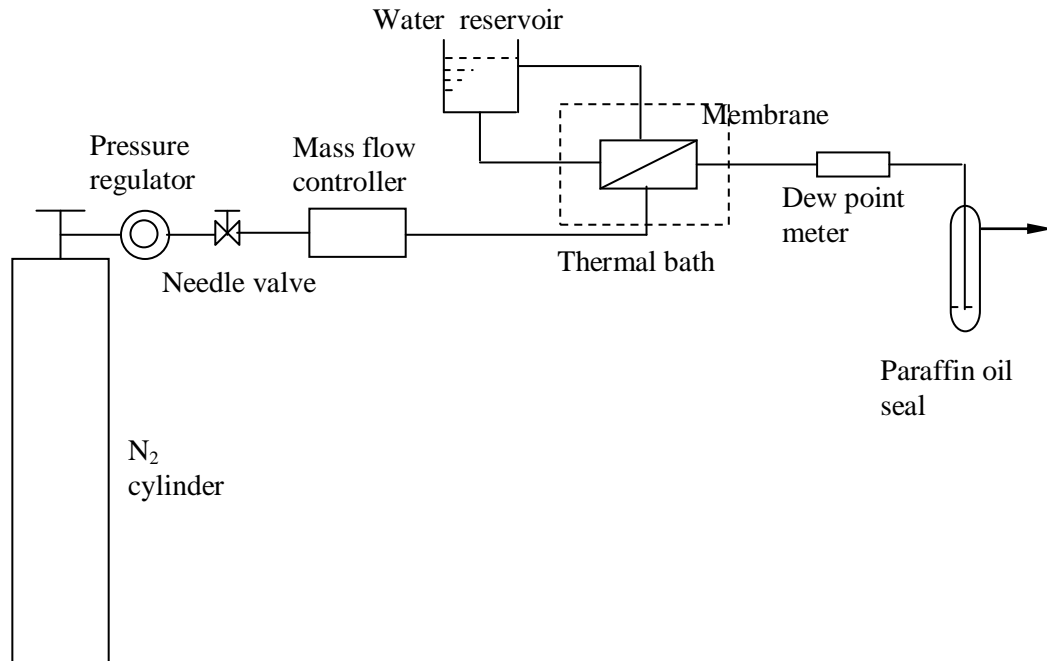
Fig. 6-2. Schematic diagram of experimental setup for gas humidification.

117

where Q_{gas} is the carrier gas flow rate (cm^3(STP)/s), and Q_{vap} is the water vapor permeation rate (cm^3(STP)/s).

6.3 Results and Discussion

6.3.1 Separation of Water Vapor from Methane

In this section, the results of the water vapor/methane permeation tests are presented. During the experiment, the feed gas was a mixture of water vapor and methane. Water vapor is a condensable gas and is able to interact strongly with itself and with the hydrophilic polymer via hydrogen bonding. Therefore, water vapor possesses a much higher solubility and diffusivity than permanent gases in polar polymeric materials. Many attempts have been made in order to describe the sorption and diffusion of water vapor in membranes. It was generally observed that there was a positive deviation of the equilibrium sorption isotherm of water vapor on polymers from Henry's law. As described by Schult and Paul [1996b], the isotherms were almost linear at low activities, following a very weak dual mode sorption, which postulated that in addition to Henry's law "dissolved" term, Langmuir "hole filling" term also contribute to sorption. Hayashi et al. [1999] found that the Langmuir sorption at low activities is significant, while the sorption isotherms follow Flory-Huggins model at high activities because the plasticization of the polymer and the clustering of water molecules [Stannett et al., 1980]. A non-Fickian diffusion behavior of water vapor was also reported due to the hydrogen bonding clusters [Schult and Paul, 1996b; Aranda et al., 1995]. It was assumed that the level of clustering was relatively small at low activities and thus water vapor diffused as individual water molecules, and the diffusion coefficient for water at low activities falls in line with those of the permanent gases. At high activities, because water molecules clustered, the effective diameter of the diffusing species increased, leading to a decreased diffusion coefficient. Nevertheless, the average diameter of the clustered water molecules is still smaller than permanent gases, thus the diffusivity of water vapor is still higher than permanent gases.

118

Generally, the interactions between the permeants and the interactions between the permeant and the polymer cause coupling effects. The strongly sorptive permeant has a strong effect on the mixed gas permeability [Zhu et al., 2005]. The vapor is preferentially adsorbed onto the membrane surface that is in contact with the feed, the sorption of water often results in swelling of the polymer matrix. In this case, the permeation rate of other gaseous species may be accelerated due to the plasticization of the polymer matrix, leading to a positive coupling effect. While the adsorbed water molecules in the membrane may effectively occupy the limited sorption sites and block the available diffusive pathways in the membrane for other gases, in this situation, water vapor may reduce the permeation rate of other gases, leading to a negative coupling effect. On the other hand, due to a large difference in the adsorption affinity between water and the permanent gases, the permanent gas in the binary mixture usually does not affect the adsorption of water significantly, especially at low temperatures. Therefore, the coupling effect of permanent gases on water vapor permeation through membranes is often insignificant.

In this chapter, however, water vapor was found to have little effect on the permeation of methane over the experimental range studied. The permeance of methane remained almost unchanged whether saturated with water or not (1.13 and 1.06 GPU at 25°C and 1 atm transmembrane pressure difference, respectively). This phenomenon is similar to the permeation of CO_2 and N_2 through humidified or dry PDMAEMA/PSF composite membranes as discussed in Chapter 5. The similar gaseous component permeation rates through the membranes in the presence or absence of water vapor are mainly due to the very low resistance of the PDMAEMA layer. The interfacial crosslinking produces an asymmetric crosslinking network structure. The high mobility of uncrosslinked side chains beneath the ultrathin crosslinked outer surface is believed to enable an effective gas transport even in the absence of water.

Fig. 6-3 shows the results of the dehydration experiments at an operating temperature of 25°C when the relative humidity of the feed was changed from 10 to 95 % (i.e., mole fractions 0.005 - 0.025). The concentration of water vapor in the permeate increased with the water content in the feed, as shown in Fig. 6-3 (a). The water vapor permeance increased
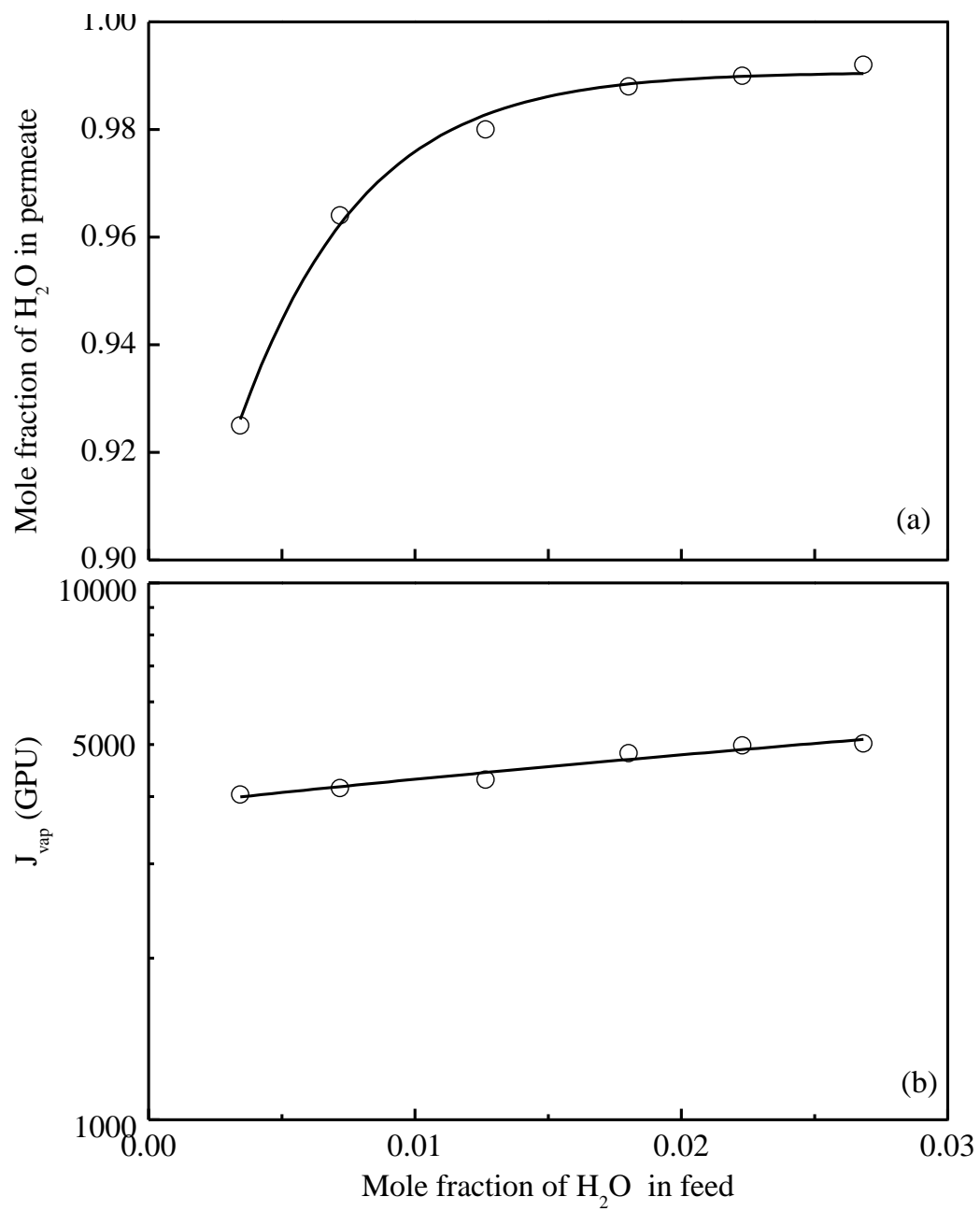
Fig. 6-3. Effect of water vapor activity in feed on (a) permeate concentration, and (b) permeance of water. Operating temperature, 25°C; permeate pressure, 1.7 kPa.

exponentially with the molar fraction of water vapor in the feed side of the membrane as shown in Fig. 6-3 (b), and can be described empirically by

$$J_{vap} = 3866 \exp(10.54X)$$ (6-5)

where X is the mole fraction of water vapor in the feed. As discussed before, the increase in the water permeance is due to the strong dependence of water sorption in the polymer.

Fig. 6-4 shows the influence of the permeate side pressure on the permeation of water vapor. The permeate pressure was changed from 1.7 to 10 kPa using a needle valve connected with the vacuum pump. The relative humidity of the feed stream was kept at around 17 % (i.e., mole fraction of water vapor 0.005). Increasing the permeate pressure significantly decreased the concentration of water in the permeate and the water flux. The permeate pressure has a large effect on the dehydration performance because the selective permeation of water vapor is driven by the partial pressure difference of water vapor across the membrane. Because of the reduced driving force, transport of the permeants was decreased. Water vapor flux was shown to follow a linear relationship with the permeate pressure as shown in Fig. 6-4 (b), and the flux decreased by about 75 % when the permeate pressure changed from 1.7 to 10 kPa.

Figs. 6-5 shows the effect of temperature on the permeance of water vapor and methane through the composite membrane plotted on a log scale versus reciprocal of operating temperature. The permeance of methane increased with an increase in temperature and follows an Arrhenius type relationship, as shown in Fig. 6-5 (a). The permeance of water vapor decreased with an increase in temperature, as shown in Fig. 6-5 (b).

The effect of temperature on the permeability is mainly determined by the effects of temperature on the diffusivity and the solubility. Based on the solution-diffusion model, the relationship between the activation energies of permeation (E_P) and diffusion (E_D) and the heat of sorption (ΔH_S) follows the equation

$$E_P = E_D + \Delta H_S$$ (6-6)
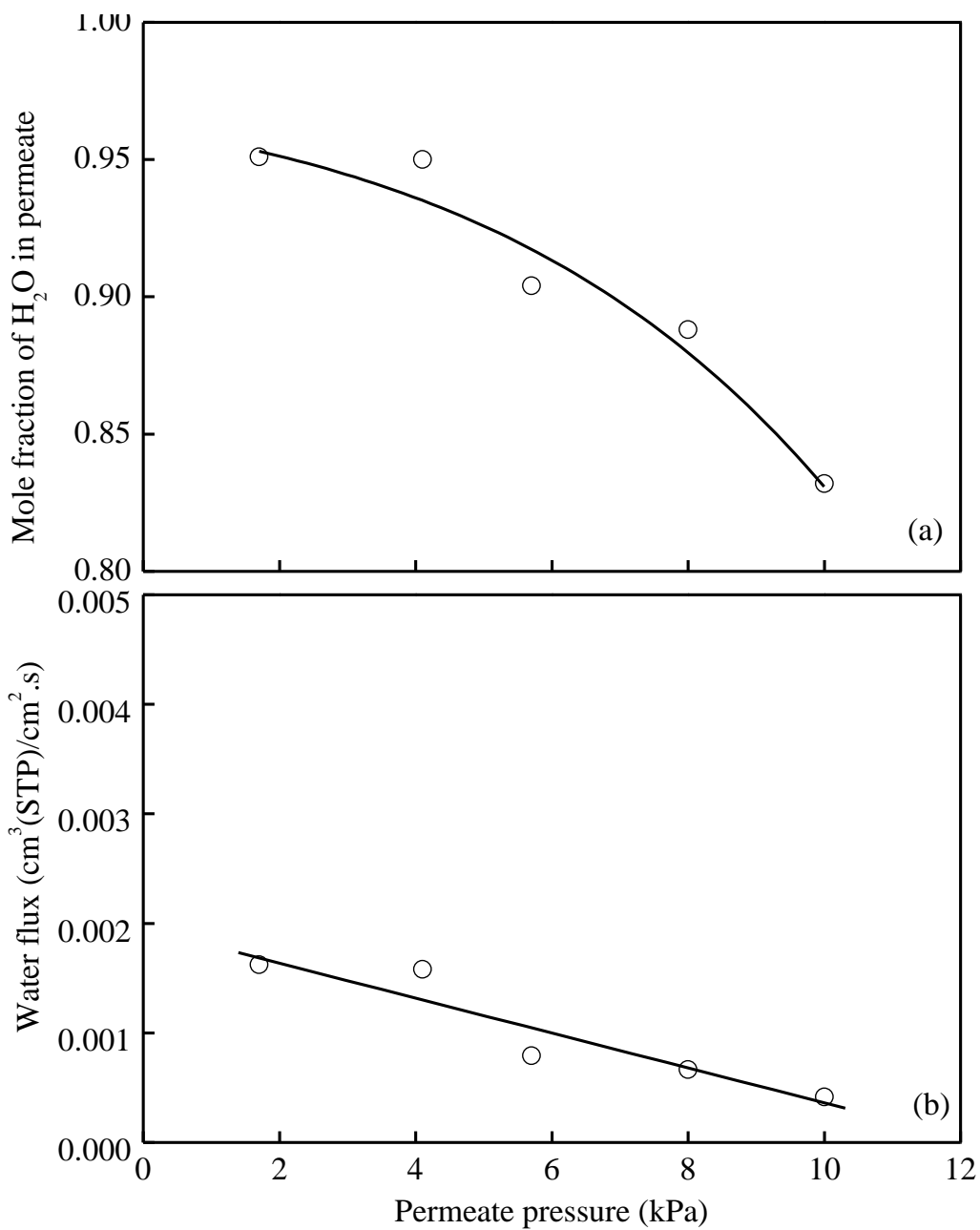
Fig. 6-4. Effect of permeate pressure on (a) permeate water concentration, and (b) water permeation flux. Operating temperature, 25°C; molar fraction of water vapor in feed, 0.005.
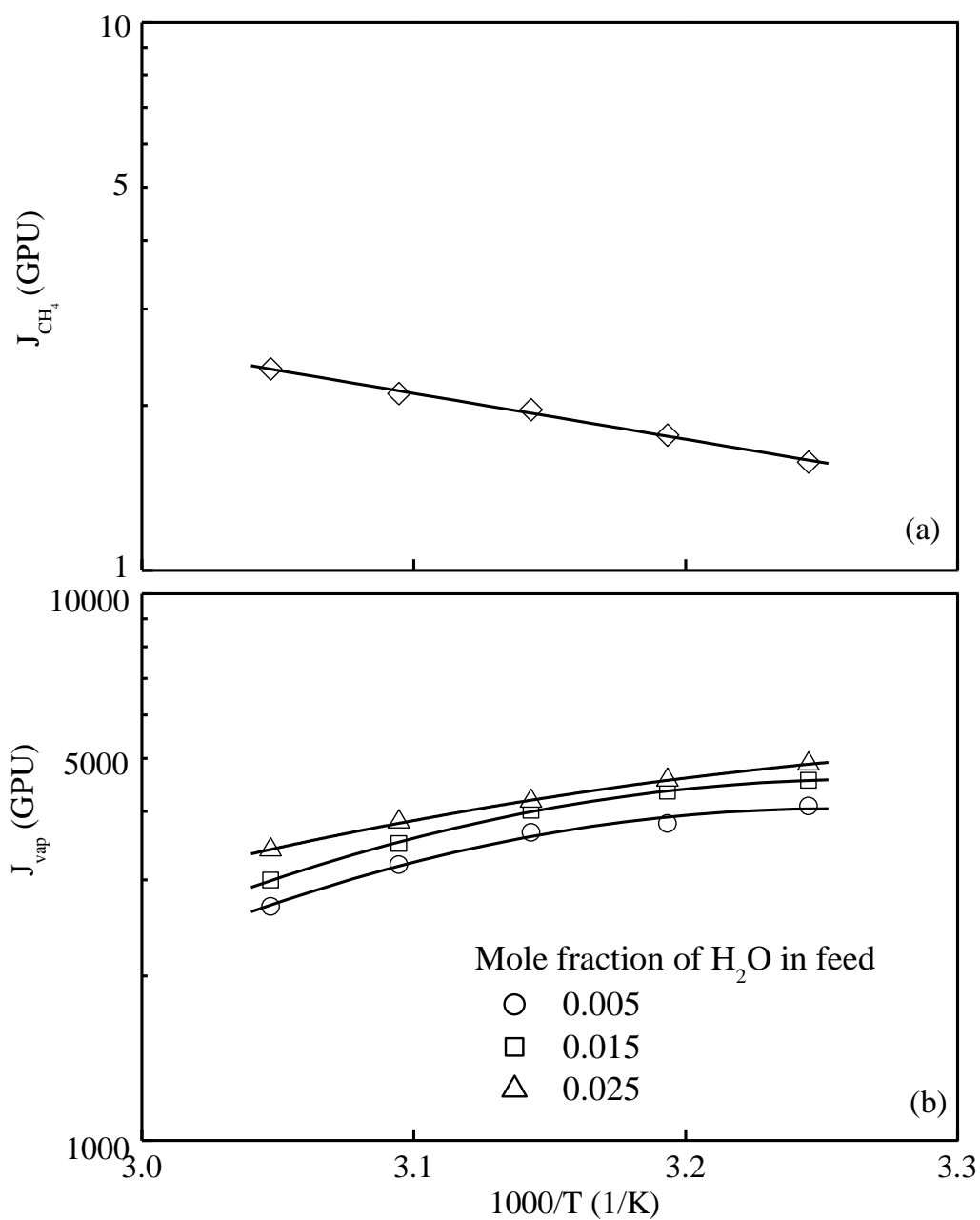
Fig. 6-5. Effect of operating temperature on permeance of methane and water vapor at different feed concentrations. Permeate pressure, 1.7 kPa.

The diffusivity increases with an increase in temperature since the diffusion activation energy is always positive, while the temperature dependence of solubility depends on the heat of sorption, which is more complicated. Dissolution of a permeant into a membrane follows two steps: "condensation" from gas-phase to a liquid-like phase; and mixing of "condensed" permeant with polymer segments. The heat of sorption can be written as

$$\Delta H_S = \Delta H_{cond} + \Delta H_{mix} \tag{6-7}$$

where ΔH_{cond} and ΔH_{mix} are the enthalpy changes associated with permeant condensation and mixing, respectively. The enthalpy change of condensation is always negative (i.e., exothermic) and increases in magnitude with an increase in the condensability of a permeant. The enthalpy change of mixing is usually positive (i.e., endothermic) because a microvoid in the polymer matrix of sufficient size and shape has to be created to accommodate a permeant [Merkel et al., 1999]. Generally, the sign and magnitude of ΔH_S are dependent on the value of ΔH_{cond}. Thus, a negative value of sorption heat indicates that the solubility decreases with increasing temperature. Hence, the different temperature dependence of the gas permeability could be ascribed to the two effects of diffusivity and solubility that are working oppositely.

For a permanent gas, the heat of sorption normally has a small negative value, and therefore, the gas permeability through polymeric membranes usually increases with an increase in temperature. As shown in Fig. 6-5 (a), the temperature dependence of methane permeance through PDMAEMA/PAN membrane followed an Arrhenius type relationship, and the activation energy of permeation was calculated to be 20.1 kJ/mol. However, for a condensable gas or vapor, the permeation behavior may be more complicated and the Arrhenius relationships may not hold. Fig. 6-5 (b) shows that the water vapor permeance decreased with an increase in temperature, indicating the exothermic sorption is more dominating. At a lower water content, the membrane swelling will be reduced. The diffusivity is usually a function of the concentration of the dissolved permeant and also depends on the swelling of the membrane. Therefore, the negative temperature effect is more significant on the vapor permeation when the vapor content in the feed is low. With an increase in temperature, the decreased water vapor permeability and the increased CH_4

permeability lead to a significant reduction in H_2O/CH_4 selectivity, which is presented in Fig. 6-6. The water content in the permeate decreased with increasing operating temperature.
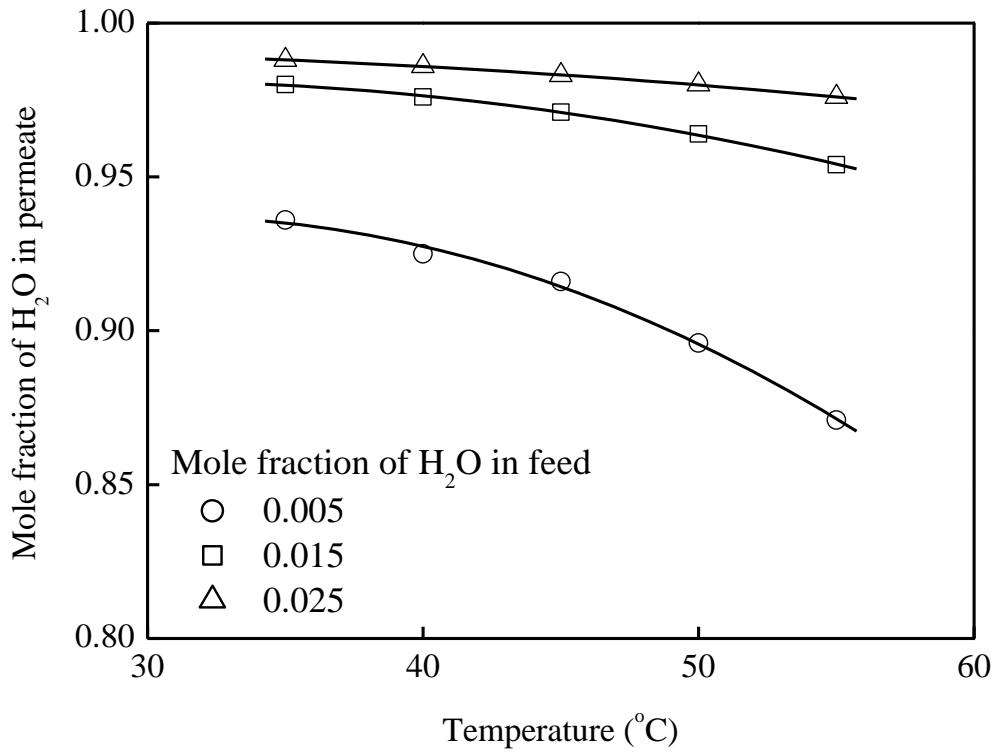
Fig. 6-6. Effect of operating temperature on permeate concentration. Permeate pressure, 1.7 kPa.

In an ideal composite membrane, separation occurs in the thin dense coating layer, while the microporous substrate provides a mechanical strength. In this case, the mass transfer resistance is controlled by the dense layer. Water vapor is much more permeable through most polymeric membranes than permanent gases. The resistance to water vapor through the substrate may have an impact on the overall performance of the composite membrane [Liu et al., 2001c]. The resistance to gas flow can be considered to be analogous to an electric circuit,

and the total resistance R_{total} consists of the resistances of the active coating layer R_{PDM} and the PAN substrate R_{PAN}. Thus,

$$R_{total} = R_{PDM} + R_{PAN} \tag{6-8}$$

The permeance is inversely proportional to the resistance,

$$R = \frac{1}{J} \tag{6-9}$$

The permeance through the coating layer J_{PDM} can be calculated with the experimentally measured permeance of the composite membrane J_{total} and the PAN substrate J_{PAN} according to Eqs. (6-8) and (6-9). The vapor permeance through the PDMAEMA layer and through the PAN substrate were plotted in Fig. 6-7. Fig. 6-7 (a) shows the temperature dependence of water vapor permeation through the PAN substrate. Gas permeation through the porous media can be mainly controlled by Knudsen diffusion and viscous flow. The mean free path of a gas molecule under vacuum is so large that the pores in the substrate can be assumed small enough for Knudsen diffusion to apply [Huang and Feng, 1993]. Thus, the permeance through the substrate can be written as

$$J_{PAN} = \frac{r\varepsilon}{l}\left(\frac{32}{9\pi M R_0 T}\right)^{1/2} \tag{6-10}$$

where l is the thickness of the substrate, r the average radius of the pores, ε the area porosity of the substrate, M the molecular weight of the permeant, R_0 the ideal gas constant, and T the temperature. Eq. (6-10) shows that the resistance to the permeation through the PAN substrate increases with operating temperature, which is consistent with the experimental result. As shown in Fig. 6-7 (b), at the same operating conditions, the vapor permeance through the PDMAEMA layer was about 30 to 70 % higher than that through the composite membrane at various water vapor concentrations in the feed. The result shows that the permeation of water is also influenced by the substrate.
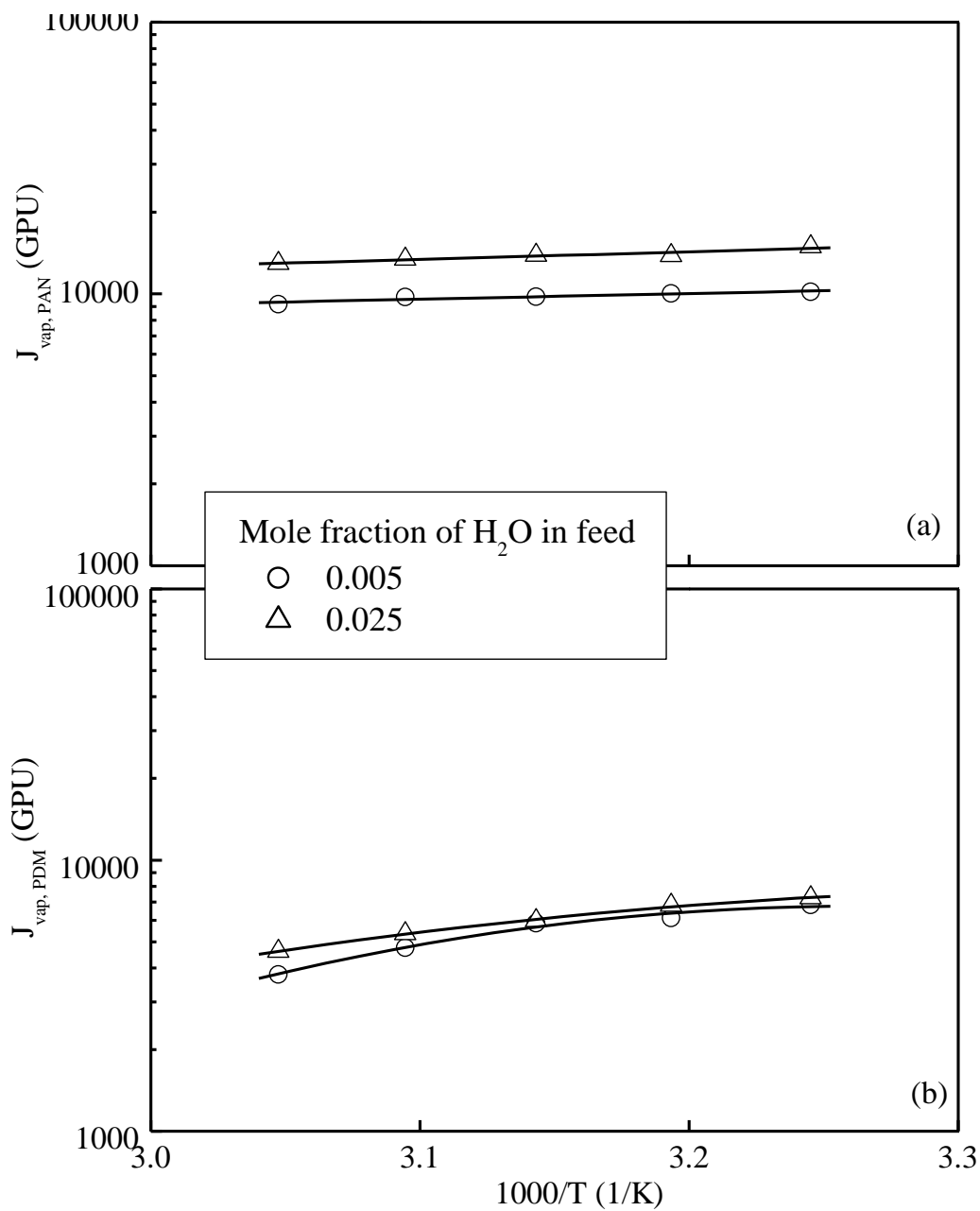
Fig. 6-7. Effect of operating temperature on water vapor permeance through (a) PAN substrate, and (b) PDMAEMA coating layer. Permeate pressure, 3.0 kPa for PAN substrate and 1.7 kPa for PDMAEMA/PAN composite membrane.

The high water vapor permeability of the PDMAEMA layer makes it a promising material for natural gas dehydration. Note that a PDMAEMA/PSF composite membrane was used for ethylene glycol dehydration by pervaporation and gave a quite high permeability as discussed in the following chapter. Therefore, PDMAEMA composite membranes can be used inintegrated natural gas production process involving a membrane dehydration unit, a glycol absorption unit and a glycol regeneration unit. Fig. 6-8 shows the ratio of the resistance to the water vapor permeation in the PAN substrate and the total resistance in the composite membrane as a function of operating temperature. The ratio of R_{PAN} and R_{total} was observed to decrease with increasing temperature, which is in agreement with the consideration that the sorption amount decreases in the PDMAEMA layer as temperature increases.
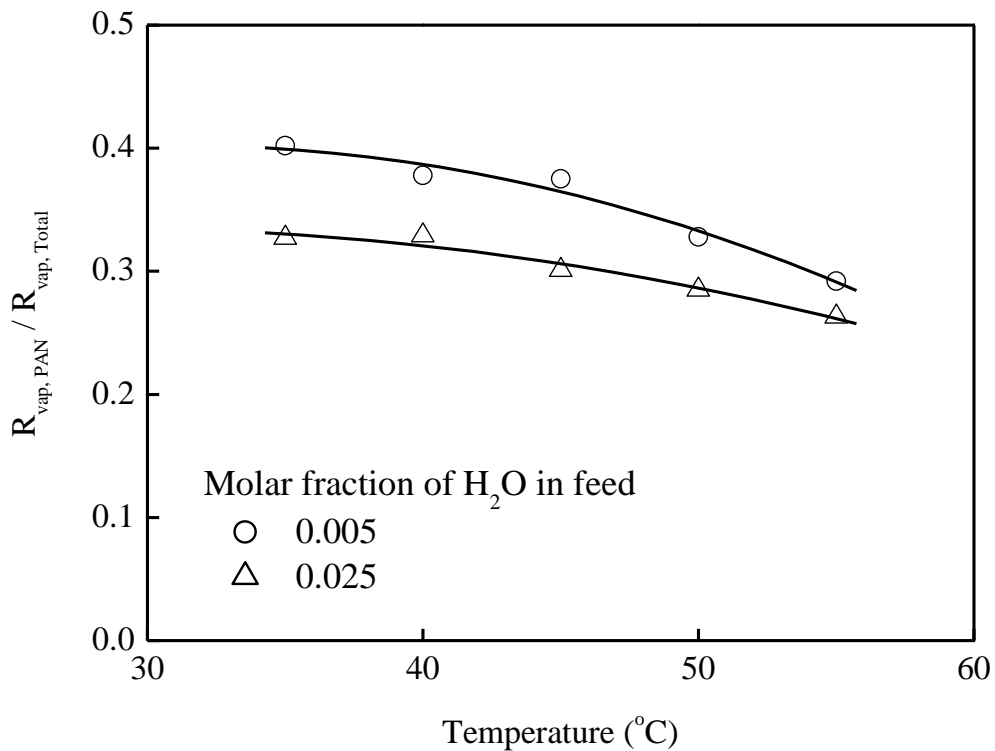
Fig. 6-8. Effect of operating temperature on the ratio of resistance from PAN substrate and the total resistance from PDMAEMA/PAN composite membrane.

6.3.2 Membrane Humidifier

The driving force for water vapor transport through the membrane was applied by purging on the permeate side with a gas stream. The membrane humidification process can be also regarded as a pervaporation process with purging instead of vacuum in the permeate side. In this section, the humidification process was tested with N_2 as the carrier gas and the results are shown in Figs. 6-9, 6-10 and 6-11.

The effect of the carrier gas flow rate, which was changed from 50 to 1750 sccm, on the humidification performance of the composite membrane is shown in Fig. 6-9. As expected, there was a decease in the relative humidity of the outlet gas stream when the inlet carrier gas flow rate increases. Due to the increased diluting effect in permeate with increased carrier gas flow rate, the partial pressure difference across the membrane (i.e., the driving force) increases and thus the water flux increased gradually, as shown in Fig. 6-9 (b). The water vapor transport performance of the membrane was evaluated on the basis of a cross flow model. Fig. 6-12 illustrates the gas transport through the membrane using a cross flow configuration, where the variations in pressure along both feed and permeate sides were assumed to be negligible. The following relations can be formulated based on permeation and mass balance equations for a differential unit of the membrane area:

$$dQ = J_{vap}(p^s - p_p Y)dA \tag{6-11}$$

$$dQ = d(QY) \tag{6-12}$$

where p^s is the saturated water vapor pressure at the operating temperature, and Q is the gas flow rate on the permeate side. At various inlet carrier gas flow rate Q_0, the flow rate and water concentration of the outlet carrier gas stream (Q_{out} and Y_{out}, respectively) can be obtained by integrating Eqs. (6-11) and (6-12) with the boundary conditions

$Q = Q_0$ and $Y = 0$ at $A=0$;

$Q = Q_{out}$ and $Y = Y_{out}$ at $A = 16.6$ cm^2.
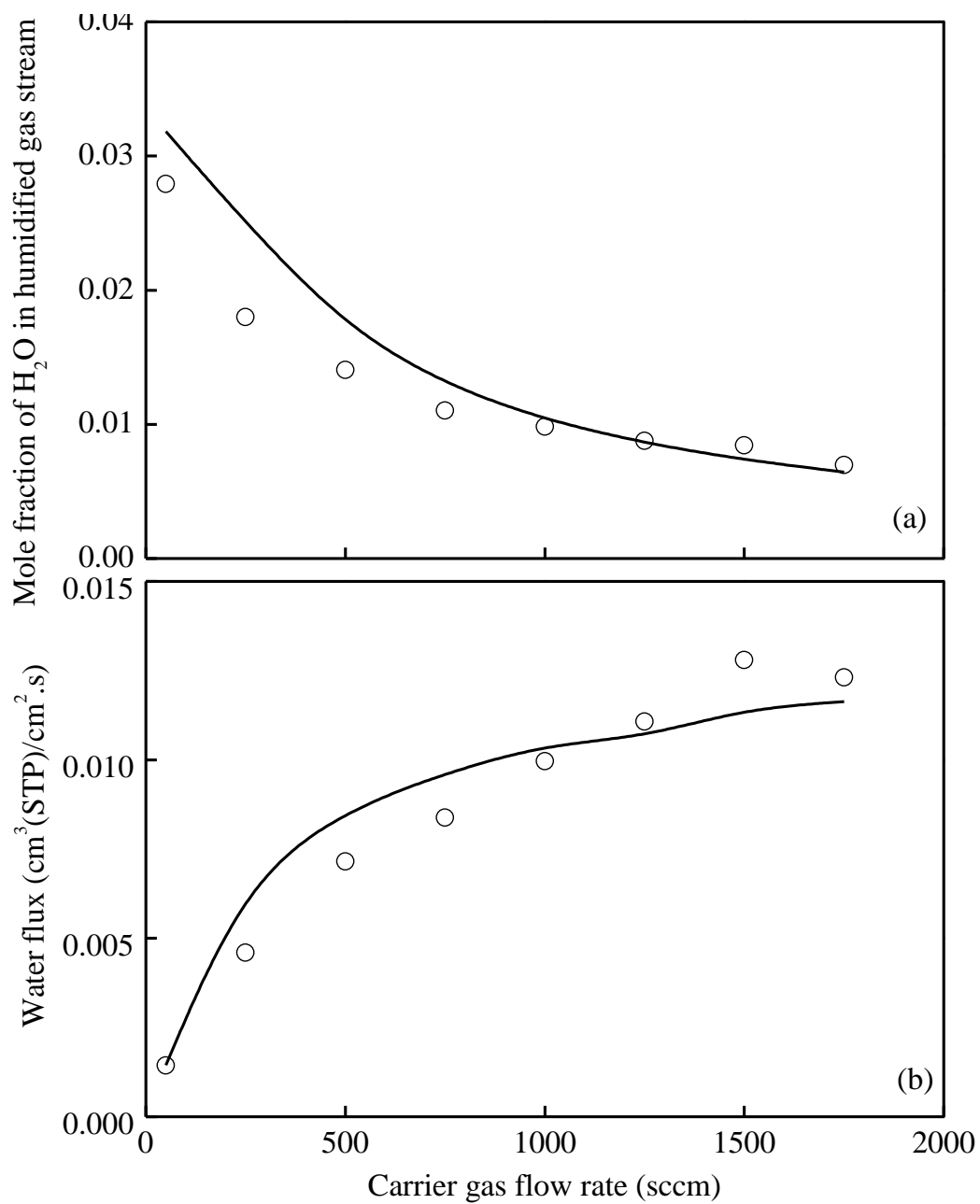
Fig. 6-9. Effect of carrier gas flow rate on (a) water vapor concentration in outlet stream, and (b) water vapor permeation flux. Operating temperature, 25°C. Symbols, experimental data; solid lines, calculated values based on the cross flow model.

The difference between the processes of dehydration and humidification is that the feed is a vapor in the first case and a liquid in the latter. In both cases the driving force for water vapor permeation through the membrane is the difference in the chemical potential of the permeant between feed and permeate side created by vacuum or purging. The permeation fluxes in the dehydration process and that in the humidification process at a saturated vapor pressure in the feed should theoretically be equal, although sometimes a difference in the permeation fluxes in these two processes was reported because of a difference in the swelling of the membranes. Some work has been done to compare the water permeation from a vaporous feed and from water liquid (i.e., pervaporation). Kataoka et al. [1991] reported that
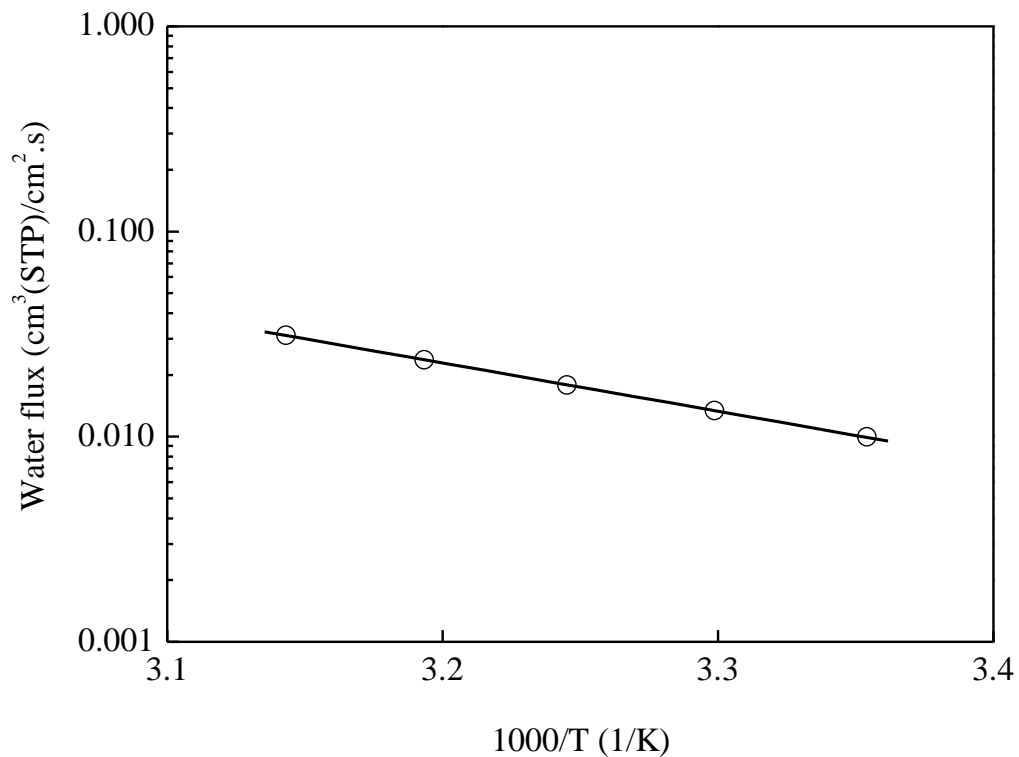
Fig. 6-10. Effect of operating temperature on water vapor permeation flux. Carrier gas flow rate, 1000 sccm.

131

PAN membranes showed good agreement between pervaporation and vapor permeation, while cellulose acetate membranes showed larger permeation flux for pervaporation. Hamada et al. [1997] observed a higher solubility and permeability of water in different hydrophilic membranes from the liquid phase than from the vapor phase. Will and Lichtenthaler [1992] found a higher flux of pervaporation than vapor permeation for the separation of methanol-water mixture by poly(vinyl alcohol)/PAN composite membranes.
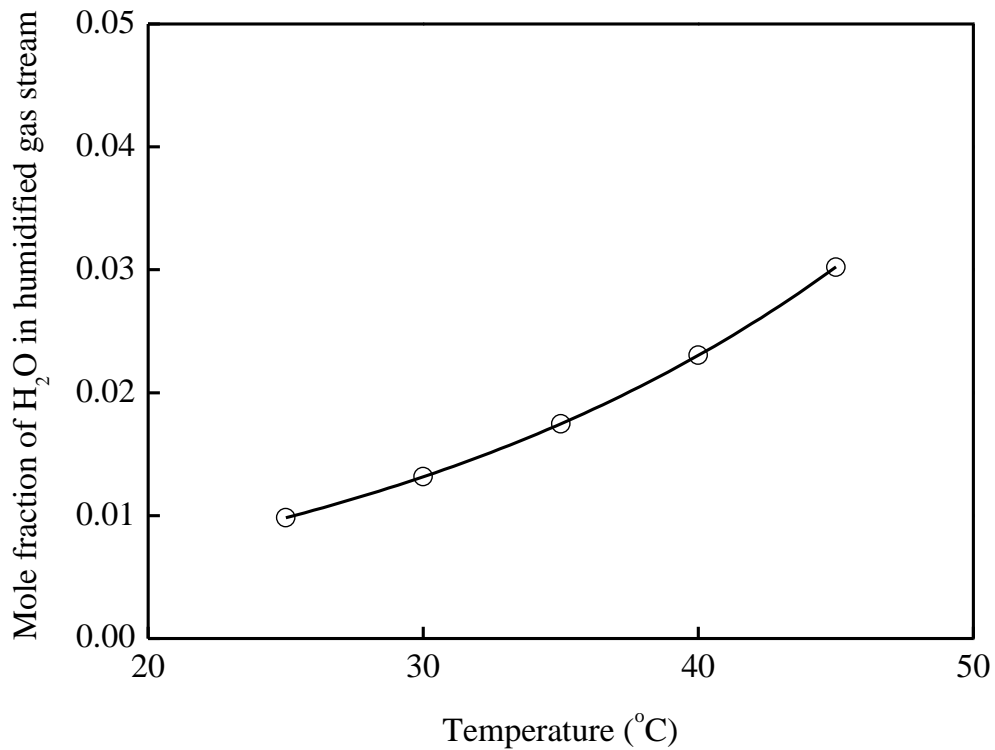
Fig. 6-11. Effect of operating temperature on water vapor concentration in outlet stream. Carrier gas flow rate, 1000 sccm.

Feed side

H_2O p^s

Membrane

Permeate side

Q_{vap} p_p

Humidified N$_2$ outlet,

Dry N$_2$ inlet, Q_{gas} $Q_{gas} + Q_{vap}$

(a)

dA

Feed side p^s

Membrane

Permeate side

Q p_p, dQ, Y $Q + dQ$

(b)
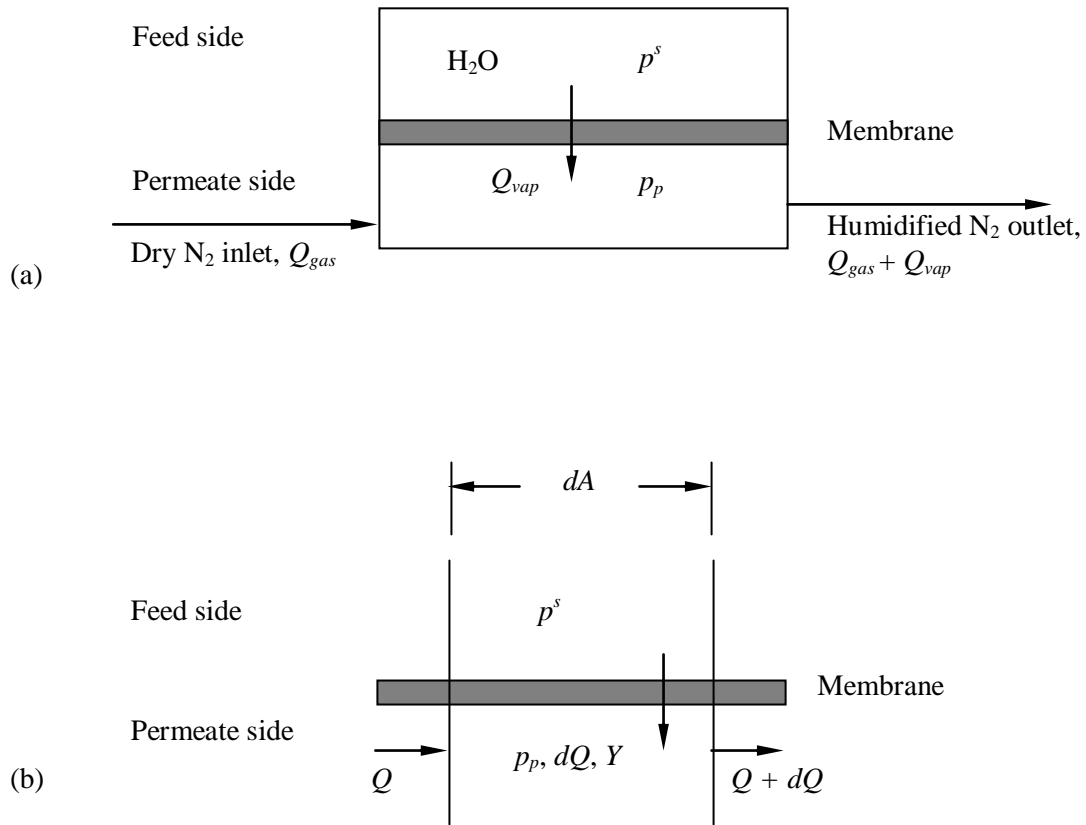
Fig. 6-12. Schematic of cross flow model for membrane humidifier.

Based on Eq. (6-5) for gas dehydration, the permeance of water through the PDMAEMA/PAN membrane was estimated to be 5350 GPU at 100 % relative humidity in the feed (i.e., molar fraction of water vapor ~ 0.03). Assuming that the water vapor permeance from a liquid feed is identical to that with a vapor feed, a J_{vap} of 5350 GPU was used in Eq. (6-11). The calculated water vapor flux and the outlet concentration using this value of J_{vap} are also shown in Fig. 6-9 (solid lines). The agreement between the experimental and calculated results demonstrates that the assumptions made above regarding the vapor permeance is reasonable, although the swelling of the membrane may be higher with water liquid than water vapor in the feed.

Figs. 6-10 and 6-11 show the effect of operating temperature on water permeation through the composite membrane in gas humidification. As the temperature increases, the saturated vapor pressure in the feed will increase, and thus the driving force for water transport increases. The increase in temperature also favours the movement of polymer segments, and increases the diffusivity of water in the membrane. As a result, the vapor permeation flux increased significantly with an increase in temperature, following an Arrhenius type of relation as shown in Fig. 6-11. Fig. 6-12 shows that the relative humidity in the outlet carrier gas stream increased from 30 to almost 100 % when the temperature changed from 25 to 45°C with a constant inlet carrier gas flow rate of 1000 sccm.

6.4 Conclusions

Interfacially formed PDMAEMA/PAN composite membranes were studied for applications involving water vapor permeation. For gas dehydration where water vapor/methane mixtures were on the feed side and vacuum was applied on the permeate side, the permeance of water vapor through the composite membrane was found to increase exponentially with the water vapor concentration in the feed. Reducing the permeate pressure favored the vapor permeation due to the increased driving force. Increasing temperature, however, had a negative effect on water vapor permeability, and the temperature effect was more significant when the vapor content in the feed is low. Due to the high permeability of water vapor through the membrane, the PAN substrate also had an impact on water vapor permeation. When tested for gas humidification where water liquid flowed on one side and N_2 gas flowed on the permeate side, an increase in the gas flow rate enhanced the permeation flux of water vapor. Temperature was also found to have a significant effect on water vapor permeation, and the temperature dependence of the water flux followed an Arrhenius type of relationship. Although it is sometimes perceived that the permeability of liquid water through a hydrophilic membrane is higher than water vapor, this study shows that no significant difference in the permeability of liquid water and saturated water vapor. Both have a permeance of 5350 GPU at 25°C.

Chapter 7

Pervaporation Dehydration based on PDMAEMA membranes[*]

7.1 Introduction

Currently, the application of pervaporation is mainly in the dehydration of alcohols [Jonquiàres et al., 2002], and ethylene glycol (EG) dehydration has attracted significant interest. At present, ethylene glycol is commercially produced from the hydrolysis of ethylene oxide, where a large excess of water is used in the hydrolysis reaction to enhance the conversion. The excess water needs to be removed for product (i.e., ethylene glycol) purification. On the other hand, ethylene glycol is an important chemical. It is a raw material for the manufacture of polyester and many other industrial products [Considine and Kulik, 2002]. In addition, because of its low freezing point, it is widely used as an antifreeze in automobiles and a deicing agent for aircrafts. What is more, the high boiling point (197°C) of ethylene glycol and its good affinity to water makes it an ideal absorbent for natural gas dehydration by scrubbing. All the above applications involve separation of water from ethylene glycol, and this is often done by multi-stage evaporation followed by distillation. Although ethylene glycol and water do not form an azeotrope over the entire composition range, separation of ethylene glycol/water mixtures by evaporation or distillation is still energy intensive because of the high boiling point of ethylene glycol [Bravo et al., 1986]. Pervaporation is considered to be a favorable alternative technology for ethylene glycol/water separation.

Hydrophilic membranes are generally used to remove water from organic solvents. These membranes usually have hydrophilic functional groups with relatively high polarities and strong interactions with water through hydrogen bonding. A literature search reveals that chitosan- and poly(vinyl alcohol)-based membranes are most widely used for ethylene glycol dehydration (see, for example, [Feng and Huang, 1996; Nam and Lee, 1999; Rao et al., 2007;

---

[*] Portions of this work have been submitted to *Sep. Purif. Technol.*

Chen and Chen, 1996; 1998; Bartels and Reale, 1990; Guo et al., 2007a]). The favorable membrane permeability to water is mainly derived from the hydrophilicity of the membrane. However, if the membrane is too hydrophilic, the membrane will be substantially swollen in aqueous solutions, resulting in a decreased membrane selectivity and long term stability. Therefore, membrane crosslinking is often used to suppress excessive swelling. While crosslinking is effective to help retain a good permselectivity, the permeation flux is often compromised.

One way to retain a high flux is the use of composite membranes where a thin active layer is supported on a microporous substrate. Among the various techniques for fabricating composite membranes, interfacial reaction for polymerization or crosslinking is particularly attractive. Recently, interfacially formed membranes have been prepared for pervaporation. Kim et al. [2000] prepared a polyimide/polysulfone composite membrane by interfacial polymerization followed by thermal imidization, and the membrane had a separation factor of over 240 and a permeation flux of 92 mol/(m^2 h) for ethanol dehydration at 40°C and 22 mol% water in the feed. Huang et al. [2006] prepared a polyamide thin-film composite membrane by interfacial polymerization of triethylenetetramine and trimesoyl chloride on a polyacrylonitrile substrate for pervaporation of aqueous isopropanol mixtures; at a feed water concentration of 27 mol%, a permeation flux of 20 mol/(m^2 h) and a permeate water concentration of about 98 mol% were obtained.

In this chapter, interfacially formed PDMAEMA/PSF composite membranes were prepared for the separation of ethylene glycol/water mixtures by pervaporation. The pervaporation performance of the membrane for ethylene glycol dehydration was studied at different feed concentrations and temperatures. The sorption behavior of crosslinked PDMAEMA in aqueous ethylene glycol solutions was also investigated to gain an insight into the contribution of preferential sorption to the overall selectivity. The membrane stability was also evaluated, and the membrane performance was found to compare favorably with that reported in the literature.

7.2 Experimental

7.2.1 Materials

Ethylene glycol was purchased from Fisher Scientific, and the aqueous ethylene glycol solutions of different concentrations used in pervaporation experiments were prepared by blending ethylene glycol and deionized water. Other materials were the same as used before.

7.2.2 Membrane Preparation

The procedure for preparation of the PSF substrate membrane and the PDMAEMA/PSF composite membrane were the same as that described in Chapter 5.

7.2.3 Pervaporation

Fig. 7-1 is a schematic diagram of the experimental setup for pervaporation tests. The PDMAEMA/PSF composite membrane was mounted into the permeation cell with an effective surface area of 16.6 cm^2. Aqueous ethylene glycol solutions of various water contents were used as the feed. The feed solution was circulated by a pump from the feed tank to the permeation cell, and the retentate was recycled back to the feed tank. The permeate pressure on the downstream side of the membrane was maintained at 1.3 kPa absolute using a vacuum pump, and the operating temperature was controlled using a thermal bath. The permeation rate was determined gravimetrically by measuring the quantity of the permeate sample collected over a given period of time, and the permeate composition was analyzed with a Hewlett-Packard (Series II) gas chromatography. The separation performance was characterized by permeation flux (N) and separation factor (α), which are defined as:

$$N = \frac{Q}{A \cdot \Delta t} \tag{7-1}$$

$$\alpha = \frac{Y/(1-Y)}{X/(1-X)} \tag{7-2}$$

where Q is the quantity (mol) of the permeate collected over a time interval Δt (h), and A is the effective membrane area (m^2), X and Y are the mole fractions of water in the feed and the permeate streams, respectively. The partial permeation fluxes of ethylene glycol and water can be calculated from the total permeation flux and the permeate concentration. The permeation was considered to have reached steady state when the permeation flux and permeate composition became constant. Note that during each pervaporation run, the quantity of permeate removed by the membrane was kept below 0.1 % of the initial feed loading so that the variation in feed concentration was negligibly small; this allows the membrane to be evaluated at a given feed concentration.
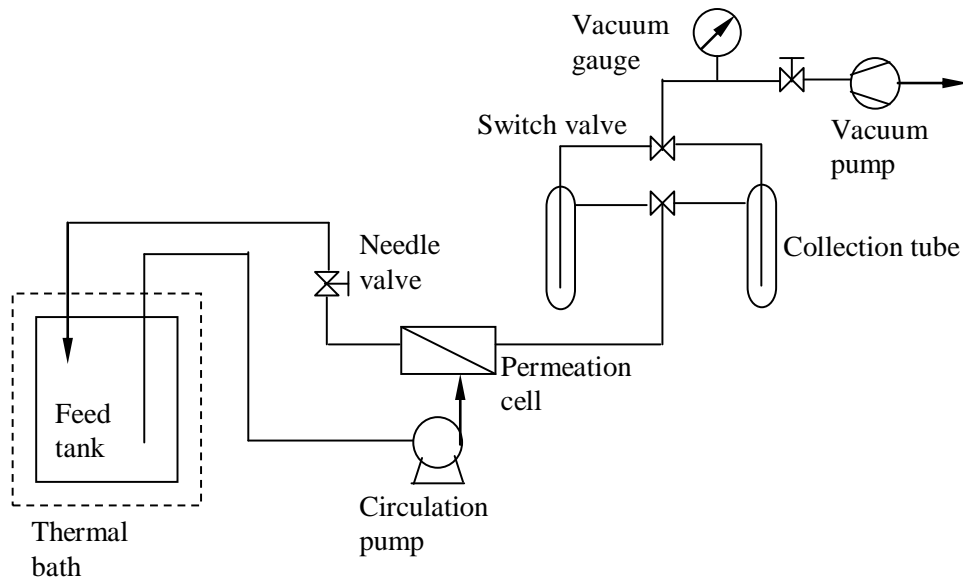
Fig. 7-1. Schematic diagram of experimental setup for pervaporation.

7.2.4 Sorption

In order to study how the preferential sorption affects the selective permeation, the sorption behavior of ethylene glycol and water in the PDMAEMA membrane was evaluated. For this

purpose, another PDMAEMA membrane was prepared using a stainless steel mesh as the substrate, which does not sorb ethylene glycol and water, to eliminate the interference of the polysulfone substrate in the composite membrane on the sorption measurements. The dried film samples of known weights were immersed in aqueous ethylene glycol solutions for 1 day at 30°C to reach sorption equilibrium. The swollen films were then taken out of the solutions and quickly blotted with Kimwipes to remove the surface liquid before being weighed. The swollen film sample was placed into a dry glass tube fitted to a vacuum system for 4 h so that desorption would occur. The desorbed vapor was condensed in a cold trap using liquid nitrogen. The experimental apparatus for desorption is shown in Fig. 7-2. The weight of the collected sorbate liquid was determined gravimetrically using a digital electronic balance, and its composition was analyzed with a gas chromatograph. This allows the determination of sorption uptake of water and ethylene glycol in the membrane, and the overall sorption uptake can be used to represent the degree of swelling of the membrane in aqueous ethylene glycol solution.
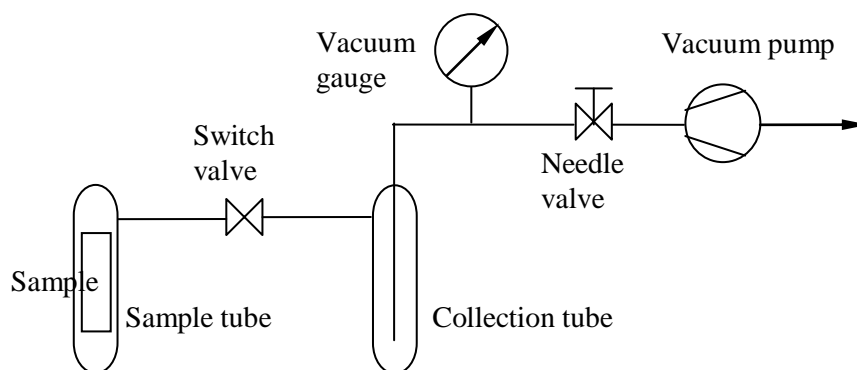
Fig. 7-2. Schematic diagram of experimental setup for sorption.

7.3 Results and Discussion

7.3.1 Effect of Feed Concentration

Fig. 7-3 shows the effects of feed concentration on the total permeation flux and the water content in permeate over the entire feed composition range at 30°C. An increase in the feed water concentration increases both the permeation flux and the permeate water concentration. The membrane appears to be very effective in selective removal of water from ethylene glycol, especially for dehydrating ethylene glycol at low water concentrations that is more relevant to practical applications. At a feed water content as low as 1 mol%, the permeate water concentration can reach 99.7 mol%, corresponding to a separation factor of ca. 32,900. As a comparison to the separation efficiency of traditional distillation, the vapor-liquid equilibrium data [Perry and Green, 1999] are also presented in the figure. It appears that the PDMAEMA/PSF composite membrane for pervaporation dehydration of ethylene glycol is most advantageous over distillation when the feed water content is relatively low. For high water concentrations in the feed, the water concentration in the permeate is not much higher than the vapor phase composition in equilibrium with the feed liquid, and the energy saving advantages of pervaporation separation gradually diminishes.

Fig. 7-3(b) shows that the total permeation flux increases progressively with an increase in the feed water concentration. Similar observations can be made for some other hydrophilic membranes for ethylene glycol dehydration, including poly(vinyl alcohol)-based GFT membranes [Jehle et al., 1995], chitosan membranes [Feng and Huang, 1996], and sulfonated poly(ether ether ketone) membranes [Huang et al., 2002]. This may be explained from the hydrophilicity of the membrane. With a higher water content in the feed, the membrane swells more significantly due to the high hydrophilicity of the polymer, and thus the free volume in the polymer increases and mobility of the polymer chains become higher, making it easier for the permeating molecules to penetrate the membrane.

The partial permeation fluxes of water and ethylene glycol are shown in Figs. 7-4 and 7-5, respectively; the dotted straight lines represent the ideal permeation flux that would be obtained if there were no coupling effects between the permeating species, which is the case
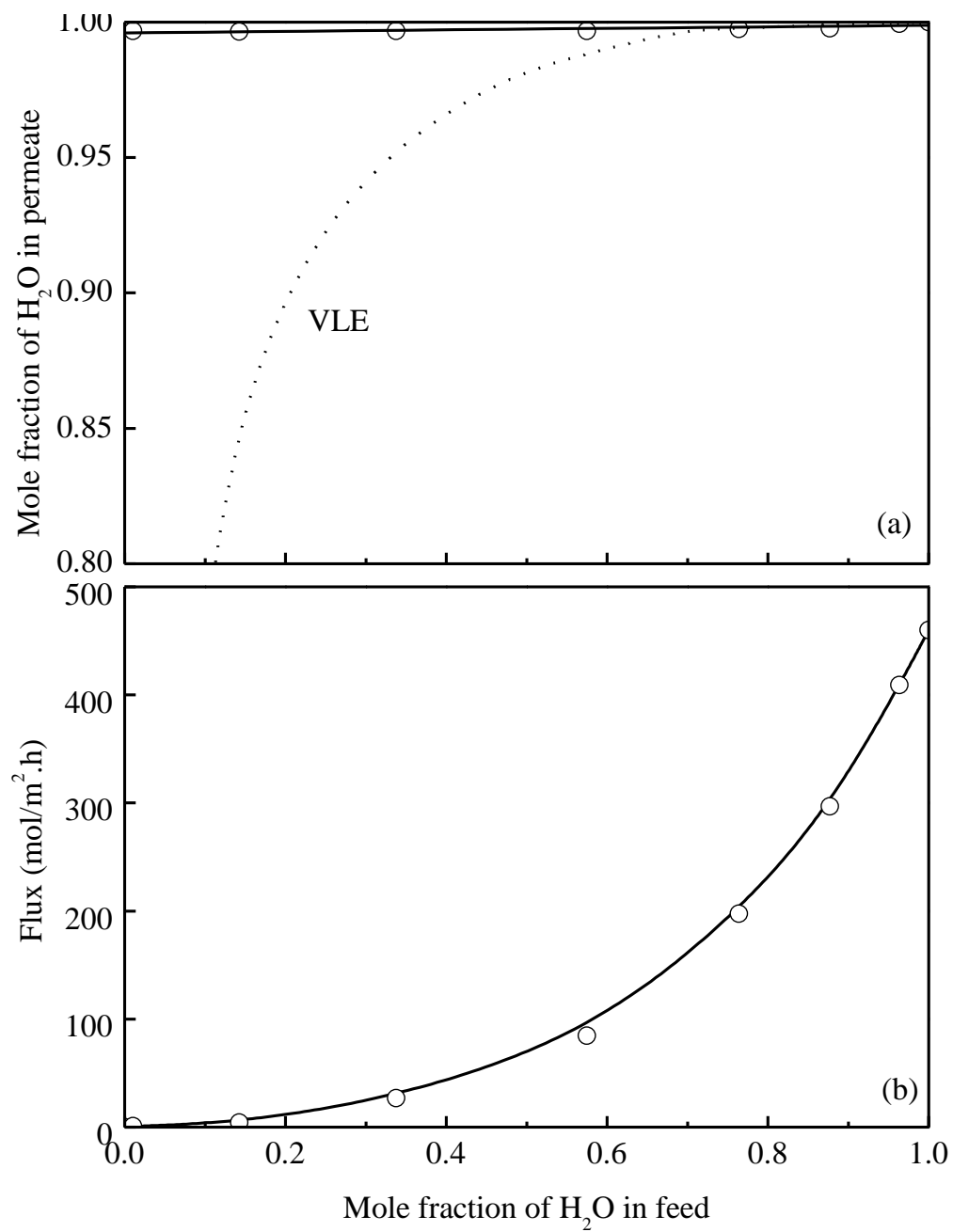
Fig. 7-3. Effect of feed concentration on (a) permeate concentration, and (b) permeation flux. Operating temperature, 30°C; downstream pressure, 1.3 kPa. Dotted line in (a) represents the vapor-liquid equilibrium (VLE) data at 40 kPa.

141
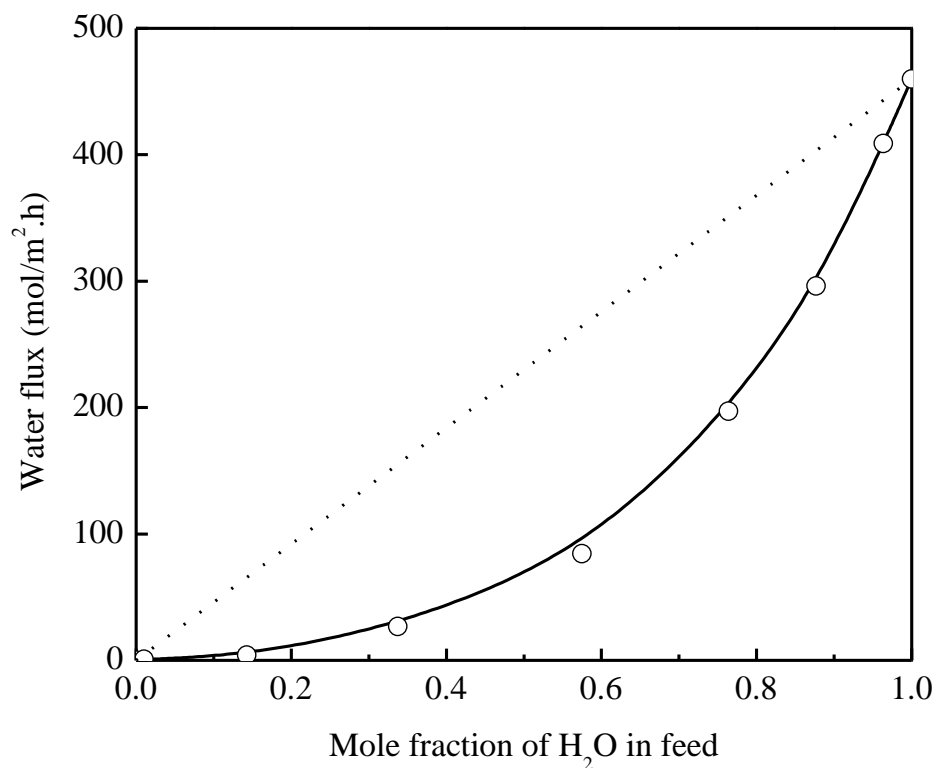
Fig. 7-4. Effect of water content in feed on partial permeation flux of water. Dotted line represents the ideal permeation flux. Operating conditions same as those specified in Fig. 7-3.

when the permeant-permeant and permeant-membrane interactions are very weak. In the case of ideal permeation, the permeation flux of a component will increase proportionally as its concentration in the feed increases. However, the coupling effects are often observed in pervaporation for both solvent dehydration with hydrophilic membranes and organic compounds removal from water with organophilic membranes due to strong interactions of at least one permeating component with the membrane. Because of the coupling effect, the permeability of one component through the membrane may be affected positively or negatively by the presence of the other component in the feed mixtures to be separated. Positive coupling will facilitate the permeation and it is often caused by plasticization of the
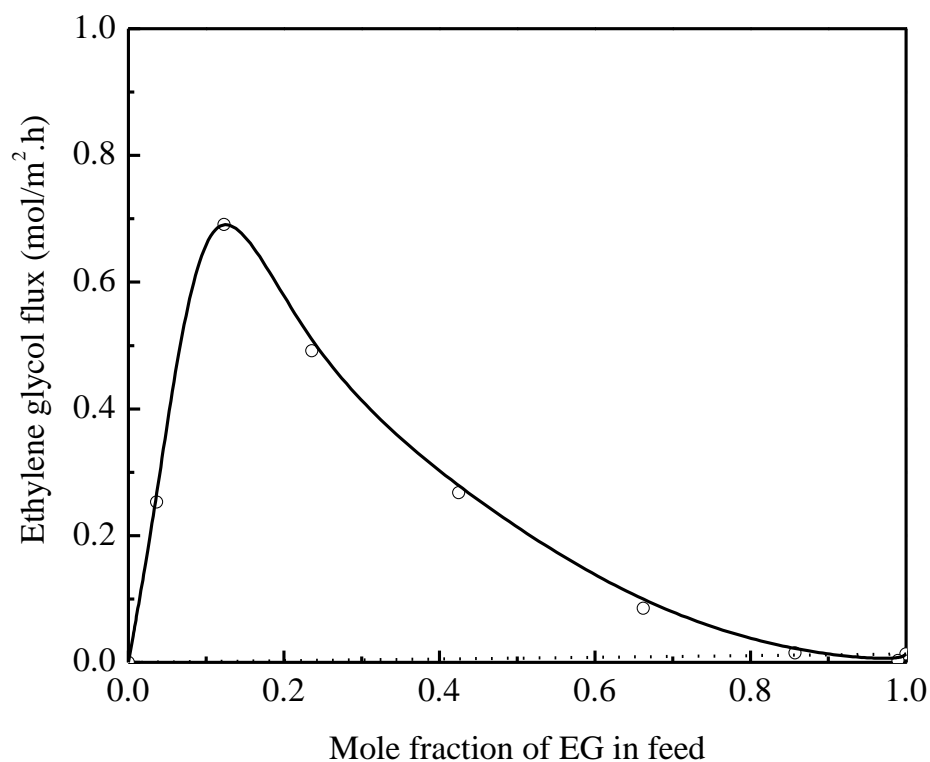
Fig. 7-5. Effect of ethylene glycol content in feed on partial permeation flux of ethylene glycol. Dotted line represents the ideal permeation flux. Operating conditions same as those specified in Fig. 7-3.

polymer matrix by the permeating species. For the membrane system studies here, the membrane can be swollen by both water and ethylene glycol because of the strong hydrogen bonding between the permeating components (i.e., water and ethylene glycol) and the polymer that contains amino groups.

The data in Fig. 7-4 show that the water permeation rate increases with an increase in the feed water content, but the water permeation rate is lower than ideal over the entire composition range. This indicates that the permeation of water through the membrane is negatively affected by ethylene glycol. This is easy to understand; there is a competition

between water and ethylene glycol molecules for the sorption sites and transport pathways in the membrane. As a result, the presence of ethylene glycol causes water molecules to permeate more slowly, that is, ethylene glycol has a negative coupling effect on water permeation. In addition, the hydrogen bonds can easily bring water or ethylene glycol molecules together [Kao et al., 2005], and they have a tendency to form water-water, water-glycol and glycol-glycol clusters, leading to a reduced diffusivity through the membrane.

On the other hand, the permeation flux of ethylene glycol did not increase monotonically with an increase in the feed ethylene glycol concentration, as shown in Fig. 7-5. Pure ethylene glycol can hardly permeate through the membrane. However, once water is present, the permeation of ethylene glycol will start to occur more easily. With an increase in the water content in the feed, the membrane becomes increasingly swollen (which will be shown later), and this facilitates the permeation of ethylene glycol. As a result, the permeation flux of ethylene glycol increases in spite of the reduced driving force for permeation due to decreased ethylene glycol concentration in the feed. However, as one may expect, this trend will not continue indefinitely. When the ethylene glycol concentration in the feed is sufficiently low, the permeation flux of ethylene glycol will begin to decrease with a further increase in water concentration (i.e., a decrease in ethylene glycol concentration). Consequently, a maximum in ethylene glycol flux results, which is shown to occur at around 13 mol% ethylene glycol in the feed. The permeation of ethylene glycol through the membrane showed a significant deviation from ideal case of permeation, and the presence of water affected the permeation of ethylene glycol positively. Very similar results were also reported by Huang and Yeom for the dehydration of ethanol using poly(vinyl alcohol) membranes [1990].

Based on the solution-diffusion model, both the solution and the diffusion aspects affects the selective permeation. Water molecules are smaller than ethylene glycol molecules, and thus the selective permeation of water is favored from a diffusion point of view. On the other hand, the membrane is hydrophilic, and the dehydration of organic solvents with hydrophilic membranes is often attributed to the selective sorption of water in the membrane. It would be of interest to know whether preferential sorption of water over ethylene glycol in the

membrane indeed occurs. However, a study on the selective sorption aspect revealed that this is not the case, as shown by Fig. 7-6 which illustrates the overall sorption uptake and the water concentration in the sorbed phase at different feed water concentrations. Although the concentration of water in the sorbed phase in the membrane increases with an increase in feed water concentration, the water content in the sorbed phase is always lower than the water concentration in the feed. This means that water is not preferentially sorbed in the crosslinked PDMAEMA membrane over ethylene glycol. From a molecular structure point of view, there is one more –OH group in the ethylene glycol molecule than in water, and as such ethylene glycol may exhibit a stronger affinity to the membrane. This has been confirmed from contact angle measurements. The contact angle of ethylene glycol on the PDMAEMA membrane surface is 41.5°, while the contact angle of water is 68.3°. These results indicate that because of the stronger affinity between ethylene glycol and the polymer, ethylene glycol is favored by the competitive sorption, and the selective permeation of water arises primarily from the selective diffusion because of the small size of water molecules.

The sorption uptake data in Fig. 7-6 showed that the crosslinked PDMAEMA membrane had a high degree of swelling in pure water (0.096 mol/g) and pure ethylene glycol (0.051 mol/g). Generally speaking, crosslinking of a polymer leads to reduced polymer chain mobility and a lower degree of swelling. The high swelling degree of the interfacially crosslinked PDMAEMA layer is mainly attributed to the asymmetric crosslinking structure. The interfacial crosslinking is a self-limiting process which results in a gradient in the crosslinking structure along the thickness of the PDMAEMA membrane. It is characterized by a highly crosslinked outer surface and a less crosslinked interior, which help maintain a high degree of swelling. On the other hand, the swelling degree as represented by the molar sorption uptake increases with an increase in feed water content. This is understandable because ethylene glycol molecules are much larger than water and thus for a given sorption "site" in the membrane fewer ethylene glycol molecules can be accommodated because of the steric hindrance effect.

The individual sorption uptakes of ethylene glycol and water in the membrane can be calculated from the total uptake and the composition of the sorbate and they are shown in
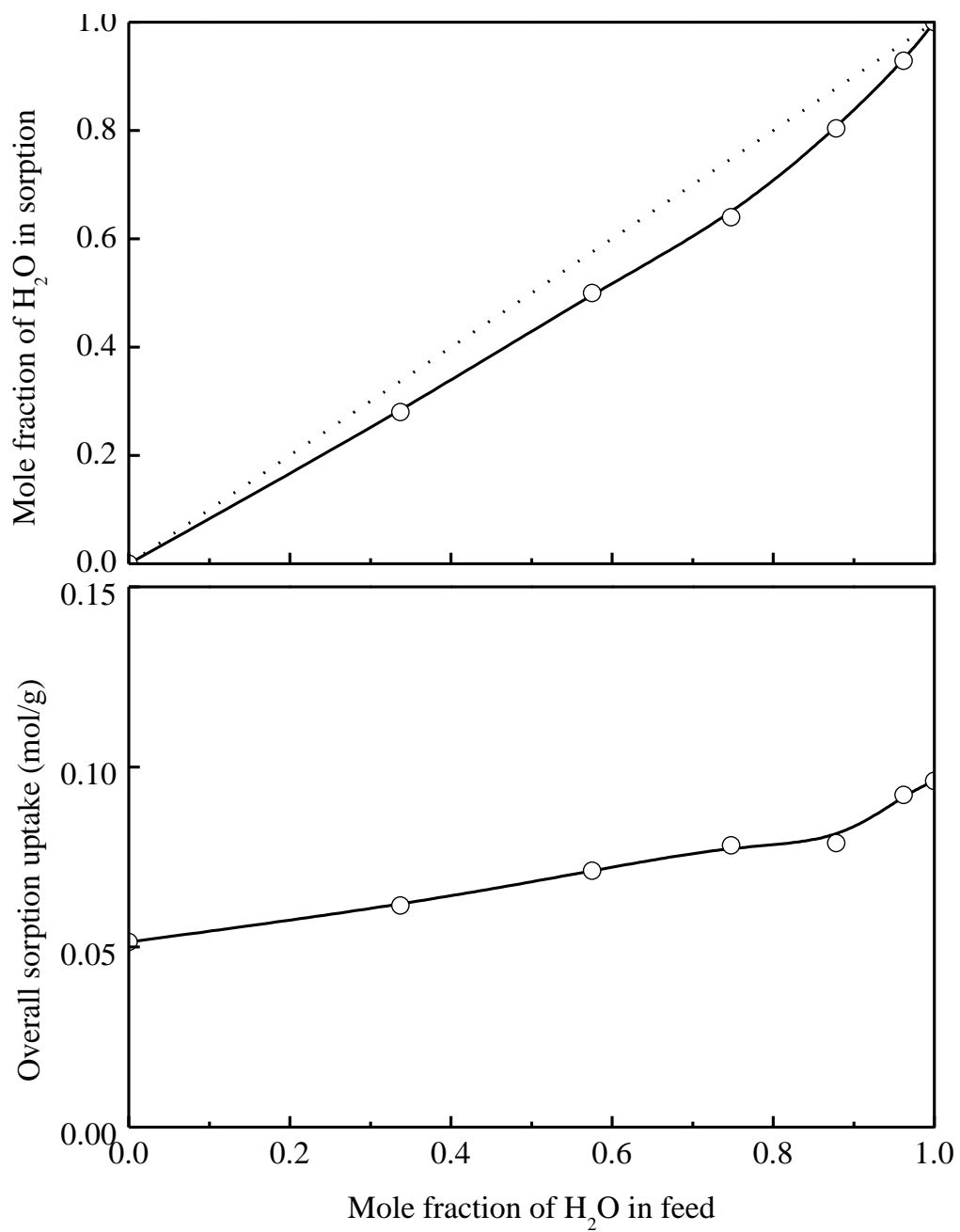
Fig. 7-6. Effect of feed concentration on sorption. Operating temperature, 30 $^{\circ}$C.

Fig. 7-7. It can be seen that the sorption uptake of an individual permeant increases with an increase in its concentration in the liquid. However, water sorption uptake was lower than ideal whereas the opposite is true for the sorption uptake of ethylene glycol over the entire concentration range. This again indicates that because of the interactions among the permeating species and the membrane, the sorption of ethylene glycol in the membrane was enhanced by the presence of water, while water sorption was influenced by ethylene glycol negatively. This is consistent with the preferential sorption of ethylene glycol over water observed earlier.
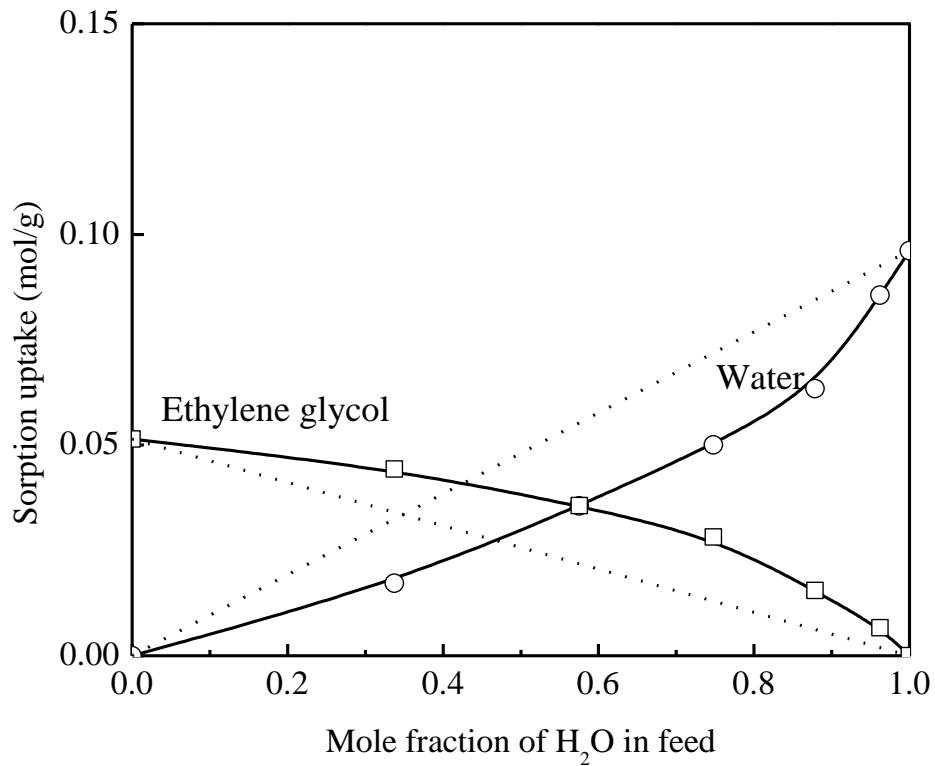
Fig. 7-7. Effect of water content in feed on sorption uptake of water and ethylene glycol. Operating temperature, 30 $^{\circ}$C.

Hydrophilic membranes are normally appropriate for solvent dehydration where water should preferentially permeate through the membrane. However, the above analysis suggests that unlike the dehydration of organic solvents with low or moderate hydrophilicities, because of the strong hydrophilicity of the diol compound, it would be difficult to find a hydrophilic polymer material that has a high affinity to water but not to ethylene glycol. Nevertheless, the results from the present study show that in spite of the less favorable sorption selectivity, a good performance in ethylene glycol dehydration can still be achieved with a highly hydrophilic membrane for enhanced permeation rate provided that the macromolecular network is dense enough (at least in the skin layer) so as to achieve a high selectivity based on diffusivity differences.

7.3.2 Effect of Operating Temperature

The composite membrane showed good thermal stability over the temperature range (30 to 60°C) tested. The partial permeation fluxes of water and ethylene glycol at various temperatures are shown in Fig. 7-8 where the logarithmic flux is plotted against the reciprocal of temperature. It is shown that the permeation fluxes increase with an increase in the temperature, and the temperature dependence of permeation fluxes follows an Arrhenius type of relationship,

$$N_i = N_{i0} \exp(-\frac{E_{Ni}}{RT})$$ (7-3)

where E_{Ni} is the activation energy for component i permeation that characterizes the overall temperature dependence of permeation flux. The activation energies for the permeation of ethylene glycol and water are determined to be 53 and 51 kJ/mol, respectively. When the temperature was increased from 30 to 60 ℃, the total flux increased from 27 to 171 mol/(m^2 h). However, there was little change in water concentration in the permeate (as shown in Fig. 7-9), which is determined by the relative permeation rates of ethylene glycol and water, because of the similar E_N values for the permeating components.
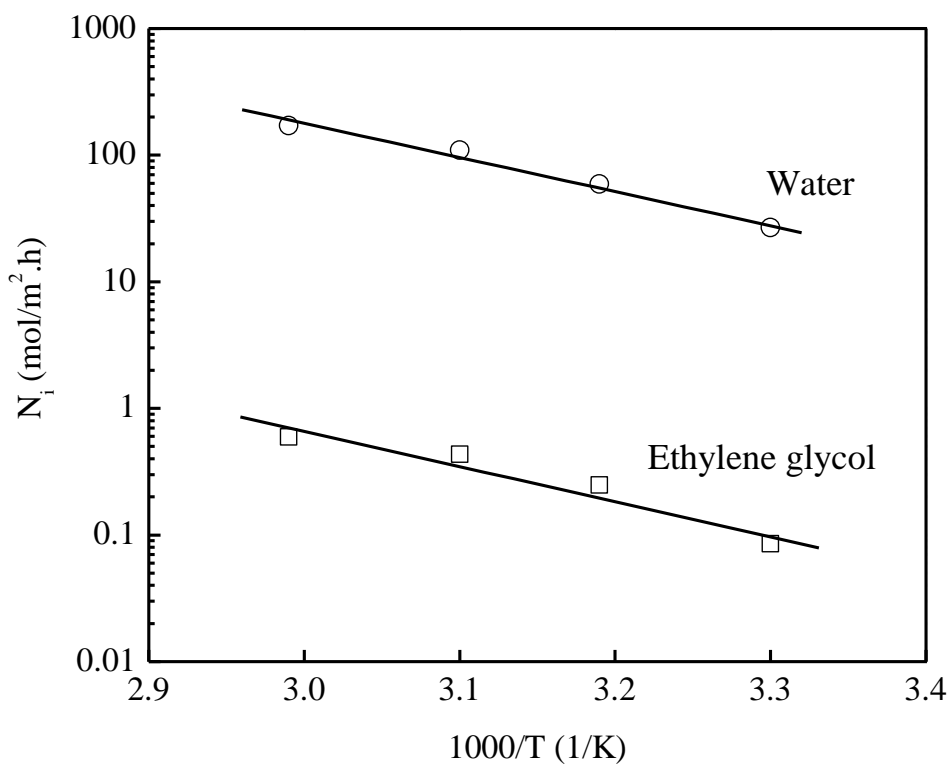
Fig. 7-8. Effect of operating temperature on partial permeation flux. Feed concentration, 34 mol% water; downstream pressure, 1.3 kPa).

It should be pointed out that temperature affects permeation on two aspects: One is the driving force, and the other the membrane permeability. An increase in temperature increases the saturated vapor pressure of the permeant, resulting in an increase in the driving force for mass transport through the membrane. In order to evaluate how the membrane permeability was influenced by temperature, the membrane permeance was estimated from the permeation flux normalized by the partial pressure driving force in analog to gas permeation [Namboodiri and Vane, 2007], and the temperature dependence of membrane permeance was also found to follow an Arrhenius relationship,

149
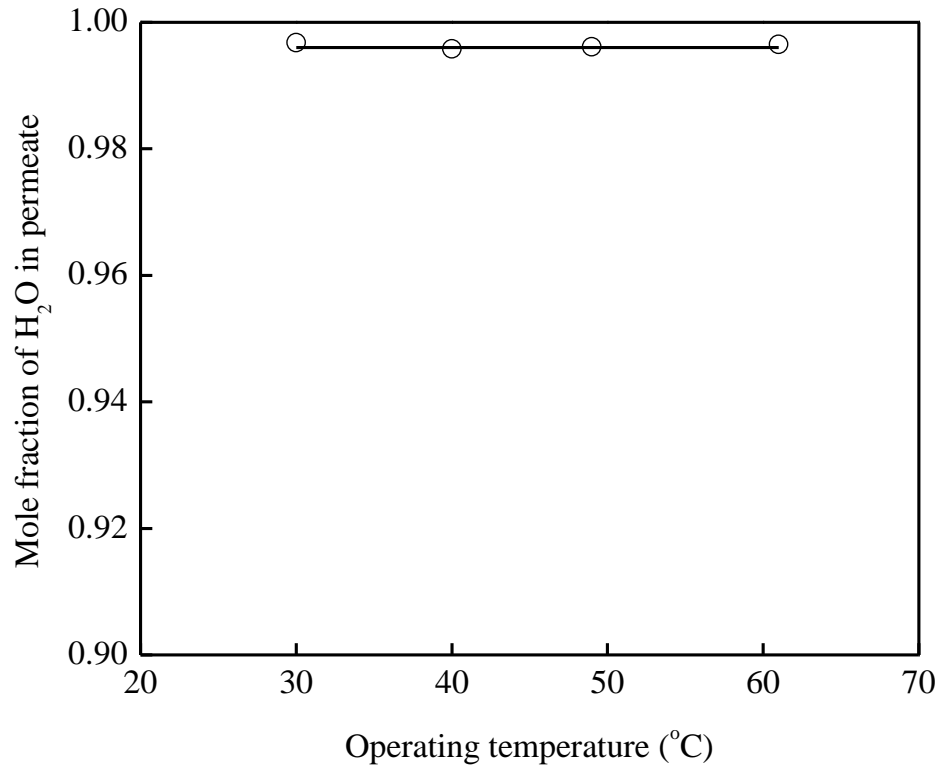
Fig. 7-9. Effect of operating temperature on permeate concentration. Operating conditions same as those specified in Fig. 7-8.

$$\left(P_i/l\right) = \frac{N_i}{p_i^s x_i \gamma_i - p_i^p y_i} = (P_{i0}/l)\exp(-\frac{E_{Pi}}{RT}) \tag{7-4}$$

where E_P the permeation activation energy characterizing the effect of temperature of the membrane permeability, (P_i/l) the permeance of the membrane, p^s the saturated vapor pressure of the permeant, γ the activity coefficient in the liquid phase, and p^p the permeate pressure. This is shown in Fig. 7-10; the membrane permeance decreased with an increase in temperature, and the E_P values for ethylene glycol and water were found to be -24 and -47 kJ/mol, respectively. Based on the solution-diffusion mechanism, the activation energy for permeation E_P is a combination of the heat of sorption ΔH_s and the activation energy for
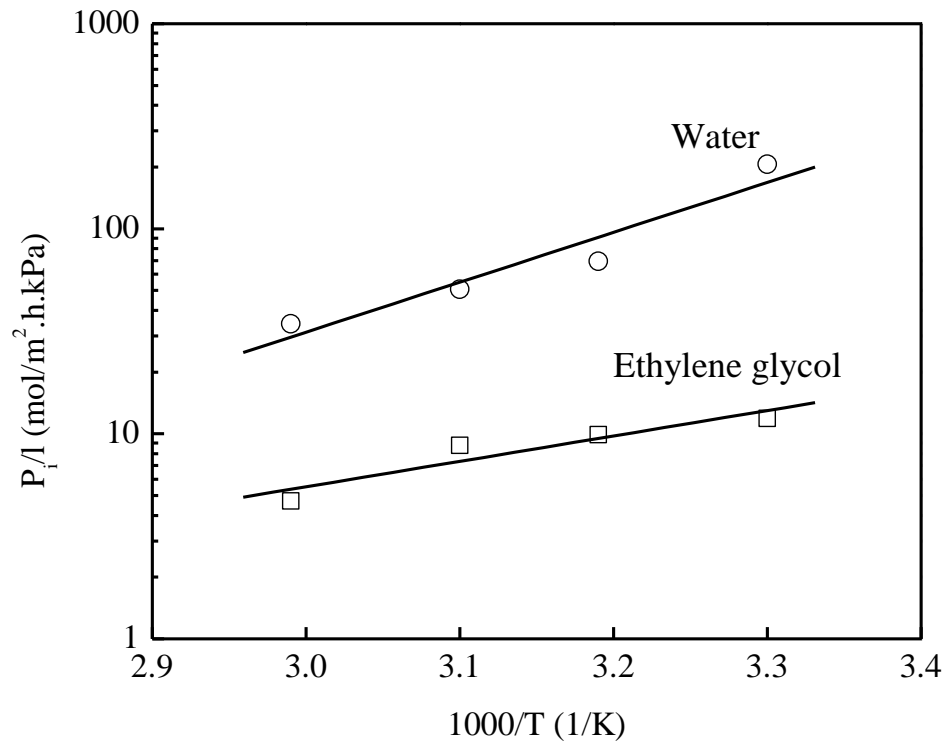
Fig. 7-10. Effect of operating temperature on partial permeance. Operating conditions same as those specified in Fig. 7-8.

diffusion E_D; as a first approximation, E_P can be considered to be equal to $(\varDelta H_s + E_D)$. Generally speaking, the activation energy for diffusion is the energy needed for diffusion to start, and its numerical value is thus positive. The sorption process, on the other hand, is often exothermic. The negative values of E_P appear to suggest that the negative $\varDelta H_s$ of the exothermic sorption process outweighs the positive E_D of the diffusion process. That is to say, as the temperature increases, the reduction in solubility prevails over the increase in diffusivity, resulting in a decrease in the membrane permeability. Therefore, the above observed increase in permeation flux with an increase in temperature is primarily due to the increased driving force.

151

7.3.3 Membrane Stability

The long-term stability of a membrane is an important factor for practical use. As mentioned before, because of the high hydrophilicity and the asymmetric crosslinked structure, the PDMAEMA membrane exhibited a quite high permeation flux. To test the membrane stability, a pervaporation run was carried out continuously with the composite PDMAEMA membrane for a duration of over 3 weeks, and the results are presented in Fig. 7-11. Essentially no reduction in the permselectivity was observed over the test period. The good stability of the membrane is expected considering the highly crosslinked surface layer of the PDMAEMA membrane which also functions as a protective layer to the less crosslinked interior from excessive swelling by feed.

7.3.4 A Comparison of Pervaporation Performance for Ethylene Glycol Dehydration

Several membranes have been studied for dehydration of ethylene glycol by pervaporation. To compare the performance of the PDMAEMA membrane studied here with membranes reported in the literature, the selectivity is plotted versus permeation flux in Fig. 7-12. In 1996 Feng and Huang [1996] reported pervaporation dehydration of ethylene glycol using lab-made chitosan/polysulfone composite membranes. Since then chitosan-based membranes and poly(vinyl alcohol)-based membranes for ethylene glycol dehydration have been studied extensively. For instance, Nam and Lee [1999] and Rao et al. [2007] used sulfuric acid and phosphoric acid respectively to crosslink the chitosan membranes, while Hu et al. [2007a;b] attempted to use chitosan-poly(acrylic acid) polyelectrolyte complex membranes. On the other hand, many studies on poly(vinyl alcohol)-based membranes (including the commercial GFT membranes) for ethylene glycol/water separation are reported [Chen and Chen 1996; 1998; Bartels and Reale, 1990; Guo et al., 2006; 2007a;b; Jehle et al., 1995]. Interpenetrating polymer network membranes of poly(vinyl alcohol)/poly(acrylic acid) and poly(vinyl alcohol)/poly(acryl amide) [Burshe et al., 1998] are also developed in order to provide a high permeation flux, but the selectivity was relatively low as compared to the conventional composite membranes. Sulfonated polymer membranes (e.g., sulfonated poly(ether ether ketone) [Huang et al., 2002; Shao, et al., 2005], sulfonated polyethylene [Pasternak and
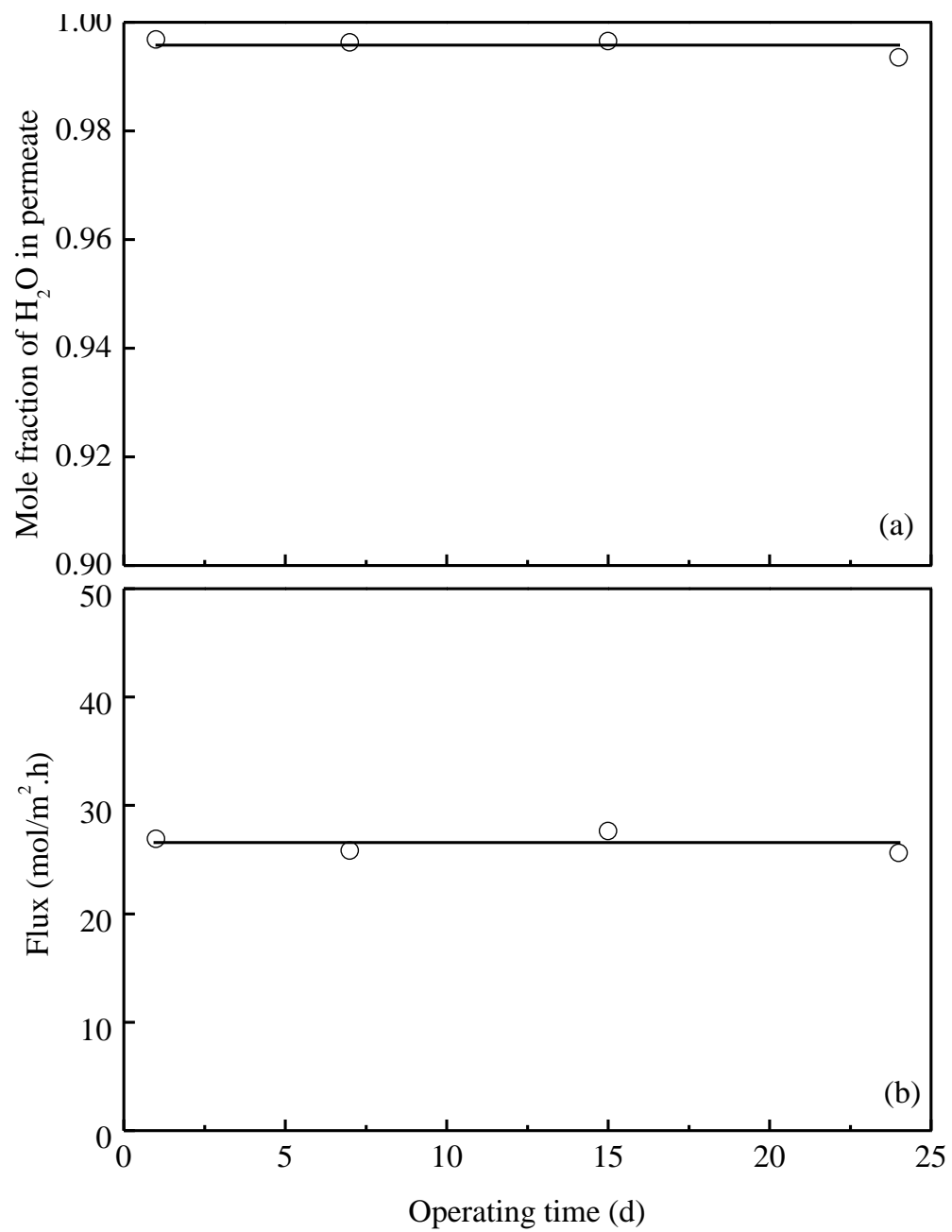
Fig. 7-11. Time dependence of (a) permeate concentration, and (b) permeation flux. Operating conditions same as those specified in Fig. 7-3.

153

Fig. 7-12. Comparison of pervaporation performance for ethylene glycol dehydration. Water content in feed: 28~60 mol%.

154

Reale, 1993]), which represent another category of polymer membranes for ethylene glycol dehydration, have a good selectivity, but the permeability is relatively low.

In addition to polymeric membranes, inorganic membranes (mainly zeolite membranes (type A and T) from Mitsui of Japan and silica membranes from ECN and Pervatech of the Netherlands) have also been used [Nik et al., 2006; Sommer and Melin, 2005]. In spite of their good permselectivity, the applications of the inorganic membranes are presently still limited because of the relatively high capital cost and poor processability. It should be pointed out that some of the performance data reported in the literature are not always consistent, and it is unclear whether the discrepancy is caused by issues related to reproducibility or uniformity of the membranes. For instance, Nik et al. [2006], who tested Mitsui zeolite membrane (type A, tubular id/od ~10/12.5 mm) for ethylene glycol dehydration at 70 °C, reported that at a feed water concentration of 28 mol%, the permeation flux and permeate water concentration were 35 mol/(m^2 h) and 99.6 mol%, respectively, and the permeation flux was shown to increase with temperature. However, the data of Sommer and Melin [2005] show that at 100 °C the Mitsui zeolite membrane (id/od 9/12 mm) had a much lower permeation rate of 1.7 mol/(m^2 h), while the water concentration in the permeate was higher (99.997 mol%). These differences cannot be fully attributed to the difference in the vacuum levels used on the permeate side because the permeances (which can be calculated from the permeation flux normalized by the partial pressure difference across the membrane) are significantly different for the two cases.

It can be seen from Fig. 7-12 that performance of the PDMAEMA/PSF membrane compares favorably with other membranes at similar operating conditions. Note that the PDMAEMA/PSF composite membrane used in this work was not prepared under optimized conditions, and it is possible to further improve the membrane performance by adjusting the parameters involved in the membrane formation process.

7.4 Conclusions

The pervaporation performance of interfacially formed PDMAEMA/PSF composite membranes for dehydration of ethylene glycol was investigated, and the following conclusions can be drawn

(1) The PDMAEMA/PSF composite membranes prepared by solid-liquid interfacial crosslinking were selective to water permeation over the entire concentration range for ethylene glycol dehydration.

(2) The preferential permeation of water through the membranes was derived from the diffusion selectivity. The membrane showed a slightly selective sorption to ethylene glycol because of the stronger affinity between the membrane and the diol.

(3) At 30°C, a permeation flux of ~1 mol/(m$^{2.}$h) and a permeate water concentration of 99.7 mol% were achieved at 1 mol% water in feed. The membrane performance compared favorably with other membranes reported in the literature.

(4) An increase in the operating temperature increased the permeation flux, and the membrane selectivity was not affected significantly. The increase in permeation flux with temperature was primarily due to the increased driving force for permeation, and the membrane permeability was shown to decrease as temperature increased.

Chapter 8

General Conclusions, Contributions and Recommendations

8.1 General Conclusions and Contributions to Original Research

8.1.1 Selection of Membrane Material and Preparation of Low Resistance Membranes

1) The water-soluble homopolymer PDMAEMA was synthesized via free radical bulk polymerization using AIBN as the initiator. PDMAEMA was chemically crosslinked with XDC at room temperature via complete alkylation reaction between the tertiary amino groups in the side chains of PDMAEMA and the chloromethyl groups in the dihalide, and converted into a quaternary ammonium salt. The chemical structure change due to crosslinking was verified by FTIR. The quaternary amino groups of crosslinked PDMAEMA made it positively charged. The polarity and hydrophilicity of the crosslinked PDMAEMA were analyzed with dyes (positively charged, negatively charged and neutral) and contact angle measurements, respectively, and the results showed that the crosslinking of the PDAMEMA membrane increased the surface hydrophilicity.

2) Both bulk crosslinked and solid-liquid interfacially crosslinked PDMAEMA membranes were formed on a microporous PSF or PAN substrate. The structure of the membrane was examined using SEM. The results showed that the PDMAEMA coating layer was thin and dense, and the adhesion of the PDMAEMA layer to the substrate was excellent. The asymmetric structure in the interfacially crosslinked PDMAEMA layer due to the "self-limiting" effect during the interfacial reaction was confirmed by mass change and SEM. The highly crosslinked outer surface was supposed to dominate the selectivity of the membrane and to protect the less crosslinked interior from excessive swelling by feed, while the unreacted amino groups in the interior offered less restricted mobility of the polymer chains and was favorable for high permeability. A three-fold increase in the membrane permeance to CO_2 was achieved without compromising the selectivity of CO_2/N_2, as compared with membranes prepared by bulk crosslinking.

8.1.2 Application of Interfacially Formed PDMAEMA Membranes

1) The permeability of the composite membrane to gases follows the order of $N_2 < CH_4 <$ $O_2 < H_2 < CO_2$, and the membrane was found to compare favorably with other membranes based on copolymerization and plasma grafting of DMAEMA in terms of CO_2/N_2 permselectivity. At $23^{o}C$ and 0.41 MPa, the membrane showed a CO_2 permeance of 85 GPU and a CO_2/N_2 ideal separation factor of 50.

Coupling effects were present in the permeation of binary gas mixtures, CO_2/N_2, CO_2/CH_4 and CO_2/H_2. The negative coupling effect was observed for CO_2 transport due to the competition between CO_2 and the other gases for the limited number of sorption sites and diffusion pathways in the membrane, while positive coupling effect was observed for inert gases because of CO_2-induced membrane swelling. The significance of the coupling depended on the molecular size of the inert gases. The permeance of CO_2 and selectivity of the binary mixtures were found to be lower than those based on pure gas permeation due to the coupling effects in the gas mixture permeation.

2) For water vapor permeation, the permeance of water vapor was 5350 GPU at $25^{o}C$ and 100 % relative humidity in the feed. An analysis based on the resistance model showed that, due to the low resistance of the interfacially crosslinked PDMAEMA layer, the resistance of the PAN substrate to water permeation was about 30 to 40 % of the total resistance of the composite membrane and could not be neglected. The membrane was tested for natural gas dehydration and gas humidification. A high vacuum level or carrier gas flow rate in the permeate side led to a high water vapor permeation flux.

3) For pervaporation dehydration of ethylene glycol, the membrane showed good permselectivity as compared with those reported in the literature due to the high hydrophilic and low resistance of the PDMAEMA layer. At $30^{o}C$, a permeation flux of ~ 1 mol/(m^2.h) and a permeate concentration of 99.7 mol% water were achieved at 1 mol% water in the feed. The swelling tests of the PDMAEMA layer in aqueous ethylene glycol solutions showed that preferential sorption was not the prerequisite to preferential permeation. The increase in

permeation flux with temperature was primarily due to the increased driving force for permeation, and the membrane permeability was shown to decrease as temperature increased.

8.1.3 Transport Mechanisms through PDMAEMA Membranes

1) Gas permeation through dry and humidified PDMAEMA membranes showed that water played an important role in the mass transport. Gases pass through the membrane via the water "path" or water "bridge" as well as polymer matrix. N_2, CH_4 and H_2 are inert gases to the polymer and water, and their transport through both dry and wet membranes follows a simple solution-diffusion model. The transport of CO_2 follows facilitated transport and the transport mechanism in the dry membrane is different from that in the wet membrane. In a dry membrane, CO_2 transport includes free molecular diffusion and CO_2-amino group complex transport based on the weak acid-base interaction between CO_2 and quaternary amino groups and reversible reaction between CO_2 and tertiary amino groups. In a wet membrane, on the other hand, part of CO_2 molecules can transform into small and easy-to-move ions HCO_3^- and can transport through the water path or through amino groups. The hydration of CO_2 can be catalyzed by amino groups.

2) The hydrophilic amino groups may also be regarded as carriers for water permeation based on hydrogen bonding. The free water molecules or water clusters can not only diffuse through the water path, but transport from one amino group to another as well.

8.2 Recommendations for Future Work

1) It has been shown that the flat sheet interfacially formed PDMAEMA membranes are promising for permeation of acid gas and water vapor. Hollow fiber has larger membrane surface per module volume. Therefore, an ultra-thin hollow fiber composite membrane is recommended here for a better performance module. The hollow fiber composite membrane may be developed by inner coating a PDMAEMA layer with a PDMAEMA solution passing through the lumen of hollow fibers.

2) The amino groups in the side chains of PDMAEMA are carriers for transport of CO_2 and water. Therefore, the alkalinity of the amino groups, entanglement of the chains and the

steric effects of the functional groups are important for the transport performance. From the point of view of materials, structure of amino groups can be changed to improve the membrane performance or to adjust the crosslinking structure of the active layer for different applications. Considering not all of the monomer is commercially available, the monomer of these polymers can be synthesized through the ester exchange reaction:

$$RCOOR' + R''OH\,(excess) \rightarrow RCOOR'' + R'OH$$
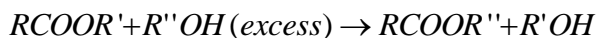
- Change alkalinity of amino groups

Different amino groups (e.g. primary, secondary, or tertiary amino group) may give different alkalinity.

$$CH_3-\underset{\underset{CH_2}{\|}}{C}-\overset{\overset{O}{\|}}{C}-O-CH_3 \quad + \quad HO-C_2H_4-\underline{\underline{NH_2}} \quad \longrightarrow$$

$$+ \quad HO-C_2H_4-\underline{\underline{NH(CH_3)}} \quad \longrightarrow$$

$$+ \quad HO-C_2H_4-\underline{\underline{N(CH_3)_2}} \quad \longrightarrow$$
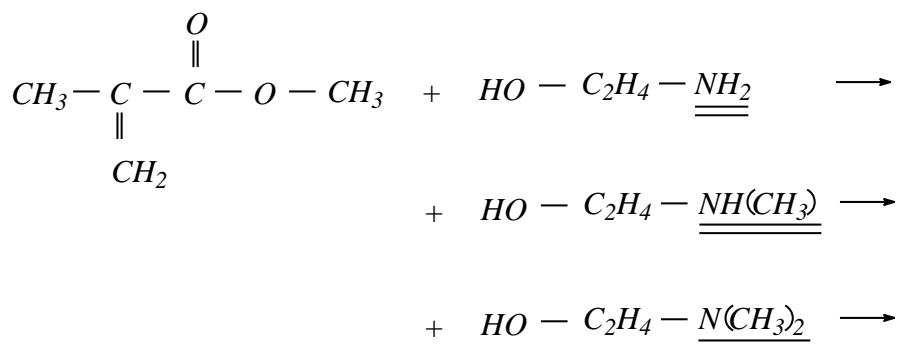
- Change length of side chain

The extent of entanglement of side chains can be adjusted by using short or long side chains.

$$CH_3-\underset{\underset{CH_2}{\|}}{C}-\overset{\overset{O}{\|}}{C}-O-CH_3 \quad + \quad HO-\underline{\underline{CH_2}}-N(CH_3)_2 \quad \longrightarrow$$

$$+ \quad HO-\underline{\underline{C_2H_4}}-N(CH_3)_2 \quad \longrightarrow$$

$$+ \quad HO-\underline{\underline{C_3H_6}}-N(CH_3)_2 \quad \longrightarrow$$
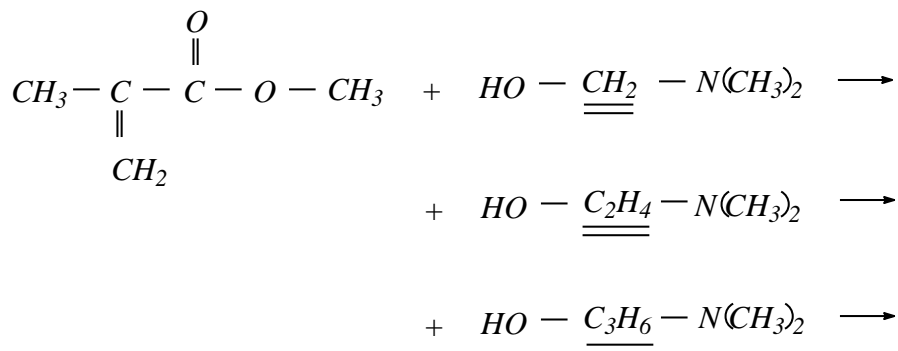
- Change steric effects

The size of substitute groups on the amino groups will give different steric effects.

160

$$CH_3-\underset{\underset{CH_2}{\|}}{\overset{\overset{O}{\|}}{C}}-C-O-CH_3 \quad + \quad HO-C_2H_4-N(CH_3)_2 \quad \longrightarrow$$

$$+ \quad HO-C_2H_4-N(CH_2CH_3)_2 \quad \longrightarrow$$
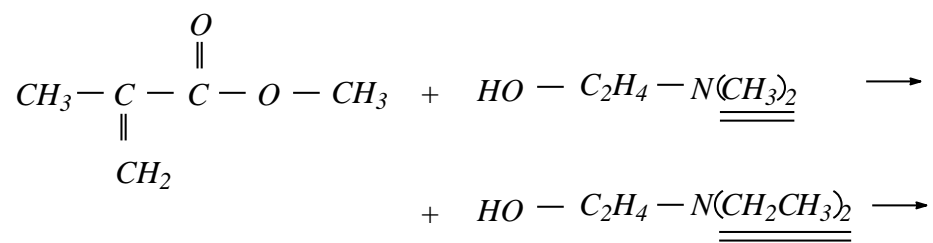
Notation

A	Effective area of membrane
C	Permeant concentration
D	Diffusion coefficient
E_P	Apparent activation energy of permeation
F_J	F parameter based on permeance defined in Eq. (3-4)
J	Permeance
k_D	Henry's law constant
l	Membrane thickness
N	Permeation flux
P	Permeability coefficient
p	Gas partial pressure
Δp	Transmembrane pressure difference
Q	Permeation rate
R	Resistance of membrane
R_0	Ideal gas constant
r	Average radius of the pores of porous membrane
S	Solubility coefficient
T	Absolute temperature
t	Permeation time
V	Permeate volume collected over a period of time
W	Weight
W_a	Work of adhesion

X	Concentration in feed
x	Position coordinate along the flow direction
Y	Concentration in permeate

Greek Letters

α	Ideal separation factor
β	Contact angle
γ	Surface free energy
δ	Solubility parameter
ε	Area porosity of porous membrane in Eq. (6-10) or volume fraction of water in water-saturated membrane in Eq. (5-2)
θ	Permeation ratio defined in Eq. (5-5)
τ	Tortuosity of water path defined in Eq. (5-2)

Subscripts

i	Fast permeating gas
j	Slow permeating gas
f	Feed side of a membrane
p	Permeate side of a membrane

Glossary

AIBN	2,2'-azobisisobutyronitrile
DEA	Diethanolamine
DMAc	N,N-dimethylacetamide
EDA	Ethylenediamine
EG	Ethylene glycol
MEA	Monoethanolamine
PAN	Polyacrylonitrile
PDMAEMA	Poly(N,N-dimethylaminoethyl methacrylate)
PDMS	Polydimethylsiloxane
PEI	Polyethylenimine
PSF	Polysulfone
PVA	Poly(vinyl alcohol)
PVP	Polyvinylpyrrolidone
XDC	p-xylylene dichloride

Structure of Membrane Materials

$$\left[CH_2-CH \atop C\equiv N \right]_n$$ PAN
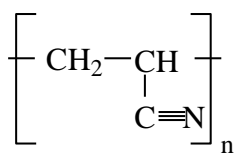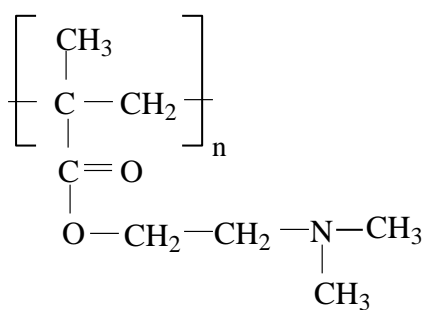
$$\left[\begin{array}{c} CH_3 \\ C-CH_2 \\ C=O \\ O-CH_2-CH_2-N-CH_3 \\ CH_3 \end{array} \right]_n$$ PDMAEMA
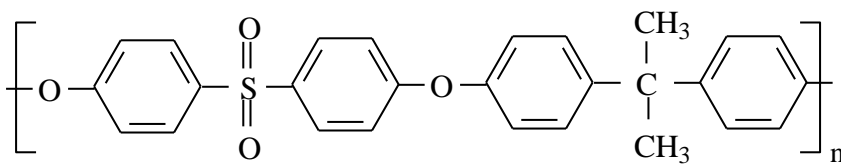
PSF

PVP

PDMS
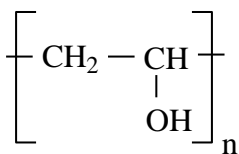
PVA
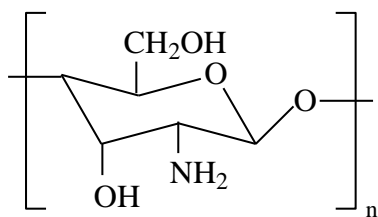
Chitosan

Bibliography

Ahmed, C., Roudesli, S., Metayer, M., Labbe, M., Langevin, D., Reaction in ion-exchanges: characterization of the ethylene-diamine protonation equilibrium in a sulfonic membrane devoted to carbon dioxide facilitated transport, Reactive Polymers, 24 (1995) 213-218.

Ahn, S.M., Ha, J.W., Kim, J.H., Lee, Y.T., Lee, S.B., Pervaporation of fluoroethanol/water and methacrylic acid/water mixtures through PVA composite membranes, J. Membr. Sci., 27 (2005) 51-57.

Amiji, M.M., Biocompatible articles and method for making same, US Patent, 5,885,609 (1999).

Aptel, P., Challard, N., Cunny, J., Neel J., Application of the pervaporation process to separate azeotropic mixtures, J. Membr. Sci., 1 (1976) 271-287.

Aranda, P., Chen, W.J., Martin, C.R., Water transport across polystyrenesulfonate/alumina composite membranes, J. Membr. Sci., 99 (1995) 185-196.
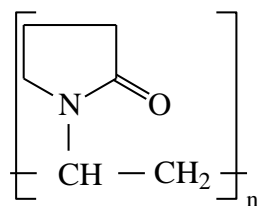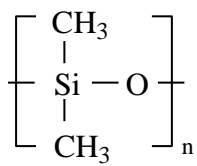
Atkinson, S., A brief history of membrane science, Filtration and Separation, (1999) 28.

Baines, F.L., Billingham, N.C., Armes, S.P., Synthesis and solution properties of water- soluble hydrophilic-hydrophobic block copolymers, Macromolecules, 29 (1996) 3416-3420.

Baker, R.W. Membrane technology and applications, 2nd ed., Wiley, New York, 2004.

Barbari, T.A., Polymeric membranes based on bisphenol-a for gas separations, J. Membr. Sci., 42 (1989) 69-86.

Barrer, R.M., Diffusivities in glassy polymers for the dual mode sorption model, J. Membr. Sci., 18 (1984) 25-35.

Barrie, J.A., Machin, D., Nunn, A., Transport of water in synthetic cis-1,4-polyisoprenes and natural rubber, Polymer, 16 (1975) 811-814.

Bartels, C.R., Reale Jr., J., Dehydration of glycols, US Patent 4,941,976 (1990).

Bartsch. R.A., Way, J.D., Chemical separations with liquid membranes: an overview, in: Bartsch. R.A., Way, J.D. (Eds.), Chemical Separations with Liquid Membranes, ACS Symp. Series, 642 (1996) 1-15.

Basu A., Akhtar J., Rahman M.H., Islam M.R., A review of separation of gases using membrane systems, Petrol. Sci. Technol., 22 (2004), 1343-1368.

Boddeker, K.W., Bengston, G., Bode, E., Pervaporation of low volatility aromatics from water, J. Membr. Sci., 53 (1990) 143-158.

Bravo, I.J., Fair, J.R., Humphery, J.L., Martin, C.L., Seibert, A.F., Joshi, S., Fluid mixture separation technologies for cost reduction and process improvement, Noyes Data Corp., Park Ridge, NY., 1986.

Brueschke, H., Multilayered membrane and its use in separating liquid mixtures by the pervaporation method, German Patent, DE 3220570A1, 1983-12-01.

Brun, J.P., Larchet, C., Bulvestre, G., Auclair, B., Sorption and pervaporation of dilute aqueous solutions of organic compounds through polymer membranes, J. Membr. Sci., 25 (1985) 55-100.

Burshe, M.C., Sawant, S.B., Joshi, J.B., Pangarkar, V.G., Dehydration of ethylene glycol by pervaporation using hydrophilic IPNs of PVA, PAA and PAAM membranes, Sep. Purif. Technol., 13 (1998) 47-56.

Cadotter, J.E., Evolution of composite reverse osmosis membranes, in: Lloyd, D.R. (Ed.), Materials Science of Synthetic Membranes, American Chemical Society, Washington, DC, 1985.

Castro, R.P., Baker, R.W., Wijmans, J.G., Multilayer interfacial composite membrane, US Patent 5,049,167 (1991).

Cha, J.S., Li, R., Sirkar, K.K., Removal of water vapor and VOCs from nitrogen in a hydrophilic hollow fiber gel membrane permeator, J. Membr. Sci., 119 (1996) 139-153.

Chakma, A., Separation of CO_2 and SO_2 from flue gas streams by liquid membranes, Energy Conversion and Management, 36 (1995) 405-410.

Charati, S.G., Stern, S.A., Diffusion of gases in silicone polymers: molecular dynamic simulations, Macromolecules, 31 (1998) 5529-5535.

Chen, F.R., Chen, H.F., A diffusion model of the pervaporation separation of ethylene glycol-water mixtures through crosslinked poly(vinyl alcohol) membrane, J. Membr. Sci., 139 (1998) 201-209.

Chen, F.R., Chen, H.F., Pervaporation separation of ethylene glycol-water mixtures using crosslinked PVA-PES composite membranes. Part I. Effects of membrane preparation conditions on pervaporation performances, J. Membr. Sci., 109 (1996) 247-256.

Clasen, C., Wilhelms, T., Kulicke, W.M., Formation and characterization of chitosan membranes, Biomacromolecules, 7 (2006) 3210-3222.

Considine, G.D., Kulik, P.H., Van Nostrand's Scientific Encyclopedia, 9th Ed., Wiley, New York, 2002.

Credali, L., Chiolle, A., Parrini, P., New completely aliphatic anionic membranes from polymers of unsaturated tertiary amines, Part I. Preparation and properties, Die Makromolekulare Chemie, 154 (1972) 201-214.

Creutz, S., Teyssie, P., Jerome, R., Living anionic homopolymerization and block copolymerization of (dimethylamino)ethyl methacrylate, Macromolecules, 30 (1997) 6-9.

Cunningham, V.L., Crosslinked, macroreticular poly(dimethylaminoethyl methacrylate) ion-exchange resins and method of preparation by aqueous suspension polymerization using trialkylamine phase extender, US Patent 4,052,343 (1977).

Cunningham, V.L., Poly(dimethylaminoethyl methacrylate) and method of preparation, US Patent 4,129,534 (1978).

Cussler, E.L., Aris, R., Bhown, A., On the limits of facilitated diffusion, J. Membr. Sci., 43 (1989) 149-164.

Dhingra, S.S., Marand, E., Mixed gas transport study through polymeric membranes, J. Membr. Sci., 141 (1998) 45-63.

Dogihere, F., Nardella, A., Sarti, G.C., Valentini, C., Pervaporation of methanol/MTBE through modified PPO membranes, J. Membr. Sci. 91 (1994) 283-291.

Donohue, M.D., Permeation behaviour of carbon dioxide-methane mixtures in cellulose acetate membranes, J. Membr. Sci., 42 (1989) 197-214.

Du, R., Zhao, J., Positively charged composite nanofiltration membrane prepared by poly(N,N-dimethylaminoethyl methacrylate)/polysulfone, J. Appl. Polym. Sci., 91 (2004a) 2721-2728.

Du, R., Zhao, J., Properties of poly (N, N-dimethylaminoethyl methacrylate)/polysulfone positively charged composite nanofiltration membrane, J. Membr. Sci., 239 (2004b) 183-188.

Fang, J., Kita, H., Okamoto, K., Gas separation properties of hyperbranched polyimide membranes, J. Membr. Sci., 182 (2001) 245-256.

Farhat, T., Yassin, G., Dubas, S.T., Schlenoff, J.B., Water and ion pairing in polyelectrolyte multilayers, Langmuir, 15 (1999) 6621-6623.

Feng, X., Huang, R.Y.M., Liquid separation by membrane pervaporation: a review, Ind. Eng. Chem. Res., 36 (1997) 1048-1066.

Feng, X., Huang, R.Y.M., Pervaporation with chitosan membranes. I. Separation of water from ethylene glycol by a chitosan/polysulfone composite membrane, J. Membr. Sci., 116 (1996) 67-76.

Feng, X., Shao, P., Huang, R.Y.M., Jiang, G., Xu, R., A study of silicone rubber/polysulfone composite membranes: correlating H_2/N_2 and O_2/N_2 permselectivities, Sep. Purif. Technol., 27 (2002) 211-223.

Freeman, B.D., Basis of permeability/selectivity tradeoff relations in polymeric gas separation membranes, Macromolecules, 32 (1999) 375-380.

Freeman, B.D., Pinnau I., Gas and liquid separations using membrane: an overview, ACS Symp. Series, 876 (Advanced materials for membrane separations) (2004) 1-23.

Freger, V., Nanoscale heterogeneity of polyamide membranes formed by interfacial polymerization, Langmuir, 19 (2003) 4791-4797.

Freger, V., Srebnik, S., Mathematical model of charged and density distributions in interfacial polymerization of thin films, J. Appl. Polym. Sci., 88 (2003) 1162-1169.

Fu, H., Jia, L., Xu, J., Studies on the sulfonation of poly(phenylene oxide) (PPO) and permeation behaviour of gases and water vapor through sulfonated PPO membranes. II. Permeation behaviour of gases and water vapor through sulfonated PPO membranes, J. Appl. Polym. Sci., 51 (1994) 1405-1409.

Fujita, H., Diffusion in polymer-diluent systems, Fortschritte der Hochpolymeren -Forschung, 3 (1961) 1-47.

Fukutomi, T., Takizawa, M., Nakamura, M., Charged mosaic membrane and production process thereof, US Patent 5,543,045 (1996).

Gierke, T.D., Munn an, G.E., Wilson, F.C., The morphology in Nafion perfluorinated membrane products, as determined by wide-and small angle X-ray studies, J. Polym. Sci. Phys. Edn., 19 (1981) 1687-1704.

Gómez, P., Daviou, M.C., Ibáñez, R., Eliceche, A.M., Ortiz, I., Comparative behaviour of hydrophilic membranes in the pervaporative dehydration of cyclohexane, J. Membr. Sci., 279 (2006) 635-644.

Greiveldinger, M., Shanahan, M.E.R., Acid base contributions to interfacial free energy: self-consistency considerations, C. R. Acad. Sci. Ser. II, 327 (1999) 275-283.

Guha, A.K., Majumdar, S., Sirkar, K.K., A large-scale study of gas separation by hollow-fiber-contained liquid membrane permeator, J. Membr. Sci., 62 (1991) 293-307.

Guha, A.K., Majumdar, S., Sirkar, K.K., Facilitated transport of CO_2 through an immobilized liquid membrane of aqueous diethanolamine, Ind. Eng. Chem. Res., 29 (1990) 2093-2100.

Guha, A.K., Majumdar, S., Sirkar, K.K., Gas separation modes in a hollow fiber contained liquid membrane permeator, Ind. Eng. Chem. Res., 31 (1992) 593-604.

Guo, R., Hu, C., Li, B., Jiang, Z., Pervaporation separation of ethylene glycol/water mixtures through surface crosslinked PVA membranes: Coupling effect and separation performance analysis, J. Membr. Sci., 289 (2007a) 191-198.

Guo, R., Hu, C., Pan, F., Wu, H., Jiang, Z., PVA-GPTMS/TEOS hybrid pervaporation membrane for dehydration of ethylene glycol aqueous solution, J. Membr. Sci., 281 (2006) 454-462.

Guo, R., Ma, X., Hu, C., Jiang, Z., Novel PVA-silica nanocomposite membrane for pervaporative dehydration of ethylene glycol aqueous solution, Polymer, 48 (2007b) 2939-2945.

Hamada, T., Taya, M., Tone, S., Pervaporation and vapor permeation behaviour of water and 2-propanol in water-selective membranes, J. Chem. Eng. Japan, 30 (1997) 600-608.

Hansen, C.M., Hansen Solubility Parameters: A User's Handbook, 2nd ed., CRC Press, Boca Raton, 2007.

Hayashi, Y., Sugiyama, S., Kawanishi, T., Shimizu, N., Kinetics of sorption and permeation of water in glassy polyimide, J. Membr. Sci., 156 (1999) 11-16.

Heaney, M.D., Pellegrineo, J., Increased facilitated transport related to microstructural changes in heat-treated ion-exchange membranes, J. Membr. Sci., 47 (1989) 143-161.

Higuchi, A., Abe, M., Komiyama, J., Iijima, T., Gas permeation through hydrogels I. Gel cellophane membranes, J. Membr. Sci., 21 (1984) 113-121.

Hofmann, D., Fritz, L., Ulbrich J., Schepers C., Böhning M., Detailed-atomistic molecular modeling of small molecule diffusion and solution processes in polymeric membrane materials, Macromol. Theory Simul., 9 (2000) 293-327.

Hong, J.M., Kang, Y.S., Jang, J., Kim, U.Y., Analysis of facilitated transport in polymeric membrane with fixed site carrier. 2. Series RC circuit model, J. Membr. Sci., 109 (1996) 159-163.

Hong, S.U., Won, J., Park, H.C., Kang, Y.S., Estimation of penetrant transport properties through fixed site carrier membranes using the RC circuit model and sensitivity analysis, J. Membr. Sci., 163 (1999) 103-108.

Hu, C., Guo, R., Li, B., Ma, X., Wu, H., Jiang, Z., Development of novel mordenite-filled chitosan-poly(acrylic acid) polyelectrolyte complex membranes for pervaporation dehydration of ethylene glycol aqueous solution, J. Membr. Sci., 293 (2007) 142-150.

Hu, C., Li, B., Guo, R., Wu, H., Jiang, Z., Pervaporation performance of chitosan-poly(acrylic acid) polyelectrolyte complex membranes for dehydration of ethylene glycol aqueous solution, Sep. Purif. Technol., 55 (2007) 327-334.

Huang, J., Cranford, R., Matsuura, T., Roy, C., Water vapor permeation properties of aromatic polyimides, J. Membr. Sci., 215 (2003) 129-140.

Huang, R.Y.M., Feng, X., Resistance model approach to asymmetric polyetherimide membranes for pervaporation of isopropanol/water mixtures, J. Membr. Sci., 84 (1993) 15-27.

Huang, R.Y.M., Lin, V.J.C., Separation of liquid mixtures by using polymer membranes. I. Permeation of binary organic liquid mixtures through polyethylene, J. Appl. Polym. Sci., 12 (1968) 2615-2631.

Huang, R.Y.M., Moreira, A., Notarfonzo, R., Xu, Y.F., Pervaporation separation of acetic acid-water mixtures using modified membranes. I. Blended polyacrylic acid (PAA)-Nylon 6 membranes, J. Appl. Polym. Sci., 35 (1988) 1191-1200.

Huang, R.Y.M., Pal, R., Moon, G.Y., Characteristics of sodium alginate membranes for the pervaporation dehydration of ethanol-water and isoporpanol-water mixtures, J. Membr. Sci., 160 (1999a) 101-113.

Huang, R.Y.M., Rhim, J.W., Separation characteristics of pervaporation membrane separation processes, in: Huang, R.Y.M. (Ed.), Pervaporation Membrane Separation Processes, Elsevier, Amsterdam, (1991) 111-180.

Huang, R.Y.M., Shao, P., Feng, X., Anderson, W.A., Separation of ethylene glycol-water mixtures using sulfonated poly(ether ether ketone) pervaporation membranes: membrane relaxation and separation performance analysis, Ind. Eng. Chem. Res., 41 (2002) 2957-2965.

Huang, R.Y.M., Yeom, C.K., Pervaporation separation of aqueous mixtures using crosslinkied poly(vinyl alcohol)(PVA). II. Permeation of ethanol-water mixtures, J. Membr. Sci., 51 (1990) 273-292.

Huang, S.H., Li, C.L., Hu, C.C., Tsai, H.A., Lee, K.R., Lai, J.Y., Polyamide thin-film composite membranes prepared by interfacial polymerization for pervaporation separation, Desalination, 200 (2006) 387-389.

Huang, X.D., Goh, S.H., Lee, S.Y., Zhao, Z.D., Wong, M.W., Miscibiltiy and interactions in blends and complexes of poly [2-(dimethylamino)ethyl methacrylate] with poly (*p*-vinylphenol), Macromolecules, 32 (1999b) 4327-4331.

Hurlock, J.R., Process for preparing hydrophilic dispersion polymers for treating wastewater, US Patent 6,025,426 (2000).

Hyun, D., Kim, J., Study of external humidification method in proton exchange membrane fuel cell, J. Power Sources, 126 (2004) 98-103.

Inui, K., Tsukamoto, K., Miyata, T., Uragami, T., Permeation and separation of benzene cyclohexane mixtures through benzoyl chitosan membranes, J. Membr. Sci., 138 (1998) 67-75.

Islam, M.A., Buschatz, H., Gas permeation through a glassy polymer membrane: chemical potential gradient or dual mobility mode? Chem. Eng. Sci., 57 (2002) 2089-2099.

Ismail, A.F., Dunkin, I.R., Gallivan, S.L., Shilton, S.J., Production of super selective Polysulfone hollow fiber membranes for gas separation, Polymer, 40 (1999) 6499-6506.

173

Ismail, A.F., Lorna, W., Penetrant-induced plasticization phenomenon in glassy polymers for gas separation membrane, Sep. Purif. Tech., 27 (2002) 173-194.

Ito, A., Dehumidification of air by a hygroscopic liquid membrane supported on surface of a hydrophobic microporous membrane, J. Membr. Sci., 175 (2000) 35-42.

Itoh, T., Toya, H., Ishihara, K., Shinohara, I., Design of polymer membrane with permselectivity for water-ethanol mixture. II. Preparation of crosslinked poly(methyl acrylate) membrane with diethylene triamine and its permselectivity, J. Appl. Polym. Sci., 30 (1985) 179-188.

Jacob, P.N., Berg, J.C., Acid-base surface energy characterization of microcrystalline cellulose and two wood pulp fiber types using inverse gas chromatography, Langmuir, 10 (1994) 3086-3093.

Jae, S.Y., Kim, H.J., Jo, W.H., Kang, Y.S., Analysis of PV for MTBE/Methanol mixtures through CA and CTA membranes, Polymer, 39 (1998) 1381-1385.

Jehle, W., Staneff, Th., Wagner, B., Steinwandel, J., Separation of glycol and water from coolant liquids by evaporation, reverse osmosis and pervaporation, J. Membr. Sci., 102 (1995) 9-19.

Ji, J., Dickson, J.M., Childs, R.F., McCarry, B.E., Mathematical model for the formation of thin-film composite membranes by interfacial polymerization: porous and dense films, Macromolecules, 33 (2000) 624-633.

Jonquières, A., Clément, R., Lochon, P., Néel, J., Dresch, M., Chrétien, B., Industrial state-of-the-art of pervaporation and vapor permeation in the western countries, J. Membr. Sci., 206 (2002) 87-117.

Kang, Y.S., Hong, J.M., Jang, J., Kim, U.Y., Analysis of facilitated transport in solid membranes with fixed site carriers. 1. Single RC circuit model, J. Membr. Sci., 109 (1996) 149-157.

Kao, M.J., Tien, D.C., Jwo C.S., and Tsung, T.T., The study of hydrophilic characteristics of ethylene glycol, J. Physics: Conference Series, 13 (2005) 442-445.

Kapantaidakis, G.C., Koops, G..H., Wessling, M., Kaldis, S.P., Sakellaropoulos, G.P., CO_2 plasticization of polyethersulfone/polyimide gas-separation membranes, AIChE J., 49 (2003) 1702-1711.

Karakane, H., Tsuyumoto, M., Maeda, Y., Honda, Z., Separation of water-ethanol by pervaporation thrgouh polyion complex composite membrane, J. Appl. Polym. Sci., 42 (1991) 3229-3239.

Kataoka, T., Tsuru, T., Nakao, S., Kimura, S., Membrane transport properties of pervaporation and vapor permeation in ethanol-water system using polyacrylonitrile and cellulose acetate membranes, J. Chem. Eng. Japan, 24 (1991) 334-339.

Kim, E. J., Cho, S. H., Yuk, S. H., Polymeric microspheres composed of pH/temperature-sensitive polymer complex, Biomaterials, 22 (2001) 2495-2499.

Kim, J.H., Lee, K.H., Kim, S.Y., Pervaporation separation of water from ethanol through polyimide composite membranes, J. Membr. Sci., 169 (2000) 81-93.

Koros, W.J., Evolving beyond the thermal age of separation processes: Membrane can lead the way, AIChE J., 50 (2004) 2326-2334.

Koros, W.J., Fleming, G.K., Jordan, S.M., Kim, T.H., Hoehn, H.H., Polymeric membrane materials for solution-diffusion based permeation separations, Prog. Polym. Sci., 13 (1988) 339-401.

Koros, W.J., Fleming, G.K., Membrane-based gas separation, J. Membr. Sci., 83 (1993) 1-80.

Koros, W.J., Gas separation membranes: Needs for combined materials science and processing approaches, Macromol. Symp., 188 (2002) 13-22.

Koros, W.J., Ma, Y.H., Shimidzu, T., Terminology for membranes and membrane processes, J. Membr. Sci., 120 (1996) 149-159.

Koros, W.J., Paul, D.R., Current aspects of membrane-based separation of gases, in: Chenoweth, M.B. (Ed.), Synthetic Membranes, Harwood Academic Publisher, New York, 1984.

Koros, W.J., Paul, D.R., Huvand, G.S., Energetics of gas sorption in glassy polymers, Polymer, 20 (1979) 956-960.

Köstler, S., Delgado, A.V., Ribitsch, V., Surface thermodynamic properties of polyelectrolyte multilayers, J. Colloid Interf. Sci., 286 (2005) 339-348.

Landro, L.D., Pegoraro, M., Bordogna, L., Interactions of polyether-polyurethanes with water vapour and water-methane separation selectivity, J. Membr. Sci., 64 (1991) 229-236.

Langevin, D., Pinoche, M., Selebny, E., Metayer, M., Poux, R., CO_2 facilitated transport through functionalized cation-exchange membranes, J. Membr. Sci., 82 (1993) 51-63.

LeBlance, O.H. Jr., Ward, W.J., Matson, S.L., Kimura, S.G., Facilitated transport in ion-exchange membrane, J. Membr. Sci., 6 (1980) 339-343.

Lee, Y.M., Nam, S.Y., Woo, D.J., Pervaporation of ionically surface crosslinked chitosan composite membranes for water-alcohol mixtures, J. Membr. Sci., 133 (1997) 103-110.

Lehermeier, H.J., Dorgan, J.R., Way, J.D., Gas permeation properties of poly (lactic acid), J. Membr. Sci., 190 (2001) 243-251.

Li, J., Chen, C., Han, B., Peng, Y., Zou, J., Jiang, W., Laboratory and pilot-scale study on dehydration of benzene by pervaporation, J. Membr. Sci., 203 (2002) 127-136.

Liang, W., Martin, C.R., Gas transport in electronically conductive polymers, Chem. Mater., 3 (1991) 390-391.

Lide, D. R. (Ed.), CRC Handbook of Chemistry and Physics, 88th Ed., 2007-2008.

Lin, W.H., Chung, T.S., Gas permeability, diffusivity, solubility, and aging characteristics of 6FDA-durene polyimide membranes, J. Membr. Sci., 186 (2001) 183-193.

Liu, L., Chakma, A., Feng, X., CO_2/N_2 separation by poly(ether block amide) thin film hollow fiber composite membranes, Ind. Eng. Chem. Res., 44 (2005) 6874-6882.

Liu, L., Chakma, A., Feng, X., Preparation of hollow fiber poly(ether block amide)/Polysulfone composite membrane for separation of carbon dioxide from nitrogen, Chem. Eng. J., 105 (2004) 43-51.

Liu, L., Chen, Y., Kang, Y., Deng, M., An industrial scale dehydration process for natural gas involving membranes, Chem. Eng. Technol., 24 (2001a) 1045-1048.

Liu, L., Chen, Y., Li, S., Deng, M., The effect of a support layer on the permeability of water vapor in asymmetric composite membranes, Sep. Sci. Technol., 36 (2001c) 3701-3720.

Liu, Y., Wang, R., Chung, T. S., Chemical cross-linking modification of polyimide membrane for gas separation, J. Membr. Sci., 189 (2001b) 231-239.

Maier, G., Gas separation with polymer membrane, Angewandte Chemie International Edition, 37 (1998) 2960-2974.

Matson, S.L., Lopez, J., Quinn, J.A., Separation of gases with synthetic membranes, Chem. Eng. Sci., 38 (1983) 503-524.

Matsumoto, K., Xu, P., Nishikimi, T., Gas permeation of aromatic polyimides. I. Relationship between gas permeabilities and dielectric constants, J. Membr. Sci., 81 (1993) 15-22.

Matsuyama, H., Hirai, K., Teramoto, M., Selective permeation of carbon dioxide through plasma polymerized membrane from diisopropylamine, J. Membr. Sci., 92 (1994b) 257-265.

Matsuyama, H., Matsui, K., Kitamura, Y., Maki, T., Termoto, M., Effects of membrane thickness and membrane preparation condition on facilitated transport of CO_2 through ionomer membrane, Sep. Purif. Technol., 17 (1999a) 235-241.

Matsuyama, H., Terada, A., Nakagawara, T., Kitamura, Y., Teramoto, M., Facilitated transport of CO_2 through polyethylenimine/poly(vinyl alcohol) blend membrane, J. Membr. Sci., 163 (1999b) 221-227.

Matsuyama, H., Teramoto, M., Facilitated transport of carbon dioxide through functional membranes prepared by plasma graft polymerization using amines as carrier, in: Bartsch, R.A., Way, J.D., (Eds.) Chemical Separations with Liquid Membranes, ACS Symp. Series, 642 (1996a) 252-269.

Matsuyama, H., Teramoto, M., Facilitated transport of CO_2 through various ion exchange membranes prepared by plasma graft polymerization, J. Membr. Sci., 117 (1996b) 251-260.

Matsuyama, H., Teramoto, M., Iwai, K., Development of a new functional cation-exchange membrane and its application to facilitate transport of CO_2, J. Membr. Sci., 93 (1994a) 237-244.

Matsuyama, H., Teramoto, M., Sakakura, H., Selective permeation of CO_2 through poly{2-(N,N-dimethyl) aminoethyl methacrylate} membrane prepared by plasma-graft polymerization technique, J. Membr. Sci., 114 (1996) 193-200.

Meares, P., The diffusion of gases through polyvinyl acetate, J. Am. Chem. Soc., 76 (1954) 3415-3422.

Mensitieri, G., Del Nobile, M.A., Sommazzi, A., Nicolais, L., Water transport in a polyketone terpolymer, J. Polym. Sci. B: Polym. Phys., 33 (1995) 1365-1370.

Merkel, T.C., Bondar, V., Nagai, K., Freeman, B.D., Yampolskii, Y.P., Gas sorption, diffusion and permeation in poly(2,2-bis(trifluoromethyl)-4,5-difluoro-1,3-dioxole-co-tetrafluoroethylen), Macromolecules, 32 (1999) 8427-8440.

Merkel, T.C., Bondar, V.I., Nagai, K., Freeman, B.D., Gas sorption, diffusion, and permeation in poly (dimethylsiloxane), J. Polym. Sci. B: Polym. Phys., 38 (2000) 415-434.

Metz, S.J., van de Ven, W.J.C., Mulder, M.H.V., Wessling, M., Mixed gas water vapor/N$_2$ transport in poly(ethylene oxide) poly(butylene terephthalate) block copolymers, J. Membr. Sci., 266 (2005b) 51-61.

Metz, S.J., van de Ven, W.J.C., Potreck, J., Mulder, M.H.V., Wessling, M., Transport of water vapor and inert gas mixtures through highly selective and highly permeable polymer membranes, J. Membr. Sci., 251 (2005a) 29-41.

Mochizuki, A., Sato, Y., Ogawara, H., Yamashita, S., pervaporation separation of water/ethanol mixtures through polysaccharide membranes: the permselectivity of the chitosan membranes, J. Appl. Polym. Sci., 37 (1989) 3375-3384.

Mulder, M.H.V., Kruitz, F., Smolders, C.A., Separation of isomeric, xylenes by pervaporation through cellulose ester membrane, J. Membr. Sci., 11 (1982) 349-363.

Nagaya, J., Tanioka, A., Miyasaka, K., Preparation and characterization of membranes with positively charged main chain from polyethylenimine, J. Appl. Polym. Sci., 48 (1993) 1441-1447.

Nakabayashi, M., Okabe, K., Fujisawa, E., Hirayama, Y., Kazama, S., Matsumiya, N., Takagi, K., Mano, H., Haraya, K., Kamizawa, C., Carbon dioxide separation through water-swollen-gel membrane, Energ. Convers. Manage., 36 (1995) 419-422.

Nakano, H., Seita, K., Imamura, K., Watanabe, T., Blood-purifying membrane, US Patent 4,787,977 (1988).

Nam, S.Y., Lee, Y.M., Pervaporation of ethylene glycol-water mixtures. I. Pervaporation performance of surface crosslinked chitosan membranes, J. Membr. Sci., 153 (1999) 155-162.

Namboodiri, V.V., Vane, L.M., High permeability membranes for the dehydration of low water content ethanol by pervaporation, J. Membr. Sci., 306 (2007) 209–215.

Neplenbroek, A.M., Bargeman, D., Smolder, C.A., Supported liquid membrane: Stabilization by gelation, J. Membr. Sci., 67 (1992) 149~165.

Nik, O.G., Moheb A., Mohammadi, T., Separation of ethylene glycol/water mixtures using NaA zeolite membranes, Chem. Eng. Technol., 29 (2006) 1340-1346.

Nitsche, V., Ohlrogge, K., Stürken, K., Separation of organic vapors by means of membranes, Chem. Eng. Technol., 21 (1998) 925-935.

Noble, R.D., Analysis of facilitated transport with fixed site carrier membrane, J. Membr. Sci., 50 (1990) 207-214.

Noble, R.D., Generalized microscopic mechanism of facilitated transport in fixed site carrier membrane, J. Membr. Sci., 75 (1992) 121-129.

Noble, R.D., Kinetic efficiency factors for facilitated transport membranes, Sep. Sci. Technol., 20 (1985) 577-585.

Noble, R.D., Pellegrino, J.J., Grosgogeat, E., Sperry, D., Way, J.D., CO_2 separation using facilitated transport ion-exchange membranes, Sep. Sci. Technol., 23 (1988) 1595-1609.

Odian, G., Principles of polymerization, 4th edition, Wiley, New York, 2004.

Pandey P., Chauhan R.S., Membrane for gas separation, Prog. Polym. Sci., 26 (2001) 853-893.

Park, Y. I., Lee, K. H., Preparation of water-swollen hydrogel membranes for gas separation, J. Appl. Polym. Sci., 80 (2001) 1785-1791.

Pasternak, M., Reale Jr., J., Dewatering of concentrated aqueous solutions by pervaporation, US Patent 5,182,022 (1993).

Paul, D.R., Koros, W.J., Effect of partially immobilizing sorption on permeability and the diffusion time lag, J. Polym. Sci. B: Polym. Phys., 14 (1976) 675-685.

Perry, R.H., Green, D.W. (Eds.), Perry's Chemical Engineers' Handbook, McGraw-Hill, 1999.

Petersen, J., Peinemann, K.V., Novel polyamide composite membranes for gas separation prepared by interfacial polycondensation, J. Appl. Polym. Sci., 63 (1997) 1557-1563.

Peterson, R.J., Composite reverse osmosis and nanofiltration membranes, J. Membr. Sci., 83 (1993) 81-150.

Petropoulos, J.H., Mechanisms and theories for sorption and diffusion of gases in polymers, in: Paul, D.R., Yampol'skii, Y.P. (Eds), Polymeric Gas Separation Membranes, CRC Press, Boca Raton, (1994) 17-81.

Petropoulos, J.H., Quantitative analysis of gaseous diffusion in glassy polymers, J. Polym. Sci., A2: 8 (1970) 1979-1801.

Pinnau, I., Toy, L.G., Solid polymer electrolyte composite membranes for olefin/paraffin separation, J. Membr. Sci., 184 (2001) 39-48.

Quinn, R., Laciak, D.V., Polyelectrolyte membranes for acid gas separations, J. Membr. Sci., 131 (1997) 49-60.

Rao, K.S.V.K., Subha, M.C.S., M., Sairam, M., Mallikarjuna, N.N., Aminabhavi T.M., Blend membrane of chitosan and poly(vinyl alcohol) in pervaporation dehydration of isopropanol and tetrahydrofuran, J. Appl. Polym. Sci., 103 (2007) 1918-1926.

Rao, P.S., Sridhar, S., Ming, Y.W., Krishnaiah, A., Pervaporative separation of ethylene glycol/water mixtures by using cross-linked chitosan membranes, Ind. Eng. Chem. Res., 46 (2007) 2155-2163.

Ray, S.K., Sawant, S.B., Joshi, J.B., Pangarkar, V.G., Development of new synthetic membranes for separation of benzene-cyclohexane mixtures by pervaporation: a solubility parameter approach, Ind. Eng. Chem. Res., 36 (1997) 5265.

Reid, C.E., Breton, E.J., Water and ion flow across cellulosic membranes, J. Appl. Polym. Sci., 1 (1959) 133-143.

Reineke, C.E., Jagodzinski, J.A., Denslow, K.R., Highly water selective celluslosic polyelectrolyte membranes for the pervaporation of alcohol-water mixtures, J. Membr. Sci., 32 (1987) 207-221.

Ren, J., Chung, T.S., Li, D., Wang, R., Liu, Y., Development of asymmetric 6FDA-2,6 DAT hollow fiber membranes for CO_2/CH_4 separation. 1. The influence of dope composition and rheology on membrane morphology and separation performance, J. Membr. Sci., 207 (2002) 227-240.

Ren, J., Wang, R., Chung, T.S., Li, D., Liu, Y., The effects of chemical modifications on morphology and performance of 6FDA-ODA/NDA hollow fiber membranes for CO_2/CH_4 separation, J. Membr. Sci., 222 (2003) 133-147.

Robeson, L.M., Correlation of separation factor versus permeability for polymeric membranes, J. Membr. Sci., 62 (1991) 165-185.

Romano Jr., C.E., Gallo, E.A., Ink jet pringting method, US Patent 6,224,202 (2001).

Salem, A., Ghoreyshi, A.A., Modelling of water/organic vapor dehydration by glassy polymer membranes, Desalination, 193 (2006) 25-34.

Sander, U., Janssen, H., Industrial application of vapour permeation, J. Membr. Sci., 61 (1991) 113-129.

Schult, K.A., Paul, D.R., Techniques for measurement of water vapor sorption and permeation in polymer films, J. Appl. Polym. Sci., 61 (1996a) 1865-1876.

Schult, K.A., Paul, D.R., Water sorption and transport in a series of polysulfones, J. Polym. Sci. B: Polym. Phys., 34 (1996b) 2805-2817.

Schult, K.A., Paul, D.R., Water sorption and transport in blends of polyethyloxazoline and polyethersulfone, J. Polym. Sci. B: Polym. Phys., 35 (1997b) 993-1007.

Schult, K.A., Paul, D.R., Water sorption and transport in blends of poly(vinylpyrrolidone) and polysulfone, J. Polym. Sci. B: Polym. Phys., 35 (1997a) 655-674.

Schultz, J., Peinemann, K.V., Membranes for separation of higher hydrocarbons from methane, J. Membr. Sci., 110 (1996) 37-45.

Semenova S.I., Ohya H., Soontarapa K., Hydrophilic membranes for pervaporation: An analytical review, Desalination, 110 (1997) 251-286.

Shah, V. M., Stern, S. A., Ludovice, P. J., Estimation of the free volume in polymers by means of a Monte Carlo technique, Macromolecules, 22 (1989) 4660-4662.

Shao, P., Huang, R. Y. M., Polymeric membrane pervaporation, J. Membr. Sci., 287 (2007) 162-179.

Shao, P., Huang, R.Y.M., Feng, X., Anderson, W.A., Pal, R., Burns, C.M., Composite membranes with an integrated skin layer: preparation, structural characteristics and pervaporation performance, J. Membr. Sci., 254 (2005) 1-11.

Shieh, J.J., Chung, T.S., Gas permeability, diffusivity, and solubility of poly (4-vinylpyridine) film, J. Polym. Sci. B: Polym. Phys., 37 (1999) 2851-2861.

Shimidzu, T., Yoshikawa, M., in: Huang, R.Y.M. (Ed.), Synthesis of novel copolymer membranes for pervaporation, Pervaporation Membrane Separation Processes, Elsevier, Amsterdam, (1991) 321-361.

Sirkar, K.K., Hollow fiber-contained liquid membranes for separations: an overview, in: Bartsch, R.A., Way, J.D. (Eds.), Chemical Separations with Liquid Membranes, ACS Symp. Series, 642 (1996) 222-238.

Smitha, B., Suhanya, D., Sridhar, S., Ramakrishna, M., Separation of organic-organic mixtures by pervaporation-a review, J. Membr. Sci., 241 (2004) 1-21.

Sommer, S., Melin, T., Performance evaluation of microporous inorganic membranes in the dehydration of industrial solvents, Chem. Eng. Proc., 44 (2005) 1138-1156.

Song, Y., Sun, P., Henry, L.L., Sun, B., mechanisms of structure and performance controlled thin film composite membrane formation via interfacial polymerization process, J. Membr. Sci., 251 (2005) 67-79.

Sridhar, S., Susheela, Reddy, G.J., Khan, A.A., Crosslinked chitosan membranes: characterization and study of dimethylhydrazine dehydration by pervaporation, Polym. Int., 50 (2001) 1156-1161.

Stannett, V., Haider, M., Koros, W. J., Hopfenberg, H. B., Sorption and transport of water vapor in glassy poly(acrylonitrile), Polym. Eng. Sci., 4 (1980) 300-304.

Stern, S.A., Koros, W.J., Separation of gas mixtures with polymer membranes: A brief overview, Chimie Nouvelle, 18 (2000) 3201-3215.

Stern, S.A., Polymers for gas separations: The next decade, J. Membr. Sci., 94 (1994) 1-65.

Streicher, C., Ethyl tertio-butyl ether purification process combining a membrane method and distillation, US Patent 5,607,557 (1997).

Terada, I., Nakamura, M., Nakao, M., Water/ethanol permeation properties through poly(hydroxymethylene) and poly(hydroxymethylene-co-fluoroolefin) membrane by pervaporation method, Desalination, 70 (1988) 455-463.

Teramoto, M., Approximate solution of facilitation factors for the transport of CO_2 through a liquid membrane of amine solution, Ind. Eng. Chem. Res., 34 (1995) 1267-1272.

Teramoto, M., Nakai, K., Ohnishi, N., Huang, Q., Watari, T., Matsuyama, H., Facilitated transport of carbon dioxide through supported liquid membranes of aqueous amine solutions, Ind. Eng. Chem. Res., 35 (1996) 538-545.

Teramoto, M., Takeuchi, N., Maki, T., Matsuyama, H., Facilitated transport of CO_2 through liquid membrane accompanied by permeation of carrier solution, Sep. Purif. Technol., 27 (2002) 25-31.

Teramoto, M., Takeuchi, N., Maki, T., Matsuyama, H., Gas separation by liquid membrane accompanied by permeation of membrane liquid through membrane physical transport, Sep. Purif. Technol., 24 (2001) 101-112.

Tsuchida, E., Nishide, H., Ohyanagi, M., Kawakami, H., Facilitated transport of molecular oxygen in the membranes of polymer-coordinated cobalt Schiff base complexes, Macromolecules, 20 (1987) 1907-1912.

van de Watering, P., Zuidam, N.J., van Steenbergen, M.J., van der Houwen, O.A.G.J., Underberg, W.J.M., Hennink, W.E., A mechanistic study of the hydrolytic stability of poly (2-(dimethylamino)ethyl methacrylate), Macromolecules, 31 (1998) 8063-8068.

van den Broeke, L.J.P.W., Bakker, J.W., Kapteijn, F., Moulijn, J.A., Binary permeation through a Silicalite-1 membrane, AIChE J., 45 (1999) 976-985.

van Oss, C. J., Good, R.J., Chaudhury, M.K., Determination of the hydrophobic interaction energy-application to separation processes, Sep. Sci. Technol., 22 (1987) 1-24.

van Oss, C.J., Giese, R.F., Wu, W., On the predominant electron-donicity of polar solid surfaces, J. Adhesion, 1997 (63) 71-88.

van Oss, C.J., Interfacial Forces in Aqueous Media, Dekker, New York, 1994.

Visser, T., Koops, G. H., Wessling, M., On the subtle balance between competitive sorption and plasticization effects in asymmetric hollow fiber gas separation membranes, J. Membr. Sci., 252 (2005) 265-277.

Volpe, C.D., Siboni, S., Acid-base surface free energies of solids and the definition of scales in the Good-van Oss-Chaudhury theory, J. Adhesion Sci. Technol., 14 (2000) 235-272.

Volpe, C.D., Siboni, S., Some reflections on acid-base solid surface free energy theories, J. Colloid Interf. Sci., 195 (1997) 121-136.

Wang, H., Tanaka, K., Kita, H., Okamoto, K., Pervaporation of aromatic/non-aromatic hydrocarbons through plasma grafted membranes, J. Membr. Sci., 154 (1999) 221-228.

Ward, W.J., Robb, W.L., Carbon dioxide-oxygen separation: Facilitated transport of carbon dioxide across a liquid film, Science, 156 (1967) 1481-1484.

Way, J.D., Noble, R.D., Reed, D.L., Ginley, G.M., Jarr, L.A., Facilitated transport of CO_2 in ion exchange membranes, AIChE J., 33 (1987) 480-487.

Wijmans, J.G., Baker, R.W., The solution-diffusion model: A review, J. Membr. Sci., 107 (1995) 1-21.

Will, B., Lichtenthaler, R.N., Comparison of the separation of mixtures by vapor permeation and by pervaporation using PVA composite membranes. I. Binary alcohol-water systems, J. Membr. Sci., 68 (1992) 119-125.

Wu, F., Li, L., Xu, Z., Tan, S., Zhang, Z., Transport study of pure and mixed gases through PDMS membrane, Chem. Eng. J., 117 (2006) 51-59.

Wu, J., Yuan, Q., Gas permeability of a novel cellulose membrane, J. Membr. Sci., 204 (2002) 185-194.

Wu, W., Giese Jr., R.F., van Oss, C.J., Evaluation of the Lifshitz-van der Waals/acid-base approach to determine surface tension components, Langmuir, 11 (1995) 379-382.

Wu, Y., Peng, X., Liu, J., Kong, Q., Shi, B., Tong, M., Study on the integrated membrane processes of dehumidification of compressed air and vapor permeation processes, J. Membr. Sci., 196 (2002) 179-183.

Yamaguchi, T., Boetje, L.M., Koval, C.A., Noble, R.D., Bowman, C.N., Transport properties of carbon dioxide through amine functionalized carrier membranes, Ind. Eng. Chem. Res., 34 (1995) 4071-4077.

Yamasaki, A., Mizoguchi, K., Pervaporation of benzene/cycloxane and benzene/hexane mixtures through PVA membranes, J. Appl. Polym. Sci., 64 (1997) 1061-1065.

Yasuda, H., Tsai, J.T., Pore size of microporous polymer membranes, J. Appl. Polym. Sci., 18 (1974) 805-819.

Yeom, C.K., Lee, K.H., Pervaporation separation of water-acetic acid mixtures through poly(vinyl alcohol) membranes crosslinked with glutaraldehyde, J. Membr. Sci., 109 (1996) 257-265.

Yoshikawa, M., Ezaki, T., Sanui, K., Ogata, N., Selective permeation of carbon dioxide through synthetic polymer membranes having pyridine moiety as a fixed carrier, J. Appl. Polym. Sci., 35 (1988) 145-154.

Yoshikawa, M., Fujimoto, K., Kinugawa, H., Kitao, T., Ogata, N., Selective permeation of carbon dioxide through synthetic polymeric membranes having amine moiety, Chem. Lett., (1994) 243-246.

Yoshikawa, M., Ogata, N., Shimidzu, T., Polymer membrane as a reaction field. III. Effect of membrane polarity on selective separation of water-ethanol binary mixtures through synthetic polymer membranes, J. Membr. Sci., 26 (1986) 107-113.

Yoshikawa, M., Yokoi, H., Ogata, N., Shimidzu, T., Polymer membrane as a reaction field. II. Effect of membrane environment on permselectivity for water-ethanol binary mixtures, Polym. J., 16 (1984) 653-656.

Zhang, L., Yu, P., Luo Y., Comparative behavior of PVA/PAN and PVA/PES composite pervaporation membranes in the pervaporative dehydration of Caprolactam, J. Appl. Polym. Sci., 103 (2007d) 4005-4011.

Zhang, L., Yu, P., Luo Y., Dehydration of caprolactam-water mixtures through cross-linked PVA composite pervaporation membranes, J. Membr. Sci., 306 (2007e) 93-102.

Zhang, Y., Wang, Z., Wang, S., Novel fixed-carrier membranes for CO_2 separation, J. Appl. Polym. Sci., 86 (2002b) 2222-2226.

Zhang, Y., Wang, Z., Wang, S., Selective permeation of CO_2 through new facilitated transport membranes, Desalination, 145 (2002a) 385-388.

Zhang, Y., Wang, Z., Wang, S., Synthesis and characteristics of novel fixed carrier membrane for CO_2 separation, Chem. Lett., 3 (2002c) 430-431.

Zhao, J., Wang, Z., Wang, J., Wang, S., Influence of heat-treatment of CO_2 separation performance of noel fixed carrier composite membranes prepared by interfacial polymerization, J. Membr. Sci., 283 (2006) 346-356.

Zhu, W., Gora, L., van de Berg, A.W.C., Kapteijn, F., Jansen, J.C., Moulijn, J.A., Water vapour separation from permanent gases by a zeolite-4A membrane, J. Membr. Sci., 253 (2005) 57-66.

Zhu, Y., Minet, R.G., Tsotsis, T.T., A continuous pervaporation membrane reactor for the study of esterification reactions using a composite polymeric/ceramic membrane, Chem. Eng. Sci., 51 (1996) 4103-4113.

Zolandz, R.R., Fleming, G.K., Gas permeation, in: Ho, W.S.W., Sirkar, K.K. (Eds.), Membrane Handbook, Van Nostrand Reinhold, New York, (1992) 17-101.